A Study of Conventional Fuels for Unconventional Applications

BY

JAI M. MEHTA
Dip., Shri Bhagubhai Mafatlal Polytechnic, Mumbai, 2013
B.E., University of Mumbai, Mumbai, 2016
M.S., University of Illinois at Chicago, Chicago, 2018

THESIS

Submitted in partial fulfillment of the requirements for the degree of
Doctor of Philosophy
in Mechanical Engineering in the Graduate College of the
University of Illinois at Chicago, 2022

Defense Committee:

Kenneth Brezinsky (Chair and Advisor, Mechanical and Industrial Engineering)
Farzad Mashayek (Mechanical and Industrial Engineering)
Patrick T. Lynch (Mechanical and Industrial Engineering)
Robert S. Tranter (Argonne National Laboratory)
Raghu Sivaramakrishnan (Argonne National Laboratory)

This thesis is dedicated to Toffee

ACKNOWLEDGEMENTS

I am grateful to my advisor Prof. Kenneth Brezinsky for giving me the opportunity to pursue doctorate in Mechanical Engineering under his guidance in the High-Pressure Shock Tube Laboratory. The advice and guidance from him during my tenure in the lab extends beyond scientific and technical knowledge to every aspect of the life and has been critical to my all-round personal development. I would like to thank Prof. Patrick T. Lynch for his support and guidance which was no less than that of an advisor. I thank all the committee members – Prof. Farzad Mashayek, Dr. Robert S. Tranter and Dr. Raghu Sivaramakrishnan for taking the time to be a part of my dissertation committee. The choice of committee members was not just influenced by the scientific stature of the members but also by the impact they have made to my progress at University of Illinois at Chicago.

I am indebted to my parents – Sonia M. Mehta and Manoj K. Mehta for their continued support throughout my academic life and beyond. I would not have been here without the sacrifices they have made over years for my academic prowess. I thank my brother – Jash M. Mehta for his support and taking care of my parents back home.

I would like to thank Rizwan A. Shaikh and Mohammed Abdul Rahman who have been on this journey with me since my first day at University of Illinois at Chicago for help and support. I want to thank the members of the High Pressure Shock Tube Laboratory – Manaf Sheyyab, Dr. Weijing Wang, Jerry Chethalan, Pedro Fernandez Jr., and Dhananjay Ambre. My successes in the lab would not have been possible without the teachings from the former members of the high pressure shock tube laboratory, particularly Dr. Miroslaw Liszka. I also thank the members of the Lynch Laboratory.

ACKNOWLEDGEMENTS (continued)

I would like to extend my gratitude to Richard Striebich – *University of Dayton Research Institute* for extensive guidance with the GCxGC analysis and thoughtful suggestions for overcoming several challenges and problems faced in the analysis.

I would also like to mention the college of engineering machine shop staff – David Mecha and Eric Schmidt, and physics machine shop staff - David Kuntzelman for their help with solving the many design and manufacturing problems faced over years.

The various parts of this dissertation were financially supported by different organizations. The work on natural gas was sponsored by the *Air Force Office of Scientific Research (AFOSR)* through grant no. FA9550-16-1-0079 with Dr. Chiping Li as the program manager. The work on functional group analysis of jet fuels was supported by *U.S. Army Research Laboratory (ARL)* through cooperative agreement no. W911NF-20-2-0223 with Dr. Mike Kweon as the program manager. The design and development of the High Pressure Shock Tube extension was funded by the *Army Research Office (ARO)* through grant no. W911NF-16-1-0063 with Dr. Ralph Anthenien as the program manager.

CONTRIBUITION OF AUTHORS

This thesis reproduces data from a previously published article - ***Experimental speciation study of natural gas oxidation using a single pulse shock tube,*** *Mehta J M., Brezinsky K., International Journal of Chemical Kinetics, 2021, 53(7), 845-867.* Jai M. Mehta wrote the manuscript and led the work in this publication – experiments, computational analysis, and data processing. Kenneth Brezinsky provided suggestion and guidance for the work.

TABLE OF CONTENTS

LIST OF TABLES

LIST OF FIGURES

LIST OF ABBREVATIONS AND SYMBOLS

NG	Natural Gas
K	Kelvin
atm	Atmospheres of pressure
ms	Milliseconds
φ	Equivalence Ratio
ppm	Parts per million
HPST	High Pressure Shock Tube
GC	Gas Chromatograph
ROP	Rate of Progress
CFG	Chemical Functional Group
GCxGC	Two Dimensional Gas Chromatograph
TOF-MS	Time of Flight – Mass Spectrometer
FID	Flame Ionization Detector
TCD	Thermal Conductivity Detector
UNIFAC	UNIQUAC Functional-group Activity Coefficient
MW	Molecular Weight
DCN	Derived Cetane Number
CN	Cetane Number
S2FG	Species to Functional Group
SMILES	Simplified Molecular Input Line Entry System
SMARTS	SMILES arbitrary target specification

SUMMARY

This study deals with the experimental and analytical analyses of different fuels to understand their combustion behavior. In addition to analyses, the design, development, and modification of an experimental apparatus was also a critical element of this study and will contribute to future studies in the laboratory.

Feasibility of using natural gas as a propulsion fuel to replace the currently used liquid fuels and pure compounds like hydrogen and methane was investigated by oxidation and pyrolysis studies of natural gas samples using a single pulse high pressure shock tube. The studies were conducted for different natural gas samples at different thermodynamic conditions. The resultant test samples from the shock tube were analyzed using gas chromatography to study the formation of various hydrocarbon species with respect to temperature at a given nominal pressure and over a nominal reaction time. The experimental observations were compared to chemical kinetic model predictions from several well established chemical kinetic models to evaluate the predictive capability of the chemical kinetic mechanisms and to recommend necessary steps for optimization of these mechanisms for use with natural gas. No single mechanism used in this study was found to be fully capable of predicting natural gas oxidation at all the experimental conditions studied in this work. Different approaches need to be undertaken to optimize each model used however, all models can benefit from optimization using new prediction targets like detailed speciation data.

Detailed gas chromatographic analysis of various jet fuel samples was conducted to understand the composition of the fuels and its implications on the properties of the fuel. A detailed GCxGC method was developed to determine the fuel composition using a flame ionization detector and time of flight mass spectrometry. The components of the fuels were identified using mass spectrometry, while they were quantified using the flame ionization detector response by

exploiting the ability of the flame ionization detector to respond linearly to the number of carbons in the species. The hydrocarbon classification method was used in the GCxGC analysis to group like compounds together and represent them by the hydrocarbon-type they belong to.

A new software package, *S2FG* (species-to-functional group), was developed to convert the species based fuel composition into chemical functional group composition of the fuel on mass basis. The software developed can be used as an independent tool to obtain chemical functional group composition of any mixture irrespective of the analytical method if species composition in weight fraction is known. The code for the software package has been provided as an additional file with the thesis.

Hydrocarbon classification analysis of complex multicomponent jet fuels was conducted to overcome the uncertainty in identification of isomers by mass spectrometry because of extremely similar fragmentation patterns. The hydrocarbon classification based composition was then converted to UNIFAC based chemical functional group composition to obtain a generalized composition of the fuel which can be correlated to various fuel properties easily since a functional group impart properties to the fuel independently, unaffected by the presence of other functional groups in the fuel. The use of this approach required the selection of a single isomer species capable of representing the overall average composition of the hydrocarbon classification. The selection of this species affects the UNIFAC group composition of the fuels. The worst case (maximum branched isomer) and best case (minimum branched isomer) species were used to obtain the upper and lower bounds within which the UNIFAC group composition of that fuel exists. The regions for various real and specialty fuels were analyzed to understand how fuels differ from one another.

1 INTRODUCTION

Burning of fuels has been the largest and most reliable source of energy for centuries and the rising global energy demand has motivated countless studies investigating fuels for decades now. Fossil fuels are the largest source of energy for the transportation sector and power generation and have been the focus of combustion studies for over a century. The studies are aimed at understanding the combustion behavior of various fossil fuels and their suitability for use in various energy generation applications like internal combustion engines, gas turbine engines and propulsion engines. These studies investigate combustion characteristic behaviors like ignition delay times (IDT) [1–7], adiabatic flame temperature (AFT), laminar and turbulent flame speeds [8–14], extinction coefficients, chemical kinetics, reaction pathway analysis [15–30] and detonation velocity of different fuels. These characteristics are used for the design and optimization of combustion devices to obtained highest thermal and volumetric efficiencies. However, with the global climate crisis and increasing prices of fossil fuel research has been driven towards analyzing fuels for obtaining environmentally important combustion behavior in the form of carbon neutral emissions, reduced unburnt hydrocarbon emissions and reduced greenhouse gas generation. Several fuels are being synthetically developed [31,32] using biowaste to reduce the carbon footprint. These fuels have shown great potential as replacements for conventional fossil fuels but extensive studies on these fuels are necessary before largescale adoption as a replacement for conventional fossil fuels. In addition to new synthetic fuel developments and their studies, parallel work is being done into reinvestigating fuels of the past as well as optimizing the fuels currently in use to meet energy needs while maintaining the environmental decorum.

The replacement of the conventional fuels with newer and cleaner fuel has also shown potential for economic benefits in the form of reduced costs and simplification of logistics. The

benefits have sparked the interest of the defense sector to investigate alternate fuels [33–36]. The U.S. Air Force is looking at replacing kerosene based fuels, pure hydrogen, and methane with a more economical substitute like natural gas for their propulsion engines.

Table I : List of recent chemical kinetic studies focusing on natural gas.

Study	Device	Measurement	Conditions	Fuel	Reference
Shao et al.	Shock Tube	IDT, Species time history	P : 10-55 atm T : 1450 – 1850 K φ : 0.2, 1.0, 5.0	NG, CH_4	[7]
Crane et al.	Detonation tube	Detonation	P : 0.03 – 0.3 atm T : 1450 – 1850 K φ :	NG	[37]
Cassady et al.	Shock tube	Species time history	P : 3.1 – 4.2 atm T : 1178 – 1527 K φ : ∞	C_2H_6	[38]
Nadiri et al.	Shock tube	IDT	P : 10, 20, 40 atm T : 850 - 1550 K φ : 0.4 -1.2	$C_1 – C_5$	[39]
Mehta et al.	Shock tube	Speciation	P : 60 atm T : 1100 - 1750 K φ : 0.5 – 3.0	NG	This work, [29]
Mehta et al.	Shock tube	Speciation	P : 240 atm T : 1100 - 1750 K φ : 0.5 – 2.0	NG	This work, [30]
Healy et al.	Shock tube, RCM	IDT	P : 8 – 30 atm T : 630 - 1550 K φ : 0.5, 1.0, 2.0	$C_1 – C_5$	[40]
Bakali et al.	Shock tube, JSR, Flame	Flame speed, speciation, IDT	P : 0.1 - 1 atm T : 298 K φ : 0.75, 1.0, 1.5	$C_1 – C_6$	[9]
Sahu et al.	Shock tube	IDT	P : 20 - 30 atm T : 840 - 1050 K φ : 0.5 – 1.5	$C_1 – C_7$	[41]
Turbiez et al.	Burner	Flames	P : 20 - 30 atm T : 600 - 1800 K φ : 1.0	C_1/C2, C_1/C2/C_3, NG	[8]
Petersen et al.	Shock tube	IDT	P : 5.3 – 31.4 atm T : 1000 - 1585 K φ : 0.5 – 3.0	C_1/C_3	[20]

Natural gas is an economical source of fuel widely used in domestic applications for centuries and it has penetrated the consumer transportation markets [42] over the last few decades. In addition to economic advantages, natural gas possesses added benefits in the form of simple chemical composition and clean combustion emission under correct thermodynamic conditions

making it environmentally friendly. Natural gas has a high hydrogen to carbon ratio resulting in larger specific energy from combustion and being in gas phase simplifies handling and mixing. Natural gas chemistry has been widely studied over the years, but with primary focus on domestic and road transport applications. These applications require a significantly lower operating pressure and temperature, usually under 50 atm pressure and 1100 K temperature. Advanced propulsion engines and turbine engines operate at high pressures (>50 atm) and high temperatures (>1100 K) and are more sensitive to combustion variations and consequently require more accurate chemical kinetic mechanisms to aid in the designing and modifying of these devices. Table I includes a non-exhaustive list of recent natural gas studies aimed towards understanding natural gas oxidation chemistry.

In this work, chemical kinetic analysis of natural gas oxidation using the UIC - single pulse high pressure shock tube [43,44] was carried out. Species generated from the oxidation of natural gas in the shock tube at a nominal pressure of ~60 atm after a nominal reaction time of ~2.5 ms over a temperature range of 1100 – 1800 K were recorded. Natural gas samples from different locations across the United States were studied at or near their stoichiometric conditions ($\varphi \sim 1.0$). The composition of all the natural gas samples varied, and the goal of this study was to understand the effect of the natural gas composition on the species formation. These results were compared to predictions from chemical kinetic models to test their capability to predict species formation from natural gas with varying composition. This was followed by oxidation of a reference natural gas sample which was artificially prepared at different equivalence ratios to study the effect of fuel-oxidizer ratio on the chemical kinetics of natural gas. The study was repeated for the reference natural gas and one real natural gas sample at a nominal pressure of ~240 atm at different equivalence ratios to observe the effect of pressure on the species formation during oxidation. All

the experimental observations were compared to predictions from well-known chemical kinetic models to ascertain the capability of these models to predict the oxidation behavior of natural gas despite the compositional variations and change in stoichiometric conditions. The observations highlighted the critical role natural gas composition can play on its oxidation behavior at conditions relevant to propulsion engines.

The other part of this study supports the United States military's single fuel forward initiative by investigating the feasibility of using a single jet fuel to meet all their fuel needs, in addition to development of fuel ignition property sensor capable of predicting fuel's ignition properties in real time and adjusting engine parameters to maintain uninterrupted operation. This sensor is envisioned towards fuel independent operation of various U.S. Army unmanned aerial systems (UAS). To develop a universal sensor capable to handle any potential fuel, the description of a fuel in a generic form is necessary. Chemical functional group based composition is a suitable generic descriptor which can be related to various fuel properties irrespective of the type and source of the fuel. Chemical functional groups are parts of a molecule which impart specific properties to the molecule irrespective of the type of molecule. The information of the chemical functional groups in a fuel can be used to predict fuel properties as shown by previous studies [45–48].

The initial studies [46,48,49] focused on using chemical functional groups for development of predictive models and used NMR (Nuclear Magnetic Resonance) spectroscopy of fuels and mixtures to estimate the functional group composition. The NMR spectroscopy provides a highly diverse set of functional groups because molecular shifts measured in NMR spectroscopy correspond to the structural arrangement of the atoms and the various bonds between them. The functional groups obtained from NMR spectroscopy include the standard functional groups of

hydrocarbons like CH3, CH2, and CH but they can be further subdivided on the basis of the primary hydrocarbon structure to which they belong [50]. For instance, the CH2 group composition obtained from NMR Spectroscopy can be divided into three different functional groups – paraffinic-CH2, aromatic-CH2, cycloparaffinic-CH2 and alkenic-CH2. Similarly, the CH groups can be further subdivided into paraffinic-CH, monoaromatic-CH and polyaromatic-CH. The comprehensive split of functional groups provides extensive information for development of a robust model; however, the overwhelming amount of information obtained can also result in in overfitted predictive models. In addition to NMR spectroscopy based studies, several recent studies have attempted to estimate the functional group composition of fuels using FTIR (Fourier Transform Infrared) spectroscopy [51,52]. Contrary to the NMR spectroscopy based studies, these FTIR spectroscopy based studies have concentrated on the CH2 and CH3 groups only. The results obtained in these studies lead to a good predictive model capable of predicting major fuel properties using only the CH2 and CH3 group composition of the fuels and mixtures. The results of the study show that overwhelming amount of functional group composition details are not necessary for developing accurate predictive models, particularly with the advancement of machine learning based model development techniques like Neural Networks. However, the error in the predictive capability of FTIR spectroscopy based studies can be reduced by inclusion of more functional groups, but not as many as the NMR spectroscopy based groups. The UNIFAC groups used for group contribution methods [53] have a potential to provide the optimum amount of information which is comprehensive and widely structurally inclusive without unnecessary information.

The GCxGC TOF-MS/FID analysis undertaken in this work provides a pathway to estimate the UNIFAC group composition of fuels and mixtures while also providing information about the

hydrocarbon composition of the fuels and mixtures. The GCxGC TOF-MS/FID analysis of fuels is considered a complementary analysis to NMR analysis because it can provide identification and quantification hydrocarbons in the fuel as well as the overall structure of the fuel [50]. In this study, GCxGC TOF-MS/FID analysis was conducted on various fuels to obtain their detailed compositions which are then converted into chemical functional group compositions of the fuel which can then be used to predict fuel properties or develop new correlations. GCxGC analysis provides a comprehensive separation of the various compounds within the fuel and the separated compounds are identified using the TOF-MS and then quantified using the FID. The final composition of the real fuels was obtained in the form of hydrocarbon classifications and not individual species. This hydrocarbon classification composition was converted into UNIFAC groups which were the choice of chemical functional groups for this study. The capabilities of predicting various properties of mixtures using UNIFAC groups has been proven [45].

A software package was developed to convert this fuel composition from the GCxGC TOF-MS/FID analysis to chemical functional group composition. The software, *S2FG*, developed uses a previously developed algorithm by Müller [54] called *Fragmenter* to split the molecules into functional groups. The input composition is fragmented into the number of functional groups for individual species by the *Fragmenter* and the aggregate functional group composition of the fuel in weight fraction is computed by S2FG. This analysis provides the UNIFAC group composition of eleven real fuels and the technical approach necessary to repeat this analysis on any fuel. The software developed for converting mixture composition to chemical functional group composition can be independently used. This can allow use of GCxGC analysis data already obtained over years, such as those in the National Jet Fuel Combustion Program [55], to estimate the functional group compositions of various fuels without the need to reanalyze the fuel samples.

2 SHOCK TUBE STUDIES OF NATURAL GAS OXIDATION

(Previously published as ***Experimental speciation study of natural gas oxidation using a single pulse shock tube,*** *Mehta J M., Brezinsky K., International Journal of Chemical Kinetics, 2021, 53(7), 845-867.)*

The shock tube studies of natural gas were conducted under oxidation conditions at different stoichiometries for various samples of natural gas. The composition of natural gas samples used, and their stoichiometric ratios have been provided in the Table II. The real natural gas samples were sourced from different locations across the United States. The samples are referred to (as shown in Table II) from where they are sourced for the remainder of this study and the reference sample is denoted by 'rf'. The variation in the composition of the different samples results in a different stoichiometry as seen in Table II for the oxidation for all samples.

Table II: Composition of various samples of natural gas in percent mole fractions. "Other" include CO2, N2 and trace hydrocarbons.

Sample Location	**CH_4**	**C_2H_6**	**C_3H_8**	**Other**	**Stoichiometric Ratio**
Reference (rf)	95.50	3.52	0.98	0.00	2.0825
Idaho (ID)	93.95	4.20	0.45	1.40	2.0485
Kentucky (KY)	91.21	7.62	0.27	0.90	2.1173
Tennessee (TN)	92.11	6.70	0.18	1.01	2.0857
Ohio (OH)	93.63	5.90	0.29	0.18	2.0935
North Carolina (NC)	95.84	3.05	0.16	0.95	2.0535
South Carolina (SC)	96.30	2.73	0.16	0.81	2.0295

The shock tube experiments were conducted using test mixtures containing dilute amounts of the fuel, natural gas, and oxidizer, oxygen, in argon. The oxidizer concentrations in the test mixture were changed to adjust the equivalence ratio while keeping the fuel concentration constant at 1000 ppm (0.1%) by mole fraction. The prepared mixtures were analyzed using gas chromatography to confirm the composition of the test mixture. The values reported in this study provide the exact measured composition of the test mixture and not the target conditions. Table III

provides the details of the test mixtures used for each experimental set. The concentration of ten target species – CH_4, C_2H_6, C_2H_4, C_2H_2, C_3H_8, CO, CO_2, O_2 and H_2 in the test sample were measured.

Table III : Details of the test mixtures used for natural gas experiments and the experiment identifiers. All experiments were conducted over the temperature range of 1100 K – 1800 K and a nominal reaction time of 2.5 ms.

Nominal Pressure (atm)	**Sample Details**	**Experiment Set**	**Equivalence Ratio (φ)**	**Mixture Composition (mole fraction - ppm)**				
				CH_4	**C_2H_6**	**C_3H_8**	**NG**	**O_2**
60	NG - Reference	NG_RF_01	0.80	809	30	8	**847**	**2160**
60	NG - Reference	NG_RF_02	0.49	858	32	9	**899**	**3840**
60	NG - Reference	NG_RF_04	1.49	876	33	9	**918**	**1280**
60	NG - Reference	NG_RF_05	3.07	873	32	9	**914**	**630**
60	NG - Reference	NG_RF_06	∞	1010	37	10	**1057**	**0**
60	NG - Reference	NG_RF_07	0.99	950	35	10	**994**	**2080**
60	NG - Idaho	NG_ID_00	0.89	982	44	5	**1031**	**2350**
60	NG - Kentucky	NG_KY_01	1.06	936	79	3	**1017**	**2060**
60	NG - Tennessee	NG_TN_01	0.99	962	70	2	**1034**	**2200**
60	NG - Ohio	NG_OH_01	1.11	998	63	3	**1064**	**1980**
60	NG - North Carolina	NG_NC_01	1.02	1050	33	2	**1085**	**2180**
60	NG - South Carolina	NG_SC_01	1.06	985	28	2	**1015**	**1960**
240	NG - Reference	NG_RF_08	1.04	956	35	10	**1001**	**2050**
240	NG - Reference	NG_RF_09	0.52	932	34	9	**975**	**3600**
240	NG - Reference	NG_RF_10	2.00	997	37	10	**1044**	**1160**
240	NG - Idaho	NG_ID_03	1.01	977	44	5	**1026**	**2150**
240	NG- Idaho	NG_ID_04	2.04	953	43	5	**1001**	**1010**
240	NG - Idaho	NG_ID_05	0.51	958	43	5	**1006**	**3670**

The first set of experiments were conducted at a nominal pressure of ~60 atm to study the effect of equivalence ratio using the reference natural gas sample. The reference natural gas sample was sourced from Linde Gas with a prescribed composition that was assumed to be a surrogate capable of representing the large variation between natural gas samples. The reference natural gas composition was prescribed by a collaborating group at Stanford University based on statistical analysis of varying natural gas compositions across United States. The experiments at different

equivalence ratios for this reference natural gas sample showed the effect of equivalence ratio on species formation under oxidation conditions and highlighted the difference in the behavior of natural gas and pure methane.

The next set of experiments used the real natural gas samples to observe the effect of compositional variation on the species formation during oxidation at near stoichiometric conditions. The target mixture composition for these experiments was 1000 ppm of fuel and 2000 ppm of oxidizer. The differences in the stoichiometric ratios for different samples resulting from composition variation resulted in slightly varying equivalence ratios of the test mixtures because the target mixture composition was constant for all mixtures. Exact details of each mixture are provided in Table III. In this study only the key components of natural gas samples (CH_4, C_2H_6 and C_3H_8) were considered as initial fuel despite the presence of trace amounts of larger hydrocarbons and impurities like N_2 and CO_2 in some natural gas samples.

The third set of experiments was conducted at a nominal pressure of ~240 atm and over the same temperature range and nominal reaction time as the previous experimental sets. The reference natural gas sample and real natural gas sample from Idaho (NG-ID) were studied at three different equivalence ratios – ~0.5, ~1.0, ~2.0 each. The objective of this study was to investigate the pressure dependency of the species generated during oxidation of natural gas. This study also obtains a large amount of high pressure data which are scarce in literature and can be used to test the chemical kinetic mechanisms at very high pressures.

2.1 Experimental Technique and Apparatus

2.1.1 Shock Tube

The shock tube is a device capable of developing high temperatures and high pressures instantaneously and maintaining them for finite amounts of time, about milliseconds, in a gas. The instantaneous rise in pressure and temperature mimics the thermodynamic conditions that occur in real combustion devices like engines and initiates chemical reactions in the test mixture that can be expected to occur in the combustion devices. After the duration of test (reaction) time, the test sample is quickly quenched to a temperature low enough so that the reaction chemistry freezes. Subsequent analysis of the test sample by GC is used to identify and quantify the species formed because of oxidation at the experimental temperature and pressure over the reaction time. The dilute nature of the test sample ensures that endo and exothermic effects do not affect the thermodynamic conditions. The observed species are purely a result of the high temperature and pressures generated in the shock tube. Shock tubes are well established and have been widely used for such chemical kinetic studies for over 50 years.

A shock tube is made of two closed end long tubes that are separated from each other. One section of the tube holds gas at an extremely high pressure, and it is called the driver section, while the other section holds the low pressure gas and is called the driven section. The two sections are separated from each other using a diaphragm or valve. A shock wave is generated in the driven section at the diaphragm location when the diaphragm is instantaneously removed, and the high pressure gas comes in direct contact with the low pressure section. At the same time an expansion wave is generated in the driver section at the diaphragm location and both the waves travel in opposite directions. The shock wave travels along the length of the driven section, away from the driver section towards the closed end of the driven section (end wall of driven section) from which

it reflects. When the shock passes through the gas, the gas is instantaneously heated and pressurized. This effect is governed by the compressible flow theory. The incident shock travelling towards the end wall raises the pressure and temperature of the gas as it travels through it and after reflecting off the wall reheats and pressurizes this gas again, which results in two-stage increase in pressure and temperature of the test gas. The resultant thermodynamic condition after the reflection of the shock is used to facilitate chemical reaction in the test gas (driven gas) when fuel is present.

An expansion wave is formed in the driver section when the diaphragm is removed which drops the pressure and temperature in the driver section. The expansion wave travels towards the driver section end wall and reflects. The reflected expansion then travels back through the driver section and into the driven section until it interfaces with the reflected shock. After the contact between the shock and expansion wave, the pressure and temperature in reaction region drops rapidly, thus freezing the chemical reactions and ending the reaction time.

The gas dynamics and thermodynamic conditions in the shock tube are described by ideal shock tube theory [56,57], in which the shock tube is divided in to five regions, as shown in Figure 1. Region 1 is the region in the driven section through which the incident shock has not passed. It also represents the initial condition of the driven section. The region 2 is the region in the driven section through which the incident shock has passed and ends at the interface between the driver and driven gases (contact surface). Region 3 is the region between the tail of the expansion wave and the contact surface. The expansion wave has passed through this region and region 4 is the region ahead of the expansion wave, through which it has not passed. It also represents the initial condition of the driver section. Another region, 5, is designated after the reflection of the incident shock from the end wall. This region represents the region through which the reflected shock has

passed, and it replaces region 1 after reflection of the shock. The region 5 is the reaction region from where the sample is extracted. The following equations provide the relations between different regions in the shock tube based on compressible flow theory, gas dynamics and thermodynamics and combined from the normal shock tube theory [56,57]. In equations 2.1 - 2.6 , ‘P’ represents the pressure, ‘T’ represents the temperature, ‘M’ represents the shock Mach number, ‘u’ represents the velocity, ‘a’ represents the velocity of sound and ‘γ’ represents the specific heat capacity ratio of the gas. The subscripts 1 – 5 represent the regions whereas ‘s’ and ‘r’ represent incident and reflected shock, respectively.

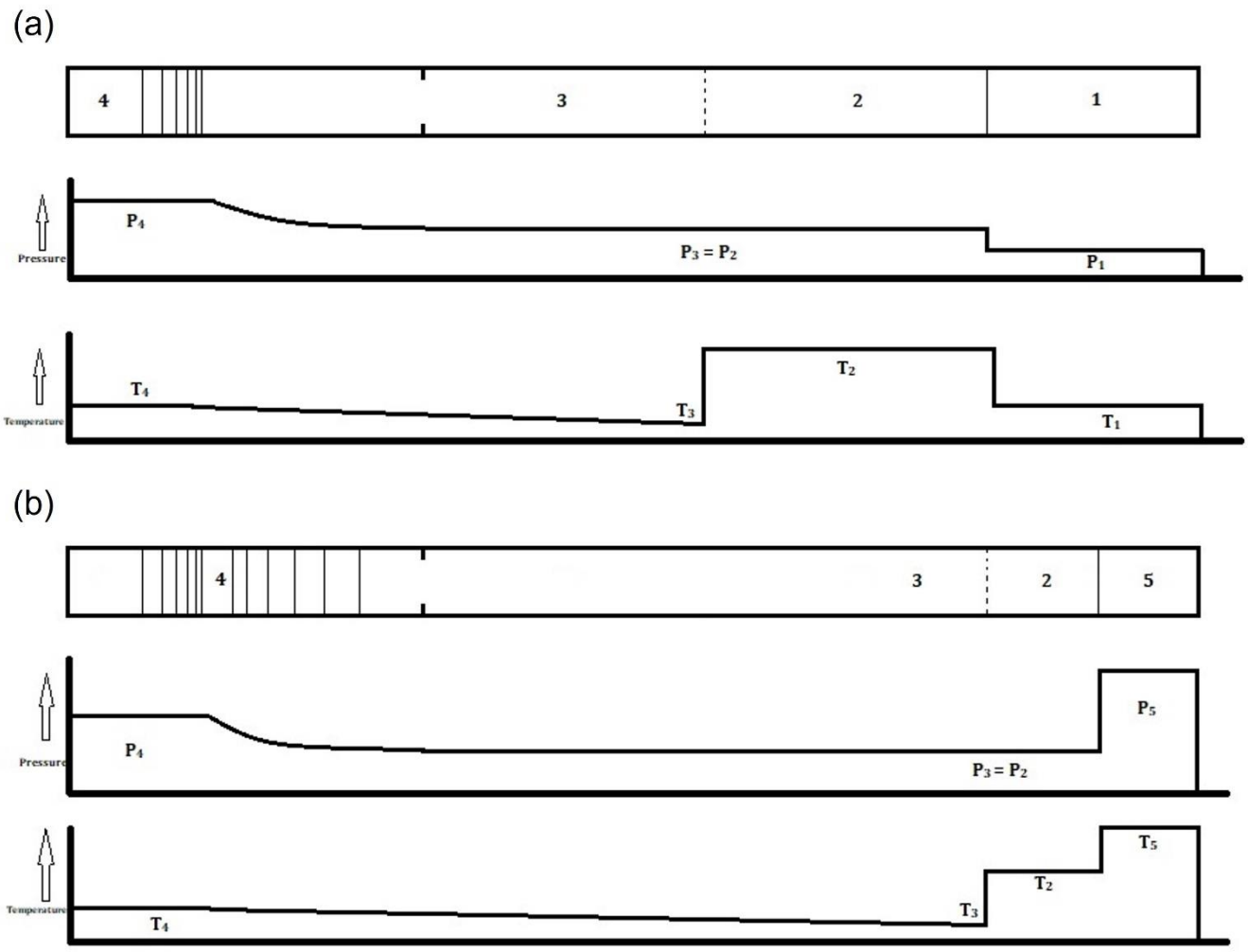

Figure 1 : Schematics of a shock tube showing different regions, before (a) and after(b) reflection of the incident shock from the end wall.

The ratio of pressures and temperatures across the incident shock can be related to the incident shock Mach number [57,58],

$$\frac{P_1}{P_2} = \frac{2\gamma_1 M_s - (\gamma_1 - 1)}{\gamma_1 + 1} \qquad 2.1$$

$$\frac{T_1}{T_2} = \frac{\left(\gamma_1 {M_s}^2 - \frac{(\gamma_1 - 1)}{2}\right)\left(\frac{(\gamma_1 - 1)}{2}.{M_s}^2 + 1\right)}{\left(\frac{\gamma_1 + 1}{2}\right)^2 .{M_s}^2}$$

2.2

Similarly, the pressures and the temperatures across the expansion wave is dependent on the velocity in the region behind the expansion wave and speed of sound in the region ahead the expansion wave,

$$\frac{P_3}{P_4} = \left(\frac{T_3}{T_4}\right)^{\frac{\gamma_4}{\gamma_4 - 1}} = \left[1 - \frac{\gamma_4 - 1}{2}\left(\frac{u_3}{a_4}\right)\right]^{\frac{2\gamma_4}{\gamma_4 - 1}}$$

2.3

The contact surface between the driver and the driven gas follows the incident shock and is assumed to be extremely thin with no mixing of driver and driven gas across the contact surface. This assumption can be used to obtain a direct relation between the incident shock Mach number and the initial pressure ratio between the driver and the driven section,

$$\frac{P_4}{P_1} = \frac{\left[\frac{2\gamma_1 M_s^2 - (\gamma_1 - 1)}{\gamma_1 + 1}\right]}{\left[1 - \frac{\gamma_4 - 1}{\gamma_1 + 1} \cdot \frac{a_1}{a_4}\left(M_s - \frac{1}{M_s}\right)\right]^{-\frac{\gamma_4}{\gamma_4 - 1}}}$$

2.4

This relation can be further extended to the ratio of initial temperature in the driven section to the reaction region temperature or the final temperature in the shock tube before the expansion wave quenches the system,

$$\frac{T_5}{T_1} = \frac{[2(\gamma_1 - 1)M_s^2 + (3 - \gamma_1)][(3\gamma_1 - 1)M_s^2 - 2(\gamma_1 - 1)}{(\gamma_1 + 1)^2 M_s^2}$$

2.5

$$\frac{P_5}{P_1} = \left[\frac{2\gamma_1 M_s^2 - (\gamma_1 - 1)}{\gamma_1 + 1}\right]\left[\frac{(3\gamma_1 - 1)M_s^2 - 2(\gamma_1 - 1)}{(\gamma_1 - 1)M_s^2 + 2}\right]$$

2.6

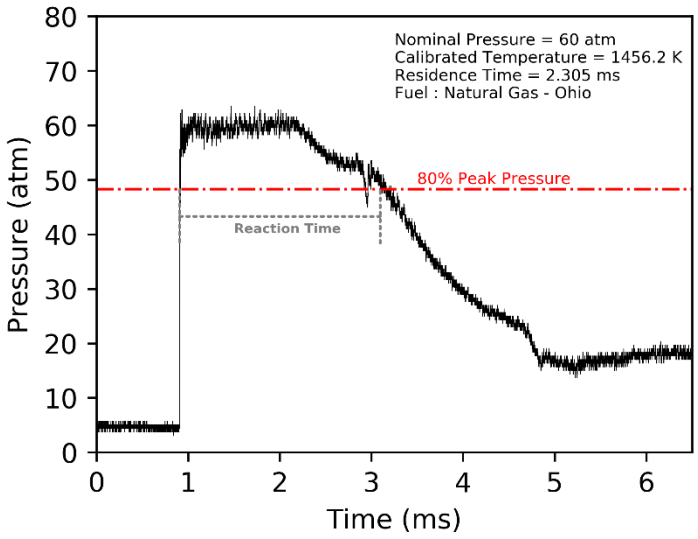

Figure 2: Pressure trace measured in the HPST at the driven section end wall for one of the natural gas experiments, depicting the typical pressure behavior in the HPST during experiments. The reaction time estimate based on the pressure drop to 80% of peak pressure is shown.

In this study the UIC Single Pulse High Pressure Shock Tube (HPST) [43,44] was used which can generate reaction region pressures from 15 atm to 1000 atm over a temperature range of 600 K to 2500 K. The reaction time in the shock tube can be varied from 0.5 ms to 10 ms [44]. The HPST can hold near constant pressure in the reaction region over the reaction time to ensure reaction chemistry is not affected by the pressure irregularities in the shock tube using optimization techniques [44] – Driver Gas Tailoring [44,59,60] and Driver Inserts [44,61]. A typical pressure trace measured at the end wall of the HPST from one of the natural gas experiments is depicted in Figure 2. The HPST uses a pre-scored metallic diaphragm made of soft brass (Grade 260) to separate the driver and the driven region and is shown in Figure 3.

The pressure measurement in the HPST is conducted at seven locations – six on the side wall and one on the driven end wall using 113B23 piezoelectric pressure sensors from PCB Piezoelectronics®. The sensors can measure pressures up to 10,000 psi and have a rise time of

<1µs. The pressure sensor data is acquired using high speed data acquisition cards, MCS Computing DAS 4020/16, controlled using an in-house developed data acquisition software in LabVIEW at a sampling rate up to 4 MHz. The side wall transducers are primarily used for measurement of the shock velocity by measuring the time taken for the pressure pulse to occur at each sensor location and dividing it by the precisely known distances between the pressure sensors. The velocity used to characterize the experiment is calculated by extrapolating the trend of velocities at the side wall transducers to the end wall. The extrapolation of the velocity is carried out to account for the shock wave attenuation. This measured shock velocity can be used to calculate the theoretical temperature in the shock as well as to compare the theoretical calculated pressure with measured pressure using the equations 2.5 and 2.6 respectively.

Figure 3 : Prescored soft brass (grade 260) diaphragms used in the UIC-HPST.

The reaction time in the shock tube is prescribed as the time taken for the peak pressure to drop to its 80% value after arrival of the incident shock at the end wall. Figure 2 illustrates the estimated reaction time for that experiment, marked by the black dotted lines. The time begins when the shock arrives at the end wall, as signaled by the instantaneous pressure rise sensed by the end wall pressure sensor and ends when the pressure drops to the 80% value (~48 atm in Figure 2) of the maximum pressure (~60 atm in Figure 2) which is the point at which the measured

pressure trace intersects the red dot dashed lines. Since the quenching is not instantaneous like the heating from the shock, the reaction time is extended beyond the constant pressure region to account for the gradual freezing of the reactions in the test region. This method of selection of reaction time assumes that reaction chemistry occurring after arrival of the quenching wave and into the tail of the pressure trace is negligible and can be accounted for by increasing the reaction time beyond the observed constant pressure region.

Direct measurement of the temperature at such small time scales is not possible in the absence of optical diagnostics so the temperature in the HPST is evaluated using a chemical thermometer [62–65]. A chemical thermometer is a compound which undergoes unimolecular decomposition under pyrolysis conditions and the rate parameters of the reaction are known. In this study, 1,1,1- trifluoroethane ($C2H_3F_3$) was used as the chemical thermometer whose rate parameters are extensively published in the literature [66–69]. TFE undergoes unimolecular decomposition over the temperature range of 1200 K to 1450 K and can be used to evaluate the temperature in the shock tube in this range and develop the calibration equation that relates the temperature with the measured velocity of the shock. The rate parameters [67] and the reaction for unimolecular decomposition of TFE used in this study are,

$$CH_3CF_3 \rightarrow CH_2CF_2 + HF$$

$$A = 3.33 \times 10^{14} \qquad {}^{-E}/_{R} = 37363$$

Pyrolysis experiments of TFE were conducted at extremely dilute conditions (~200 ppm) in the shock tube at the conditions used for the actual experiments. The shock tube bore and length for calibration experiments matched the set-up used for the actual experiments. The decomposition of TFE resulting from every shock is measured using gas chromatography. The extent of the

reaction which is the difference between the TFE concentration in the test sample and post shock sample, can be directly used to evaluate the average chemical temperature in the shock tube over the reaction time [64]. This evaluated temperature based on the decomposition of the chemical thermometer for every shock, when plotted against the shock velocity, provides the calibration equation which can be used to calculate the calibrated temperature in the shock tube for all experiments by using the measured velocity. Figure 4 shows the calibration results at ~240 atm pressures and the comparison with the temperature calculated using ideal shock tube theory from the measured shock velocity.

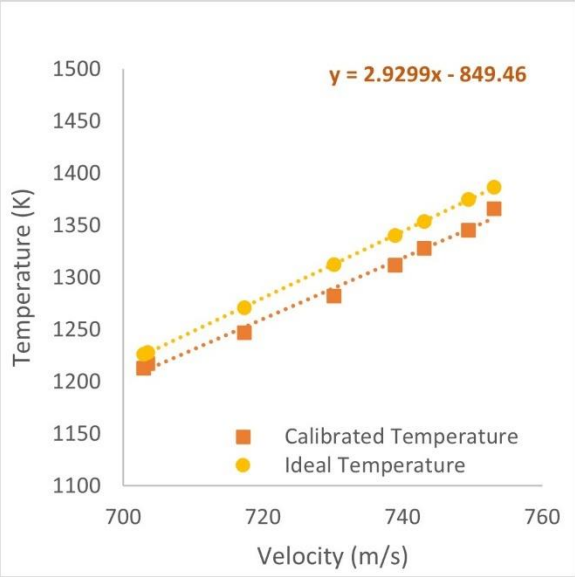

Figure 4 : Temperature calibration in the HPST using 1,1,1 trifluoroethane at a nominal pressure of 240 atm.

2.1.2 Mixture Preparation

The test mixtures used in the shock tube for experiments were highly dilute, consisting of ~1000 ppm of natural gas and 500 – 4000 ppm of oxygen (by mole fraction), dependent on the target equivalence ratio of the mixture in a balance of argon. The argon gas used for preparation of test mixture was obtained from Linde Gas with a purity of 99.999%. The mixtures were prepared in a 40 liter heated stainless steel tank using the method of partial pressures to control the mixture

composition using an in-house mixing rig. The total tank pressure of the mixtures prepared for ~ 60 atm experiments was kept at around 40 atm, whereas two tanks with a total pressure of 70 atm were required for each experiment set at nominal pressure of ~240 atm. The mixture composition for both the tanks used for a single experiment set was maintained closely. The difference between the composition of the two mixtures prepared was within one percent. The difference in composition between tanks, measured by gas chromatography was used to adjust the reported experimental data. The species measurements from the experiment using the second mixture were proportionally scaled up or down based on the difference between the two mixture such that the initial composition of the second mixture after adjustments would match the first mixture.

The mixing rig uses all stainless steel fittings and valves and is maintained at a temperature of 150°C to prevent condensation of fuel on the walls of the tubing and fittings. However, in this study the fuels analyzed were gas phase and were immune to condensation within the mixing rig during mixture preparation and storage in the mixture tank. The mixing rig consists of two sections, the low pressure section, used to vacuum the system and the mixture tank as well as to introduce the fuel and the oxidizer into the tank with precise pressure measurement and the high pressure section used to backfill the mixture tank with the bath gas – argon. The mixing rig and the mixture tank were evacuated using an Edwards RV8 rotary vane type vacuum pump to a pressure below 0.001 torr. The pressure in the low pressure section of the mixing rig was measured using high accuracy 631D series heated capacitance manometers from MKS Instruments. The evacuated mixture tank was first filled with the fuel (natural gas) until the pressure of the tank reached the target pressure required to obtain the desired concentration of the fuel in the test mixture (1000 ppm) and then oxygen was introduced into the tank until the pressure rose to a value such that the increase in pressure corresponds to the target pressure necessary to obtain the desired concentration

of oxidizer in test mixture. Then the tank was filled with 99.999% purity argon using the high pressure section until the target total tank pressure was reached. These prepared mixtures were allowed to sit overnight to homogenize. The prepared mixtures were analyzed using gas chromatography the next day to confirm the actual composition of the tank. The actual compositions are reported in the experimental data.

2.1.3 Analytical Method

The analysis of the post shock sample of the test gas is conducted using gas chromatography. Gas chromatography allows the separation of the different species present in the test gas, which are then sequentially passed to a detector for identification and quantification of the separated species. The test sample gas passes through a capillary chromatographic column which is a fine glass capillary tube with a stationary phase inside it. The test sample serves as the mobile phase that passes through the column. The stationary phase is responsible for separation because it provides different levels of resistance to the motion of different molecules in the test sample. The difference in the resistance changes the speed at which different molecules move within the column and hence changes the time each molecule takes to exit the column resulting in the separation of the different species within the test sample. There is a constant flow of low molecular weight gas through the column called the carrier gas which facilitates the movement of mobile phase through the columns and onto the detector.

Gas chromatographs can operate with a variety of detectors each of them specializing in detection and/or quantification of the species. The selection of the detector depends on the species of interest in the test sample and the chemical composition of these species. In addition to this the desired analytical accuracy of the quantification and the levels at which the species need to be measured influences the detector choices. Some detectors like the mass selective detector (MSD)

and the thermal conductivity detector (TCD) are considered universal detectors capable of analyzing a wide variety of compounds, however, they have limited accuracy and detection levels over a large variety of species. In addition, the MSD can identify unknown compounds and is often used only for identification of species in the test samples and the preliminary tests to assist in determining the suitable detector for quantification. Among several detectors available, the most suitable detector for hydrocarbon analysis is the flame ionization detector (FID) which responds to C-H bonds making it extremely sensitive towards hydrocarbons. The FID has an exceptionally good detection limit as well as detection accuracy for hydrocarbons and can easily detect hydrocarbons at ppm levels. The FID can also count the carbon atoms in a species because it responds linearly to the number of carbons in the molecule [70].

In this study, the test samples from the shock tube after every experiment are transferred to the GC directly using an online sampling [71,72] system designed in the lab and improved over the years. The sampling system is separated from the shock tube through a valve, referred to as the sampling valve, so that the delicate components of the gas chromatographs are not exposed to high pressures in the shock tube. After the sample has quenched in the shock tube (~ 200 ms after start of the experiment) the valve is opened (for 0.1 - 0.3 ms) to introduce the sample into the sampling system. The sample is first expanded in a 150cc stainless steel vessel to a lower pressure and then passed to the sampling loops connected to the GC valves. The GC headspace valves are connected to the columns and opening them injects the sample from the sampling loop into the columns where the sample is separated and exits at the detector for identification and/or quantification.

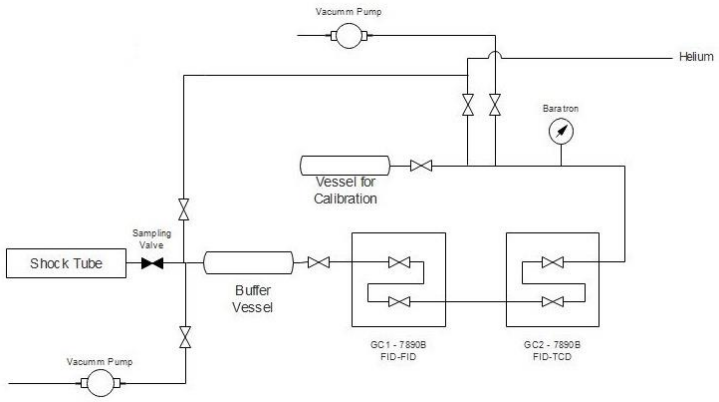

Figure 5 : Schematics of the sampling system used to extract test samples from the shock tube and analyze them using gas chromatography.

The complete sampling system and the GC valves are maintained at a temperature of 150°C and all the components are made of stainless steel and Silconert® coated to ensure no species are absorbed, adsorbed, or condensed within the sampling system. The sampling system is maintained at vacuum using Edwards RV3 vacuum pump and helium is supplied to the sampling line for flushing the sample between runs. The pressure in the sampling system is measured using the 631D series capacitance manometers from MKS Instruments with a measuring range of up to 1000 torr and accuracy of 0.5% of the reading. The pressure measurement is used for calibration of the gas chromatographs for quantifications and to normalize the GC measurements between experiments. The schematics of the sampling system are provided in Figure 5.

Two Agilent Technologies 7890B gas chromatographs are connected in series. Schematics of the set up are shown in Figure 5. One of the GC is equipped with two FIDs, whereas the other one is equipped with one FID and one TCD. In addition to the detectors the second GC has a Ni-Cat tube (methanizer) which allows accurate detection of the non-hydrocarbon species like CO and CO_2 using the FID by converting these compounds into hydrocarbons, mostly methane. The sample from the shock tube passing through the sampling system is stored in sample loops connected to the GC valves. When the valves are operated only the sample volume in the sample

loops is injected into the columns for analysis. The sampling loops have an accurately measured volume and the mass of the sample injected depends on the pressure in the loop. The target pressure in the sampling system/loop is ~16 psi, just over atmospheric pressure, to avoid contamination of the sample from uncontrollable leakage sources. However, the pressure slightly varies between the experiemnts and the measured detector response is normalized by the injection pressure for every experiment to eliminate the effect of this variation on the analysis. In this study the sample loops for all the FIDs had a volume of 100 µL and that for the TCD was 1 mL.

This study used only three out of the four available detectors with different capillary columns connected to each detector. The first detector was an FID fed by the Agilent Technologies GC-GasPro column which is capable of separating hydrocarbon right from C_1 to C_{14} and can successfully separate some key isomers like allene and propyne. In addition to purely hydrocarbon species, it can separate some oxygenated hydrocarbon species as well. However, the stationary phase can absorb water and degrades quickly when sample contains large amounts of water. The water absorption can be evident in shifting of retention times of the various compounds. The column can be regenerated to release the water by reconditioning. However frequent cycles of reconditioning can result in wearing out of stationary phase and column bleed. Column reconditioning was carried out prior to the start of a new experimental set. This column and detector were primarily used to detect and quantify purely hydrocarbon species and primary components of the fuel (CH_4, C_2H_6 and C_3H_8) and the retention time shifts from the water adsorption were negligible within the experiment set. The second detector used was also an FID connected to a capillary porous open tubular (PLOT) column, HP-Plot U, which is capable of the separation of hydrocarbons from C_1 – C_7 and oxygenated hydrocarbons like alcohols and aldehydes. This is a polar column and unlike GC-GasPro, it is not susceptible to damage by water.

This column was used to separate and detect CO and CO_2 and to use as feedback to check the measurements using the other FID. This column was also chosen so that the occurrence of any other oxygenated species could be detected. The third detector was a TCD, which was used to primarily detect permanent gases like O_2 and H_2 in the test sample and to check if the test sample is contaminated with the helium driver gas. This detector was connected to a molecular sieve type Supelco® Carboxen 1010 column which can separate the permanent gases quickly and is not susceptible to performance degradation resulting from the clogging of the sieve by large molecules like CO_2, like HP-Molsiv columns are. The details of the GC method used is provide in the Appendix D.

In the absence of an MSD, the identification of the compounds is not possible. The retention order of the species remains fixed for all the columns. The information about the order in which species elute from the column from publicly available literature, manufacturer documents and internal lab communications was used to identify the species during detector response calibration. Calibration gas samples with known quantities of species of interests are used to calibrate the detector response and since the composition is known and the information on order of elution is available the peaks can be identified. The detector response is calibrated per ppm of the species in the same exercise which can then be applied to analysis of unknown quantities of all the species from the shock tube experiments. The calibration gases used have an uncertainty of ± 2% and the other sources of uncertainty in the system arise from the injection pressure measurement and the errors in integration of the area under the peak for every species when done manually. The integration is conducted using the auto integrate function of the data acquisition software to eliminate manual errors in integration. The sample volume is kept constant by the sample loops but the pressure in the sampling system cannot be kept constant from experiment to

experiment which can affect the test sample concentration. The measured pressure is used to normalize the detector response for each run to avoid the concentration variation resulting from sampling system pressure differences between experiments. The pressure in the manifold is measured with an accuracy of ± 0.5% of the reading. . The calibration procedure is conducted using the same system as that is used during the experiments, which would account for all random sources of error within this calibration factor. Overall uncertainty in the GC measurements can only be attributed to the uncertainty of the calibration gas, which is ±2%. This uncertainty is however higher for permanent gases which are detected using the TCD because of detection limits of the detector as well as the higher uncertainty in the mixture, of ±5%. The details of the calibration for this study are provided in Appendix C.

2.2 Chemical Kinetic Modeling

Chemical kinetic modeling is used to predict the behavior of a reactive chemical system. Chemical kinetics uses reaction rate parameters of elementary reactions to determine the fate of different chemical species when external energy is supplied to the system, usually in the form of temperature, pressure, or both. The reaction rate parameters for these elementary reactions reflect the energy consumed (or generated) to surmount the activation energy barriers at different thermodynamic conditions. In addition to the rate parameters which are expressed in an Arrhenius form ($k = A\, e^{\frac{-E_a}{RT}}$), chemical reaction pathways are used to decide the probability of reactions that would occur. Elementary reactions and their associated rate parameters make up a chemical kinetic mechanism that can define the chemical behavior of the system. Several chemical kinetic mechanisms have been developed over decades that either target a specific chemical system [15,16,18,27] or provide a generic chemical kinetic mechanism [4,73–77] that can be applied to a

wide variety of systems. In general, these chemical kinetic mechanisms have a hierarchical structure.

Chemical kinetic modeling of transient systems in devices like shock tube, flow reactors, burners and rapid compression machines requires the use of reactor models which can define and modify the thermodynamic parameters of the system that are responsible for activating the chemical system and eventually quenching them. The chemical kinetic mechanism provides the information about the changes in the chemical system because of the change in the thermodynamic parameters from the reactor model. Together they provide the complete description of the chemical reactivity of the system. In shock tube studies, chemical kinetic modeling is conducted using a 0-D homogeneous reactor. The 0-D homogeneous reactor only progresses in time and does not account for spatial changes since the gas is assumed to be in steady state in the shock tube over the reaction time and it is a closed system.

In this study Cantera [78] was used to carry out chemical kinetic modeling of the ~60 atm shock tube experiments using the 0-D homogenous constant pressure reactor model. This model assumes that the pressure in the shock tube remains constant for the duration of the reaction time and then instantaneously drops to zero, quenching the reaction. The same is true for the temperature in this system. This approach has been proven by previous studies [26,29,33,63] to provide good representation of the reaction conditions in the shock tube and the selection of the reaction time in the shock tube by using the 80% pressure drop rule as previously explained accounts for any additional chemical reactions occurring during the quenching time. The calibrated temperature evaluation also assumes a similar conditions and thus provides an average temperature in the reaction region that is effective for the chemical system to progress.

However, the constant pressure approach is often questioned, especially when the shock tube behavior deviates from ideal conditions resulting in appreciable pressure variations over the reaction times. In addition, when systems being studied are dominated by reactions requiring lower activation energy to progress, there can be significant reaction occurring over the quenching period and can be missed if constant pressure approach is used. To address this possibility, a changing pressure approach [30,63] was used for the ~240 atm experimental sets where the thermodynamic conditions of the reactor model were continuously altered using the measured pressure trace from the shock tube. The custom ODE solver within Cantera was used to implement this changing pressure on the reaction kinetics which replaces the constant pressure reactor model previously used. The energy equation implementation within the reactor model solves for the temperature change resulting from the pressure change and uses it to adjust the chemical kinetic calculations. This method provides a much better representation of the actual thermodynamic changes in the shock tube at the cost of larger computation demands and the need to supply data about the experimental measurement of pressure. The results in past studies [63] have shown that there are minimal benefits of using this approach. In this study it was observed that in some cases this method provides significant improvement in the match between experiments and predictions from some of the chemical kinetic mechanisms studied. While the improvements were evident, the predictions from constant pressure approach were mostly within the error region of the experimental data. Thus, use of this method is beneficial only if extremely accurate predictions are required, or an unexpected behavior needs to be diagnosed.

Table IV : Details of the chemical kinetic mechanism used in this study.

Mechanism	**Organization**	**Species**	**Reaction**
CRECK-C1-C3-HT (1412) [73,74]	*Politecnico de Milano, Milan-Italy*	109	1999
ARAMCO 3.0 [4]	*National University of Ireland Galway, Galway - Ireland*	578	3037

San Diego Mechanism (2016-12-14) [79]	*University of California San Diego, San Diego-USA*	58	270
USC Mechanism 2.0 [76]	*University of Southern California, Los Angeles-USA*	111	784

In this study, four different chemical kinetic models were chosen for chemical kinetic modeling and the predictions were compared to the experimental results to judge the capability of these mechanisms to predict the oxidation of natural gas and adjust for compositional variations. The details of the various chemical kinetic mechanism chosen for this study are listed in Table IV. The initial conditions – pressure, temperature and reaction time used for the modeling all the experiments are the exact values measured or evaluated for each experiment and not the nominal conditions for the experiment sets. This approach allows accounting for the minor variations that can occur in experimental species measurements from the changes in the experiment parameters from experiment to experiment.

2.3 Effect of Equivalence Ratio on Oxidation of Natural Gas

2.3.1 Experiments

The experiments to test the effect of equivalence ratio on the oxidation of natural gas was studied using the reference natural gas sample. Seven sets of experiments were conducted of which six were at different equivalence ratios ranging from fuel lean ($\varphi \sim 0.5$) to fuel rich ($\varphi \sim 3.0$) the seventh experimental set was a pyrolysis experiment. The observations are not surprising in terms of fuel consumption since the temperature required for the start of fuel consumption reduces with reduction in equivalence ratio or increase in the oxygen in the system as evident in Figure 6.

However, if the individual fuel species are considered, there are some unexpected observations. Ethane concentration in the test sample for lean and stoichiometric conditions begins to rise at the start of fuel consumption (1100 – 1300 K) before eventually getting consumed like

the rest of the fuel. Over the temperature range at which the ethane concentration rises, methane starts to slowly decompose. This dissociation of methane over 1100 – 1300 K temperature range could be because of the H atom abstraction from methane which is facilitated by an abundance of oxygen (compared to stoichiometric requirements) in the fuel lean mixtures resulting in formation of CH_3 radicals. These CH_3 radicals would recombine to form ethane which can increase the ethane concentration in the system. However, H abstraction from ethane is also possible over this temperature range which would result in the dissociation of ethane into C_2H_5 radical. However, the rate at which this dissociation progresses over 1100 – 1350 K temperature range may be lower than the rate at which CH_3 recombination occurs hence resulting in the net increase in ethane concentration. At fuel rich conditions, the H abstraction from methane is significantly slower resulting in a smaller pool of CH_3 radicals available for the recombination reaction forming C_2H_6 and hence at the fuel rich conditions there is no evident rise in the ethane concentration before the dissociation.

The formation of CO and CO_2 are critical to the oxidation studies since these reaction in non-dilute conditions result in heat release. Thus, it can be assumed that the maximum heat release for an oxidation system occurs between temperatures at which CO_2 formation starts and at which the CO_2 plateaus. It can be seen from Figure 6 that the CO_2 formation starts at a lower temperature for the leaner mixtures suggesting that the temperature range over which the system is highly active shifts towards the lower temperatures compared to the stoichiometric conditions. At the fuel rich conditions, however, CO_2 formation is extremely low and instead only CO is formed since sufficient oxygen is not available for the conversion of CO to CO_2. Like CO, the formation of C_2H_2 is evident at the rich conditions since the overall temperature range over which the system is active

is high resulting in the formation of C_2H_2. The lack of oxygen in the system impedes its conversion to CO and CO_2.

Ethylene is another key species that has been focus of several chemical kinetic studies since it is assumed to be related to the ignition delay time of a fuel [27]. Accurate understanding of C_2H_4 formation and consumption can provide insight into the ignition behavior of the fuels. The ethylene peak at different equivalence ratios occurs at different temperatures which increase with the increase in fuel richness which suggests an increase in ignition delay times for fuel rich conditions. This observation goes hand in hand with the fact that consumption of fuel is slower at fuel rich conditions.

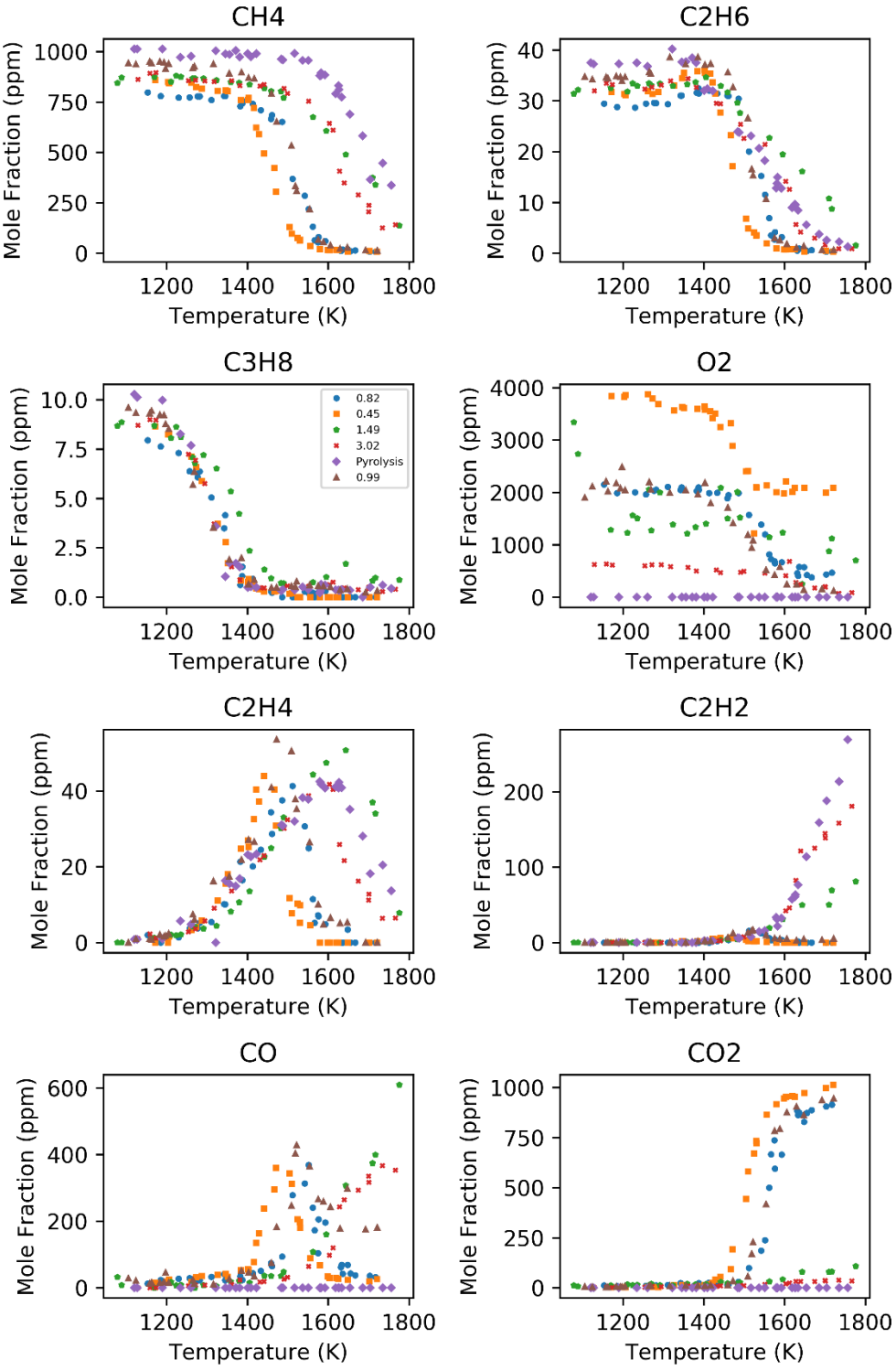

Figure 6 : Experimental speciation data for reference natural gas oxidation at different equivalence ratios.

2.3.2 Modeling

The experimental results for all the seven experiments were compared to the species concentration predicted at the end of the reaction time by the four models previously described using the constant pressure approach. The thermodynamic conditions used as input match the measured values for each experiment. The model predictions were significantly off for the CRECK and the San Diego mechanism whereas ARAMCO 3.0 performed better at the lean conditions and the USC Mech 2 performed better for the rich experiments. The comparisons with speciation are shown in Figure 7 to Figure 12.

The predictions from all models showed a particularly good agreement in the experiments at stoichiometric condition ($\varphi \sim 1.0$) and at very fuel rich conditions ($\varphi \sim 3.02$). The predictions match perfectly at the pyrolysis conditions, with the exception of C_2H_4 which is overpredicted by USC Mech 2 and ARAMCO 3.0, and underpredicted by the CRECK and the San Diego mechanism. In the experiment at the stoichiometric conditions, CRECK showed a good match for C_2H_4 but overpredicted C_2H_2 by about three times.

The models have significant differences from experimental results at the fuel lean conditions, as evident in Figure 7. The models predict complete fuel consumption at temperatures ranging from 1450 K – 1500 K whereas the experiment shows complete fuel consumption occurring at about 1600 K. Similar differences were observed for the experiment at ($\varphi \sim 0.8$) shown in Figure 8. Furthermore, there is a significant difference among predictions from different models for the fuel lean conditions which is not present for the fuel-rich and the stoichiometric conditions. This difference suggests different dominant reaction pathways for different models at different stoichiometries.

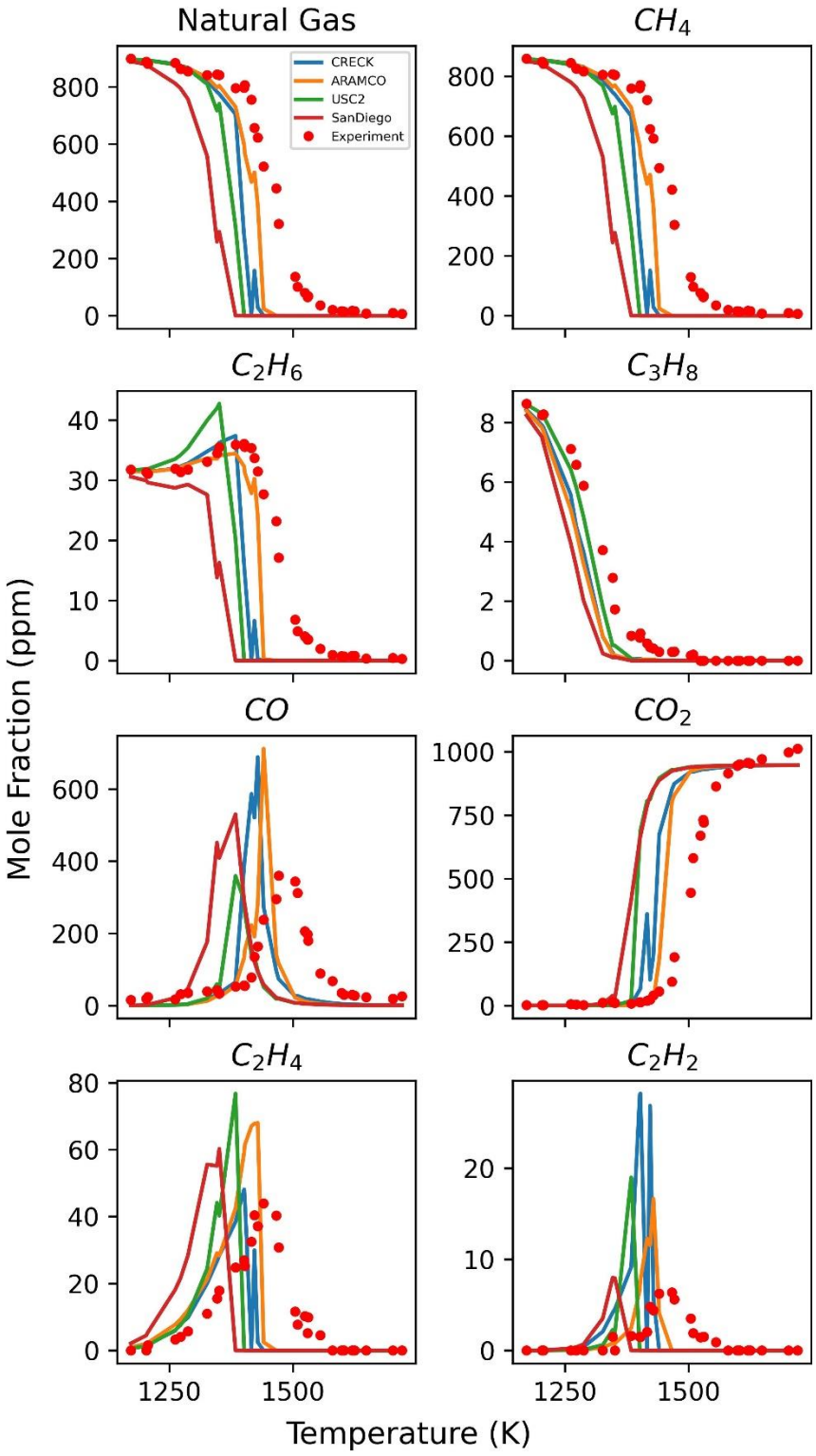

Figure 7 : Natural Gas Reference Fuel at φ=0.49 - Experimental species profiles (red circles) of Natural Gas, CH4, C2H6, C3H8, CO, CO2, C2H4 and C2H2 compared with predictions using ARAMCO 3.0 (orange), CRECK (blue), San Diego Mechanism (red) and USC Mech 2 (green).

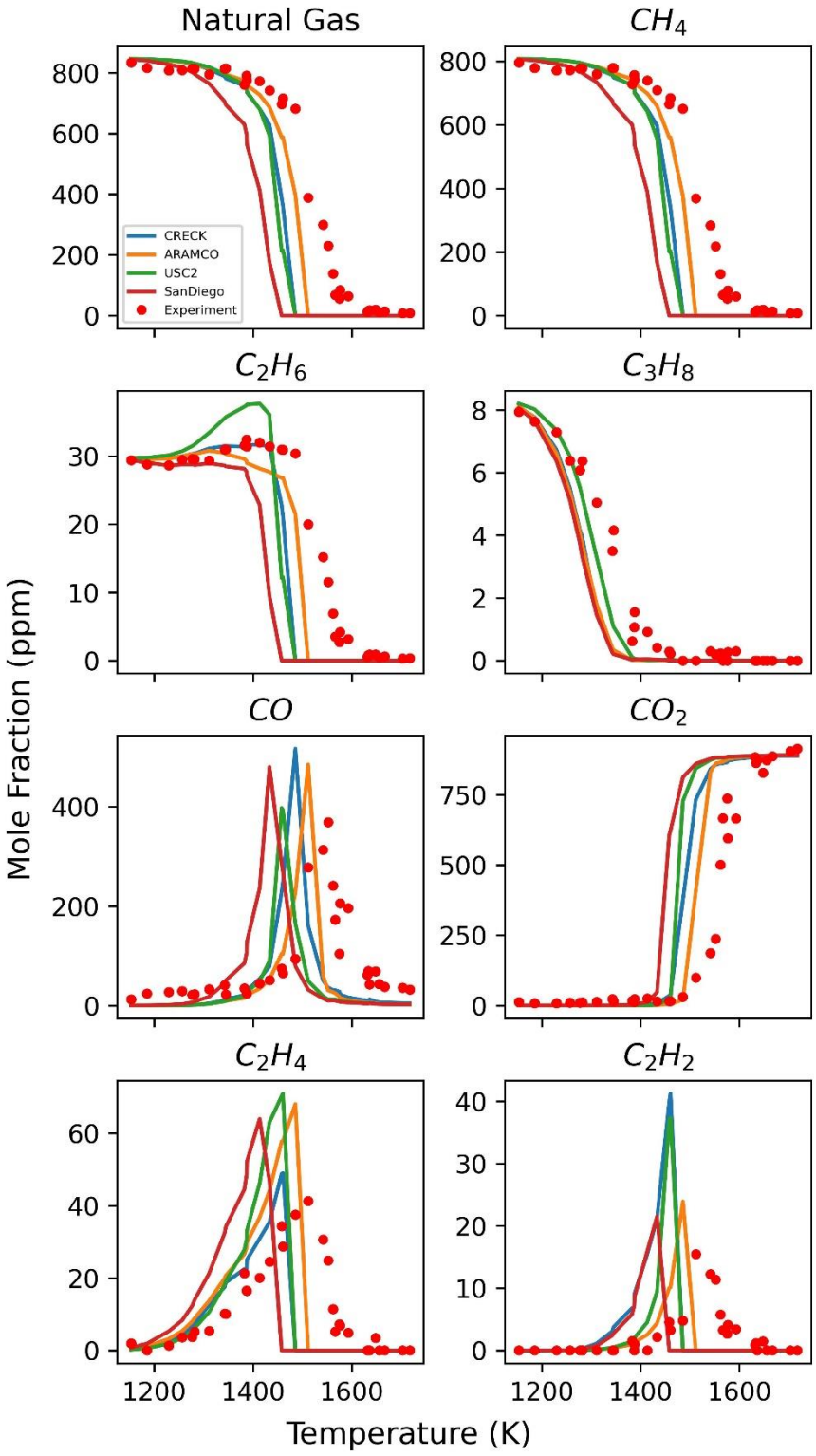

Figure 8 : Natural Gas Reference Fuel at φ = 0.80 - Experimental species profiles (red circles) of Natural Gas, CH4, C2H6, C3H8, CO, CO2, C2H4 and C2H2 compared with predictions using ARAMCO 3.0 (orange), CRECK (blue), San Diego Mechanism (red) and USC Mech 2 (green)

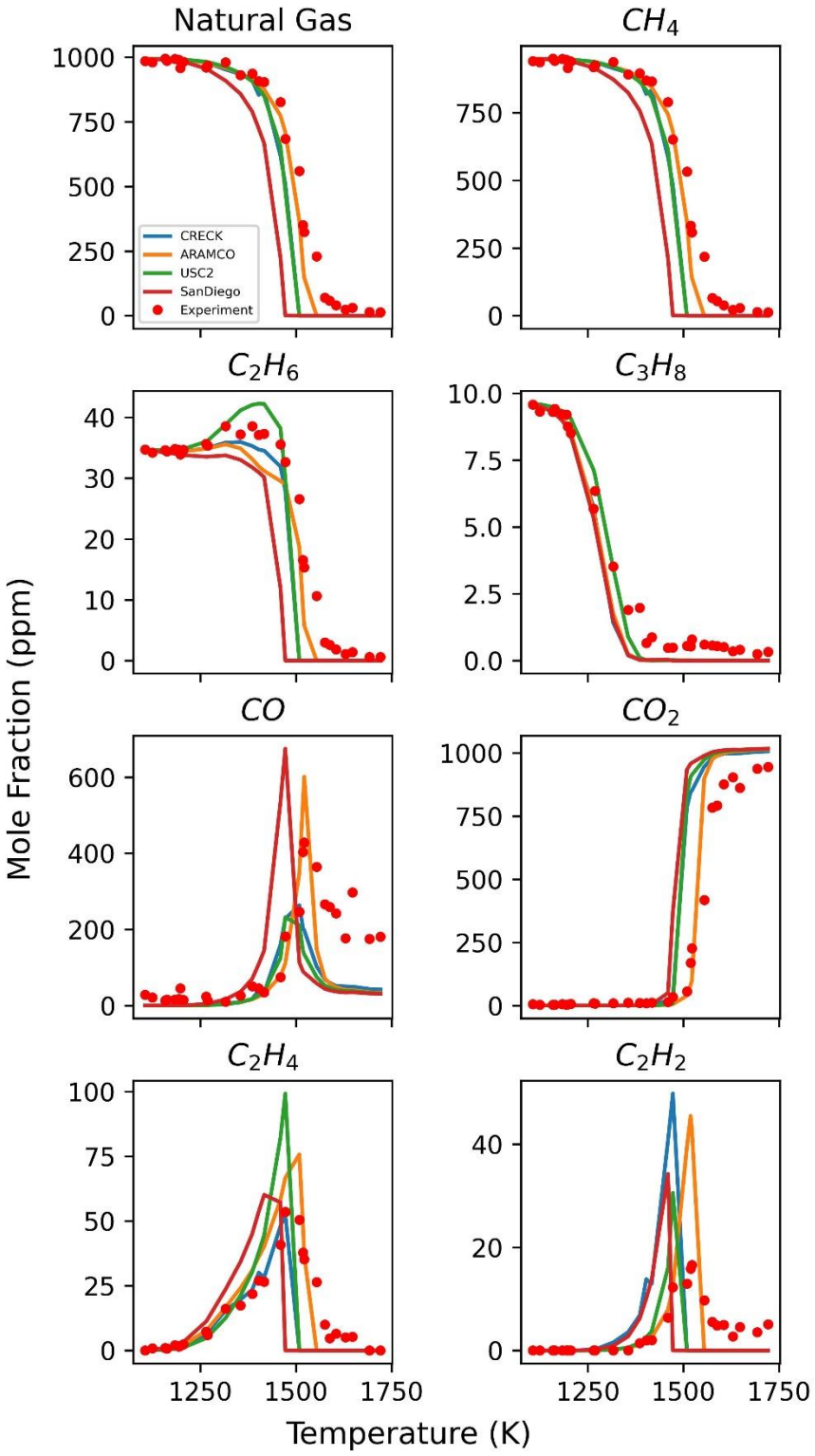

Figure 9: Natural Gas Reference Fuel at φ=0.99 - Experimental species profiles (red circles) of Natural Gas, CH4, C2H6, C3H8, CO, CO2, C2H4 and C2H2 compared with predictions using ARAMCO 3.0 (orange), CRECK (blue), San Diego Mechanism (red) and USC Mech 2 (green).

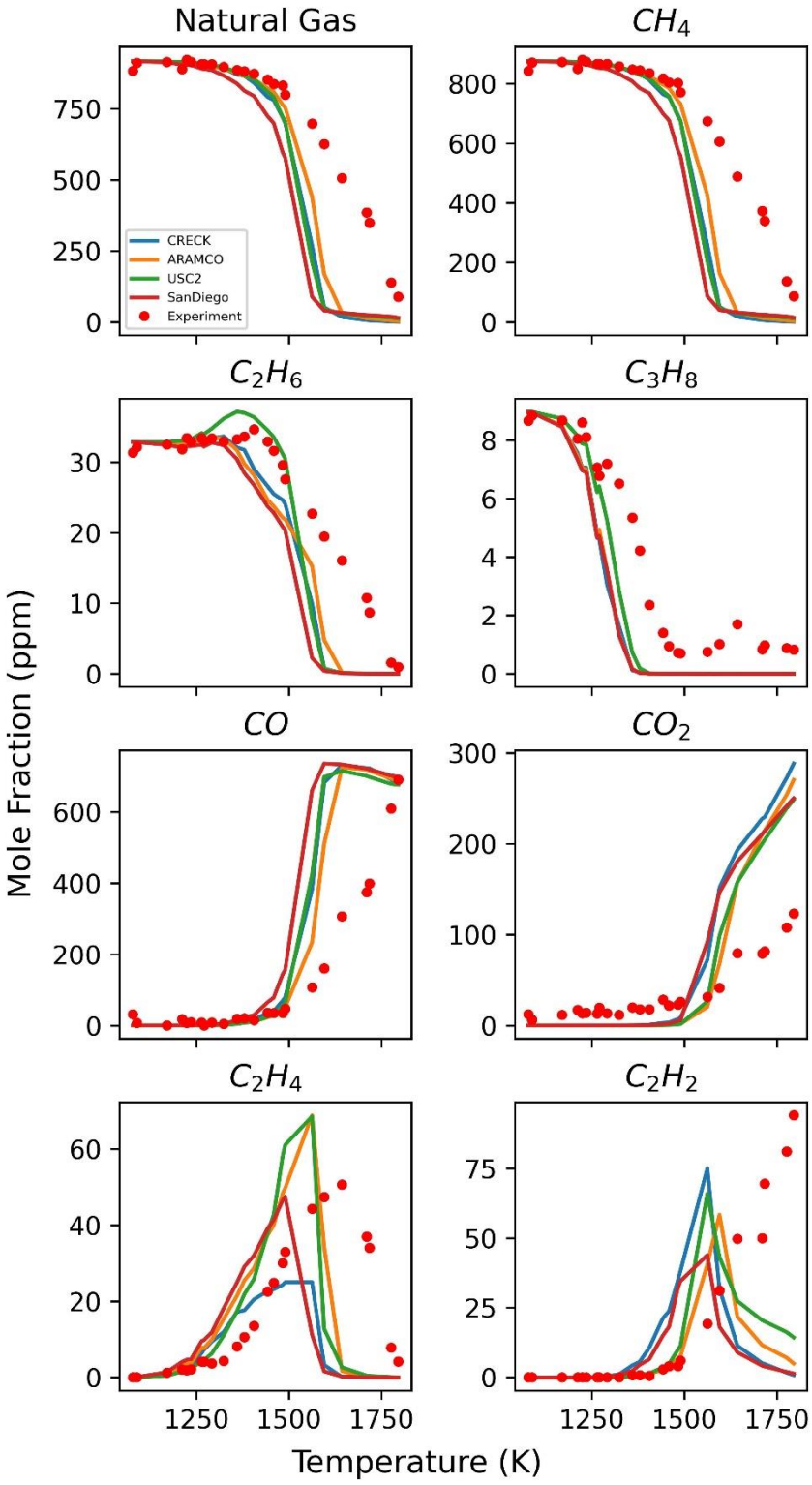

Figure 10 : Natural Gas Reference Fuel at φ=1.49 - Experimental species profiles (red circles) of Natural Gas, CH4, C2H6, C3H8, CO, CO2, C2H4 and C2H2 compared with predictions using ARAMCO 3.0 (orange), CRECK (blue), San Diego Mechanism (red) and USC Mech 2 (green).

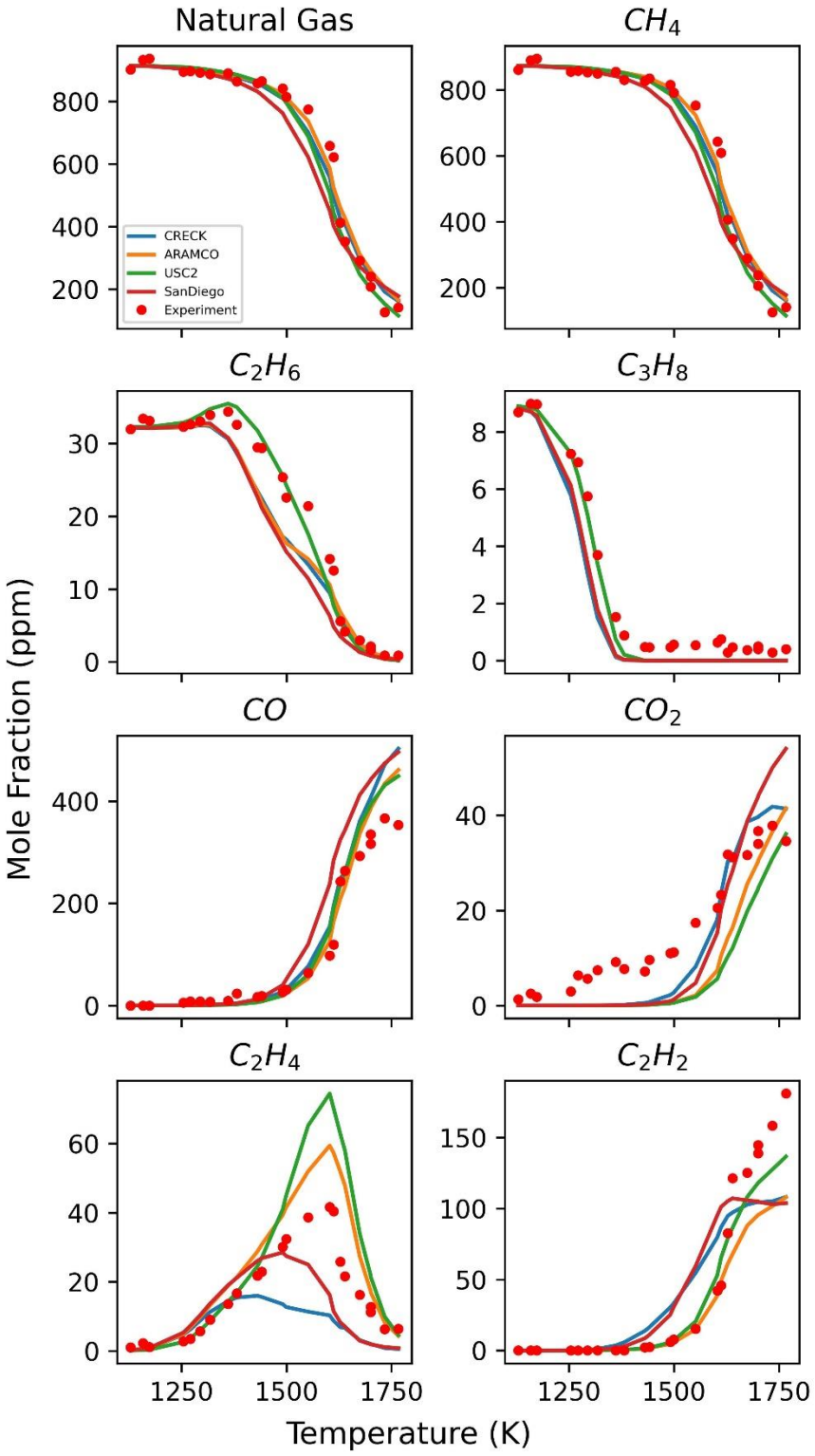

Figure 11 : Natural Gas Reference Fuel at φ=3.09 - Experimental species profiles (red circles) of Natural Gas, CH4, C2H6, C3H8, CO, CO2, C2H4 and C2H2 compared with predictions using ARAMCO 3.0 (orange), CRECK (blue), San Diego Mechanism (red) and USC Mech 2 (green).

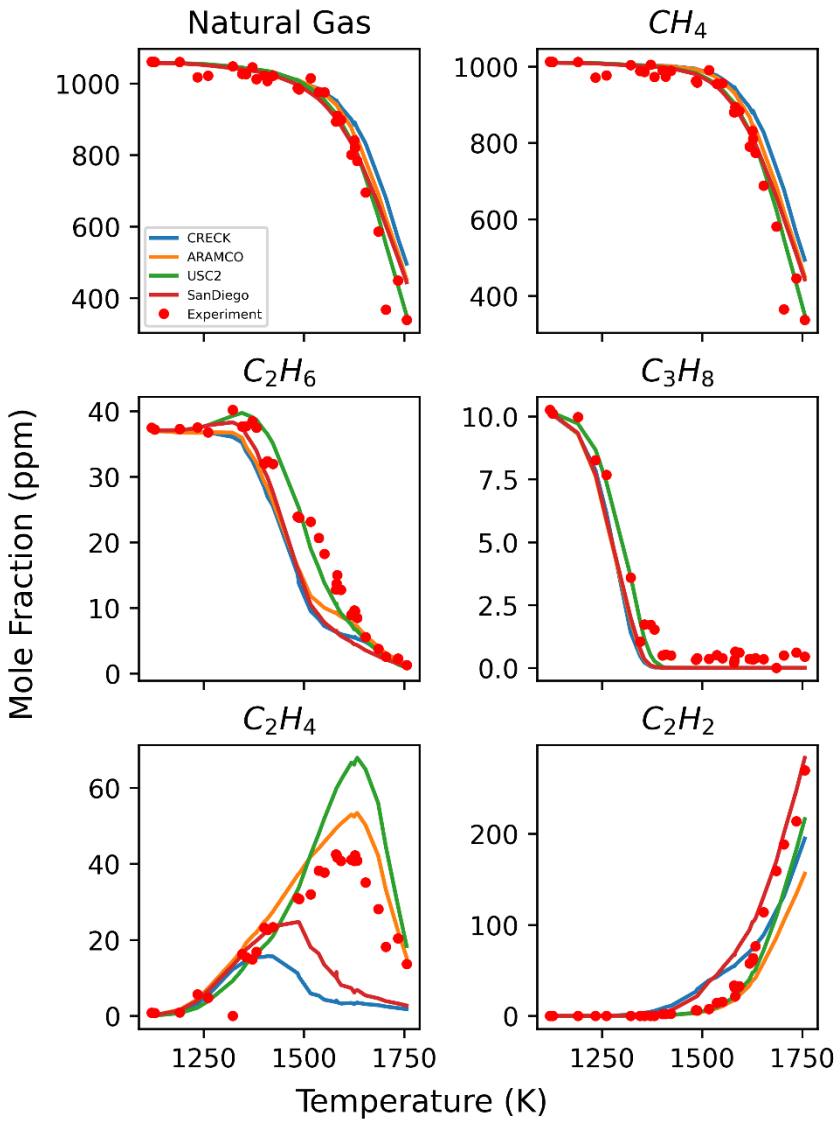

Figure 12 : Natural Gas Reference Fuel pyrolysis - Experimental species profiles (red circles) of Natural Gas, CH4, C2H6, C3H8, CO, CO2, C2H4 and C2H2 compared with predictions using ARAMCO 3.0 (orange), CRECK (blue), San Diego Mechanism (red) and USC Mech 2 (green).

The experimental data at φ ~1.49 have shown the worst match of all, not only with other experimental data but also among the models, especially in the C_2H_4 predictions. All the sources of errors in experiments were checked and none of them were found to be the contributing factors to this behavior which confirms that this behavior is not an experimental artifact. This raises

questions about the equivalence ratio being a critical condition for this fuel and thus the fuel is showing an unusual behavior. Detailed experimental studies at and around $\varphi \sim 1.49$ are needed to examine this hypothesis. The model-based sensitivity analysis and rates of production analysis may throw some light on cause of this behavior. It is evident from the comparisons in Figure 14 that the model predictions, particularly from USC Mech 2 match very well until about 1300 K after which the difference between the experiments and the model predictions keeps on increasing. This variation for this set of experiments is not just limited to the mole fraction predictions but also to the overall profile of the species.

Ethylene has been long suggested to be an important intermediate species during the pyrolysis of a fuel [15,16,27] and an accurate prediction of C_2H_4 yield is necessary for good predictions of the key fuel properties like ignition delay, laminar flame speeds and flame-extinction. The models tested in this study show a large difference in the prediction of C_2H_4 not just in terms of mole fractions but also in the temperature at which the peak concentrations are achieved. The C_2H_4 predictions from different models showed the highest variance of all the other species predicted. Even within a generous error region of the temperature and the mole fraction, the model predictions of C_2H_4 did not agree well with the experimental results. This mismatch was particularly evident even in the pyrolysis experiment (Figure 12) where all the other species predictions showed a very good match with the experimental results except for C_2H_4 whose peak temperature is well captured by USC Mech 2 and ARAMCO 3.0 but whose concentration is overpredicted by about 10 ppm and 25 ppm, respectively. CRECK and San Diego Mech significantly underpredicted C_2H_4 for the pyrolysis experiments. Optimization of the models using a vast data set from experiments over a wide set of conditions - pressure, stoichiometry and composition will be beneficial for overcoming these mismatches.

The capability of models to predict the species was especially tested when predicting the sudden rise in the mole fraction of C_2H_6 over the temperatures range of approximately 1350 — 1500 K. It was previously pointed out that the species profile of ethane shows a peculiar behavior under some of the tested conditions ($\varphi < 1.0$) for the reference natural gas sample. This behavior was not well predicted by any of the models as evident in Figure 7 - Figure 12. While the CRECK model overpredicted this behavior, all other models underpredicted the ethane profile. This significant variation in the prediction of ethane could be one of the reasons for the significant deviation in the prediction of other C_2 species by all the models as discussed above.

Rate of progress (ROP) analysis was performed for all the experiments using the three best models – USC Mech 2, ARMACO 3.0 and CRECK to further investigate the reason behind the significant difference between the model predictions and the experiments as well as among the models. The rate of progress analysis provides the reaction rates of the top 10 reactions in the system at the specified conditions. The rate of progress analysis was conducted at the temperature at which the fuel decomposition is at 50% of the initial value and at halfway through the reaction time. The rate of progress of the top 10 reactions from all the models have been compared in Figure 12 - Figure 17, to observe if the same reactions are included in the top 10 reactions based on their reaction rates at the specified condition. The top 10 reactions with highest reaction rate are different for different models, making it evident that all mechanisms follow different reaction pathways as well as use different reaction rate parameters.

For the leanest experiment set with $\varphi \sim 0.49$, the key reactions for CRECK and USC Mech2 that show significant progress at the analysis conditions are significantly different from that for ARAMCO 3.0 as evident in Figure 13. In fact, ARAMCO 3.0 shows little activity in the top 10 active reactions at these conditions. The reactions responsible for the conversion of C_2H_4 to C_2H_3

radical and H_2O by OH and the conversion of HCHO to HCO radical and H_2O by OH are the common key reactions between the models. However, the rate of progress for these reactions is extremely low for ARAMCO 3.0. The CRECK and USC Mech2 have rate of progress for these reaction similar to each other. However, in the case of $\varphi \sim 0.8$, shown in Figure 14 the most dominating reactions across all the three models are completely different with the breakdown of HCO to form CO being the most active in USC Mech 2.

The most important reactions for therich condition are same for the three models, however with different rates. The reactions are the same for experiments at both rich conditions $\varphi \sim 1.49$ and $\varphi \sim 3.09$ as evident in Figure 16 and Figure 17 respectively. However, it is worth noting that the model prediction of the fuel level at the end of reaction at lean conditions was zero, suggesting the fuel was completely consumed at the temperature where experimentally 50% of the fuel was remaining. Since the active reactions even at 50% of the reaction time show only minor activity, it is evident that in an abundance of oxygen, the models predict fuel consumption occurring over a short temperature range whereas experiments prove otherwise. The reaction mechanisms as well as the reaction pathways for these models needs to be optimized particularly at the lower temperatures where the oxygenated chemistry is highly active.

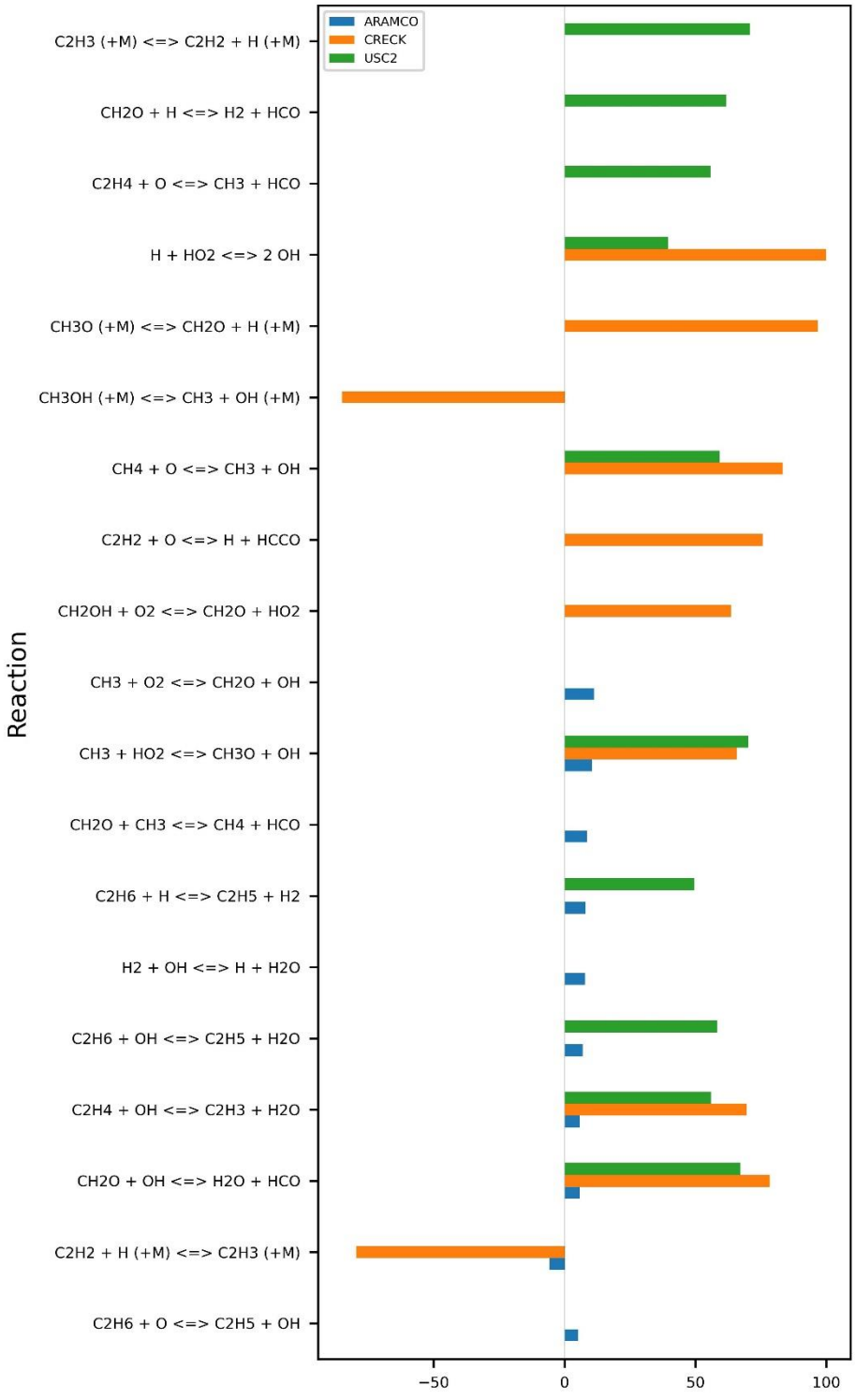

Figure 13: Rate of Progress for key reactions from three models – ARAMCO 3.0 (blue), CRECK (orange) and USC Mech 2 (blue) for the natural gas experiments at φ ~ 0.49. The analysis was conducted midway through the reaction time and at 1466 K where experimentally the fuel drops to half of its initial value. x-axis : net rate of progress in kmol/m₃/s

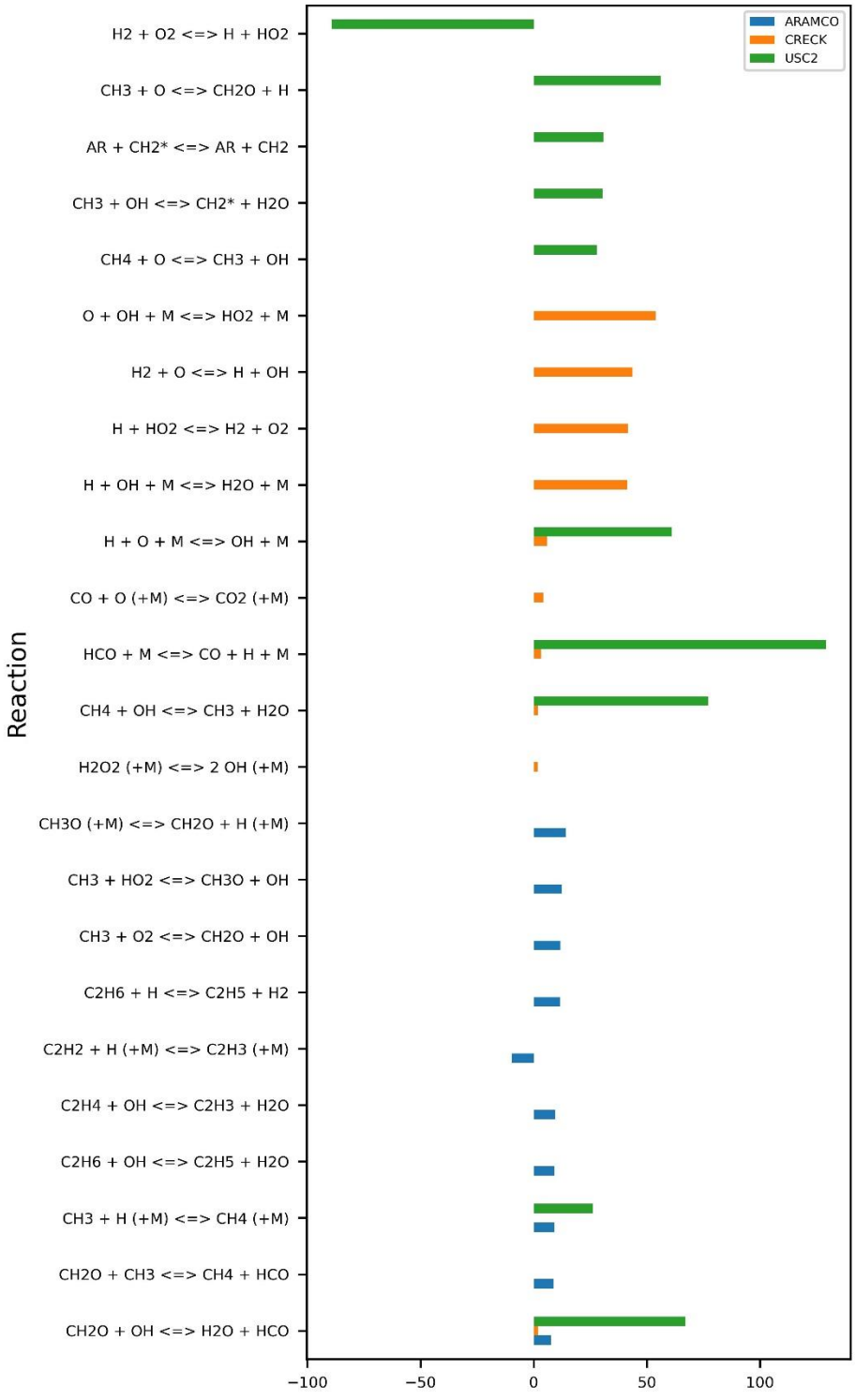

Figure 14 : Rate of Progress for key reactions from three models – ARAMCO 3.0 (blue), CRECK (orange) and USC Mech 2 (blue) for the natural gas experiments at φ ~ 0.80. The analysis was conducted midway through the reaction time and at 1511 K where experimentally the fuel drops to half of its initial value. x-axis : net rate of progress in kmol/m₃/s.

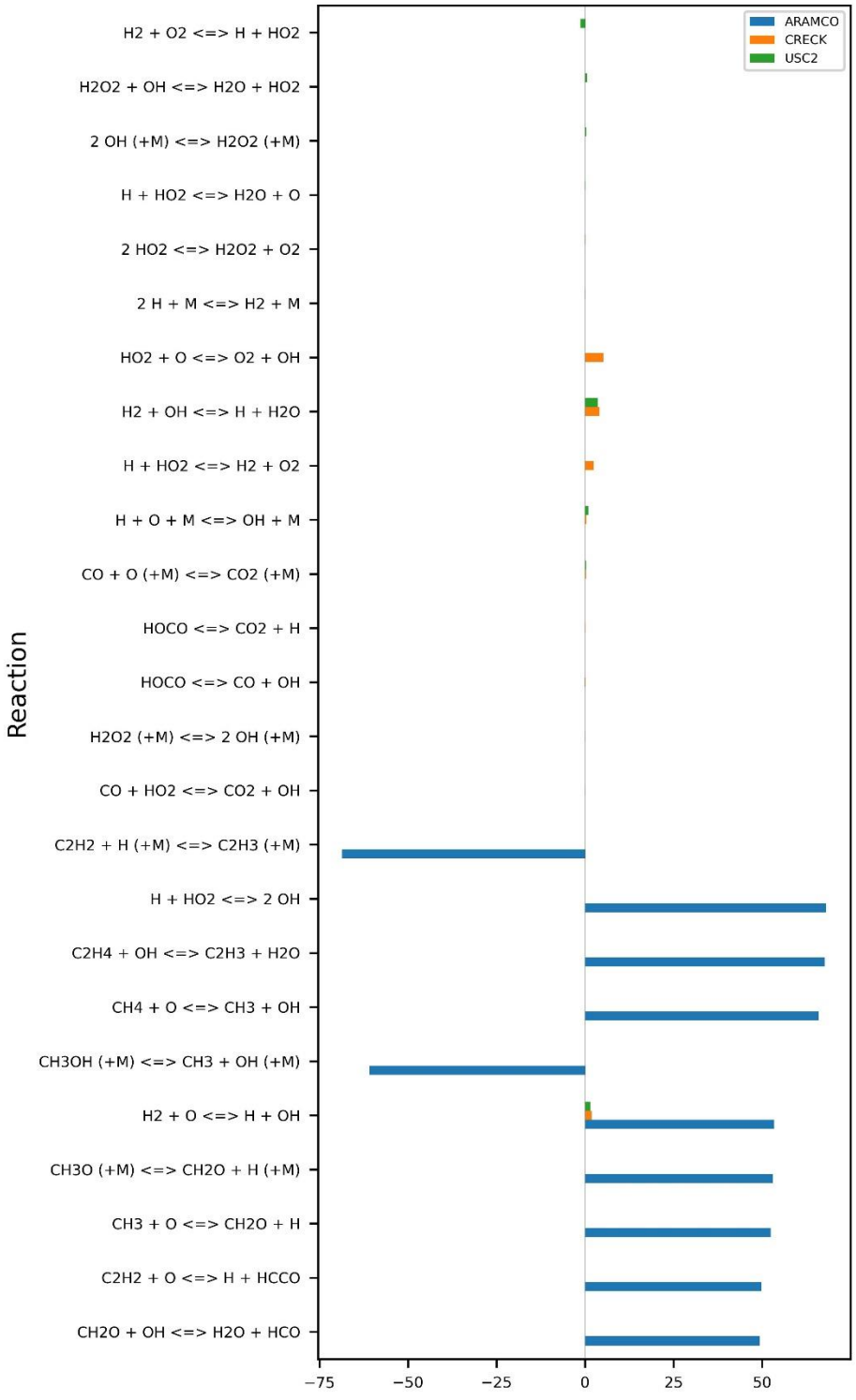

Figure 15 : Rate of Progress for key reactions from three models – ARAMCO 3.0 (blue), CRECK (orange) and USC Mech 2 (blue) for the natural gas experiments at φ ~ 0.99. The analysis was conducted midway through the reaction time and at 1509 K where experimentally the fuel drops to half of its initial value. x-axis : net rate of progress in kmol/m₃/s.

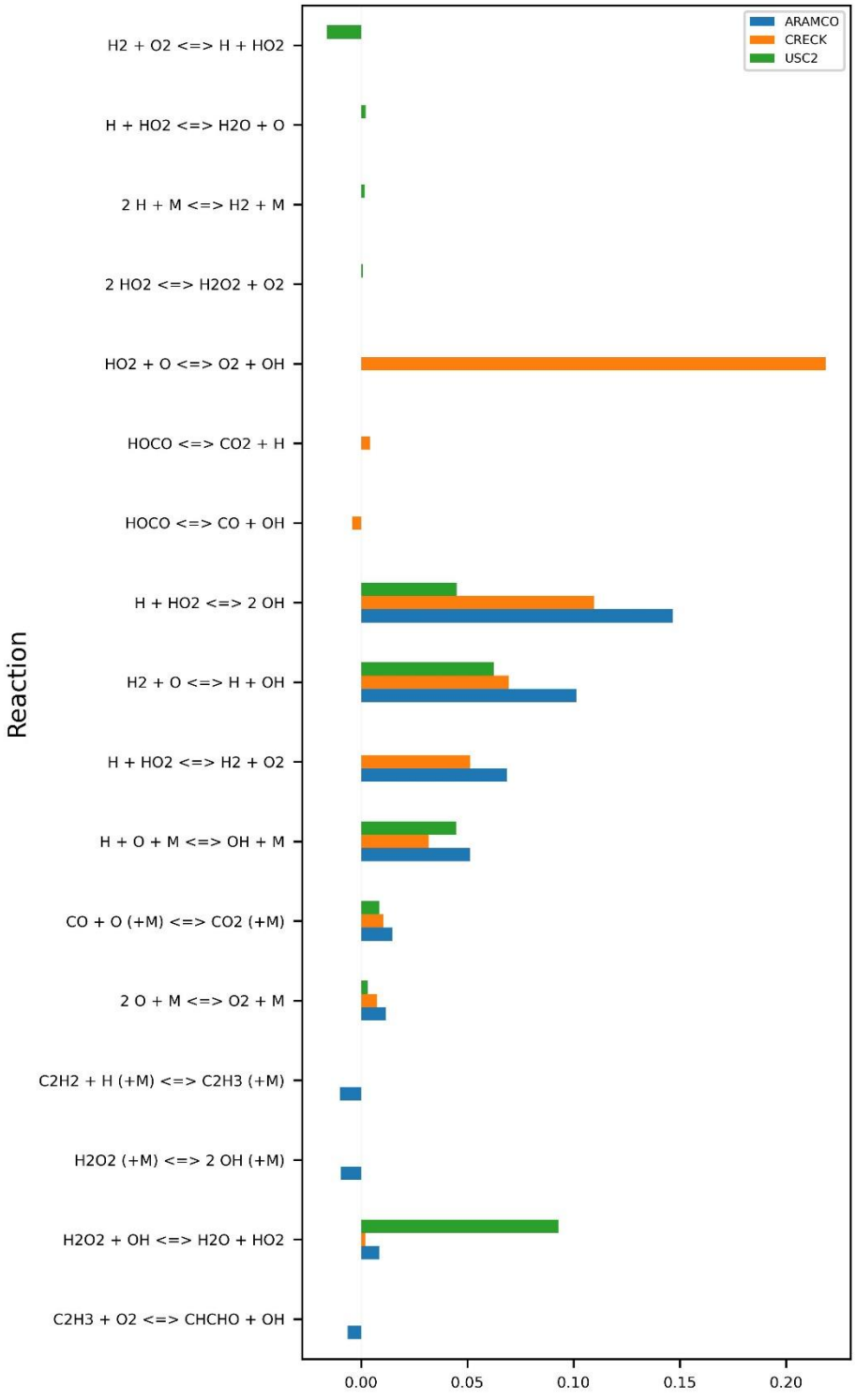

Figure 16 : Rate of Progress for key reactions from three models – ARAMCO 3.0 (blue), CRECK (orange) and USC Mech 2 (blue) for the natural gas experiments at φ ~ 1.49. The analysis was conducted midway through the reaction time and at 1643 K where experimentally the fuel drops to half of its initial value. x-axis : net rate of progress in kmol/m₃/s.

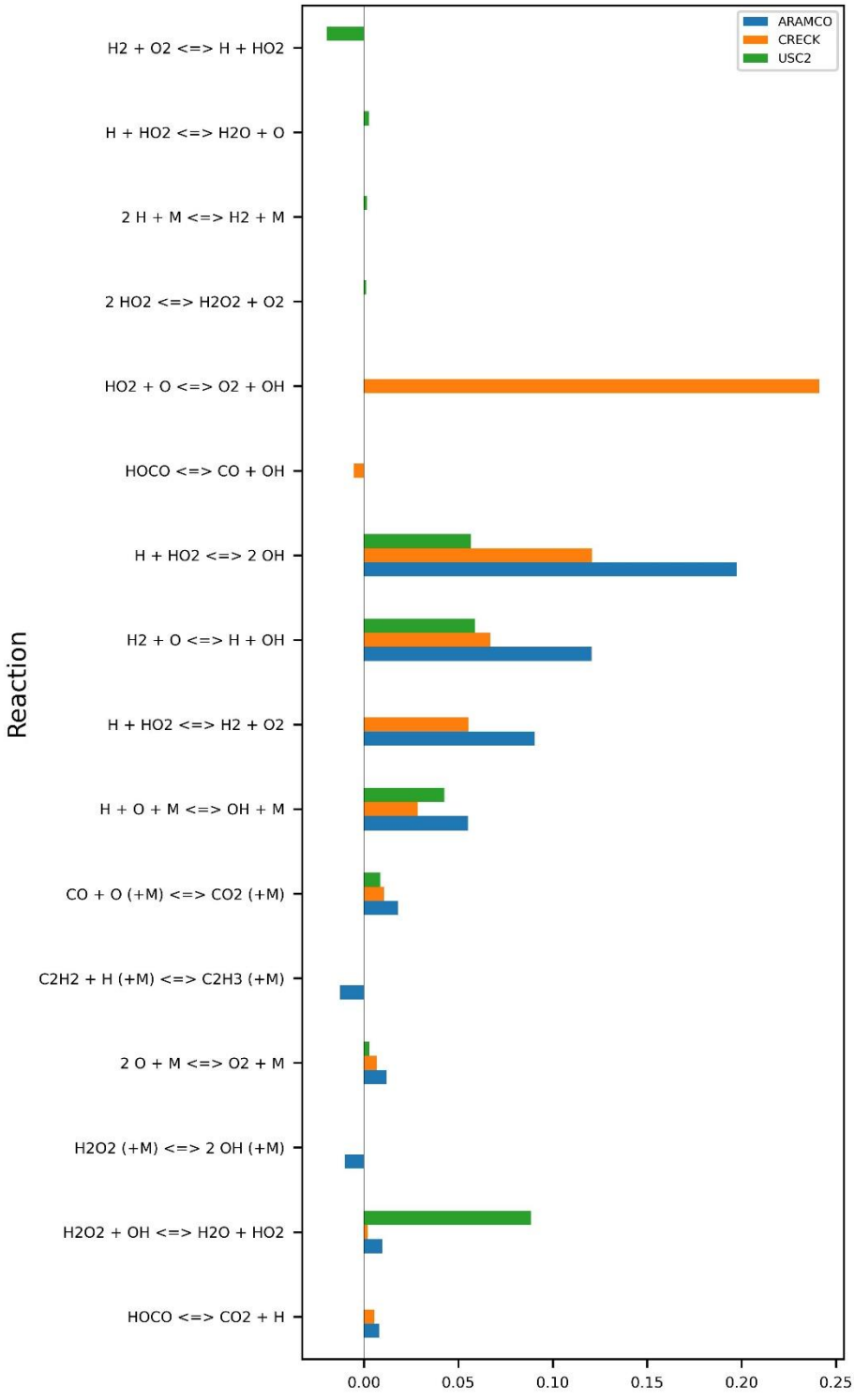

Figure 17 : Rate of Progress for key reactions from three models – ARAMCO 3.0 (blue), CRECK (orange) and USC Mech 2 (blue) for the natural gas experiments at φ ~ 3.09. The analysis was conducted midway through the reaction time and at 1604 K where experimentally the fuel drops to half of its initial value. x-axis : net rate of progress in kmol/m3/s.

2.4 Oxidation Study of Real Natural Gas Samples

2.4.1 Experiments

To study the effect of the composition of natural gas, real natural gas samples were studied at or near their stoichiometric conditions and the speciation of different samples of natural gas compared, as shown in Figure 18. The observations were in line with the expectations wherein the samples with higher methane content showed a greater resistance to reaction at lower temperatures, resulting in the fuel decomposition starting at a higher temperature than those with lower methane content. However, the relationship was not always linear since the balance composition also showed effects on how some key species were formed and consumed. For most of the samples the change in methane content was balanced by a change in ethane content. However, in some samples the impurities and propane content changed significantly like in the case of the Idaho natural gas sample (NG-ID) where despite methane content being close to the Ohio sample (NG-OH), the ethane content is lower and the propane content and impurities are higher.

The experiments show a remarkably similar trend across all the samples but if observed closely the temperature at which the fuel decomposition begins decreased between the samples as the methane content in the sample was reduced. The two samples with the maximum and the minimum methane content are the South Carolina sample (NG-SC) and the Kentucky natural gas sample (NG-KY) respectively and the difference between temperatures at which the fuel begins to decay is about 100 K. It should also be noted that while the temperature of start of fuel decomposition are 100 K apart, the temperature at which the complete fuel is decomposed has a larger difference of about 170 K with the NG-KY sample ending at a higher temperature. This difference implies that the fuel decomposition occurs more gradually over a larger temperature range for samples with lower methane content.

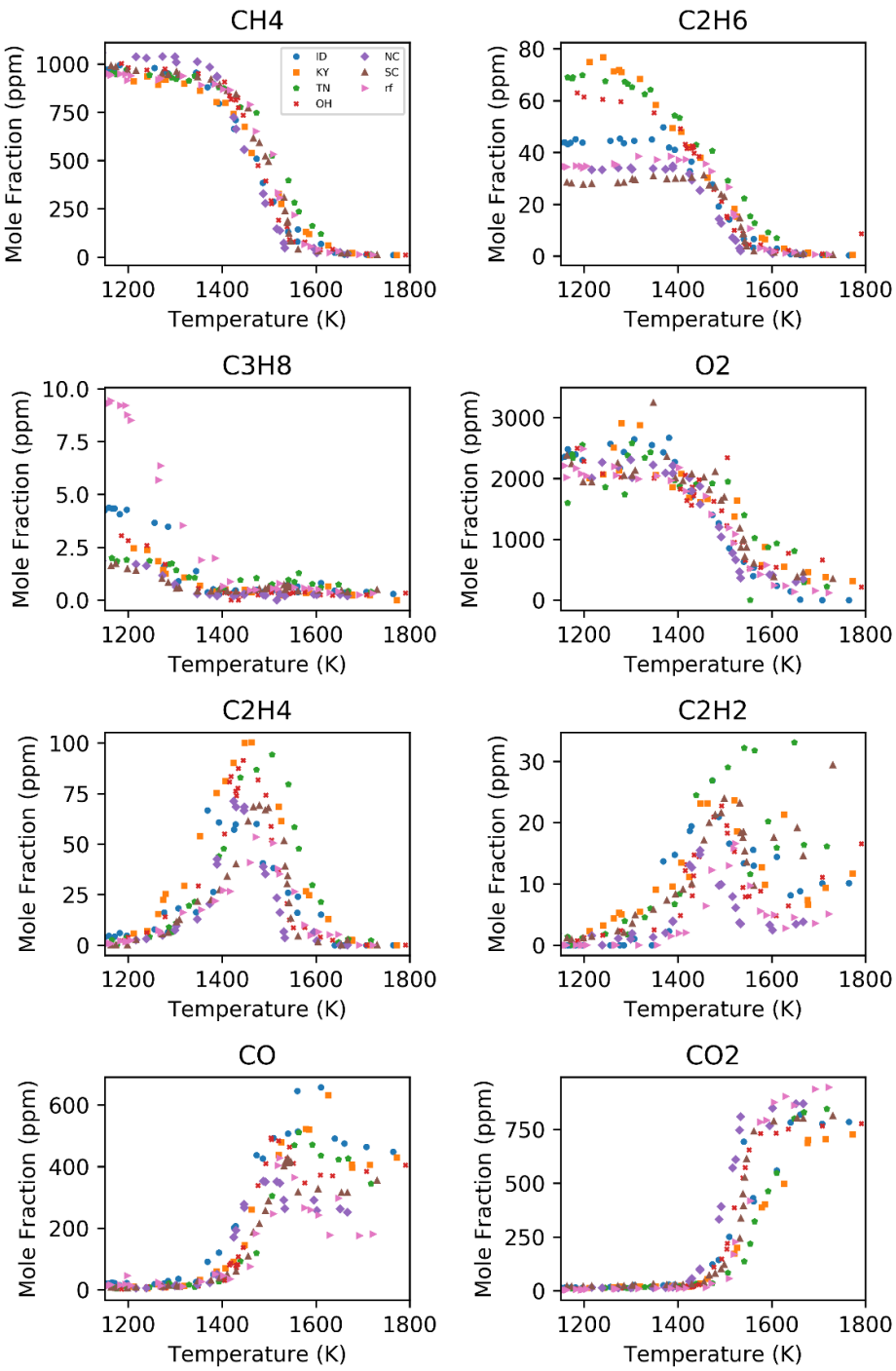

Figure 18 : Natural gas experiment speciation results comparing different experiment sets using real natural gas samples with varying compositions. The oxidation experiments were conducted at φ ~ 1.0.

This difference in the decomposition of the fuel is translated to the formation of CO_2 as well. It can be seen in Figure 20 that the CO_2 formation starts at the same temperature for all samples except for the North Carolina sample (NG-NC) for which the CO_2 formation starts about 50 K earlier which is greater than the temperature uncertainty of the experiments. However, the temperature at which the CO_2 level reaches maximum value and plateaus are significantly different between all the samples. The difference in the temperature for maximum CO_2 formation for natural gas samples with lower methane content is higher than that for the ones with higher content.

The comparison also shows that while all real natural gas samples behave differently, the reference natural gas sample does not mimic the behavior of any of the real natural gas samples. To investigate the cause for this difference, an additional study can be conducted in the future at the same experimental conditions using a synthetically prepared three component natural gas whose composition matches one of the real natural gas samples tested. This proposed experiment would confirm if the variation in the experimental results is inherent to the composition of methane, ethane and propane in the natural gas samples tested, as is hypothesized, or caused by the presence of impurities in the real natural gas samples. Based on current results the reference natural gas sample cannot be considered a surrogate for natural gas for chemical kinetic mechanism development or optimization of the method but instead should be considered as any other real natural gas sample.

2.4.2 Modeling

Figure 19 - Figure 24 show the simulation results from all four models compared to the experimental observations for all sets of experiments conducted with various natural gas samples. The model predictions from the various models do not agree with the experimental species profiles to the same extent for all samples. For example, one model may well capture a species profile with

respect to temperature but miss predicting another species whereas a different model may miss the prediction of the species that the first model captured but do well predicting the second species which was not well predicted by the other model. Furthermore, the models do not agree nor disagree systematically with each other for most cases. However, it was observed that as a general trend the models better predicted samples with higher content of CH_4. Since most models are based on or validated with pure methane oxidation/pyrolysis experiments it can be expected that their predictions will be better for fuels comprised mainly of methane. This predictability of methane suggests the need to conduct model optimizations using experimental data from fuels having varying CH_4 content to make a model suitable to use for real natural gas applications. The various models showed good agreement among themselves in capturing the primary fuel components, CH_4, C_2H_6, C_3H_8 and CO_2 but significantly missed predicting the temperature dependence of CO, C_2H_4 and C_2H_2.

The predictions of some of the key species such as CO and C_2H_4 are particularly important because these species play a significant role during design and analysis of gas turbines. To predict the gas turbine emissions, CO levels are used in industry. The models used in this study fail to capture its temperature dependence as well as yield for most of the samples of natural gas studied except for the sample from Ohio. For instance, Figure 20 shows one of the most serious discrepancies where the predicted peak for CO from the models is about 200 K lower than the experimentally observed value. The profile of CO_2 is also not very well predicted which suggests that the reactions responsible for CO to CO_2 conversion needs to be re-evaluated. A detailed rate of production and sensitivity analysis would be necessary to point out the exact reactions responsible for this difference. Optimization of the rate parameters of these models using data from additional experiments at different stoichiometric ratios for these fuels would be helpful.

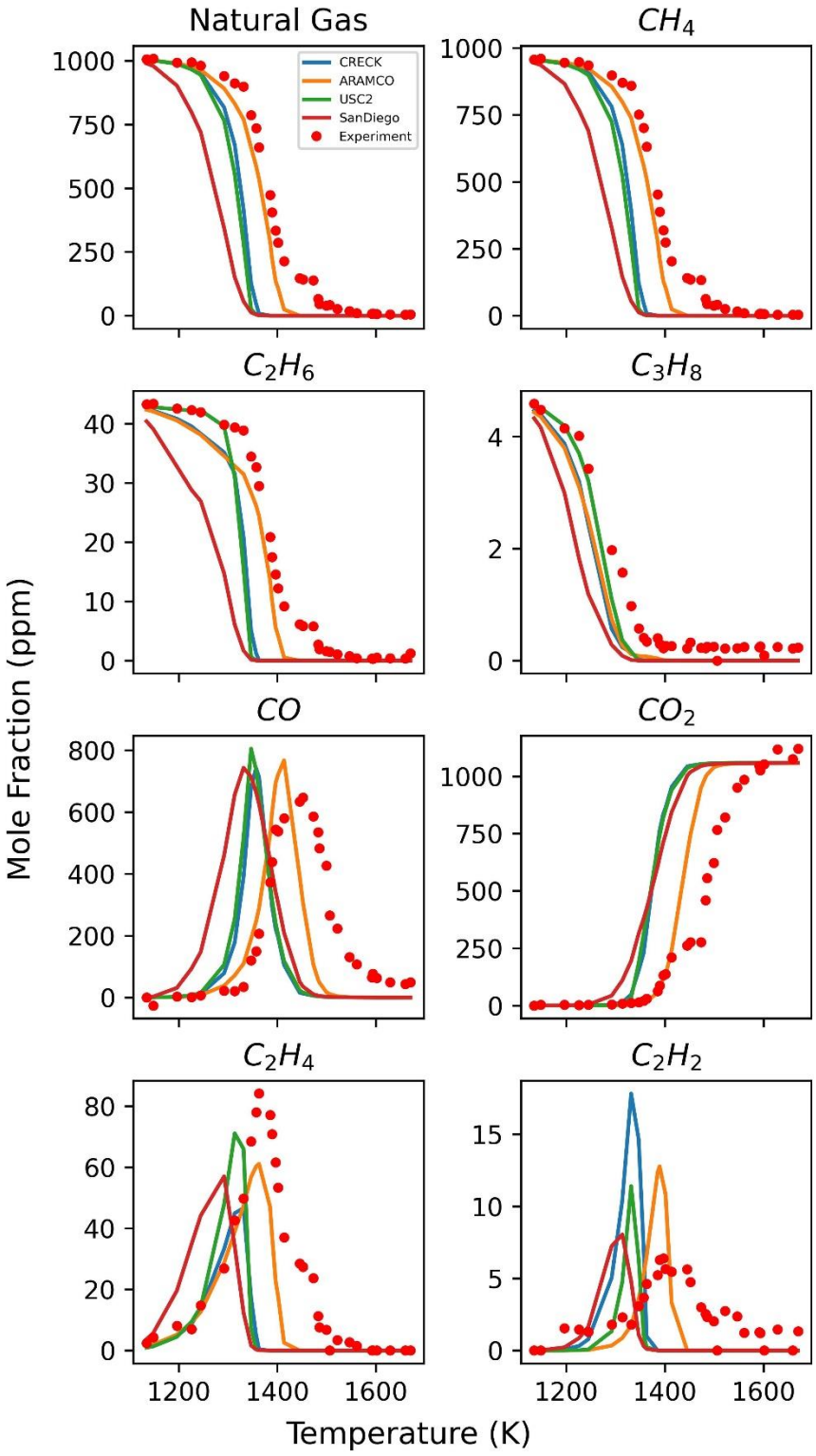

Figure 19 : Natural Gas Sample – Idaho (ID): Experimental species profiles (red circles) of CH_4, C_2H_6, C_3H_8, C_2H_4, C_2H_2, CO, CO2 and O_2 compared with predictions using ARAMCO 3 (orange), CRECK (blue), San Diego Mechanism (red) and USC Mech 2 (green).

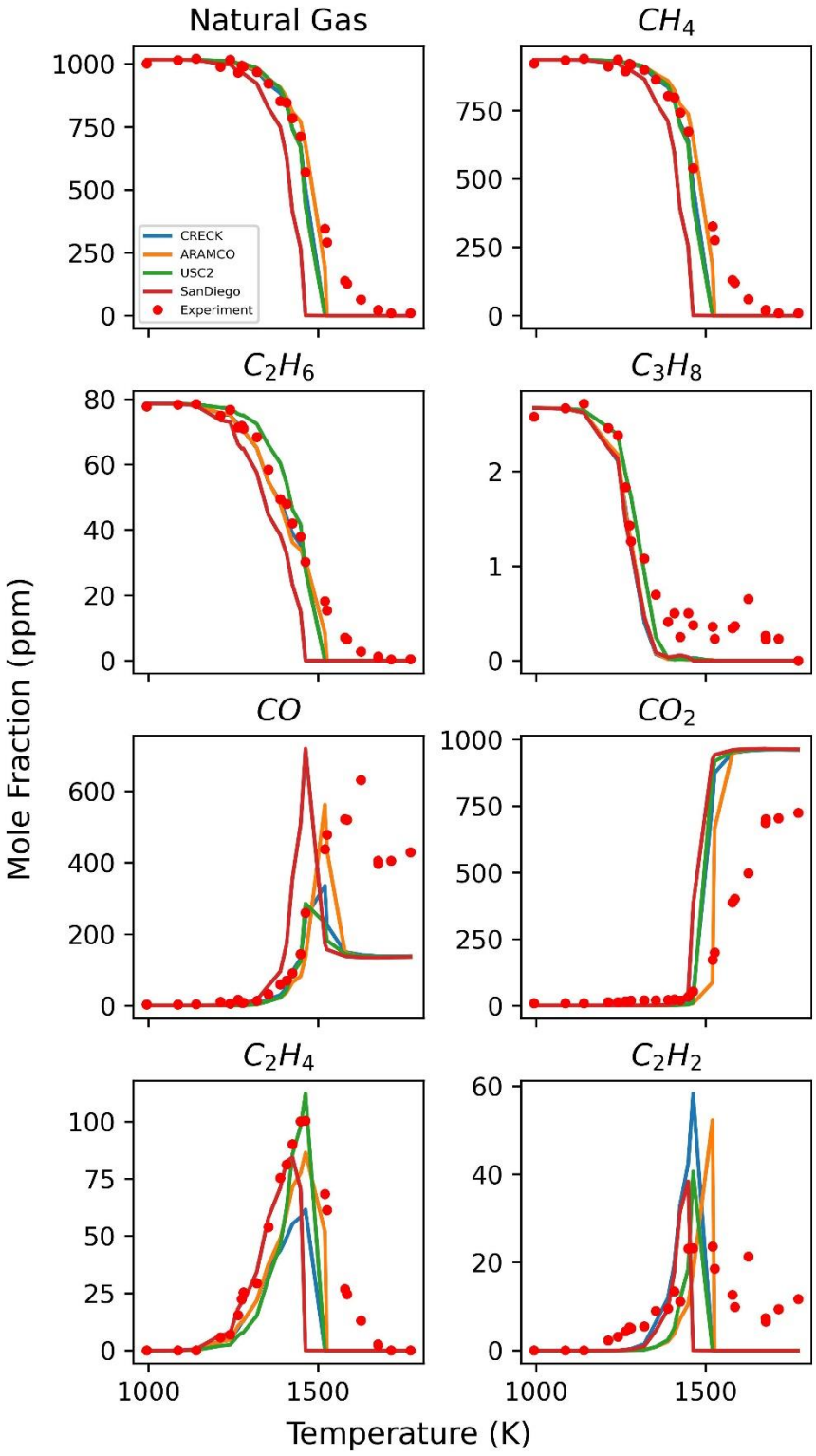

Figure 20 : Natural Gas Sample – Kentucky (KY) : Experimental species profiles (red circles) of CH_4, C_2H_6, C_3H_8, C_2H_4, C_2H_2, CO, CO2 and O_2 compared with predictions using ARAMCO 3 (orange), CRECK (blue), San Diego Mechanism (red) and USC Mech 2 (green).

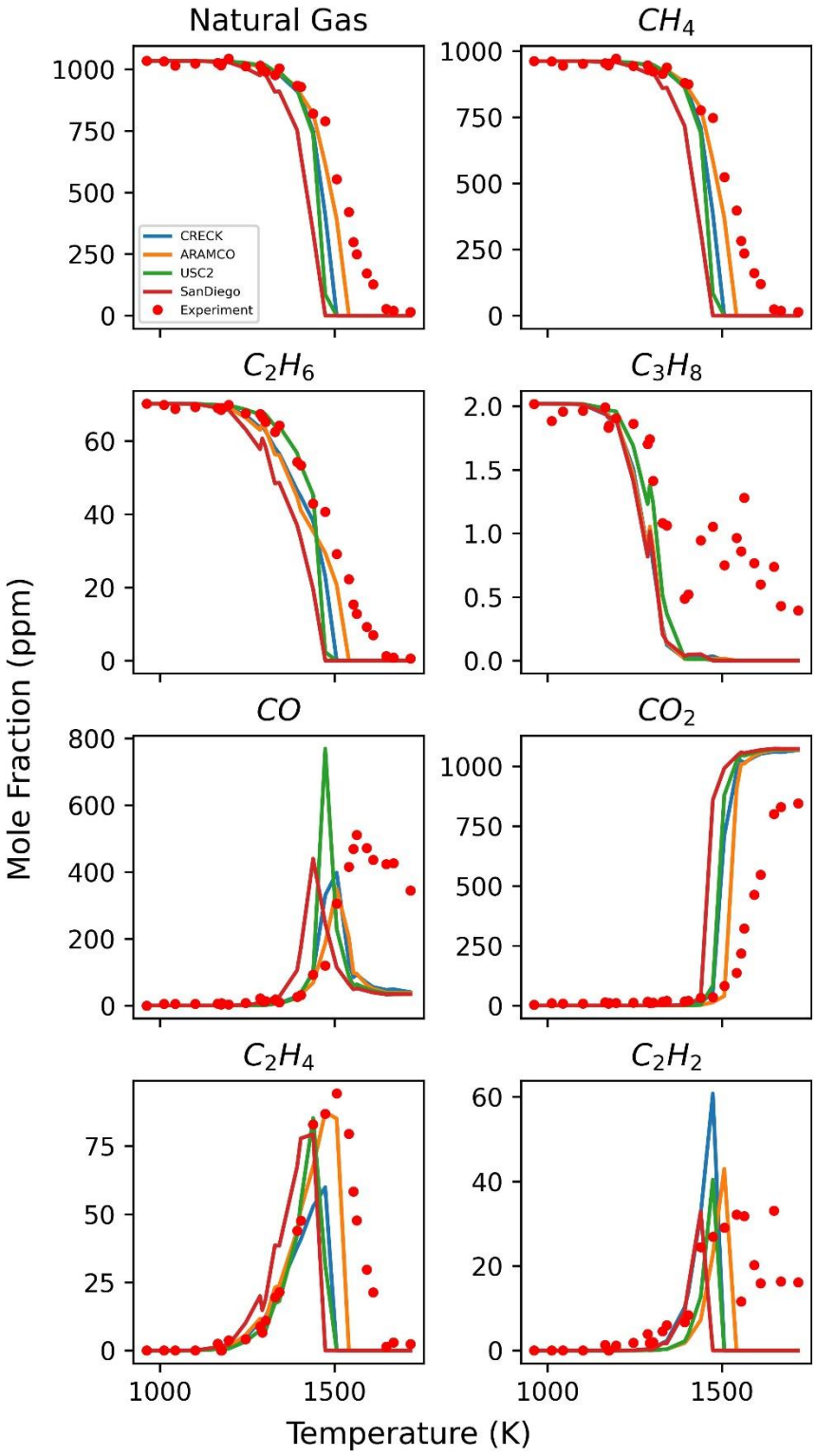

Figure 21 : Natural Gas Sample – Tennessee (TN): Experimental species profiles (red circles) of CH_4, C_2H_6, C_3H_8, C_2H_4, C_2H_2, CO, CO2 and O_2 compared with predictions using ARAMCO 3 (orange), CRECK (blue), San Diego Mechanism (red) and USC Mech 2 (green).

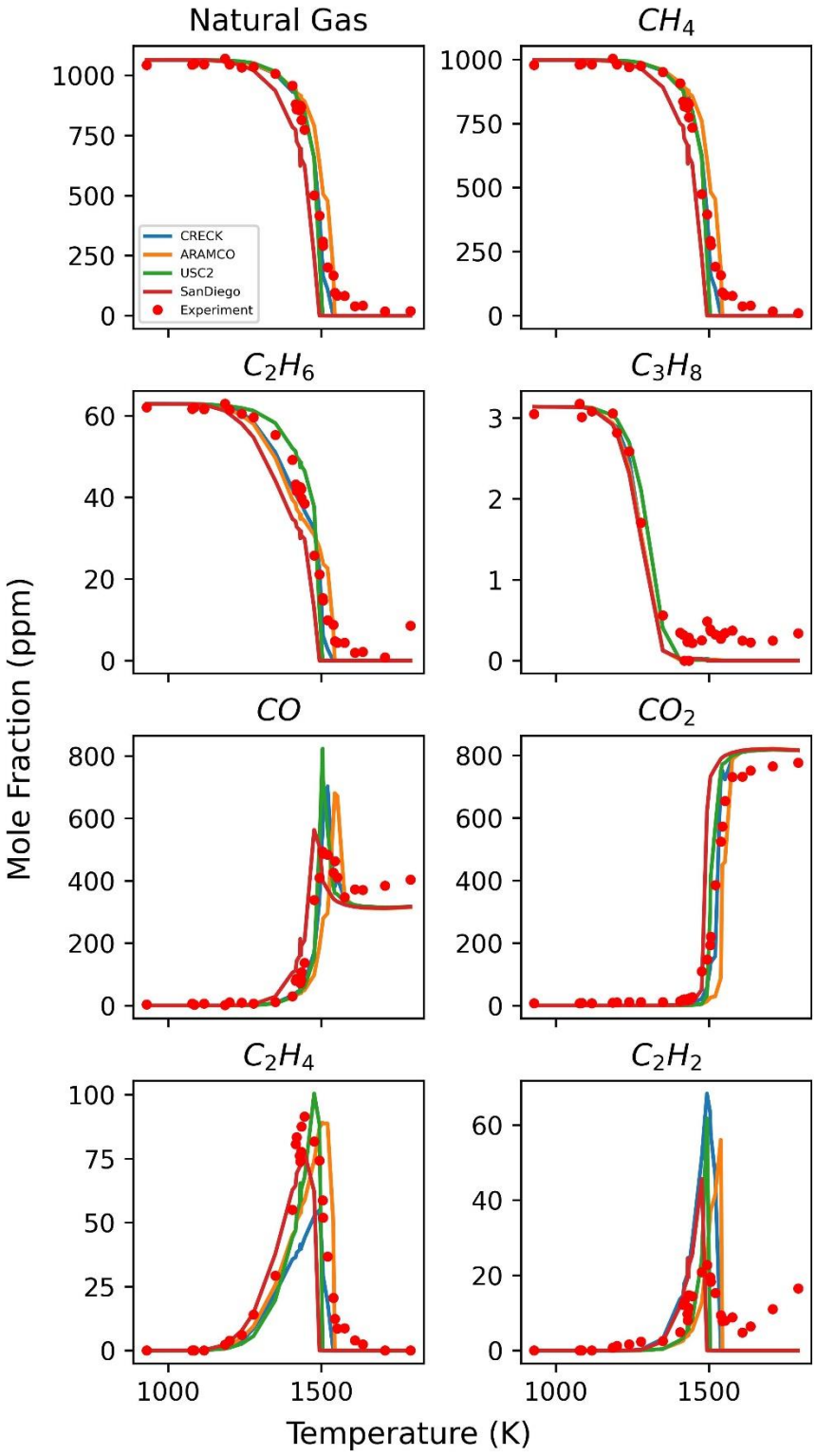

Figure 22 : Natural Gas Sample – Ohio (OH): Experimental species profiles (red circles) of CH4, C2H6, C3H8, C2H4, C2H2, CO, CO2 and O2 compared with predictions using ARAMCO 3 (orange), CRECK (blue), San Diego Mechanism (red) and USC Mech 2 (green).

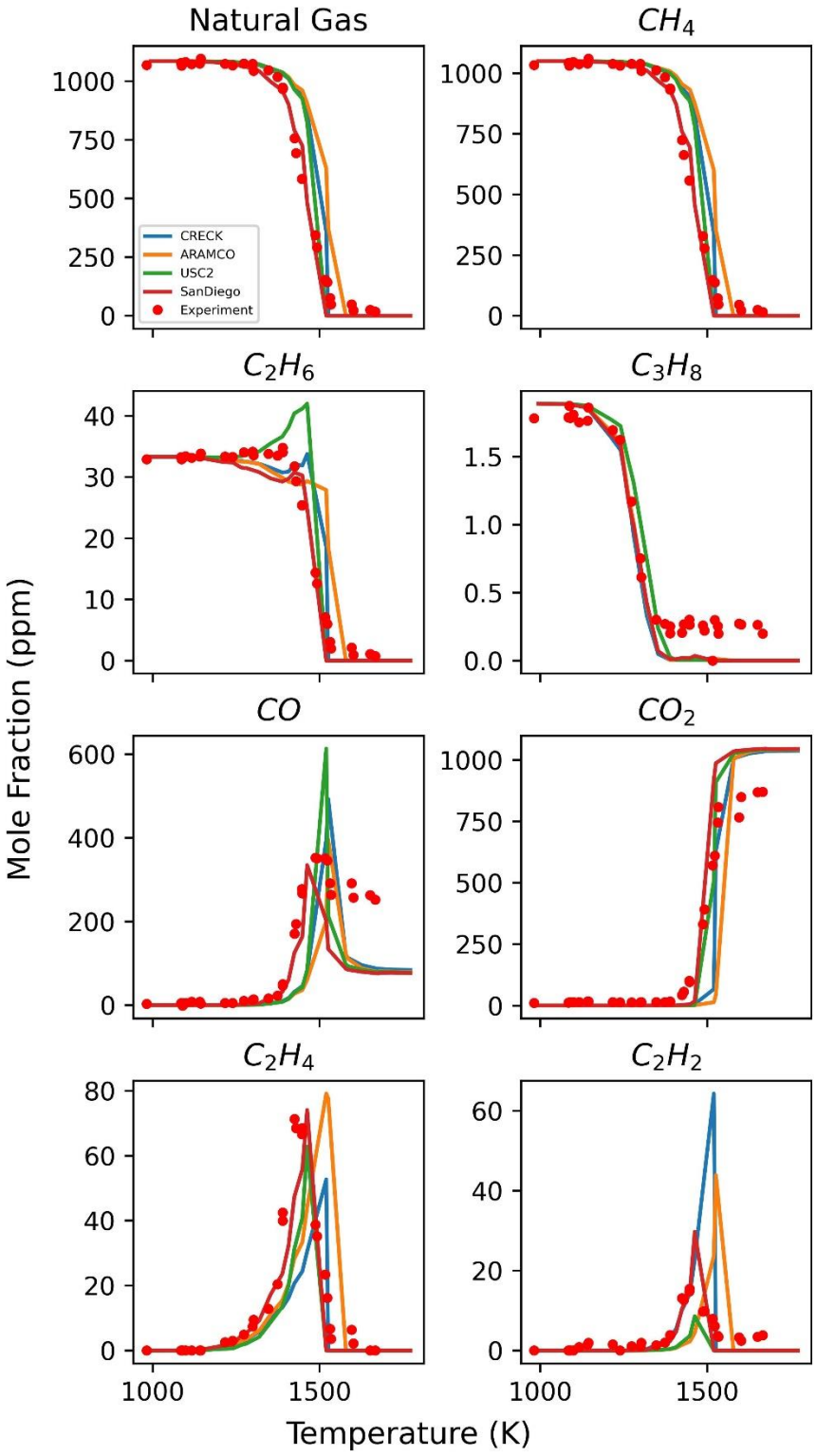

Figure 23 : Natural Gas Sample – North Carolina (NC) : Experimental species profiles (red circles) of CH4, C2H6, C3H8, C2H4, C2H2, CO, CO2 and O2 compared with predictions using ARAMCO 3 (orange), CRECK (blue), San Diego Mechanism (red) and USC Mech 2 (green).

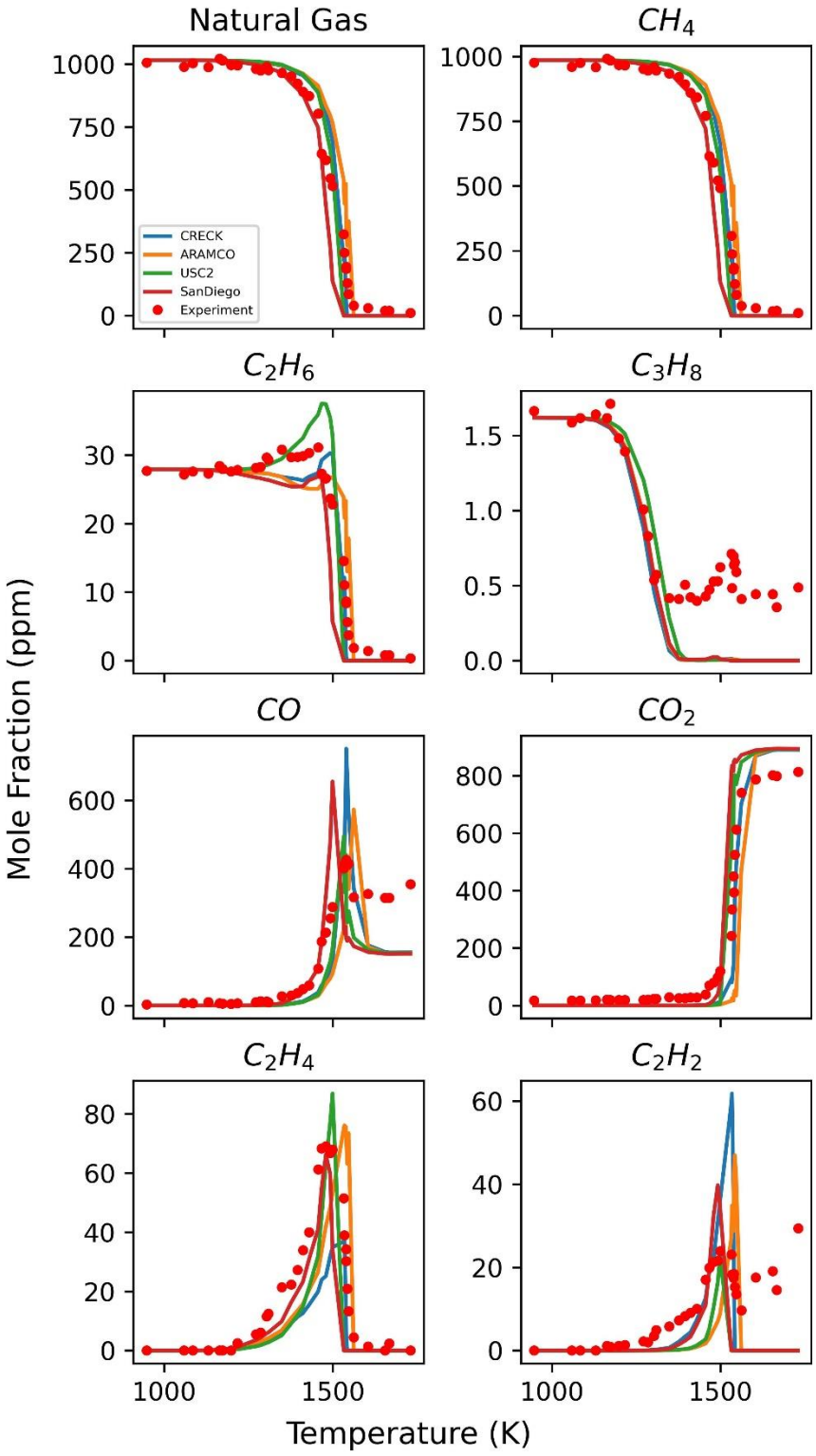

Figure 24 : Natural Gas Sample – South Carolina (SC): Experimental species profiles (red circles) of CH4, C2H6, C3H8, C2H4, C2H2, CO, CO2 and O2 compared with predictions using ARAMCO 3 (orange), CRECK (blue), San Diego Mechanism (red) and USC Mech 2 (green).

The agreement of the model predictions with experimental observations varied from experiment to experiment, with USC Mech 2 having the best overall match with experimental data. However, it did significantly overpredict C_2H_6 for the South Carolina sample – Figure 23 and the North Carolina sample - Figure 24 by about 10 ppm which is outside the experimental error. Another significant USC Mech 2 overprediction, by almost double the observed amount was for C_2H_2 in the Ohio sample, Figure 22.

All the model predictions and experimental conditions match very well for the natural gas samples from Ohio and South Carolina along with the reference natural gas except for C_2H_2 predictions which are overpredicted by a factor of greater than two. North Carolina also showed good agreement between the model predictions and experimental data except for CO_2 and C_2H_2. This latter observation supports the hypothesis that the model's performance improves for the fuels with higher initial methane concentration warranting the need for further optimization using binary and ternary gas fuel samples.

The experimental results show that the fuel samples having lower methane content such as those from Tennessee and Kentucky have a more gradual fuel decomposition with respect to the temperature since the complete fuel decomposition happens at temperatures approximately 100 K greater than that of higher methane content fuels (rf, OH, NC, SC). This effect is not well captured by any of the models, and they predict the same temperature at which fuel completely decomposes for all the natural gas samples. This can be accounted for by further optimization of the rate parameters of some key reactions involved in fuel decomposition.

The rate of progress analysis was repeated for all these experiment at conditions meeting the same requirement as before: the temperature at which experimentally fuel decays to half its initial value at end of reaction and at a time equivalent to half of the total estimated reaction time.

The top ten reactions from the different chemical kinetic mechanisms used for each experiment set have been compared in Figure 25 to Figure 30. The results show a significantly difference in the active reactions at described conditions. Additionally, no similarities are evident between the mechanisms with exception of a couple of reactions for some samples like the NG-KY and the NG-NC samples. For these experiments there is similarity between the ROP analysis of CRECK and USC Mech 2. For instance, the reaction responsible for H-atom abstraction from ethane to form the ethyl radical ($C_2H_6 + H \leftrightarrow C_2H_5 + H_2$) in both the models has a similar progress rate for all natural gas samples except the NG-TN and the NG-SC samples. The reaction does not show up in this analysis for the NG-TN and NG-SC samples at all. However, the ARAMCO 3.0 analysis shows that the same reaction is important for the NG-TN and NG-SC samples, while it has a significantly low rate for the remaining samples. It is worth noting that these two samples are the samples with the lowest and highest methane content, respectively. This result is evidence of the significantly different chemical kinetic paths that these models consider and the effect of different rate constants on the final species predictions.

Another reaction that shows the significant activity, however only for the USC Mech 2 is the reaction of formaldehyde with hydrogen to yield formyl radical and hydrogen molecule ($HCHO + H \leftrightarrow H_2 + HCO$). This reaction has significant rate of progress for all the samples except for the NG-SC and NG-TN samples. This results for USC Mech 2 mechanism at these conditions emphasizes oxygenated hydrocarbon chemistry. The close match of speciation results of USC Mech 2 with experimental data, evident in Figure 19 - Figure 24 shows that this approach is more appropriate.

To further understand how the chemistry progresses for the different mechanisms, the rate of progress for the whole experimental set were compared to each other for the three models

ARAMCO 3.0, CRECK and USC Mech 2, Figure 31, Figure 32 and Figure 33 respectively. The rate of progress analyses was carried out at the temperature and pressure at which half the fuel was consumed at the end of reaction time in the experiment set. The rate of progress discussed in this work is at 50% of the experimental reaction time.

The ARAMCO 3.0 (Figure 31) rate of progress analysis shows that four reactions out of the top ten reactions for every experiment set are common. Two of the most important reactions are H-atom abstraction from ethane by reaction with H and OH to form ethyl radical. The highest rate of progress for these reactions ($C_2H_6 + H \leftrightarrow C_2H_5 + H_2$ and $C_2H_6 + OH \leftrightarrow C_2H_5 + H_2O$) is for the NG-KY sample, with the NG-NC samples being the close second. While these reactions show a high progress rate for other samples as well, it is half that for the NG-KY and NG-NC samples, with the lowest rate for the NG-OH sample. In addition to this reaction the other key reaction is the formation of formaldehyde from methyl radicals, through two reactions – $CH_3 + HO_2 \leftrightarrow CH_3O + OH$ and $CH_3O \leftrightarrow CH_2O + H$. The rate of progress of both these reactions is the same for both the NG-KY and NG-NC samples. The NG-SC sample which has the highest methane content of all samples (>96% mole fraction) has a distinct set of reactions that have high progress rates when using the ARAMCO 3.0 mechanism and is not shared by any other samples. The samples NG-TN, NG-RF, NG-OH, and NG-ID have similar methane content, but NG-OH despite being in the similar range is showing a significantly different rates of progress.

In the case of the CRECK mechanism (Figure 32), there are no similarities in the rate of progress between all the different sets of experiments. However, several experiments are showing the same top 10 reactions. The similarities in top 10 reactions are observed in pairs, such as for NG-KY and NG-NC which have four reactions where the progress is only for these samples and no other samples. Similarly, NG-RF and NG-TN have a significant number of reactions common

among them. USC Mech 2 shows a similar trend as the CRECK mechanism and unlike ARAMCO 3.0 the distinct set of reactions in case of NG-SC are not present. There are seven reactions common to the NG-OH, NG-RF, NG-ID, and NG-TN samples which involve C_2 hydrocarbons and oxygenated hydrocarbon chemistry which are not significant for the NG-KY, NG-NC, and NG-SC samples.

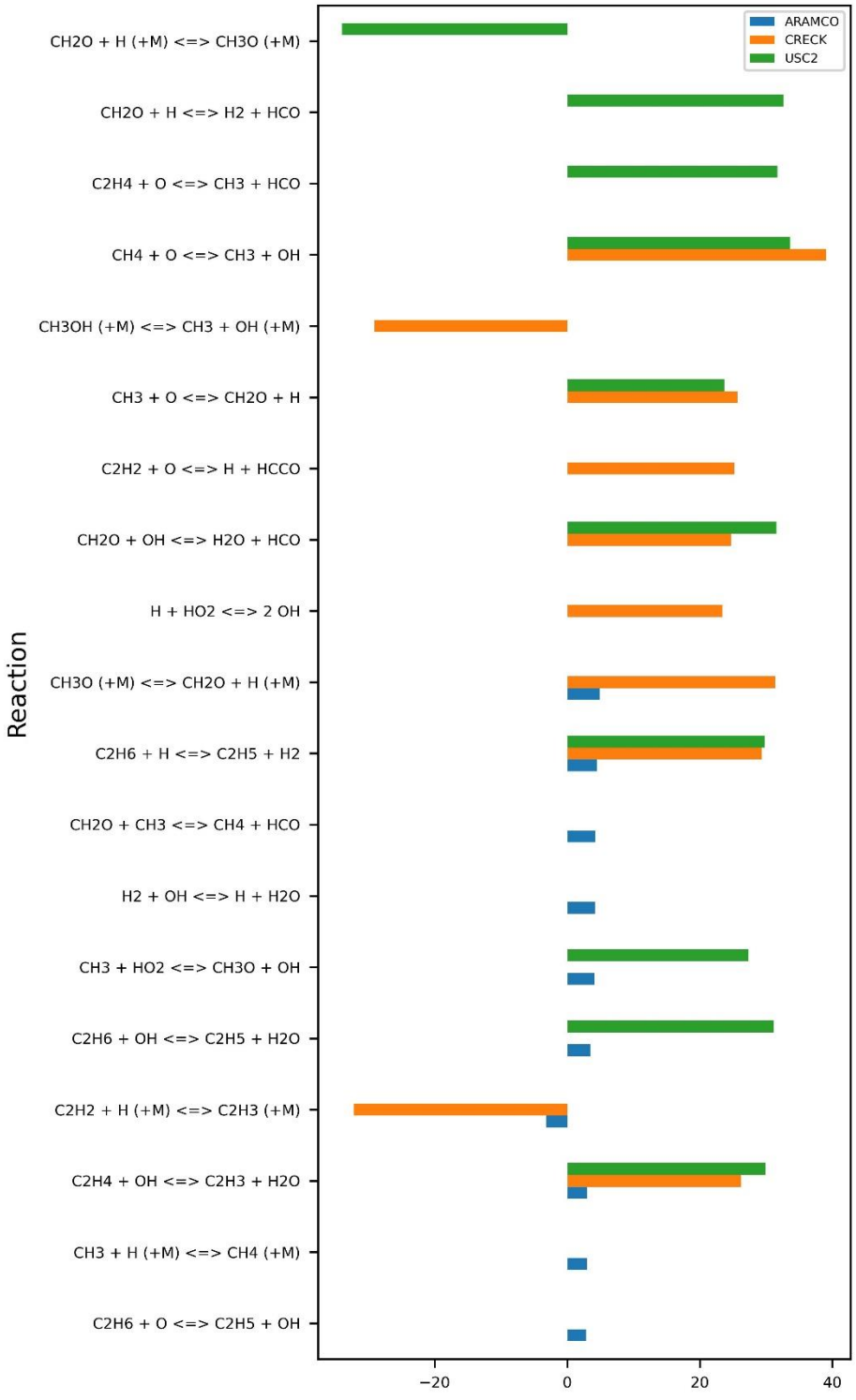

Figure 25 : Rate of Progress analysis for Natural Gas sample from Idaho (NG-ID) from three different chemical kinetic mechanisms - ARAMCO 3.0 (blue), CRECK (orange), USC Mech 2 (green). The analysis was conducted midway through the reaction time and where experimentally the fuel drops to half of its initial value. x-axis : net rate of progress in kmol/m_3/s.

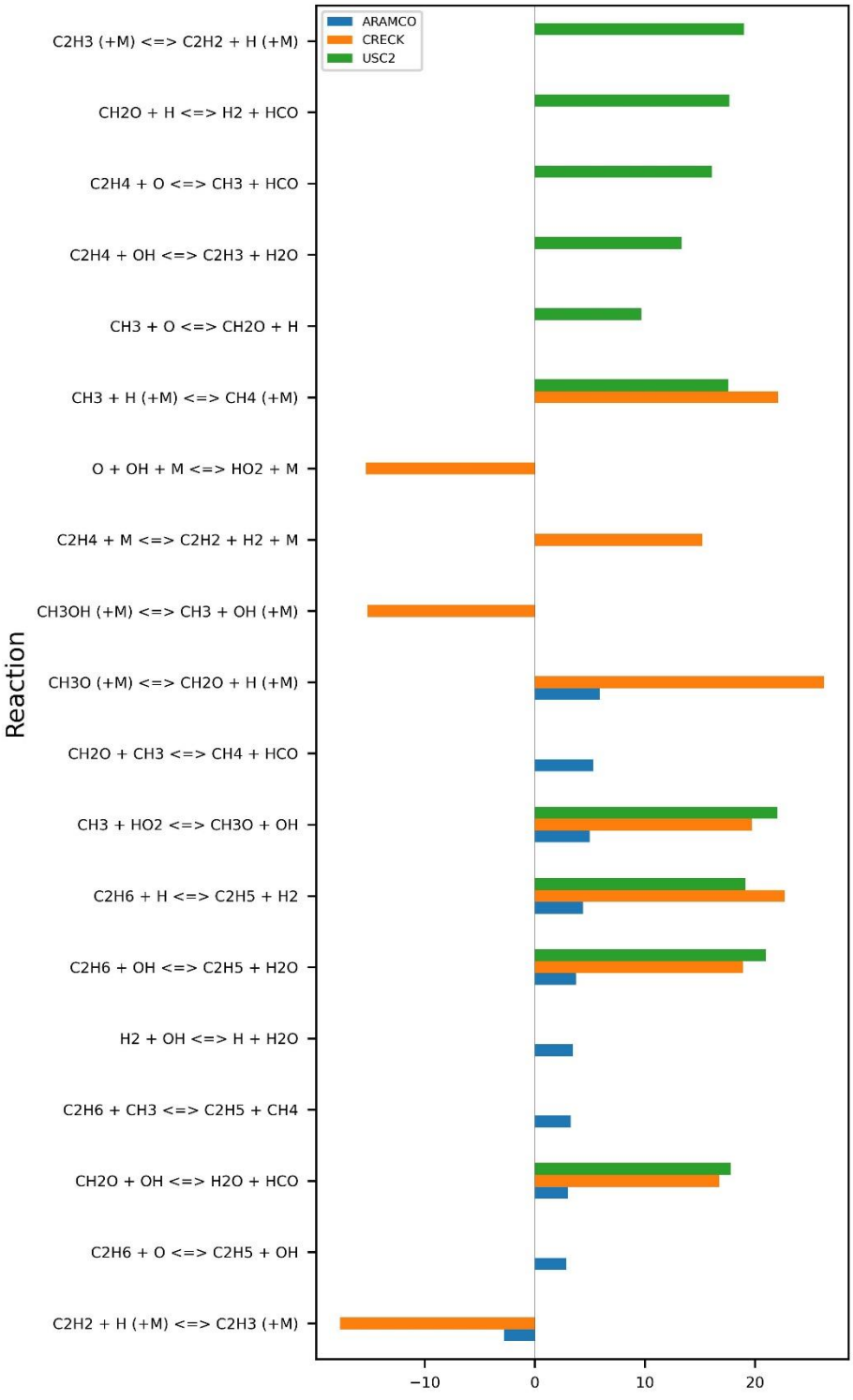

Figure 26 : Rate of Progress analysis for Natural Gas sample from Kentucky (NG-KY) from three different chemical kinetic mechanisms - ARAMCO 3.0 (blue), CRECK (orange), USC Mech 2 (green). The analysis was conducted midway through the reaction time and where experimentally the fuel drops to half of its initial value. x-axis : net rate of progress in kmol/m_3/s.

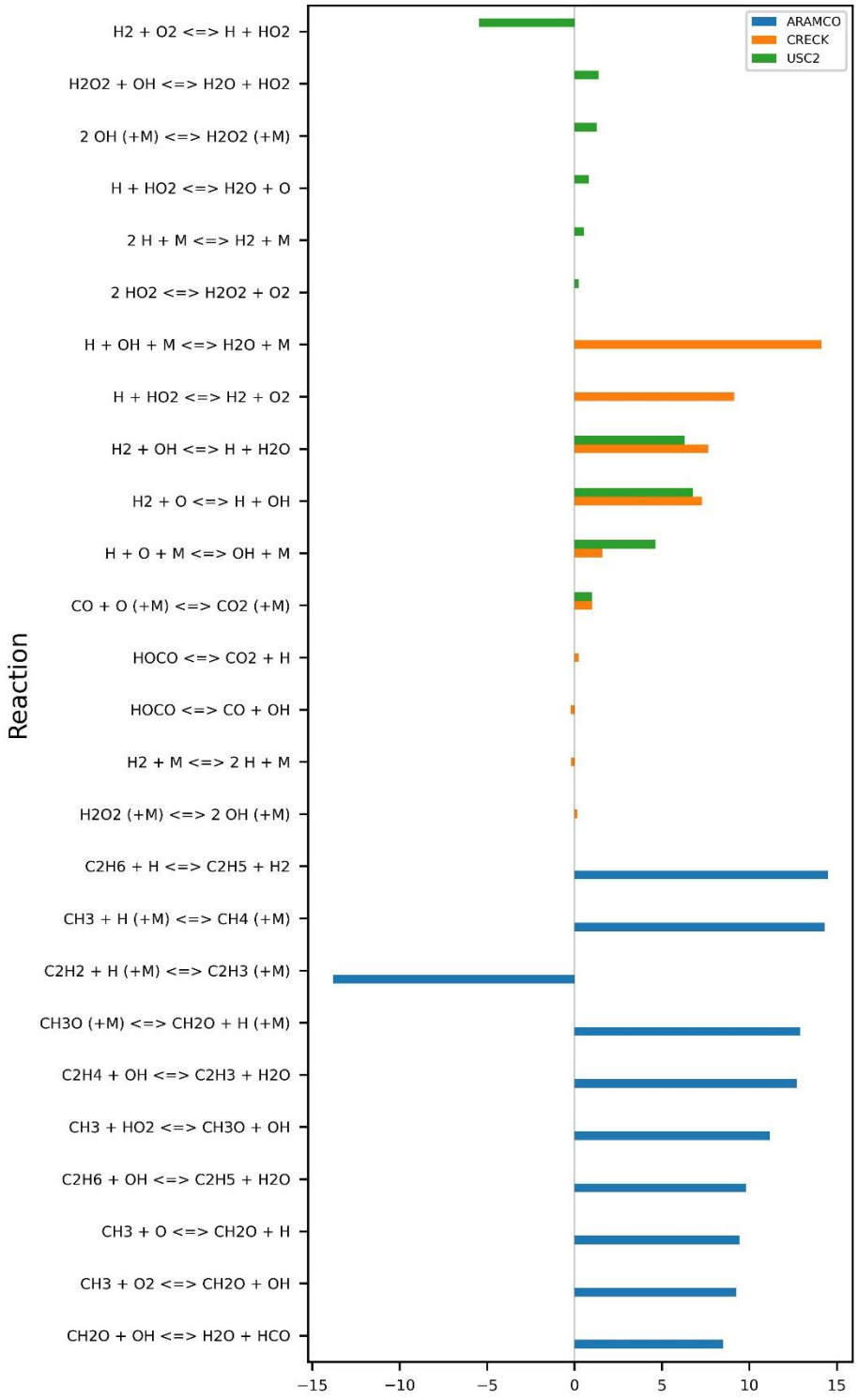

Figure 27 : Rate of Progress analysis for Natural Gas sample from Tennessee (NG-TN) from three different chemical kinetic mechanisms - ARAMCO 3.0 (blue), CRECK (orange), USC Mech 2 (green). The analysis was conducted midway through the reaction time and where experimentally the fuel drops to half of its initial value. x-axis : net rate of progress in kmol/m_3/s.

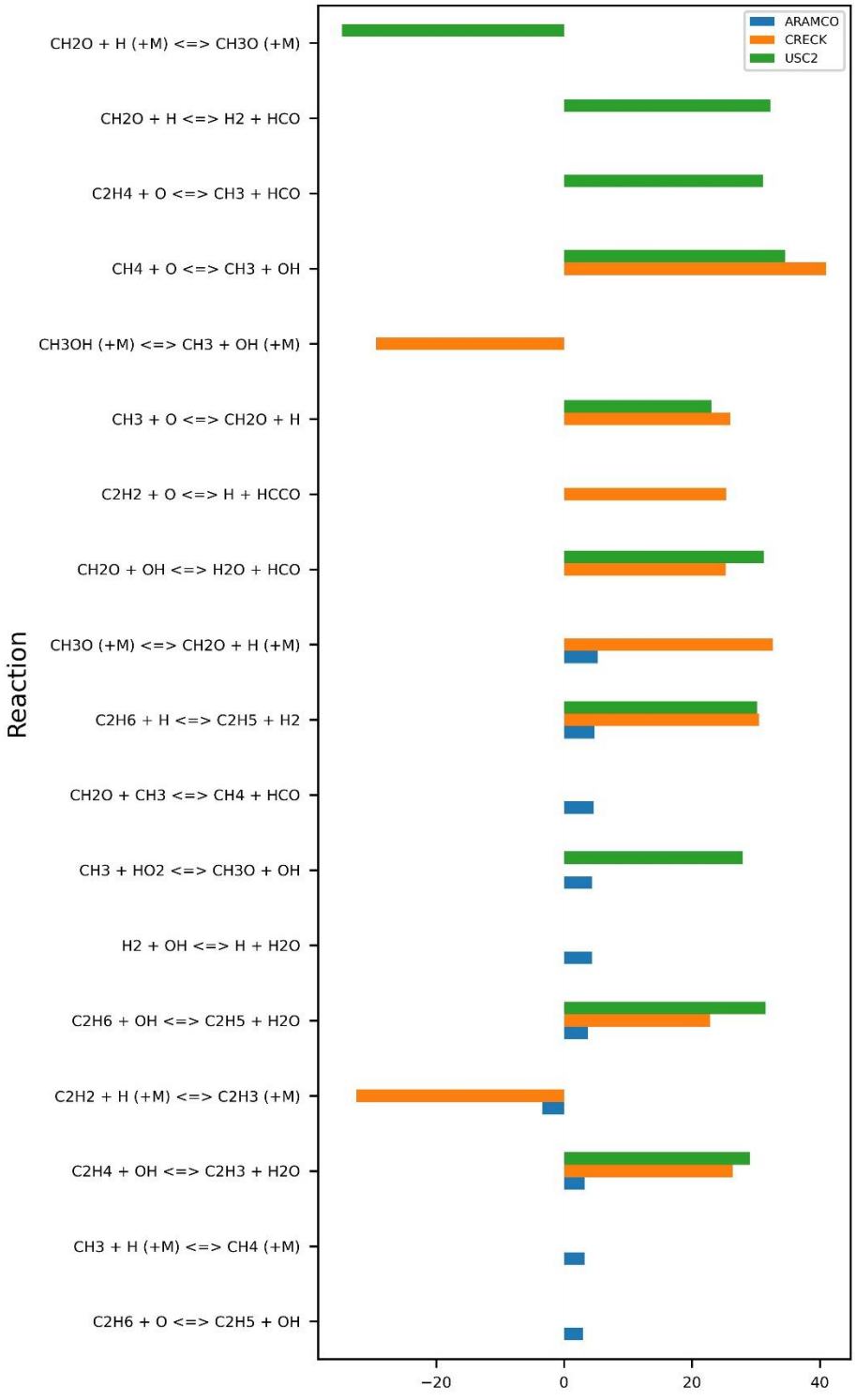

Figure 28 : Rate of Progress analysis for Natural Gas sample from Ohio (NG-OH) from three different chemical kinetic mechanisms - ARAMCO 3.0 (blue), CRECK (orange), USC Mech 2 (green). The analysis was conducted midway through the reaction time and where experimentally the fuel drops to half of its initial value. x-axis : net rate of progress in kmol/m_3/s.

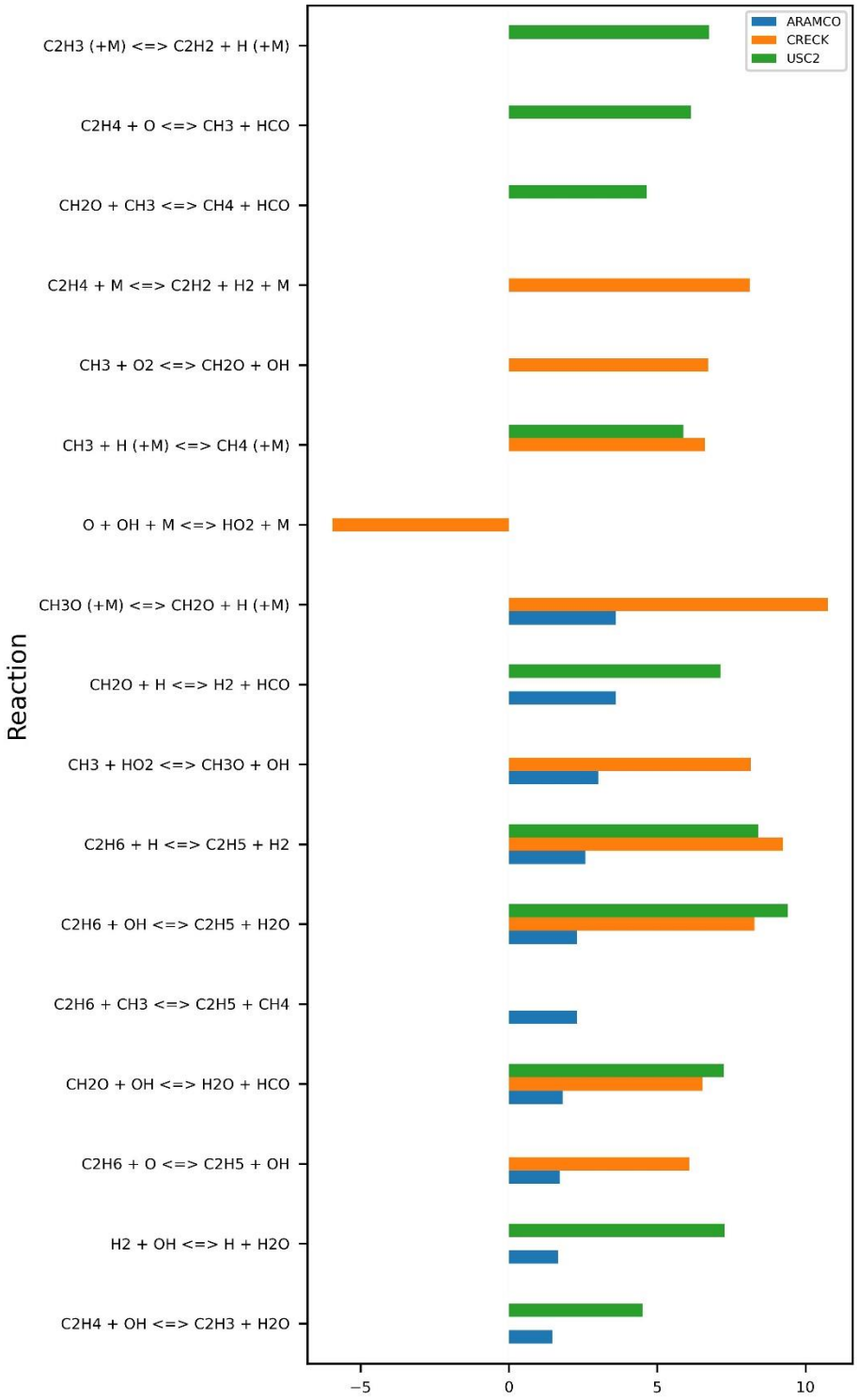

Figure 29: Rate of Progress analysis for Natural Gas sample from North Carolina (NG-NC) from three different chemical kinetic mechanisms - ARAMCO 3.0 (blue), CRECK (orange), USC Mech 2 (green). The analysis was conducted midway through the reaction time and where experimentally the fuel drops to half of its initial value. x-axis : net rate of progress in kmol/m_3/s.

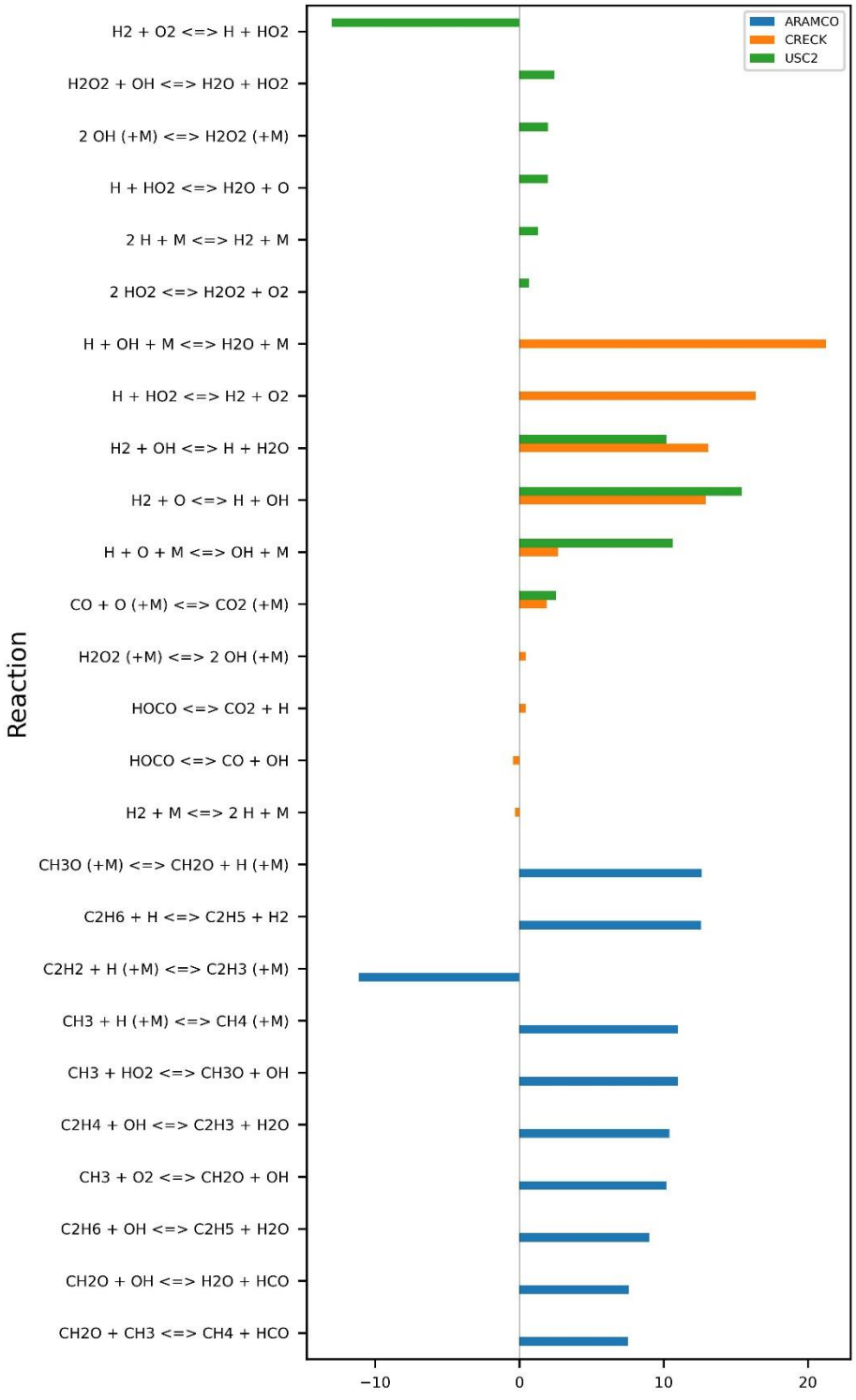

Figure 30 : Rate of Progress analysis for Natural Gas sample from South Carolina (NG-SC) from three different chemical kinetic mechanisms - ARAMCO 3.0 (blue), CRECK (orange), USC Mech 2 (green). The analysis was conducted midway through the reaction time and where experimentally the fuel drops to half of its initial value. x-axis : net rate of progress in kmol/m_3/s.

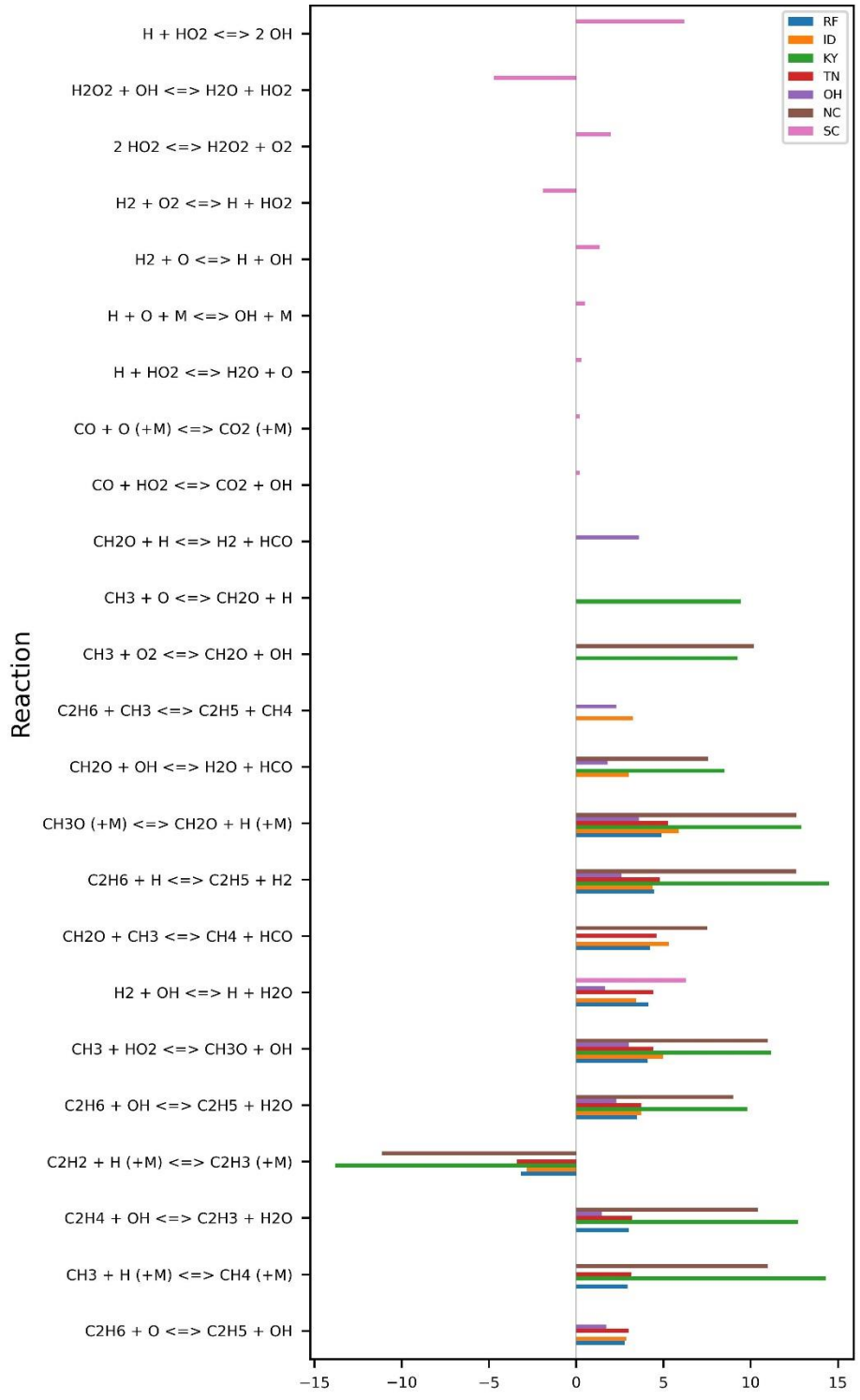

Figure 31 : Rate of progress analysis for experiments using different natural gas samples from the ARAMCO 3.0 mechanism. x-axis : net rate of progress in kmol/m3/s.

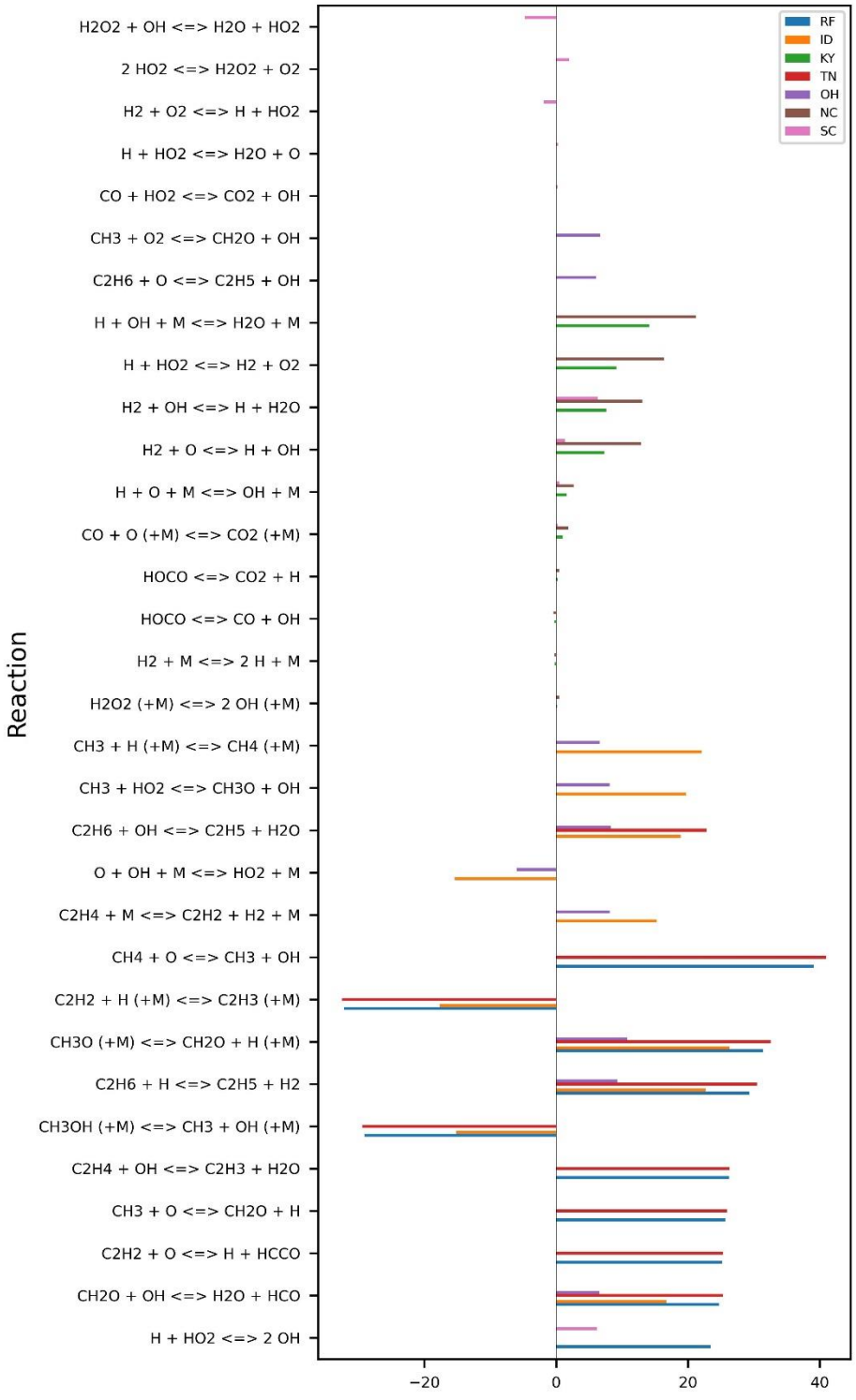

Figure 32 : Rate of progress analysis for experiments using different natural gas samples from the CRECK mechanism. x-axis : net rate of progress in kmol/m3/s.

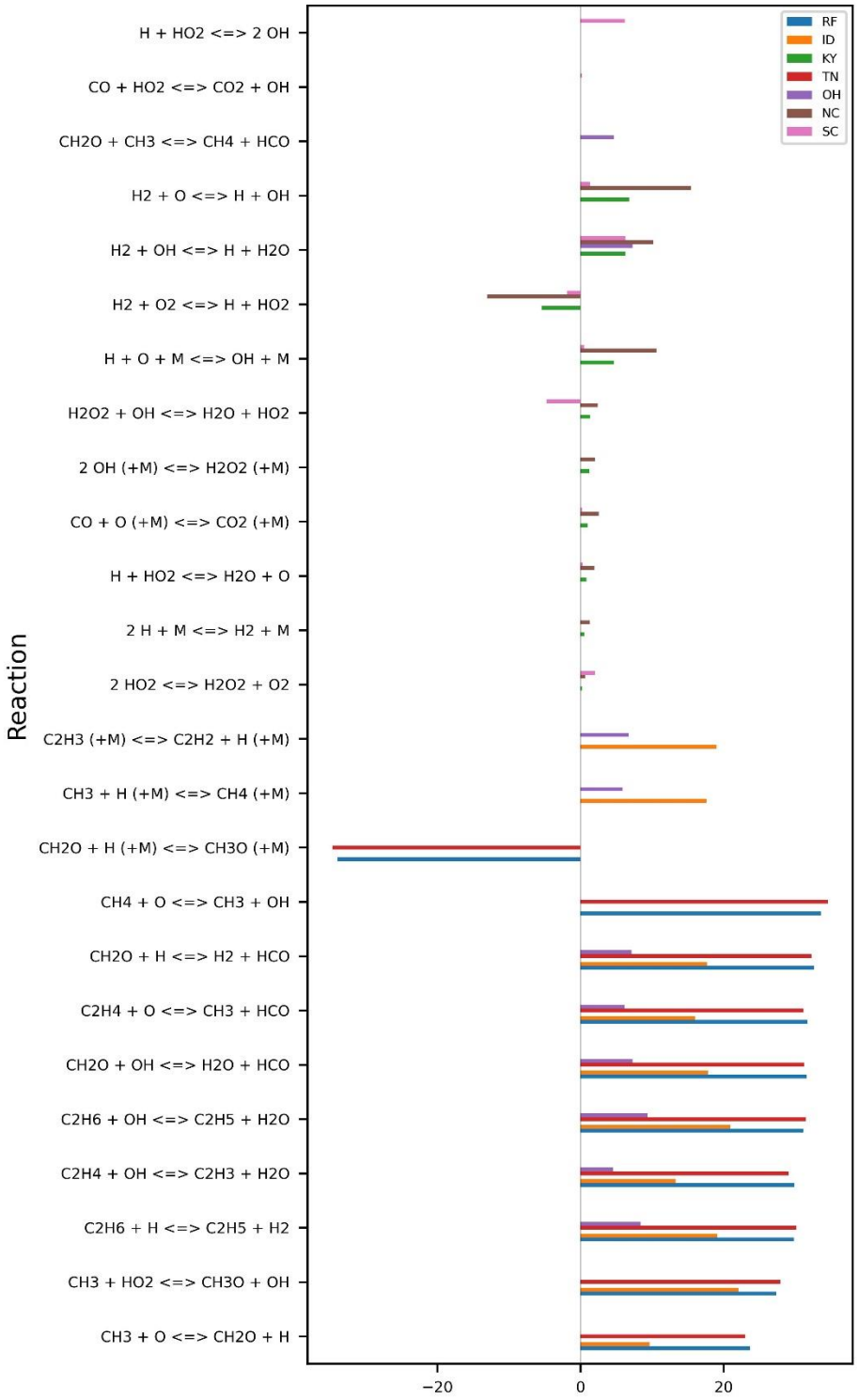

Figure 33 : Rate of progress analysis for experiments using different natural gas samples from the USC Mech 2. x-axis : net rate of progress in kmol/m3/s.

2.5 Formation of Ethane During Consumption of Natural Gas

Ethane is a constituent species of the natural gas samples analyzed in this study and it is anticipated that ethane concentration would drop as the overall natural gas composition drops but this was not the case for several experiments. Rise in the C_2H_6 concentration was observed mainly over a temperature range of 1150 K – 1450 K in NG-RF experiments. Experiments conducted at equivalence ratios below stoichiometric ($\varphi \leq 1$) showed a more significant rise in the ethane concentration. From the experimental speciation results (Figure 7 - Figure 9) it can be seen that the other two fuel constituents – CH_4 and C_3H_8, do not show any rise in their concentration over this temperature range, and are instead consumed as the temperature rises. It would be logical to assume that C_2H_6 is formed from reactions resulting in the consumption of the other two fuel constituents (CH_4 and C_3H_8).

One of the reactions responsible for formation of ethane is the methyl recombination reaction, $2CH_3 \leftrightarrow C_2H_6$. The formation of the CH_3 radical is possible by H atom abstraction from CH_4.. However, CH_4 decomposition into CH_3 + H at the temperature range under consideration is slow because of the high activation energy required for this reactions and may not result in formation of sufficient amount of CH_3 to contribute to C_2H_6 formation. Furthermore, C_2H_6 can be expected to be undergoing decomposition at the temperatures above 1100 K [80] and thus for the rise of overall concentration of C_2H_6 as seen in the experimental results, the net production rates need to be greater than the consumption rate. It is unlikely that CH_4 decomposition or methyl formation by abstraction alone are responsible for this rise in the ethane concentration.

Since C_3H_8 completely decomposes over 1150 K – 1350 K for most experiments (Figure 7 - Figure 9) it is more likely that C_3H_8 contributes to the intermediates responsible for the formation of C_2H_6 at a rate higher than its decomposition resulting in a net increase in

concentration. One of the reaction paths for C_3H_8 breakdown that can contribute to CH_3 formation is through $C_3H_8 \leftrightarrow CH_3 + C_2H_5$. The reaction rate for this C_3H_8 decomposition if higher than that for $C_2H_6 \leftrightarrow 2CH_3$ [81] it is reasonable to assume that the propane decomposition is contributing to the formation of ethane.

Since time resolved measurements were not conducted in the experiments, it is not possible to infer the cause for this C_2H_6 concentration rise. The predictions from chemical kinetic modeling of the experiments carried out using the chemical kinetic mechanisms mentioned in Table IV could provide an insight into the cause for this phenomenon, however the models were not able to reproduce this rise in the C_2H_6 concentrations. The inability of some of the mechanisms used in this study to predict the species profile for C_2 hydrocarbons during the oxidation of the same NG sample was observed by Shao et al. [7] in a complementary shock tube study using the same natural gas samples for measurement of IDT and time resolved species measurements. Another study was conducted by Shao et al. [82] to measure the rate constant for the $CH_3 + C_2H_6 \leftrightarrow CH_4 + C_2H_5$ reaction which they suspected was responsible for the discrepancy between experimental and model predictions of C_2H_4. The new measured rate constant for this reaction led to a significant improvement in match between model predictions and their experimental data for ARAMCO 2.0 and USC Mech 2. However, this reaction rate constant was temperature independent and applicable only at high temperatures.

The reaction rate parameters for $CH_3 + C_2H_6 \leftrightarrow CH_4 + C_2H_5$ reaction for all the models used in this study were replaced by the rate parameters from Shao et al. [82] as listed in Table V to test if the change in this single set of rate parameters would improve the capability of the chemical kinetic models in estimating the rise in C_2H_6 concentrations observed experimentally in this study. The C_2H_6 species profiles obtained from the experiments were then compared to the

predictions form chemical kinetic models before and after the change in the reaction rate parameters for $CH_3 + C_2H_6 \leftrightarrow CH_4 + C_2H_5$ reaction.

Table V : Original and new reaction rate parameters for the $CH_3 + C_2H_6 \leftrightarrow CH_4 + C_2H_5$ reaction.

Mechanism	Original Rate Parameters			New Rate Parameters		
	A	b	E_a (cal/mol)	A	b	E_e (cal/mol)
CRECK-C1-C3-HT (1412)	5.55×10^{-4}	4.72	-3231.0	3.9×10^{13}	0.0	-16670.0
ARAMCO 3.0	5.55×10^{-4}	4.72	-3231.0			
San Diego Mechanism (2016-12-14)	5.50×10^{-1}	4.0	-8293.5			
USC Mechanism 2.0	6.14×10^{6}	1.74	-10450.0			

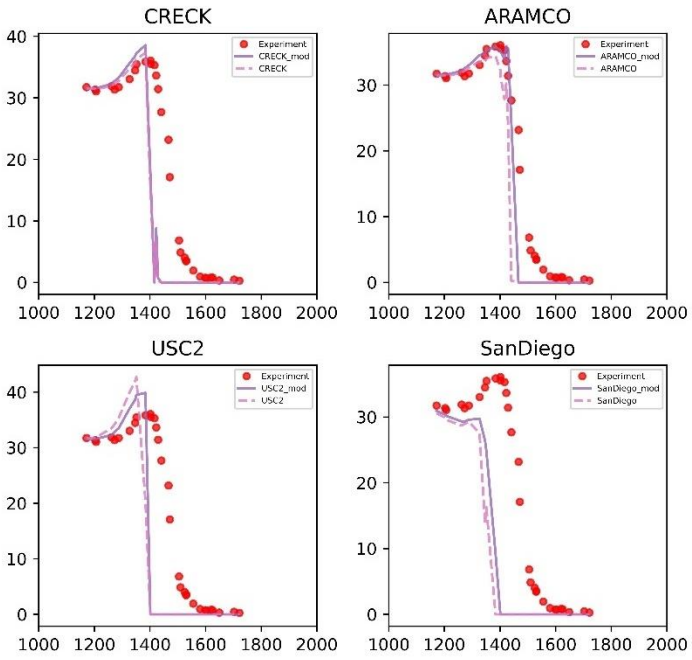

Figure 34 : Comparison between experimental species profiles of C_2H_6 and predictions from all the mechanisms used in this study, before and after changing the rate constants for NG-RF experiment at ~60 atm and φ ~ 0.5. Experiments (red dots), original mechanism (pink dot dashed line), modified mechanism (purple solid line).

Figure 34 and Figure 35 show the comparison between the experimental data and the chemical kinetic model predictions before and after the change in reaction rate parameters. The prediction of the C_2H_6 was partially captured by ARAMCO 3.0 at φ ~ 0.5 even before the change in the reaction rate parameters. The change of the reaction rate parameters did not make any evident

difference in the prediction for ARAMCO 3.0. However, in the case of CRECK and USC Mech 2 the rise was only partially captured. The modification showed only slight improvement in predictions from the CRECK mechanism. In the case of USC Mech 2.0, the change led to a better match between the predicted and the experimental values. The San Diego mechanism prediction comes nowhere close to the experimental value irrespective of the reaction rate constants used.

In the case of the experiments at $\varphi \sim 0.8$, the rise in C_2H_6 concentration observed experimentally was much more gradual with respect to the temperature. The improvement in the match between model predictions and the experiment was much better after the change in reaction rate parameters as evident in Figure 35. The changed reaction rate paramters result in nearly an exact match with experimental values for USC Mech 2.0 and CRECK. In the case of ARAMCO 3.0, the change does not result in a perfect match but however improves the trend of the species profile to better match the experimental observations. Again, the San Diego mechanism did not benefit from this change. The improvement in the predictions from the chemical kinetic models was even better for the stoichiometric conditions as shown in Figure 36. The improvements from model predictions by changing rate constants for the $CH_3 + C_2H_6 \leftrightarrow CH_4 + C_2H_5$ reaction show that the experimentally observed rise in C_2H_6 is not directly related to the previously hypothesized reactions. However, C_3H_8 decomposition results in formation of C_2H_5 through the reaction previously mentioned ($C_3H_8 \leftrightarrow CH_3 + C_2H_5$), so C_3H_8 is at least indirectly related to the formation of C_2H_6 resulting in the rise of ethane concentration over 1150 K – 1450 K. Additionally, the $CH_3 + C_2H_6 \leftrightarrow CH_4 + C_2H_5$ reaction involves the other fuel component – CH_4. If the $CH_3 + C_2H_6 \leftrightarrow CH_4 + C_2H_5$ reaction is indeed primarily responsible for the C_2H_6 concentration rise, then this is an effect of consumption of the other two fuel components (CH_4 and C_3H_8). Based on these observations we can infer that the decomposition of C_3H_8 contributes to the C_2H_5 radical in the

system which reacts with CH_4 resulting in formation of C_2H_6 through the $CH_3 + C_2H_6 \leftrightarrow CH_4 + C_2H_5$ reaction and decomposition of the CH_4 molecule to the CH_3 radical. It is plausible to assume that the CH_3 formed as a result of CH_4 decomposition would undergo recombination to form C_2H_6 further increasing the C_2H_6 concentration in the system.

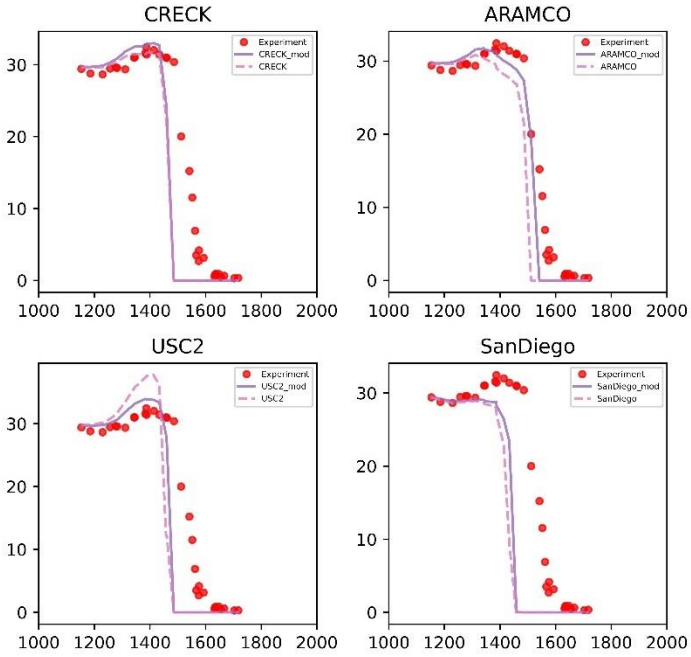

Figure 35 : Comparison between experimental species profiles of C_2H_6 and predictions from all the mechanisms used in this study, before and after changing the rate constants for NG-RF experiment at ~60 atm and φ ~ 0.8. Experiments (red dots), original mechanism (pink dot dashed line), modified mechanism (purple solid line).

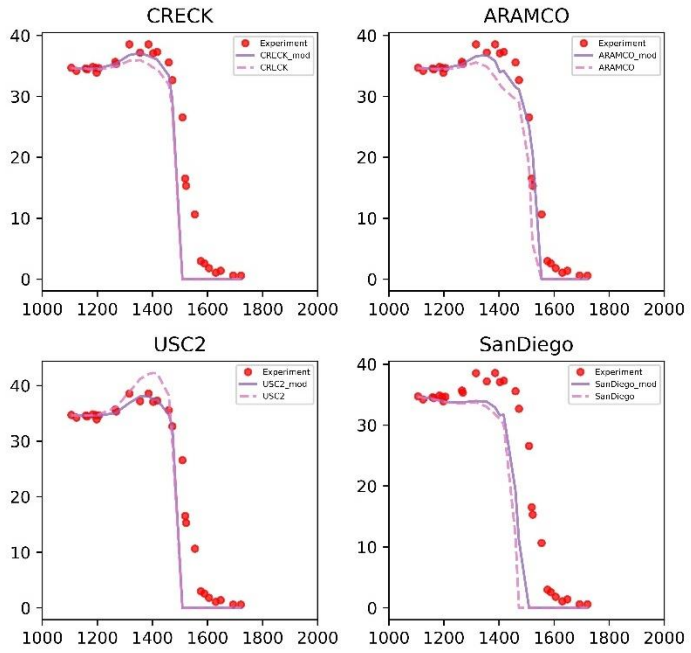

Figure 36 : Comparison between experimental species profiles of C_2H_6 and predictions from all the mechanisms used in this study, before and after changing the rate constants for NG-RF experiment at ~60 atm and φ ~ 1.0. Experiments (red dots), original mechanism (pink dot dashed line), modified mechanism (purple solid line).

2.6 Natural Gas Oxidation Experiments at Nominal Pressure of 240 atm

2.6.1 Experiments

Conventional natural gas applications like domestic heaters, power generation and internal combustion engines do not need combustion at extremely high pressures and the study of natural gas has been limited to conditions relevant to these applications. However, the recent interest in engines which operate at more extreme thermodynamic conditions such as rocket and detonation engines using natural gas has motivated natural gas studies at high pressures. Natural gas oxidation experiments for the reference sample (NG-RF) and the Idaho sample (NG-ID) were repeated at a nominal pressure of 240 atm to study the effect of pressure on the oxidation chemistry of natural gas. Extremely high pressure speciation data for natural gas and small hydrocarbon chemistry is scarce in literature and this study provided additional data for optimizing chemical kinetic mechanism at extreme conditions and to direct focus on the type of additional studies necessary for complete understanding of natural gas oxidation.

In this study, the oxidation of natural gas samples, previously described, was conducted at three different equivalence ratios each - ~0.5, ~1.0, ~2.0 in the shock tube at a nominal pressure of 240 atm over the temperature range of 1100 – 1800 K and a nominal reaction time of 2.5 ms. Figure 37 illustrates the experimental results for all the six experimental sets. Figure 37 shows the comparison between the experimental speciation measurements of different samples at same equivalence ratios as well as compares how speciation for each sample changes with equivalence ratios. In Figure 37 the NG-RF sample experiments are plotted as the solid points while the NG-ID sample experiments are plotted as hollow symbols.

The overall fuel consumption of both the samples follows a quite similar trend at fuel lean and fuel rich conditions, however at near stoichiometric conditions the fuel consumption for NG-RF

sample slows down at about 1400 K and instead a slight rise in the fuel concentration (~30ppm) is observed. This rise in fuel concentration is absent in the experiment with NG-ID sample at the stoichiometric condition. The fuel consumption trends between the two experiments deviate from each other after this increase in fuel concentration for NG-RF. This increase in the fuel concentration is observed only in the methane and ethane consumption and not in the case of propane. This variation is also evident in other species starting at around 1400 K. In the case of ethylene, the rise in fuel concentration at ~1400 K for NG-RF results as a split peak with a valley around ~1400 K. Experiments were repeated at the temperatures around 1400 K to ensure that this peculiar behavior of reference natural gas sample is not an artifact of the experimental variations. Chemical kinetic modeling study of this experimental study, which is described in the upcoming sections, also revealed a sudden bump in the fuel decays as well as a split peak for ethylene. At the lean conditions, the two fuels, NG-RF and NG-ID, show similar behavior for most of the species. The ethylene peaks at temperatures about 50 K from one another with the NG-ID sample having the earlier peak. In addition to the ethylene variation, a plateau was observed in fuel consumption around 1500 K where the fuel decay becomes constant for about 50 K, after which the fuel continues to decay, until it is fully consumed. There were no peculiar behaviors observed at the fuel-rich conditions for either of the experiments.

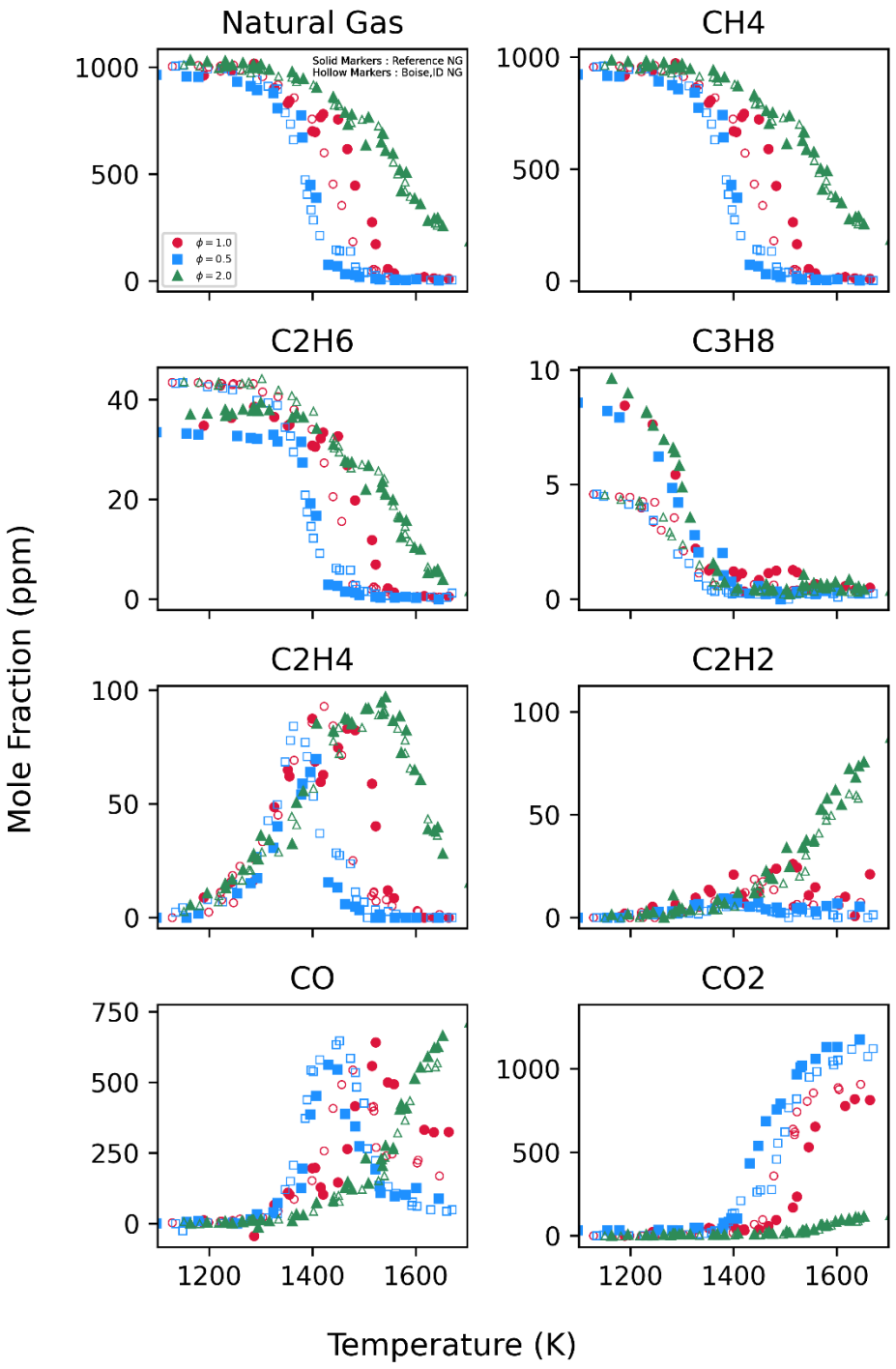

Figure 37 : Experimental speciation results for natural gas experiments at nominal pressure of 240 atm. Species measured for both NG-RF (solid markers) and NG-ID (hollow markers) experiments at φ ~ 0.5 (blue), 1.0(red) and 2.0 (green) shown.

2.6.2 Changing Pressure Approach

Chemical kinetic modeling was conducted for the ~240 atm experimental set using two established chemical kinetic mechanisms – ARAMCO 3.0 and CRECK which are the most detailed mechanisms from all the mechanism used in this study to test the capability of these mechanisms to predict speciation at very high pressures. The chemical modeling was conducted using the constant pressure approach, which was described in section 2.2 and was used for the ~60 atm oxidation experiments. The thermodynamic conditions used for the simulations matched the measured conditions in the shock tube to account for variations between experiments. In addition to the simulation based on the constant pressure, another approach called the changing pressure approach was used [63]. In this approach, the experimentally measured pressure change in the shock tube's reaction region is used to establish the temperature and pressure conditions in the reactor model. The pressure variations and resulting temperature variations are hence accounted for in the simulations.

The changing pressure approach was used for this set of the experiments since at high pressures the non-ideal effects in the shock tube [83] are more pronounced and can result in non-ideal behavior in the shock tube reaction region, usually evident in the form of a gradual pressure rise with time in the reaction region. The effect of non-ideal effects in the HPST has been minimized by the use of optimization techniques [44] that have been tailored for use with HPST based on the previously developed techniques [60,61]. However, unlike at ~60 atm nominal pressures in the shock tube, at elevated pressures (~240 atm) like those used for this experimental study, the effectiveness of these techniques is reduced, and some pressure variations are observed in the pressure measurement for the experiments. Use of the changing pressure approach allows to account for this variation in the simulations and provides a better representation of experimental

conditions when non-idealities are inevitable. The peculiar behavior observed in the speciation measurements for some of the experiments, as previously described, further warrants the need for the changing pressure approach to confirm that the behavior is not an artifact of the pressure variations in the experiment and are a result of chemical kinetic behavior of the system.

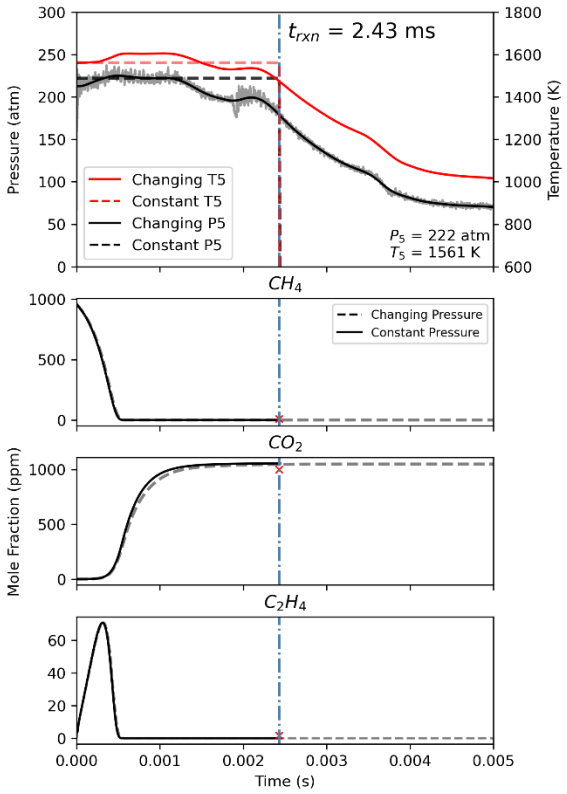

Figure 38 : Comparison between constant pressure and changing pressure approach using ARAMCO 3.0 mechanism for one of the natural gas experiments with minimal non-ideal effect. The experimentally measured value for the species is represented as a red cross ('x'). The illustrated pressure trace is from NG-ID experiment at φ ~ 0.5.

The changing pressure approach has been previously used in some studies, notably Han et al. [63] compared the changing pressure approach and the constant pressure approach to validate the use of the constant pressure approach for simulation of the shock tube experiments and to gauge the benefits of using the changing pressure approach which is computationally intensive compared to the constant pressure approach. They concluded that no significant improvement in simulations was obtained for most cases with large hydrocarbons as the fuel, with the exception

of some cases dealing with polycyclic aromatics (PAH) and that the constant pressure approximation along with the calibrated temperature from chemical thermometer can sufficiently define the experimental conditions for chemical kinetic simulations. However, in this study for several experiments there was a significant improvement in prediction by using changing pressure approach.

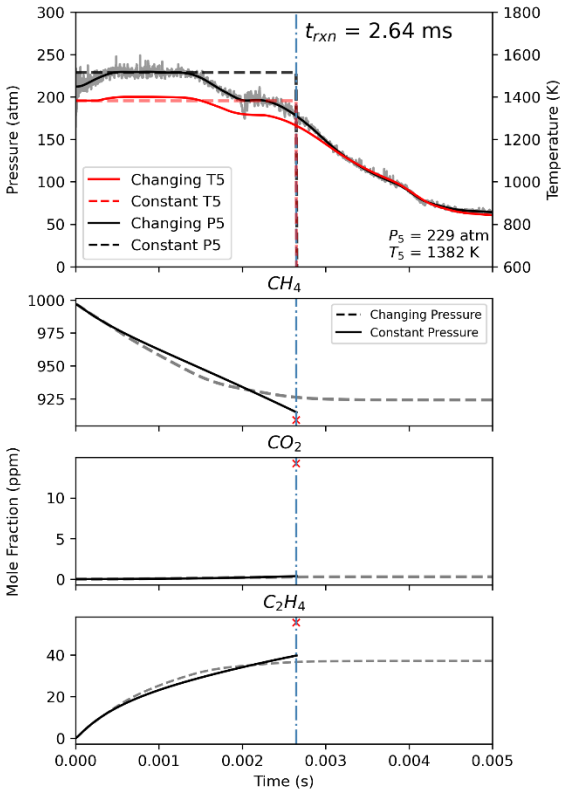

Figure 39 : Comparison between constant pressure and changing pressure approach using ARAMCO 3.0 mechanism for one of the natural gas experiments with non-ideal effects. The experimentally measured value for the species is represented as a red cross ('x'). The illustrated pressure trace is from NG-RF experiment at φ ~ 2.0.

The changing pressure approach was implemented in Cantera using the custom ODE solver available within Cantera to impose the pressure and temperature conditions resulting from the measured pressure trace in the reaction region. The pressure trace used as input considers the arrival of the incident shock at the end wall as the starting point and then follows the measured pressure trace. The assumption that the heating of the test gas by the incident shock does not induce

enough energy for reactions to occur holds true for this approach as well and the reactions are assumed to have started only after the reflected shock heats the test gas downstream.

Figure 38 compares the results from the changing pressure and constant pressure approach for one of the NG-RF experiments at the fuel rich conditions. The experiment had a nominal pressure of 229 atm and a calibrated temperature of 1382 K. The time resolved species yields for three critical species – CH_4 (major fuel component), CO_2 (key oxidation product), C_2H_4 (key pyrolytic decomposition product) from simulations are compared to the measured pressure change in the shock tube and the temperature change calculated from it. The constant pressure and temperature used for the constant pressure approach has also been illustrated using dotted lines. The blue vertical dash dotted line represents the reaction time (t_{rxn}) that is chosen using the 80% cut off rule. The selection of reaction time by the method described in 2.1.1 provides a good estimate of the actual reaction time in the shock tube since in Figure 38 at the reaction time the predicted species concentration in the shock tube is nearly the same from both the simulation approaches and the concentrations remains nearly constant thereafter for the changing pressure simulation suggesting that the expansion wave has sufficiently quenched the system and frozen the chemical reactions. When constant pressure approach is used the species concentration in the system at the end of reaction time is taken as the final value. The complete time history of the species, if the reaction time was not fixed is depicted in Figure 38 and Figure 40 but, for the constant pressure approach the species concentration at 't_{rxn}' is the final concentration of the species compared to the experimental data. These results also show that the improvement in accuracy of prediction from changing pressure approach is minimal when the non-ideal effects in the shock tube are sufficiently mitigated and the constant pressure approach can tolerate some amount of non-ideal behavior, like the initial pressure rise evident in Figure 38.

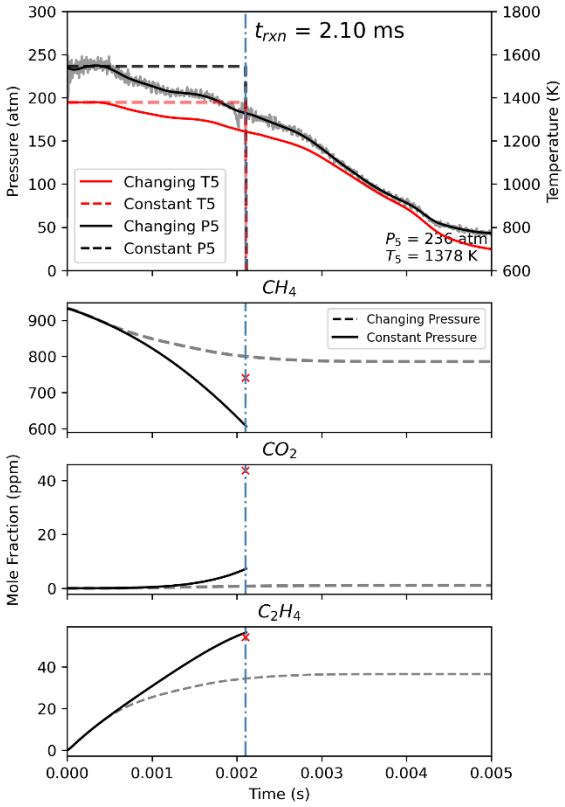

Figure 40 : Comparison between constant pressure and changing pressure approach using ARAMCO 3.0 mechanism for one of the natural gas experiments with non-ideal effects. The experimentally measured value for the species is represented as a red cross ('x'). The illustrated pressure trace is from NG-RF experiment at φ ~ 0.5.

The gain in accuracy by using the changing pressure approach is not always minimal. For experiments displaying a large amount of non-ideal behavior in the form of frequent pressure variations or slower rates of quenching, there can be significant improvement by using the changing pressure approach. Figure 40 illustrates one such experiment for NG-RF at fuel lean conditions with a nominal pressure of 236 atm and calibrated temperature of 1378 K where the non-ideal effects in the shock tube have an adverse effect on the pressure in the reaction region. The sudden rise in pressure is followed by gradual drop in pressure with some wavy behavior prior to the quenching effect by the expansion wave. This pressure variation has resulted in significant deviation of species yields at the end of reaction time (t_{rxn}) for CH_4 and C_2H_4 by about 250 ppm

and 30 ppm, respectively. This difference is nontrivial especially when the species showing the variation are key species responsible for predicting other combustion properties like ignition delay.

Routine comparisons and experiments with near ideal behavior observed in the form of nearly constant pressure in the reaction region until the arrival of the quenching wave, the constant pressure approach can be used to save computational time simplify data management. Thus, the use of the changing pressure approach provides a beneficial tool for diagnostics when the experimental observations significantly deviate from the predictions or large amount of non-ideal effects are evident in the experiments.

2.6.3 Modeling

The experimental measurements of species formed during oxidation of natural gas at different temperatures were compared to predictions from chemical kinetic mechanisms. The predictions were obtained by simulation of the shock tube experiments in Cantera. Both the constant pressure approach using the constant pressure reactor model and changing pressure approach using the custom ODE solver were used and compared. The comparison shows improvements in the match between the experimental observations and the predictions for both mechanisms when using the changing pressure approach. However, the constant pressure approach was found to be within the error region of the experimental temperature uncertainties for most cases and predicted similar trends as the changing pressure approach. Overall, the ARAMCO 3.0 mechanism showed the best match with experimental measurements and in several cases with the changing pressure approach had a nearly exact match, as evident in Figure 41, Figure 43 and Figure 46. The CRECK mechanism followed similar trends as the ARAMCO 3.0 mechanism and the experiment but missed the predictions for key species like C_2H_4, in terms of the temperature by over 100 K for

most experiments, like in Figure 43 and Figure 46. The decay of C_3H_8 was always accurately predicted by both mechanisms irrespective of the simulation approached use.

The simulations for NG-RF at near stoichiometric conditions (Figure 41) when compared to the experimental measurements showed an exceptionally good match with ARAMCO 3.0 mechanism predictions from the changing pressure approach. The decay of methane is exactly captured by the ARAMCO 3.0 predictions with the changing pressure approach, including the sudden rise in the methane mole fraction over the approximate temperature range of 1400 K – 1450 K, which was previously discussed in section 2.6.1. In addition to this, the resulting double peak for C_2H_4 for the same experiment set was well captured by the changing pressure simulation with ARAMCO 3.0 mechanism. Since the double peak behavior is slightly evident in the constant pressure simulation with ARAMCO 3.0 and the CRECK predictions, it can be concluded that this behavior is not an artifact from the experiment but a chemical kinetic effect. However, the changing pressure approach improved the reproduction of the double peak in the simulation suggesting that the behavior is an outcome of the rate constants of reactions resulting in the consumption of methane being sensitive to pressure/temperature variations in the shock tube. The CO predictions show a particularly good match in terms of peak value with experiments. The equilibrium composition of CO, at higher temperatures when there is no change in the concentration of CO with increase in temperature, measured in experiments is 200 ppm larger than that predicted by different mechanisms. This difference factors into a 200 ppm over prediction of CO_2 by the models.

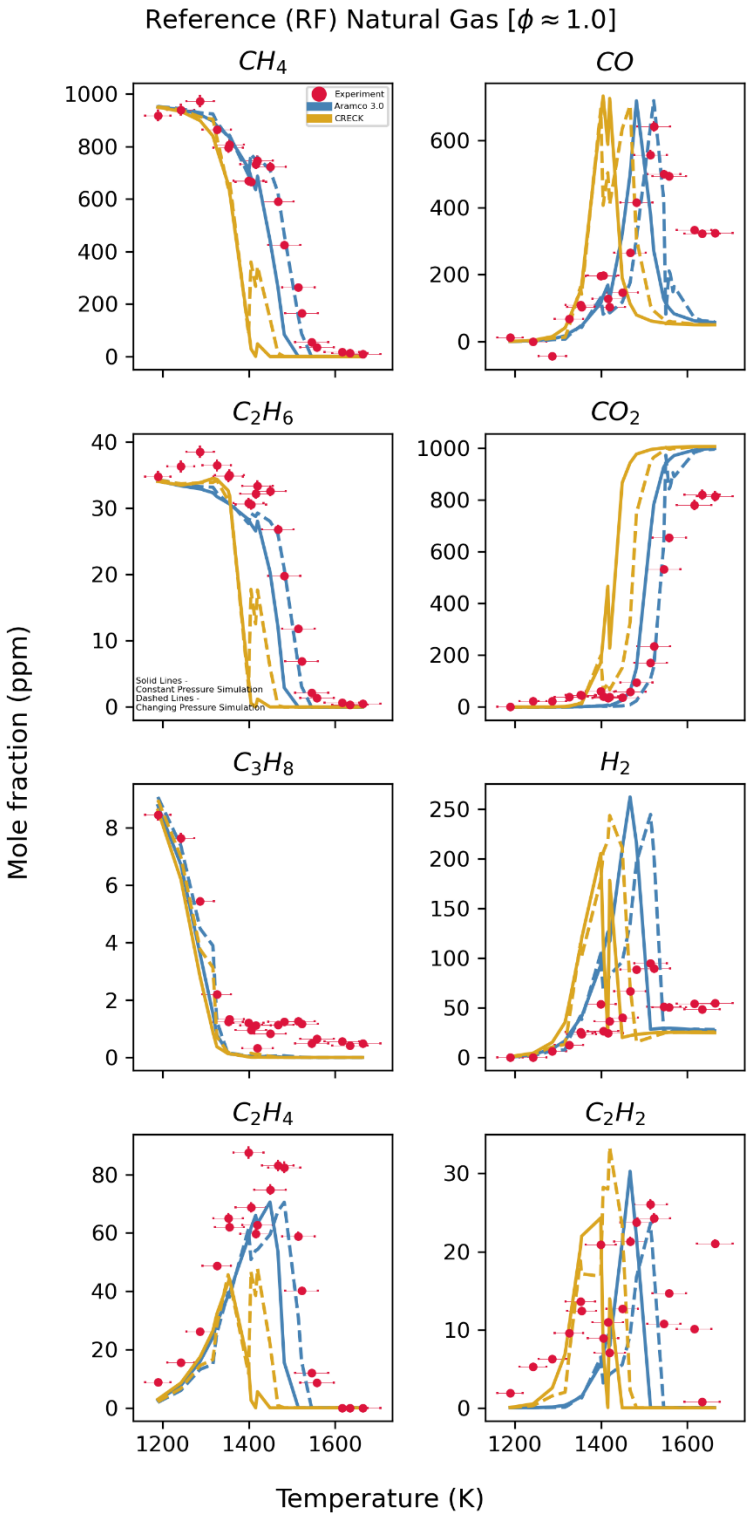

Figure 41 : Comparison between experimental measurements for NG-RF sample at φ ~ 1.0 and model predictions for CRECK (yellow) and ARAMCO 3.0 (blue), using the changing pressure (dashed) and constant pressure (solid) approach.

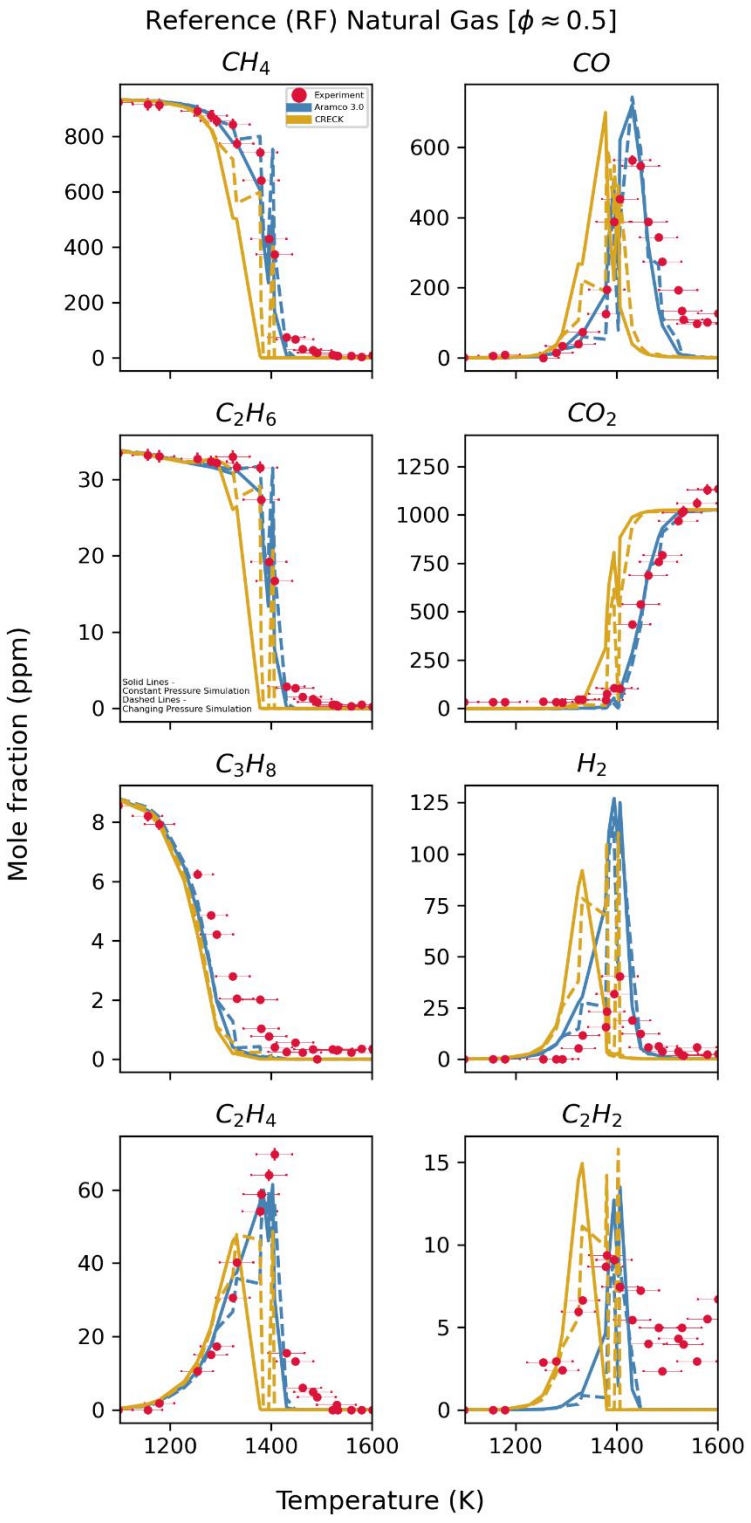

Figure 42 : Comparison between experimental measurements for NG-RF sample at φ ~ 0.5 and model predictions for CRECK (yellow) and ARAMCO 3.0 (blue), using the changing pressure (dashed) and constant pressure (solid) approach.

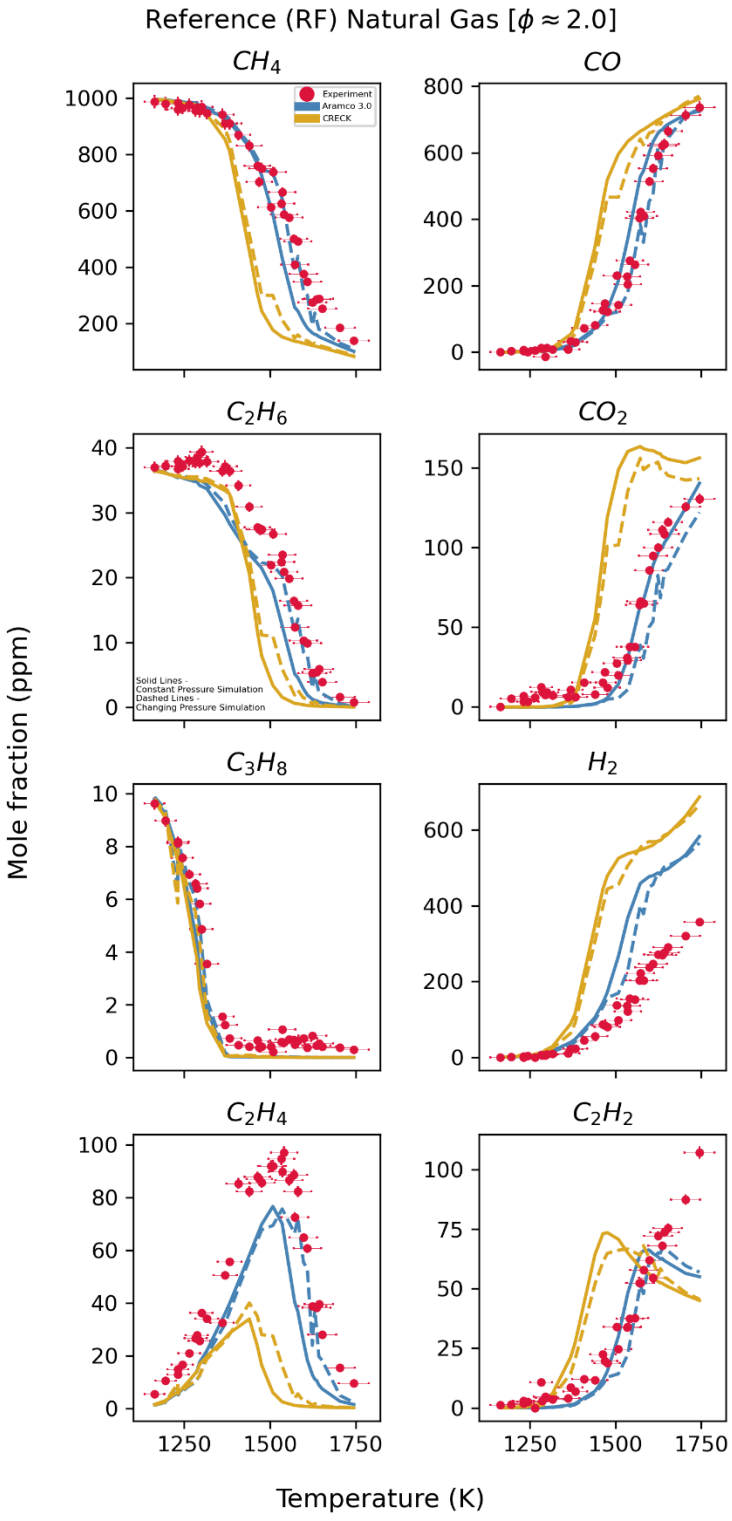

Figure 43: Comparison between experimental measurements for NG-RF sample at φ ~ 2.0 and model predictions for CRECK (yellow) and ARAMCO 3.0 (blue), using the changing pressure (dashed) and constant pressure (solid) approach.

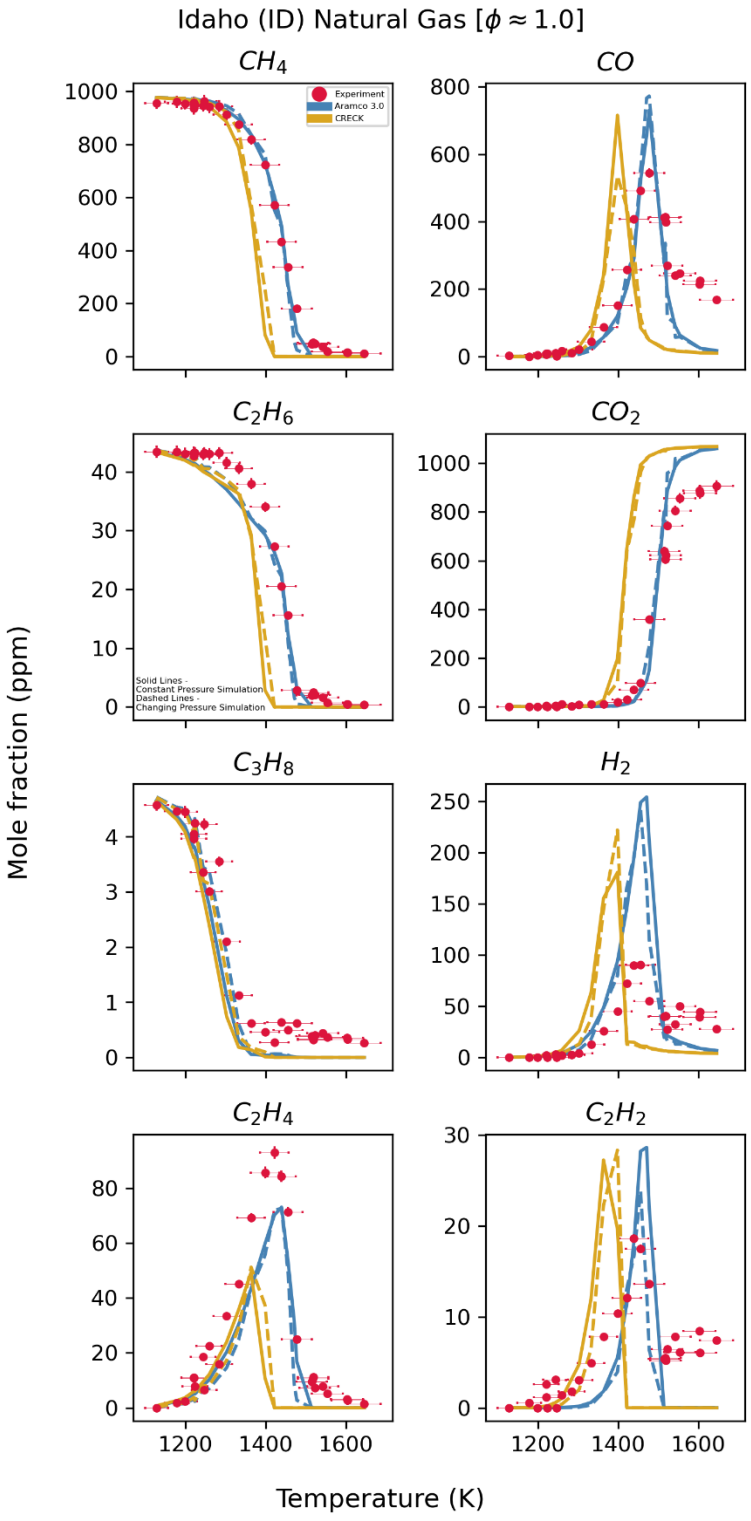

Figure 44 :Comparison between experimental measurements for NG-ID sample at φ ~ 1.0 and model predictions for CRECK (yellow) and ARAMCO 3.0 (blue), using the changing pressure (dashed) and constant pressure (solid) approach.

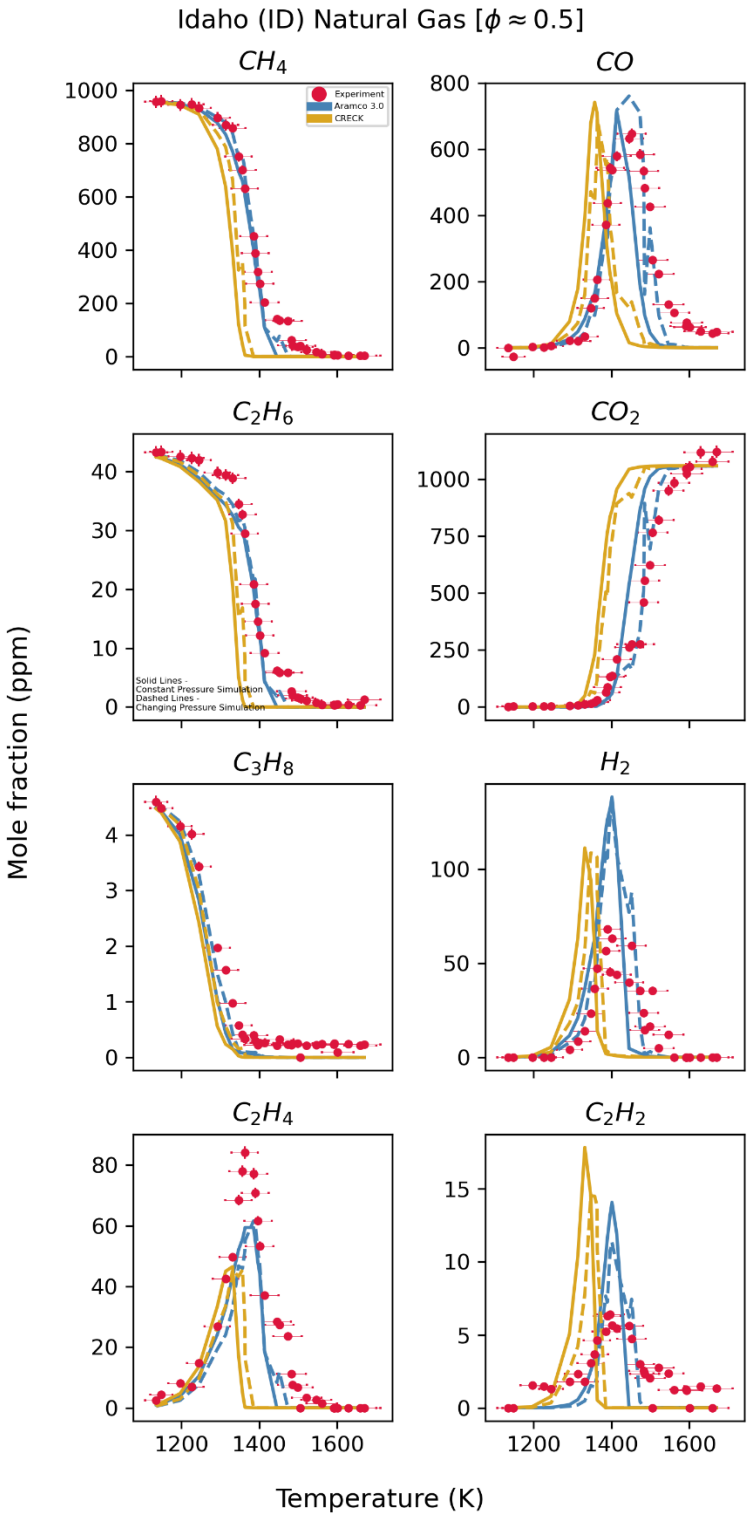

Figure 45 : Comparison between experimental measurements for NG-ID sample at φ ~ 0.5 and model predictions for CRECK (yellow) and ARAMCO 3.0 (blue), using the changing pressure (dashed) and constant pressure (solid) approach.

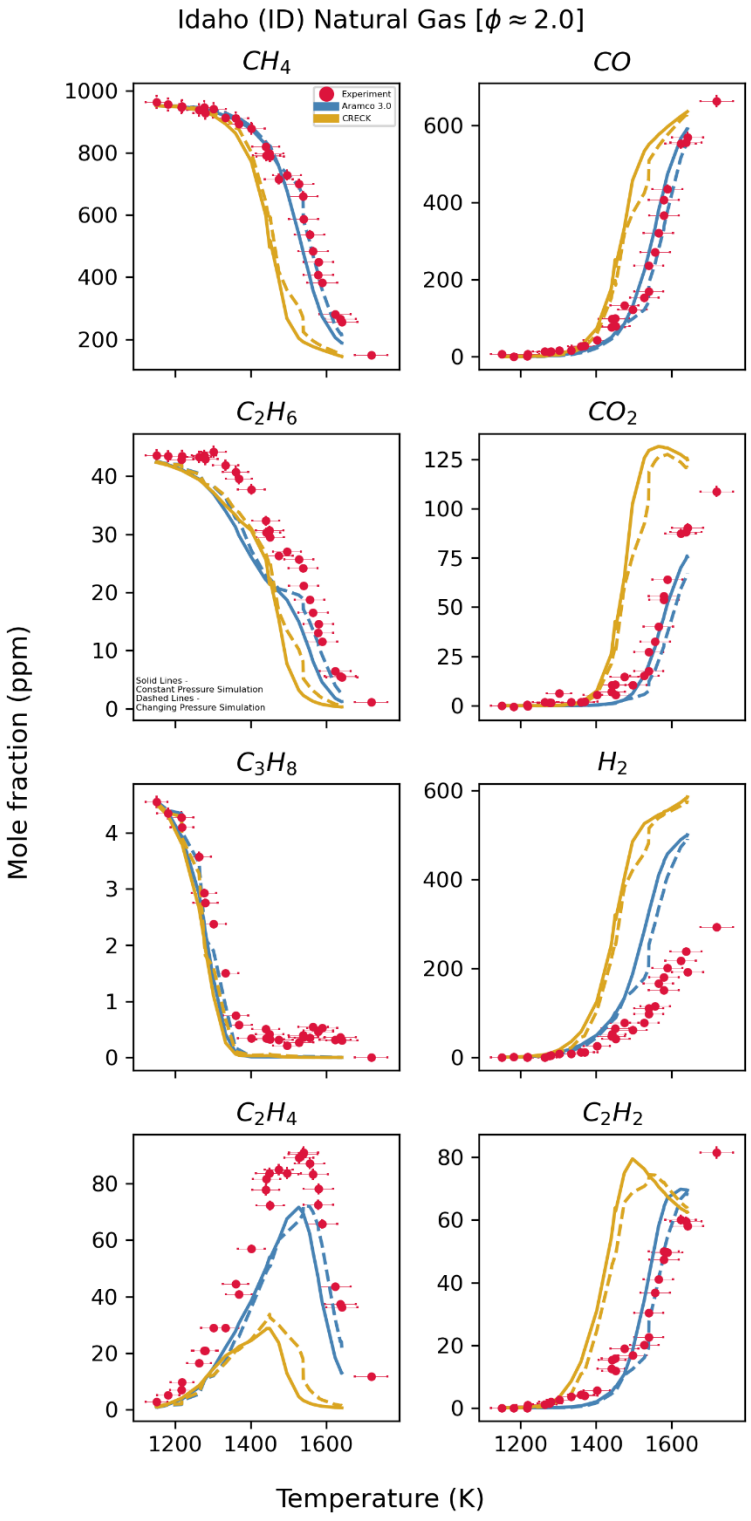

Figure 46 : Comparison between experimental measurements for NG-ID sample at φ ~ 2.0 and model predictions for CRECK (yellow) and ARAMCO 3.0 (blue), using the changing pressure (dashed) and constant pressure (solid) approach.

At the lean conditions (φ ~ 0.5) for the NG-RF sample (Figure 42), the model predictions match the experiments very well. The improvement from using changing pressure approach is minimal for the lean experiment sets. In this experiment set also, experimental measurements show that CO never gets completely consumed after the peak value is obtained but the model predictions show that the value drops down to zero. The models also overpredict the H_2 peak by approximately 50 ppm. In case of the experimental set for NG-RF (Figure 43) at the fuel rich condition (φ ~ 2.0) the ARAMCO 3.0 predictions match the experimental values very well for all the species except for H_2. The CRECK mechanism follows the trend of the experiments but under predicts the fuel consumption and the species formation by over 100 K. The CRECK mechanism also severely under predicts the C_2H_4 formation with the peak value being approximately 60 ppm below the experimental measurements. Overall, for the experiments with NG-RF, ARAMCO 3.0 has done an incredibly good job in predicting speciation and the changing pressure approach has not significantly improved predictions but has helped reproduce peculiar results observed experimentally.

The same comparison was made for the experiment set with NG-ID as the fuel and were compared to model predictions. The ARAMCO 3.0 mechanism again showed a much better match with the experimental results while CRECK mechanism showed a much worse overall match than that for NG-RF experiment sets. In case of NG-ID the discrepancy between CO and CO_2 at temperatures above 1550 K which was observed for NG-RF experiment sets was not present for the fuel lean and the fuel rich conditions. However, a similar trend of greater amount of remaining CO at higher temperatures and a lower maximum CO_2 concentration were observed for the NG-ID experiment set at near stoichiometric conditions (Figure 44). In addition to the differences between CO and CO_2 there was a mismatch between C_2H_6 for all sets, but the trend was captured

by ARAMCO 3.0. The CRECK mechanism under predicted C_2H_4 in these experiment sets also, suggesting that the rate constants for key reactions responsible for consumption of C_2H_6 and formation of C_2H_4 need to be optimized or remeasured.

2.7 Effect of Pressure on Natural Gas Oxidation

The natural gas experiments for the NG-RF and NG-ID at near stoichiometric condition ($\varphi \sim 1.0$) were compared to each other to study the effect of pressure on the oxidation of natural gas. Figure 47 compares the experimental speciation results obtained for NG-RF and NG-ID at pressures of ~60 atm and ~240 atm. It can be observed from the results that at higher pressures the fuel decay starts gradually at a lower temperature of about 1300 K for both the samples, but at ~60 atm the fuel consumption of NG-RF at approximately 1350 K and for NG-ID at approximately 1375 K. The higher pressure does speed up the reaction slightly and results in a smaller temperature range over which the fuel decays to complete consumption. This difference is more pronounced in CO and CO_2 formation where the peaks of CO for the NG-ID sample are about 100 K apart, with the higher pressure experiments having the peak at a lower temperature. In case of CO_2 the starting temperature of formation for NG-ID is similar however the maximum CO_2 value is reached at a higher temperature for the lower pressure experiments.

The formation of CO and CO2 for the NG-RF experiments are remarkably similar at both the pressures. However, the consumption of CH_4 and C_2H_6 is different in trend and the temperature range. In addition to this difference in trend and temperature, the rise in the fuel concentration at approximately 1400 K previously discussed for the NG-RF experiments at ~240 atm is absent in the ~60 atm experimental set. The rise in fuel concentration at ~1400 K observed in ~240 atm experiments results in a 20 K shift between fuel consumption in both the experimental sets while maintaining a similar trend. While there is some pressure effect evident in this comparison, it is

difficult to assess true extent of this effect since the measurements for both the experiments fall within the error bounds of the experiments. The pressure dependent effect observed could be a reflection of the increased effective concentration of the test gas in the reaction region because of the different experimental pressures (~60 atm and ~240 atm).

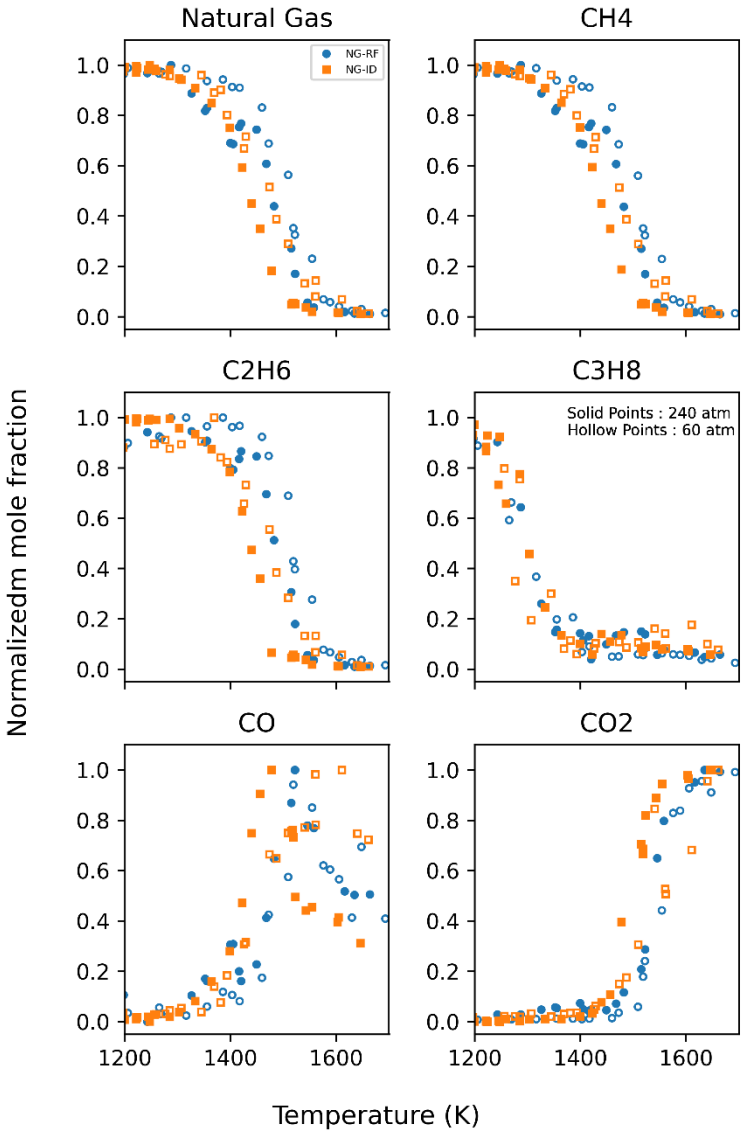

Figure 47 : Comparison of natural gas experiments at ~60 atm (hollow points) and ~240 atm (solid points) for the NG-RF sample (blue circles) and NG-ID sample (orange squares) at φ ~ 1.0. The mole fractions are normalized by the maximum value for each set to eliminate the effect of initial test mixture fuel concentration variation.

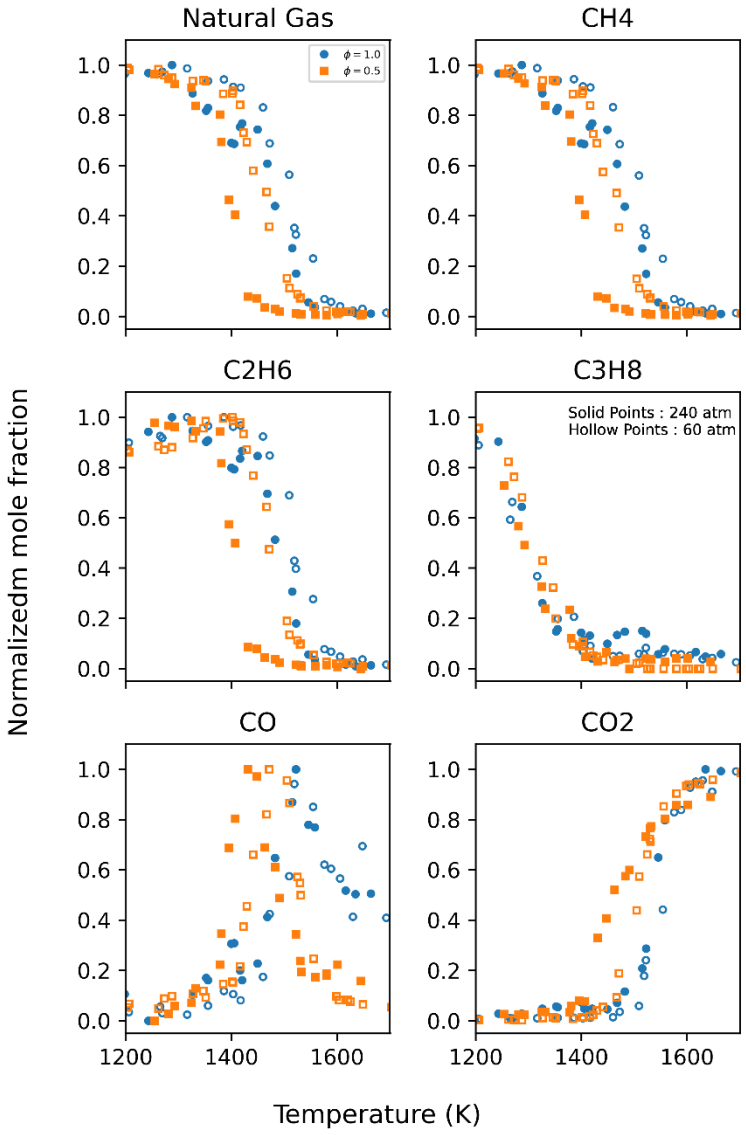

Figure 48 : Comparison of natural gas experiments at ~60 atm (hollow points) and ~240 atm (solid points) for the NG-RF sample at φ ~ 1.0 (blue circles) and φ ~ 0.5 (orange squares). The mole fractions are normalized by the maximum value for each set to eliminate the effect of initial test mixture fuel concentration variation.

A similar comparison was made between the NG-RF experiments at near stoichiometric conditions (φ ~ 1.0) as well as at the fuel lean conditions (φ ~ 0.5) and is illustrated in Figure 48. At the fuel lean conditions, the difference in the speciation results at the two pressures is much greater than that at stoichiometric condition. The fuel decay shows a similar trend however over a temperature range that is approximately 200 K apart. Despite this difference in fuel decay, the CO peaks are not proportionally far apart, just approximately 50 K apart. The difference in CO_2

formation of is also large, with the formation starting at a lower temperature for ~240 atm experiments compared to ~60 atm experiments; however, it is more gradual. This results in having the same temperature at which the maximum concentration of CO_2 is reached. There is a very slight rise in the mole fraction of fuel in the ~240 atm experiments for the lean conditions as well which is absent in the ~60 atm experiments.

2.8 Inference

Natural gas is perceived as a well understood fuel owing to its simple composition. Most chemical kinetic studies and design exercises are conducted with the assumption that the behavior of natural gas is similar to methane and using pure methane as the fuel for studies is sufficient for developing and optimizing chemical kinetic mechanism for use with natural gas applications. The oxidation study of natural gas at high pressures and temperatures reveal that the breakdown paths of natural gas vary based on the true composition of natural gas. The temperature over which the natural gas breaks down also varies from sample to sample even at the same stoichiometric conditions. A small variation in the methane content can significantly affect how the fuel breaks down and which species are formed, such as for the NG-RF and NG-NC whose methane concentration is just 0.3 % by mole fraction apart, with NG-NC having he higher concentration but the fuel decomposition and species formation have significant differences. This difference in the fuel decomposition is not proportional to the methane concentration of natural gas because, in addition to the slight difference in methane, there is an increase of about 0.5% and 0.8% by mole fraction of ethane and propane in NG-RF, respectively. The slight change in the natural constituents show a large effect on its chemical kinetic behavior which needs to be accounted for when designing devices for operation on natural gas, especially in the absence of any fuel specification standards for natural gas.

The modeling results show that the well-established models like those used in this study in their current state cannot capture the effect of compositional variation even when they are highly detailed like ARAMCO 3.0 and CRECK. These models need to be rigorously optimized with different target outputs beyond ignition delay time which is the conventional target property of choice. New experimental measurements or theoretical calculation of rate parameters for reactions responsible for formation of key species would benefit the optimization of these mechanism and development of new models. Shao et al. [82,84] recently conducted measurements of rate constants for two key reactions responsible for decomposition of the major components of natural gas – methane and ethane and showed the significant improvement in model predictions for some of the models used in this study. While this justifies the need for new rate constant measurements for optimizing the chemical kinetic mechanisms, these measurements are limited to high temperature and have provided a non-temperature dependent reaction rate which may not be accurate over a larger temperature range. Additional studies [85–87] have been done which have validated measurements of rate parameters for small hydrocarbon chemistry using molecular theory and provide a larger range over which the rate constants are applicable.

In addition to the inability of the mechanism to capture the composition effects very well they also lacked in predicting the fuel decomposition and species formation at the fuel-lean conditions while doing an excellent job at the fuel-rich conditions. For the fuel lean conditions, the match among the models themselves was found to be minimal. Rate of progress analyses showed that there is significant involvement of oxygenated hydrocarbon chemistry, particularly formaldehyde (HCHO) reactions in the breakdown of natural gas under oxidation conditions. Additional studies with a focus on studying the oxygenated hydrocarbon reactions in natural gas decomposition would be beneficial. The study of oxygenated hydrocarbon reactions will also

benefit the understanding of low temperature chemical kinetics as well as the ignition behavior of natural gas.

The study of natural gas at high pressures and temperature, relevant to high power applications like propulsion and detonation engines makes it clear that natural gas despite its simple composition has a complex oxidation reaction mechanism. The compositional variation of natural gas is easily manageable for conventional applications like domestic heating and cooking as well as internal combustion engines. However, propulsion engines are sensitive to this variation and smaller time scales over which combustion events occur in these engines make it difficult for devices to respond to the combustion anomalies arising from the natural gas composition variation when in operation.

Research studies focusing on small hydrocarbons (C_1-C_4) and their mixtures (binary, ternary, and tertiary) are necessary to understand the effect of chemical composition on the combustion behaviors. Studies targeting speciation in shock tubes or flow reactors would benefit testing the chemical kinetic models which are used for prediction of ignition delay times. Experimental measurements of ignition delay times can complement these studies to anchor the reaction mechanism. In addition to the species measurements of these mixtures, key reaction rates need to be evaluated individually and confirmed with experimental data from studies focusing on real natural gas samples. Several studies have been conducted in the past [8,40] and some newer studies [7,25,37,38,41] however, large scale research campaigns are necessary for making natural gas a promising fuel of choice for high power applications.

2.9 Future Work

2.9.1 Low Temperatures and Long Reaction Times

This study was conducted at very high temperatures which are relevant to propulsion devices. Reactions at high temperatures occur very fast and details about intermediate reactions involved in breakdown of natural gas cannot be easily studied. The ROP analysis discussed in previous sections pointed out some key reactions that need to be addressed, including the reactions involving formaldehyde. Formaldehyde is a key species, especially to study the low temperature ignition of fuels. Formaldehyde is highly elusive especially at high temperatures where it undergoes rapid breakdown making high temperature studies inappropriate for studying its reactions. Thus, low temperature studies of natural gas would be beneficial to study intermediate reactions involving species that are short lived at high temperatures and their effect on the final dissociation products of natural gas and validate chemical kinetic mechanisms. The low temperature and long reaction time studies can also help study if there is an NTC (negative temperature coefficient) regime of natural gas.

Since natural gas breakdown occurs through reactions that have a high activation energy barriers, long reaction times are required to overcome these barriers at low temperatures. Shock tube experiments with reaction times greater than 8 ms would be needed to study the chemistry at low temperature in the range of around 800 K, where the reactions progress slowly making it easy to study the intermediate reaction chemistry for natural gas breakdown during combustion. A new driver section extension for the UIC-HPST has been designed, manufactured, and installed which is capable of theoretically creating a reaction time in the shock tube of up to 12 ms without any gas dynamic optimizations to facilitate low temperature chemical kinetic studies of fuels. The use of the optimization techniques [44] can further increase the reaction time by over three times. The

extension increases the length of the driver of the current HPST by another 200 inches converting it to UIC-HPSTex (Figure 49), having a total driver length of 260 inches. The extension includes a 180° bent section connected to the original driver section; the bend makes the rest of the section parallel to the shock tube extending along the driven section of the shock tube. The bend is necessary to overcome space restrictions and accounts for 60 inches of the driver length.

Figure 49 : UIC-HPSTex

The straight section of the driver extension is comprised of three separate pieces of 40 inches each and one piece of 20 inches making a total length of 140 inches. This section is made in pieces to allow changing the overall length of driver section to adjust the reaction time to a required value. Additional resolution in drive length can be achieved by using internal cylindrical plugs. The design of the linear sections of the extension matches the design of the driven section pieces to allow interchangeability between them. This interchangeability allows for extending the driver length further however at the loss of driven section length. In addition to this feature, the driven section of the UIC-HPSTex uses the maximum designed length for UIC-HPST which is 180 inches. The bore of the extension is one inch to limit the gas consumption and simplify manufacturing. The original driver of the shock tube is maintained at two inches, with an option to operate with a one inch bore using a modified area reducing insert [44].

The coupler designed to connect the current driver to the extension converts the buttress threaded end of the original driver into a flange set-up necessary for connecting the bent section. Two versions of the coupler are designed and manufactured. The version ‘A’ is used when the complete driver section is operated with a one inch bore diameter (with area reducing insert [44]) and the version ‘C’ allows taking advantage of the convergent shock tube set-up for obtaining higher experiment pressures and temperatures by connecting the two inch bore of the original driver section to the one inch extension using a convergent nozzle within the coupler. All the parts of the extension were hydraulically tested at the manufacturing location to a pressure of 14,000 psi. The end caps used for hydraulic testing were the same end-caps which serve as the driver end wall. Detailed design drawings of the UIC-HPSTex are provided in Appendix E.

In addition to the extension of the HPST, additional components were redesigned and replaced to make way for the extension as well as to update the system to current technology

standards. A new fuel mixing rig was designed and procured to replace the old mixing rig. The new mixing rig was moved to a satellite location from the shock and its dependence on the auxiliary systems of the shock tube was eliminated. The high pressure gas storage tanks for the driver gas of the HPST were moved away from the shock tube and secured to a wall to make space for the extension. The vacuum system of the HPST was also replaced with a new system, including an Edwards RV12 rotary vane vacuum pump for the driver and an Edwards RV5 rotary vane pump coupled to Edwards nEXT-85 turbo molecular pump for the driven section.

The shock tube operating computer was upgraded to the latest software and hardware to make the system capable of incorporating anticipated future projects easily. The new DAQ computer uses a National Instruments PCIe-6376 for high speed data acquisition of the pressure sensors and National Instruments PCIe-6351 for low speed data acquisition and valve control. The National Instruments BNC 2090A serves as the I/O interface for both the cards (one each). Additional details related to the extension have been provided within the Appendix F.

With the extended high pressure shock tube, low temperature experiments (~750 K) with long reaction time for the natural gas samples studied in this work would provide an insight into how the composition variation affects the combustion of natural gas at operating conditions of internal combustion engines used for automotive and stationary applications like power plants. It will also provide the chemical kinetic data necessary to more effectively model natural gas powered engines. Additionally, binary mixtures of methane and ethane at different ratios could be analyzed to understand the effect of chemical compositions on the chemical kinetics of the natural gas.

2.9.2 Multi Time Point Sampling Valve

The study of individual reactions and their rate constants would benefit from time resolved measurements in mixtures that are extremely sensitive to the reaction [69,82,84,88]. To track target species, time resolved studies usually require optical methods which are challenging to perform at high pressures such as those considered in this study. Thus, capability to extract test samples from the shock tube at different time points within the experiment and analyzing with gas chromatography would provide an alternative method of obtaining time resolved speciation data for the experiment. This approach would provide the time histories of several species in the experiment and result in a large comprehensive data set over different times and temperatures for a given pressure. The motivation for this approach has inspired some studies [89] in the past but no large scale advancement is made in this approach.

This technique when applied to the UIC-HPSTex can take advantage of long reaction times to obtain several samples over the reaction time and analyze them in parallel using gas chromatography. A new sampling valve system would need to be developed which is capable of swift operation (over μs) to extract samples and introduce them into the sampling system. The valve would need to be fast as well as be capable of diverting paths of different samples into different sampling lines. Each of the sampling lines would need to then be connected to one gas chromatograph where the sample would be analyzed, without the need for storage. The current upgrades to the analytical instruments will allow using four dedicated GCs for the multi-sampling analysis and if each GC is used to analyze one sample, then four samples at four time points per experiment can be analyzed. The number of time points can be doubled by analyzing each sample using only one detector of the GC which would allow two samples to be analyzed in a single GC simultaneously,

To move towards this approach, two new gas chromatographs have been procured, each equipped with three detectors (2xFID and 1xTCD), which expand the current two GC setup to a four GC setup. The current GCs have also been upgraded, making one GC a replica of the new GCs with three detectors (2xFID and 1xTCD) while the other GC is now equipped with an MSD in addition to the FID and the TCD. The complete set-up is capable of operating as a single time point system which samples at the end of reaction with all GCs in series or it can be modified to allow multiple time point sampling where several test samples at different time points within the experiment can be analyzed by different GCs simultaneously. Some preliminary concept designs and discussion have been completed. However significant work is necessary to study the feasibility of this system and to investigate technology already available to assist the development of this valve.

3 CHEMICAL FUNCTIONAL GROUP ANALYSIS OF FUELS

3.1 Background

Jet fuels are hydrocarbon based fuels used in jet engines and gas turbine engines. Jet fuels are complex multicomponent mixtures of hydrocarbons extracted from crude oil in the kerosene band. The physical and chemical properties of the fuels vary since jet fuels are obtained from crude oil. Their absolute composition can vary from source to source and batch to batch. The fuels are further categorized within jet fuels based on the physical and chemical properties, based on guidelines from standard specifications such as the MIL-STD-3004D [90]. The specifications provide a range for critical fuel properties that a fuel needs to be qualified for, for use in different applications. Thus, fuels categorized for a single application can have a difference in the property if they are within the specified range. In addition to the hydrocarbon based fuels several synthetic fuels like ATJ [91] have been developed in the interest of sustainability which possess the necessary properties to be qualified as jet fuels.

The large variations in the fuel properties make interoperability a challenge. The U.S. military has taken up the single fuel forward initiative to tackle this problem and move towards using a single fuel for all applications. The use of a single fuel simplifies logistics of fuel sourcing, transportation, and testing. The U.S. Army has taken this initiative one step further towards developing a multi-fuel capable engine which can operate using any fuel, rather than a single fuel, available at the point of application. The multi-fuel capable engine will allow fuel independence in the battlefield as well as remote installations where delivering military spec fuel is challenging. The initial goal of this engine is to be able to power unmanned aerial vehicles (UAS) used by the U.S. Army. This study is a part of the large Versatile Tactical Power and Propulsion (VICTOR) project moving towards developing this technology. The primary goal at hand is to develop an on-

board fuel property sensor capable of sensing the fuel's ignition properties in real time and can provide feedback to the engine control system to adjust engine operating parameters to ensure uninterrupted operation of the engine. The sensor is expected to use optical or spectroscopic technology to measure the composition of the fuel being fed to the engine and predict the ignition property of the fuel. The ignition property predictions will be based on data science and machine learning techniques. However, to ensure that the predictions are not purely statistical a chemically informed prediction model needs to be developed and this study will provide the necessary fuel composition analysis to determine the fuel properties based on fuel chemistry.

The jet fuels as previously mentioned contain thousands of components which can vary from batch to batch despite being fit for use. Detailed analysis of the composition of a fuel requires time consuming and sophisticated laboratory methods such as liquid chromatography (LC), gas chromatography (GC), Nuclear Magnetic Resonance Spectroscopy (NMR) and Mass Spectrometry (MS) which cannot be used on the fly for a portable sensor. Hence the composition of the fuel needs to be defined using general quantities which can be easily measured or estimated using optical and spectroscopic methods. Chemical functional groups (CFG) composition of the fuels can be used as general description of the fuel which can be used to predict its properties. This is possible since the chemical functional group is a part of a molecule which imparts specific properties to the molecule independent of the presence of any other functional group in the molecule. Hence the properties of a molecule can be directly predicted with the knowledge of its functional group composition. In addition, when the fuel is analyzed using optical methods specific spectral features are observed based on the chemical functional groups present in the fuel. This makes chemical functional groups a viable choice the measurement of general fuel composition.

Several studies have successfully attempted correlating and predicting the fuel properties using functional groups [46,47,92].

In this study, the evaluation of chemical functional groups of fuels and mixtures is done using GCxGC TOF-MS/FID analysis of the fuel. The GCxGC analysis allows superior separation of the constituents of a fuel and provides the species composition of the fuels which can be used directly to predict different physical and chemical fuel properties like molecular weight and H-C ratio or can be converted in chemical functional group based composition which can be used to predict additional combustion properties like ignition delay.

In this study, a GCxGC method was developed which uses a TOF-MS to identify the components of the fuel after separation using GCxGC, while a flame ionization detector is used for quantification of each component because of its high sensitivity to hydrocarbons and carbon counting ability [70]. A new software package *S2FG* (species-to-functional-group) was developed to convert the quantified species composition into quantified chemical functional group composition. This software uses the fragmenting algorithm from the literature [54] to split the molecules into the number of chemical functional group fragments. The input to the code is a list of chemical species in the fuel or mixture and their weight fractions, which is then converted into the chemical function group weight fractions in the fuel as the output. The composition is provided in the form of the UNIFAC groups [53], which were the chemical functional groups of choice in this study. The UNIFAC chemical functional groups chosen [84] are proven groups capable of predicting various fuel/mixture properties. The UNIFAC groups were developed to predict the activity coefficients of liquid mixtures based on their UNIFAC group composition to adjust for real liquid behavior. These groups have further found use to predict other fuel properties as well [45].

The analysis developed as a part of this study was applied to eleven different jet fuels to estimate their chemical functional group (UNIFAC) compositions. These functional group data are provided for development of prediction models using machine learning as well as to correlate the spectral features from optical methods like FTIR, Raman Spectroscopy, NDIR, ATR, and NIR. In addition to real fuels, *S2FG* was used to compute the chemical functional group composition of various jet fuel surrogates from the literature as well as custom mixtures prepared in the laboratory to develop a large database of mixtures having known functional group composition and measured ignition properties like derived cetane number (DCN).

3.2 Challenges

Over the course of this work several challenges were faced in obtaining the chemical functional group based composition of real jet fuels as well as developing the technique that is applicable to most jet fuels. The challenges were an outcome of practical problems, technical limitations, and scientific possibilities because of which some compromises and assumptions were necessary. This section discusses the challenges and the measures taken to overcome them.

- The GCxGC analysis is two dimensional gas chromatographic (GC) analysis which allows the separation of constituents of analyte in two dimensions. In the second dimension, the co-eluting peaks of the primary separation (first dimension) are separated out and thus highly similar isomers can be separated easily. This is greatly beneficial for fuel analysis. However, the manufacturer specified column configuration (HP-5MS + DB-10MS) had a limited separation in the second dimension resulting in basically a one dimensional chromatogram with the exception of polycyclic aromatics which were well separated in the second dimensions. This was in part because of the remarkably similar nature of the constituents of the jet fuel as well

as the fact that both the columns had non-polar phases. This configuration resulted in lack of separation in the second dimension.

- The approach for this analysis was simultaneous measurement using the TOF-MS detector as well as the FID so that analytes can be identified using the TOF-MS signal while the FID response can be used to quantify each analyte to obtain the complete quantified fuel composition. However, for the success of this approach to happen, the two chromatograms for either detector need to perfectly match so that one to one comparisons of detected species can be made so that the TOF-MS chromatogram can be used as an identification template over the FID chromatogram. However, in the initial configuration even with equivalent column lengths to both detectors and identical flow parameters, the chromatograms were significantly skewed since both detectors operate in different environments (vacuum for the TOF-MS and atmospheric pressure for the FID) which results in overall change in the flow pattern through the columns. Additionally, the FID is susceptible to atmospheric pressure variation while the TOF-MS is maintained at the same degree of vacuum. The ideal way to adjust for this is to manually adjust the column length by trial and error to obtain the necessary equivalent column configuration. This is a resource intensive task and does not guarantee the perfect outcome. Another way to account for this chromatogram mismatch is by adjusting carrier gas flow across the columns to align the chromatograms. This method was the one used. The flows were adjusted by trial and error and informed calculation based on multiple runs at different flow rates. This flow adjustment combined with the minor adjustments to the chromatogram offsets within the acquisition software were done to obtain a near exact match. However, some region of chromatograms still suffered from mismatch.

- The use of mass spectrometry for identification of unknown analytes in a compound is well established and successful. However, in the case of hydrocarbon fuels the constituents of the fuel are almost all hydrocarbons and many have the same masses. Additionally, there are a large number of isomers present in the fuel which have nearly the same mass fragmentation pattern resulting in misidentifications across the TOF-MS chromatograms. This misidentification and the similar spectra for neighboring peaks also affected the peak deconvolution feature that the acquisition software used to separate the partially or fully overlapping peaks even after second dimension separation. The result was several misidentified analytes, some of which could be manually corrected but not all. This is a technical limitation of using mass spectrometry and a scientific barrier since many of the fuel components have the same identification masses. The only way to overcome this problem is to use the classification approach in which groups with like constituents of the fuel are grouped together as one single compound. This approach provides a particularly good estimate of the hydrocarbon composition of the fuel. However, it introduces a large uncertainty in functional group composition estimation.
- The quantification of the analytes using the FID requires calibration of the response of the detector using calibration mixtures having known composition which can then be applied to analysis of unknown samples (explained in detail in section 2.1.3). This is not possible when the sample under question consists of thousands of species and the goal is to try to quantify as many components as possible. The ability of the FID to respond linearly to the number of carbon atoms [70] in each molecule makes possible estimating its response to each species with high accuracy without rigorous calibration. The effective carbon number (ECN) approach was used to estimate the weight fractions of different species/classifications in the fuels.

3.3 GCxGC Method Development

In GCxGC analysis, unlike one dimensional gas chromatography explained in section 2.1.3 the separation occurs in two dimensions, or to put it simply, twice. Two columns are connected in series. The first column is called the primary column and the second column is called the secondary column. In the primary column, the first stage separation occurs where the sample being analyzed is separated into several parts or packages. Each package has the tendency to have multiple compounds within itself and all of them would enter the detector as one if the secondary column is not used. The detector response would be an aggregate of all the compounds in the package. The packages separated in the primary column (first dimension) then enter the secondary column (second dimension) for further separation of the individual compounds from within the package before being introduced into the detector. The introduction of the compounds from primary column to the secondary column is controlled, either thermally or by flow, and this is called modulation. The separation in the secondary column is a result of the column as well as the modulation. Modulation plays a key role in successfully separating all the compounds at the end of the secondary column as well as prevents the doubling up of the compounds in the secondary column, which negates the separation in the primary column.

In this study, the LECO Corporations Pegasus 4D system was used which has a time-of-flight mass spectrometer (TOF-MS) coupled to a modified Agilent Technologies 7890A GC. The 7890A GC's oven is used as the primary oven in which the primary column sits while LECO Corporation has added the modulator and the secondary oven within the primary oven as shown in Figure 50. The secondary oven is used to house the secondary column and is usually maintained at a temperature above that of the primary oven. The columns exit the secondary oven and enter the detector. A thermal modulation system is used in Pegasus 4D to control the introduction of

exiting analytes from primary column into the secondary column. Two sets of identical column setups connected to each detector were used. The column configuration and the paths are shown in Figure 50.

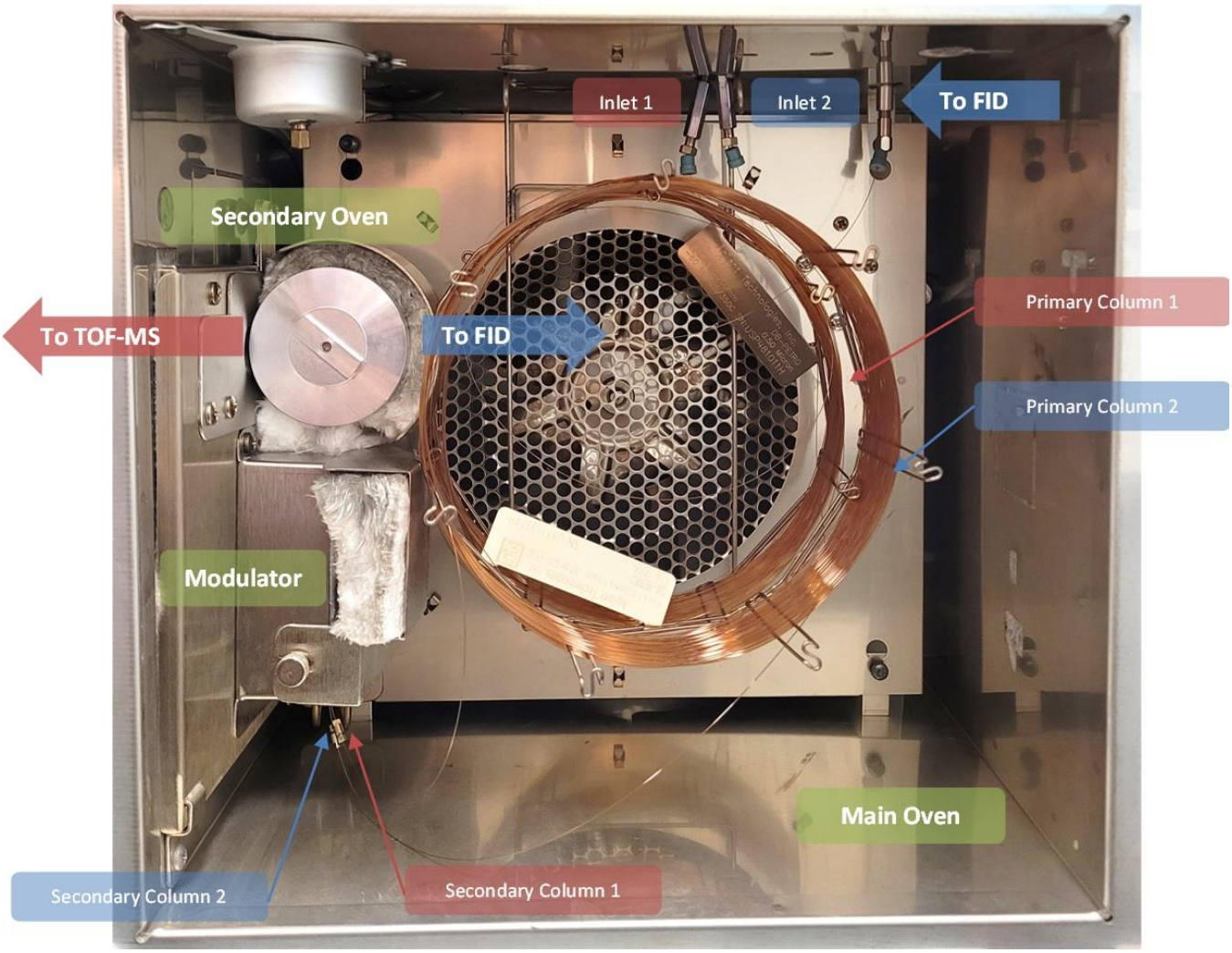

Figure 50 : Interior of the Leco Pegasus 4D system gas chromatograph, showing various columns and their flow path to their respective detectors. FID – blue and TOF-MS – red.

3.3.1 Thermal Modulation

The thermally modulated system uses two pairs of hot and cold jets which spray hot or cold nitrogen, respectively. The jets spray on the starting section of the secondary column. The cold jet freezes (cryo-focuses) the mobile phase and causes it to stop while the hot jet heats the frozen flow

back to the initial temperature allowing the flow to continue. The sequence of jet operation is hot-cold-cold-hot. This is done to ensure that any analyte that evades the first jet is trapped within the second jet and moves to the detector sequentially. The selection of various parameters of the modulation system are key and have significant effect on the results of the analysis.

The time taken for the complete modulation activity to occur is called the modulation time. This time is the maximum time that an analyte can take to exit the secondary column and hence provides the upper bound for the second dimensions. One modulation activity is one cycle of hot and cold jets for each stage. The modulation can be adjusted in the acquisition system by changing the total modulation time and the opening time for hot and cold jets (modulation period). Thus, the total modulation time becomes double of the sum of hot jet open time and cold jet open time. This value is critical since this value needs to exceed the time that any expected analyte would take to exit the secondary column after exiting the modulator. For this study, the critical species were the polycyclic aromatics (PAH) like naphthalene and biphenyls which took the longest time to reach the detector while in the secondary column. The duration for which the hot and cold jets operate are also critical to ensure that all the analytes from the primary column are cryo-focused (cold jet) and sufficient heat (hot-jet) is provided to ensure they become mobile and move ahead. As a rule of thumb, the hot jet time should always be greater than the cold jet time to ensure complete evaporation of all the cryo-focused analytes. In addition to the timing, the temperature of the modulator can be controlled. The modulator temperature controls the hot jet temperature, while the cold jet temperature is fixed since the cold jet uses liquid nitrogen (LN2). The analysis is usually not sensitive to the modulator jet temperature if the temperature and the open timing of the hot jet provide sufficient heating to evaporate the frozen flow. When short modulation times are used, a higher modulator temperature is favorable to ensure sufficient heat can be provided,

especially when analytes with high boiling points are anticipated in the test mixture. However, care needs to be taken when selecting the jet temperature to ensure that the maximum method temperature of the jet does not exceed the column maximum temperature. When short modulation times are used, there is a chance of having peak wrap around if the analytes do not get enough time to exit the secondary column before the next modulation activity begins. Wrap around results in the analyte mixing into the next analyte package from the primary column and results in the peak showing up in unexpected parts of the chromatogram. In this study, an 8 second modulation time was chosen to ensure that all the high boiling point analytes like PAH have sufficient time to reach the detector and avoid the wrap around.

3.3.2 Sample Preparation and Introduction

The analysis of fuels in this study is done using gas phase samples of the fuel, diluted in helium, and introduced into the GC column using gas phase head space valves. The headspace valves are connected to an in-house designed sampling system [71,72] capable of directly handling gas phase samples as well as preparing samples using liquid injections. This sampling system is also capable of introducing test sample from experimental apparatus like shock tube directly to analyze combustion products from chemical kinetic experiments.

The sampling system uses a high accuracy temperature controlled MKS 631D capacitance manometer capable of reading pressures of up to 1000 torr with accuracy of 0.5% of the reading. The pressure measurements are used while preparing the mixtures from liquid injection and to measure the head pressure on the valve before injecting the sample into the columns. The complete system uses Sulfinert® coated lines and is heated to 150°C to prevent the loss of sample components by adsorption and absorption in lines and condensation. The sample is transferred to a fixed volume sample loop (250 µL) connected to gas phase valves, from which it is introduced

into the columns. Measurement of the injection head pressure allows normalization of acquired data between runs, since sample volume is constant.

In this study the test mixtures were prepared in the sampling system and the concentrations were maintained using partial pressures. Liquid fuel (3 µL) was injected using a high accuracy zero dead volume glass syringe in a 150cc stainless steel Sulfinert® coated vessel at vacuum to ensure complete vaporization. Then the vessel was filled with helium as the dilutant to ~950 torr and allowed to homogenize for ~20 minutes. The sample is then transferred to the sample loops of the gas phase valves and injected into the column after the injection pressure is stabilized.

3.3.3 Hydrocarbon Classification

Hydrocarbons in general are organic compounds that consist of hydrogen and carbon only, but these can be categorized based on their primary structures like straight chains, rings, aromaticity, or type of bonding between carbon atoms – single bonds, double bonds, and triple bonds. These categories can be sub-divided based on the sub-structure of the molecule which have similar properties and behaviors. Figure 51 illustrates the overall categorization of hydrocarbons. When the subcategories of hydrocarbons are combined with the size of the molecule (number of carbon atoms), they can be further divided into hydrocarbon group-types [93] or hydrocarbon classifications. Hydrocarbons in each classification possess similar properties and usually have the similar molecular weight with slight variations in other physical and chemical properties like density, vapor pressure and boiling point.

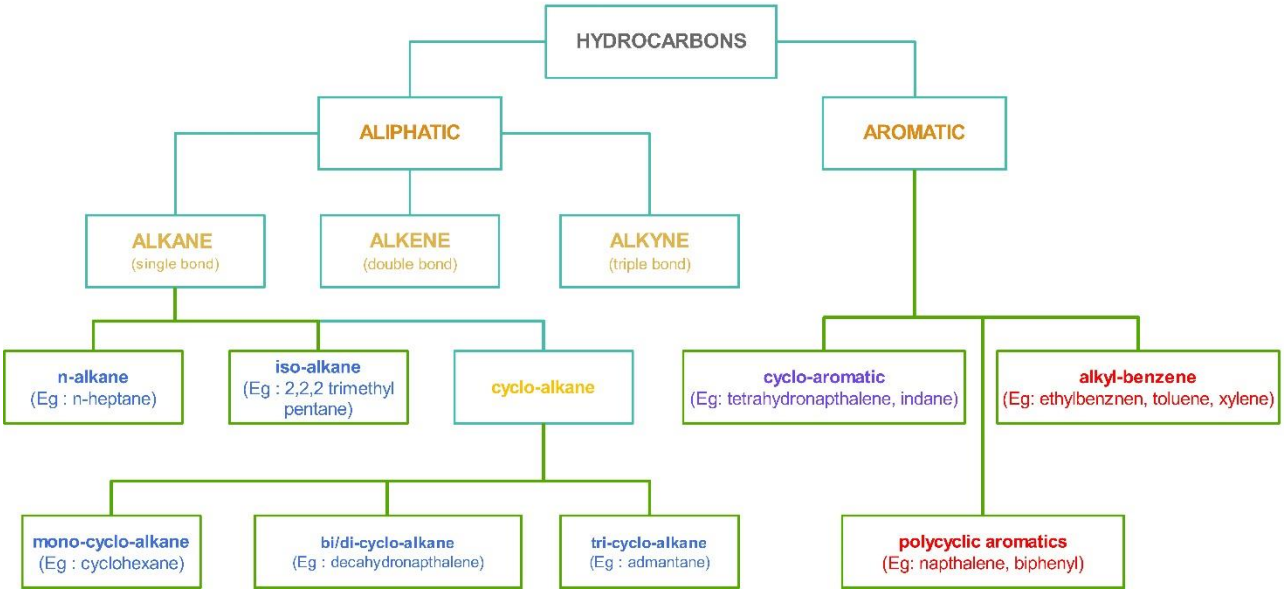

Figure 51 : Chart showing hydrocarbon categories and subcategories. Green boxes represent the classification groups used in this analysis

The ability to combine large number of hydrocarbons into a single classification simplifies the analysis of the fuels while providing the necessary details to compute physical and chemical properties. It is this property that allows eliminating the problem of misidentifications based on fragmentation patterns from the TOF-MS since each classification can be represented as a characteristic species. The separation of the hydrocarbons in a mixture or fuel during chromatographic analysis also follow these classifications and elute in groups pertaining to the classifications. This behavior results in a two dimensional chromatogram that can be easily divided into regions that pertain to the different classifications and accurate quantification of each classification can be carried out without the need for knowing the exact species composition within the classifications. Figure 52 shows a schematic of a two dimensional chromatogram of a jet fuel, F-24, with regions for different classifications annotated. Along the first dimension retention time (x-axis) the size of the molecule increases. The second dimension retention time (y-axis) splits the different subcategories of hydrocarbons for the same molecule size. The two dimensional

chromatograms can be split along the y-axis into hydrocarbon subcategories (Figure 52) and can be split along the x-axis based on the molecule size to provide classification regions. The TOF-MS signal can be used to identify the species, to obtain the boundaries of each classification and to check for any non-conforming hydrocarbons that elute outside the expected region.

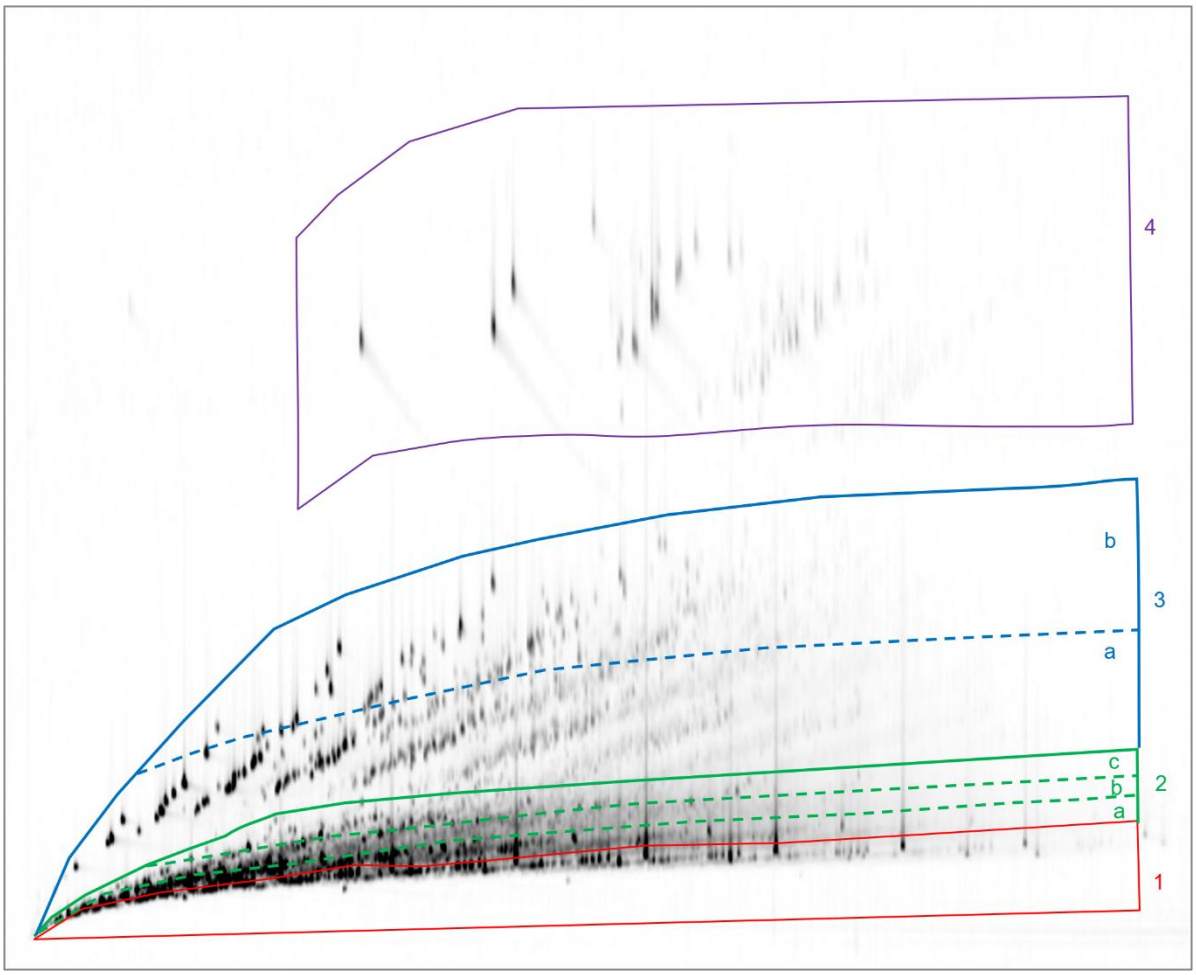

Figure 52 : A typical two dimensional chromatogram depicting various classification regions in jet fuel analysis, classifications, x-axis – 1D retention item (min) and y-axis – 2D retention time (sec). Region 1: n-paraffin and iso-paraffin; Region 2 : cycloparaffin (a : monocycloparaffins, b : dicycloparaffins, c : tricycloparaffins) ; Region 3 : alkylbenzene (a : monoaromatic, b : cycloaromatic) ; Region 4 : diaromatics. This particular chromatogram corresponds to analysis of F-24 fuel.

The TOF-MS identifications from analysis of a reference jet fuel, F24, allowed dividing the chromatogram vertically based on the molecule sizes. Evident patterns are visible within the chromatogram that assist making this division. For instance, the normal alkane for a molecular

size (defined by the number of carbon atoms in the molecule throughout this study unless otherwise specified) usually appears as the last species in the region, followed by iso-alkanes for the next molecular size at the baseline value of second dimension time. The other hydrocarbon families span along the second dimension. Compounds with same molecular size usually remain within the vertical region boundary, with few exceptions. Figure 53 shows the vertical regions superimposed on the reference fuel analysis chromatogram showing the approximate vertical regions based on molecule size.

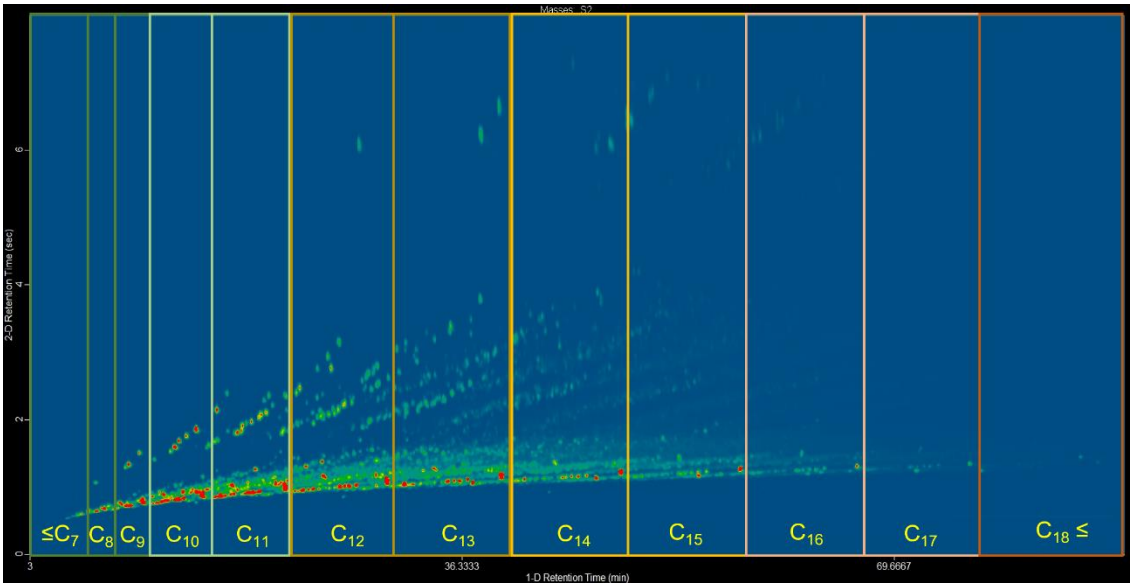

Figure 53 : Two dimensional chromatogram from reference fuel – F-24 analysis showing approximate vertical division of the chromatogram based on molecule size.

The various regions corresponding to the hydrocarbon family and the molecule size (number of carbon atoms) were marked on the FID chromatogram using the 'Classifications' tool of ChromaTOF® software. Identifications by the TOF-MS were used to identify the boundaries of the regions. The classification tool of the ChromaTOF® software allows for calculation of total area of all the peaks under each region to provide the total area of a classification or percentage area of the classification. This area can then be used to quantify the hydrocarbon classification

present in the fuel. A classification template was prepared for the gas chromatographic method using a real fuel (F-24) analysis as reference to anchor the different classification regions on the chromatogram using the TOF-MS identifications, marking all the classifications that are listed within Table VI. Templates can be directly applied within the software to analyze any sample and area (or area percent) under each classification can be obtained.

Table VI provides the list of different classification regions within the template along with their molecular weights and atomic composition details. The correction factor used for quantification, explained in section 3.3.4, is also provide in Table VI. The various classifications follow a naming convention which is a combination of the primary structure of the molecule along with the substructure size (in carbon numbers). For example, Benzene+C03 stands for a molecule having a mono aromatic ring (benzene) as the primary structure with three additional carbons attached to the primary structure making it a C_9 hydrocarbon. These species can be present with multiple substitutions like in the case of 1,3,5 trimethylbenzene (C_9H_{12}) or single substitution of long hydrocarbon chains like n-propyl benzene (C_9H_{12}). Similarly, the Naphthalene groups represent a primary structure having two fused aromatic rings (diaromatic or bi-aromatic) along with the substitution carbon atoms present in the molecule. In case of alkanes, the classifications are formed as n-alkanes which consist of a single normal alkane that represents that group and iso-alkanes which are comprised of all the branched isomers of the alkane having the carbon number as stated within the classification name. Cycloparaffins are either split based on the primary structure plus the substituting carbon numbers or as a single family of cycloparaffins with the total carbon atoms in the molecule like C15-tricyclo. This is done when too many different primary structures such as endo-cyclo, exo-cyclo, and spiro can exist for the same family while no clear

positional difference on the chromatogram is evident to separate the classification regions. Figure 54 shows the various classification regions listed in Table VI within the chromatogram.

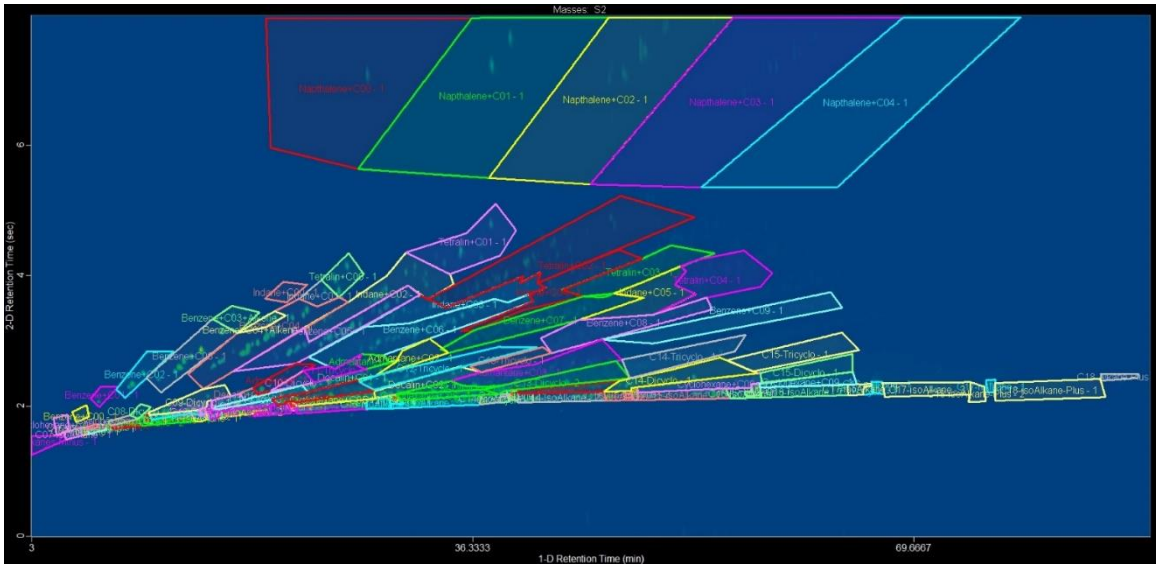

Figure 54 : Two dimensional chromatogram from GCxGC analysis of F-24 illustrating he different classification regions.

When building the template (Figure 54) as previously explained some compounds were found to be present outside the expected region of the chromatograms. These compounds were highly branched paraffins, one of the most branched isomers of the corresponding alkanes. These branched paraffins can elute with compounds that are up to two carbons smaller than the branched paraffin itself and would be counted with all the compounds in the smaller size classification. This elution can result in quantification errors for the two classifications which can create errors with the estimation of fuel properties as well as conversion of the composition into chemical functional group composition. These compounds are usually present at a second dimension retention time earlier than that for normal alkane and can be identified within the chromatogram and confirmed with the TOF-MS based identifications. An additional region was set-up within the template to accommodate this effect consisting of the peaks in which would contribute to the total area in the correct classification while being present in a different classification. One of the most significant

compounds that had this behavior was 2,2,4,6,6 pentamethyl heptane (PMH) which eluted at the same first dimension retention time as n-decane (C_{10}) and contributed to the C10-nAlkane classification region. This compound was critical since the jet fuels tested in this study had large amounts of PMH. The second most critical species having this behavior was 2,2,4,4,6,8,8 heptamethyl nonane (HMN) which eluted within the iso-pentadecane (C_{15}) classifications. ATJ was the only fuel that was significantly affected by the shift of HMN into a different classification.

Table VI : List of classifications used in this study with F-24 as the reference fuel for building the template.

Sr No.	***Classification Name***	***C***	***H***	***Class MW (g/mol)***	***Correction Factor***
1	Napthalene+C00	10	8	128.16	1.07
2	Napthalene+C01	11	10	142.19	1.08
3	Napthalene+C02	12	12	156.21	1.08
4	Napthalene+C03	13	14	170.24	1.09
5	Napthalene+C04	14	16	184.27	1.10
6	Indane+C00	9	10	118.17	1.09
7	Indane+C01	10	12	132.19	1.10
8	Tetralin+C00	10	12	132.19	1.10
9	Indane+C02	11	14	146.22	1.11
10	Tetralin+C01	11	14	146.22	1.11
11	Indane+C03	12	16	160.25	1.11
12	Tetralin+C02	12	16	160.25	1.11
13	Tetralin+C03	13	18	174.27	1.12
14	Benzene+C00	6	6	78.11	1.08
15	Benzene+C01	7	8	92.13	1.10
16	Benzene+C02	8	10	106.16	1.10
17	Benzene+C03	9	12	120.18	1.11
18	Benzene+C04	10	14	134.21	1.12
19	Benzene+C03+Alkene	9	11	119.18	1.10
20	Benzene+C04+Alkene	10	13	133.20	1.11
21	Benzene+C05	11	16	148.24	1.12
22	Benzene+C06	12	18	162.26	1.13
23	Indane+C04	13	18	174.27	1.12
24	Benzene+C07	13	20	176.29	1.13
25	Indane+C05	14	20	188.30	1.12
26	Tetralin+C04	14	20	188.30	1.12
27	C16-nAlkane	16	34	226.43	1.18
28	C15-nAlkane	15	32	212.40	1.18
29	C14-nAlkane	14	30	198.38	1.18

30	C13-nAlkane	13	28	184.35	1.18
31	C12-nAlkane	12	26	170.32	1.18
32	C11-nAlkane	11	24	156.30	1.18
33	C10-nAlkane	10	22	142.27	1.18
34	C09-nAlkane	9	20	128.25	1.19
35	C08-nAlkane	8	18	114.22	1.19
36	C07-nAlkane	7	16	100.20	1.19
37	C06-Alkanes-Minus	6	14	86.17	1.20
38	C17-nAlkane	17	36	240.45	1.18
39	C18-Alkane-Plus	18	38	254.48	1.18
40	Decalin+C00	10	18	138.24	1.15
41	Decalin+C01	11	20	152.27	1.15
42	Decalin+C02	12	22	166.29	1.15
43	Benzene+C08	14	22	190.31	1.13
44	Benzene+C09	15	24	204.34	1.13
45	Adamantane	10	16	136.23	1.13
46	Adamantane+C01	11	18	150.25	1.14
47	Adamantane+C02	12	20	164.28	1.14
48	Adamantane+C03	13	22	178.30	1.14
49	C16-Cyclo	16	32	224.41	1.17
50	C15-Cyclo	15	30	210.39	1.17
51	C14-Cyclo	14	28	196.36	1.17
52	C13-Cyclo	13	26	182.33	1.17
53	C18-isoAlkane-Plus	18	38	254.48	1.18
54	C07-isoAlkane	7	16	100.20	1.19
55	C08-isoAlkane	8	18	114.22	1.19
56	C09-isoAlkane	9	20	128.25	1.19
57	C10-isoAlkane	10	22	142.27	1.18
58	C11-isoAlkane	11	24	156.30	1.18
59	C12-isoAlkane	12	26	170.32	1.18
60	C13-isoAlkane	13	28	184.35	1.18
61	C14-isoAlkane	14	30	198.38	1.18
62	C15-isoAlkane	15	32	212.40	1.18
63	C16-isoAlkane	16	34	226.43	1.18
64	C17-isoAlkane	17	36	240.45	1.18
65	Cyclohexane+C08	15	30	210.39	1.17
66	Cyclohexane+C09	14	28	196.36	1.17
67	Cyclohexane+C07	13	26	182.33	1.17
68	Cyclohexane+C06	12	24	168.31	1.17
69	Cyclohexane+C05	11	22	154.28	1.17
70	Cyclohexane+C04	10	20	140.26	1.17
71	Cyclohexane+C03	9	18	126.23	1.17
72	Cyclohexane+C02	8	16	112.21	1.17
73	Cyclohexane+C01	7	14	98.18	1.17

74	C08-Dicyclo	8	14	110.19	1.15
75	C09-Dicyclo	9	16	124.22	1.15
76	C10-Dicyclo	10	18	138.24	1.15
77	C11-Dicyclo	11	20	152.27	1.15
78	C12-Dicyclo	12	22	166.29	1.15
79	C13-Dicyclo	13	24	180.32	1.15
80	C14-Dicyclo	14	26	194.34	1.16
81	C11-Tricyclo	11	18	150.25	1.14
82	C12-Tricyclo	12	20	164.28	1.14
83	C14-Tricyclo	13	22	178.30	1.14
84	C13-Tricyclo	14	24	192.33	1.14
85	C15-Dicyclo	15	26	206.35	1.15
86	C15-Tricyclo	16	28	220.38	1.15
87	Unclassified	16	16	208.29	1.08

3.3.4 Quantification

Gas chromatography can be used for quantitative analysis of composition of test sample if appropriate detectors are used. The detector response needs to be calibrated as previously explained for accurate quantitative measurements, especially when trace species analysis is conducted. However, when using the FID for quantitative analysis of a complete mixture, its unique ability to respond linearly with respect to number of carbons [70] in molecule can be exploited to carryout quantitative analysis without the need for calibrations. Since the detector responds proportionally to the molecule size. The area under the peaks in the chromatogram for different species is proportional to the weight fraction of the compounds in the test sample when detected using FID. This is also true for the classifications since the classifications are grouped by the molecule size. The total area under the peak for all the constituent peaks of a classification is directly proportional to the weight of the classification within the test sample. Since most of the fuels tested have unknown molecular weights and densities, the exact weight of the sample injected cannot be known, hence we can use the fraction of the total area that is within the classification to obtain the weight fraction of the classification within the sample being analyzed. Thus, calculation

of area percentage under each peak(s) will provide the weight fraction of that compound/classification in the test sample.

Theoretically the response of each species in the sample is proportional to the weight fraction of the species, making the area percent under each peak equal to the weight percent of the species in the complete sample. However, in practice the effect of unmatching number of hydrogen atoms between species despite the same carbon count affects the detector response. A small correction factor can then be applied to the area percent to convert it into the accurate weight fractions. The correction factor, greater than one, is the ratio of total molecular weight of the compound/classification to the total molecular weight contribution of carbon atoms for that compound/classification which is mathematically represented by equation 3.1. The correction factors for various classifications are provided within Table VI.

$$Correction\ Factor_{compound} = \frac{(Number\ of\ Carbon\ Atoms \times 12.01) + ((Number\ of\ Hydrogen\ Atoms \times 1.01)}{(Number\ of\ Carbon\ Atoms \times 12.01)} \quad 3.1$$

The area percentage obtained from the analysis for all the classifications was multiplied with the correction factor calculated from the equation 3.1. The obtained value provides the effective area percent of the classification. The total of the effective area percent can be expected to be higher by approximately 15%, making the total peak area percent ~115% when adjusted by the correction factors to include the effect of hydrogen in the molecule. The exact weight fraction can then be calculated by dividing the effective area percentage of each compound/classification by the total effective area percentage, which normalizes the total effective area percentage back to 100%. The final value obtained is equal to the weight percent of each classification in the test sample. Once the weight percentage is known, this can be converted into the mole fractions if necessary.

The weight fractions can be converted to the number of moles of the classification per gram of the compound. The sum over all classifications provides the number of moles of test sample per gram. This number can be converted to obtain the average molecular weight of the test sample. Similar calculations can be carried out by splitting the number of moles into number of moles of carbon and hydrogen if the number of carbon atoms and hydrogen atoms in the classification constituents is known. Table VI lists the number of carbon and hydrogen atoms for each classification in this study. The sum over their respective atoms provides the molar contribution of that atom to a mole of the sample and this value can be used to back-calculate the average molecular formula for the sample along with the H-C ratio. The final composition of various classifications in all the fuels tested along with the number of carbon and hydrogen atoms is provided within Appendix H.

3.3.5 Post Processing

An input file comprising of the weight fraction of various compounds/classification is generated for conversion of the fuel composition to chemical functional group composition. The input file is a '.csv' file with three columns having, IUPAC (International Union of Pure and Applied Chemistry) name, the SMILES representation of the compound or the representative species for the classification, and the weight fraction. This input file is used by the software *S2FG*, explained in section 3.5 for further processing.

The preparation of input file when analysis uses exact constituent compounds is straightforward, however when hydrocarbon classifications are used it requires allotting a representative species to each classification whose SMILES format will be used for further processing. Since classifications are comprised of several constituents which are isomers, the chosen species should be able to represent the structures within the classification well. Several

assumptions need to be made when selecting this species, particularly for larger hydrocarbons which have several isomers. If accurate identifications are available from the TOF-MS for various constituent species, then an appropriate species can be easily chosen. The choice of this species affects the computation of the functional group composition of the fuel because the functional group composition is dependent on the structure of the molecule and selection of incorrect species can result in large errors. In this study however, species that would represent the classification well was not evident from the TOF-MS analysis and hence the species representing two extreme scenarios were chosen. As a result, the range over which the different functional group composition can exist in a fuel has been provided.

3.4 GCxGC Analysis of Fuels

The developed GCxGC analysis method was used to analyze eleven different jet fuels. The tested fuels included four distillate jet fuels - Jet A1 [94], Jet A2 [94], Jet A3 [94] and F-24 [33,34], six specialty jet fuels - CN30 [95], CN35 [95], CN40 [95], CN45 [95], CN50 [95], and CN55 [95], and one synthetic jet fuel – ATJ [91,96]. The specialty fuels (referred to as CN fuels in this study) are fuels prepared to obtain a specific cetane number (CN) rating. Cetane number is a non-dimensional rating assigned to the fuels based on their auto-ignition capability under standard conditions and is widely used to specify fuels for compression-ignition engines. The cetane number is measured using the CFR engine. However, a modern instrument called the Ignition Quality Tester (IQT) has been developed to estimate the cetane number of fuels based on their ignition delay time at specified conditions. This value is called the derive cetane number (DCN) and is prescribed by the ASTM D6890 standard. The four distillate fuels tested in this study include a commercial jet fuel (Jet A2 – Jet A), and three military spec jet fuels (Jet A1 – JP-8, Jet A3 – JP-5 and F-24). The properties of these jet fuels have been specified by military standards and are

expected to be similar to each other, with the exception of JP-5. This study reveals the compositional differences between these fuels, despite their similar physical properties. Another jet fuel considered in this study has been synthetically prepared from bio-derived butanol [96]. This fuel is called ATJ (alcohol-to-jet), and it meets the military specification for use as a jet fuel. Nevertheless, it is mainly composed of iso-paraffins [91] and has an extremely low cetane rating.[82]

Table VII : Estimated molecular weight, hydrogen and carbon percentage and average molecular formula for fuels analyzed.

Sr No.	***Fuel***	***Molecular Weight (g/mol)***	***H %***	***C %***	***Average Molecular Formula***
1	Jet A1 (JP-8 POSF10264)	149.7	14.0	86.0	$C_{10.7}H_{20.8}$
2	Jet A2 (Jet A POSF10325)	158.6	13.6	86.4	$C_{11.4}H_{21.3}$
3	Jet A3 (JP-5 POSF10289)	165.4	13.1	86.9	$C_{12}H_{21.5}$
4	CN30	163.5	14.3	85.7	$C_{11.7}H_{23.2}$
5	CN35	160.1	14.4	85.6	$C_{11.4}H_{22.9}$
6	CN40	163.5	14.2	85.8	$C_{11.7}H_{23}$
7	CN45	161.0	14.3	85.7	$C_{11.5}H_{22.8}$
8	CN50	155.2	14.2	85.8	$C_{11.1}H_{21.9}$
9	CN55	161.0	14.2	85.8	$C_{11.5}H_{22.7}$
10	F-24	158.4	13.9	86.1	$C_{11.3}H_{21.9}$
11	ATJ (alcohol-to-jet)	171.1	15.3	84.7	$C_{12.1}H_{25.9}$

The comprehensive classifications described in section 3.3.3 were used to obtain detailed compositions of these fuels, which are provided in Appendix H. The comprehensive compositions of the fuels were simplified by combining like classifications (irrespective of molecular size) into the larger hydrocarbon families that they belong as shown in Figure 51. The simplified composition of the fuels tested is illustrated in Figure 55 and large differences are evident.

The fuel ATJ is comprised of ~98% iso-paraffins based on the analysis. However, it should contain 100% iso-paraffins as shown in previous studies [33,91,94,96] and based on theory of synthesizing this fuel from fermentation of bio waste [96]. In this study, the remaining ~2% appeared as normal alkanes, which is an outcome of the classification regions of n-alkanes and

iso-alkanes coinciding in some locations, particularly when highly branched iso-alkanes are expected. The major species of ATJ is 2,2,4,6,6 pentamethyl heptane (PMH), which comprises above 65% of the total fuel by mass. It was discussed previously that this species overlaps with n-decane and is often misclassified with the C10-nAlkane group. However, in this case the amount of PMH is extremely high. This results in a part of the peak falling in the C10-nAlkane region, outside the additional C12-isoAlkane region marked near the C10-nAlkane region causing this error, as shown in Figure 56. This interference of PMH in other classification has proven to be a critical problem for this analysis since most artificial fuels analyzed in this study include exceptionally large amounts of PMH as discussed ahead.

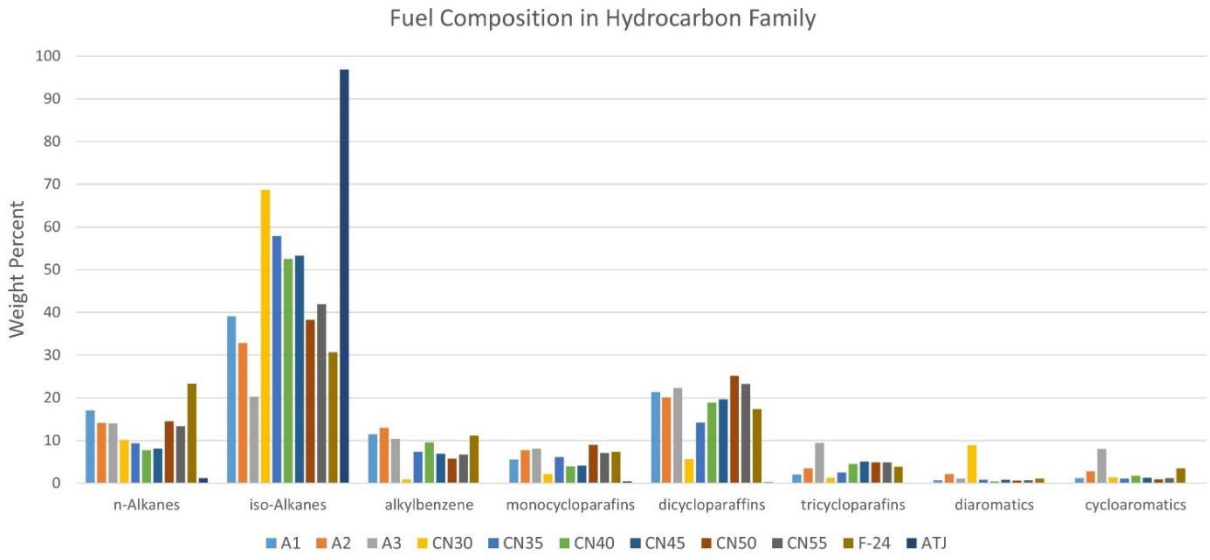

Figure 55 : Composition of tested fuels based on hydrocarbon families.

The analysis of CN fuels showed how the fuel composition changes with change in cetane number. However, these changes are not uniquely linked, and other compositions are possible for obtaining similar cetane numbers. The lowest cetane number fuel among all CN fuels is CN30. The chromatogram from the GCxGC analysis is shown in Figure 56. This fuel is comprised of over 55% of PMH by mass as unveiled by the GCxGC analysis. It is as if a standard fuel is blended

with large amount of PMH. Additionally in this fuel, there are a substantial number of diaromatic species like substituted naphthalene and substituted bi-phenyls, which are present in significantly lower quantities in other CN fuels. The content of the monoaromatic and the cyclo-aromatic species is also extremely low in CN30 fuel making it a mixture of PMH with some smaller hydrocarbon ($\leq C_{12}$). Additionally, the GCxGC analysis reveals a lack of large hydrocarbon ($\geq C_{13}$) in this CN30 fuel. However, the average molecular weight of this fuel is remarkably similar to the remaining CN fuels as evident in Table VII, with the exception of CN50 which has a much lower average molecular weight.

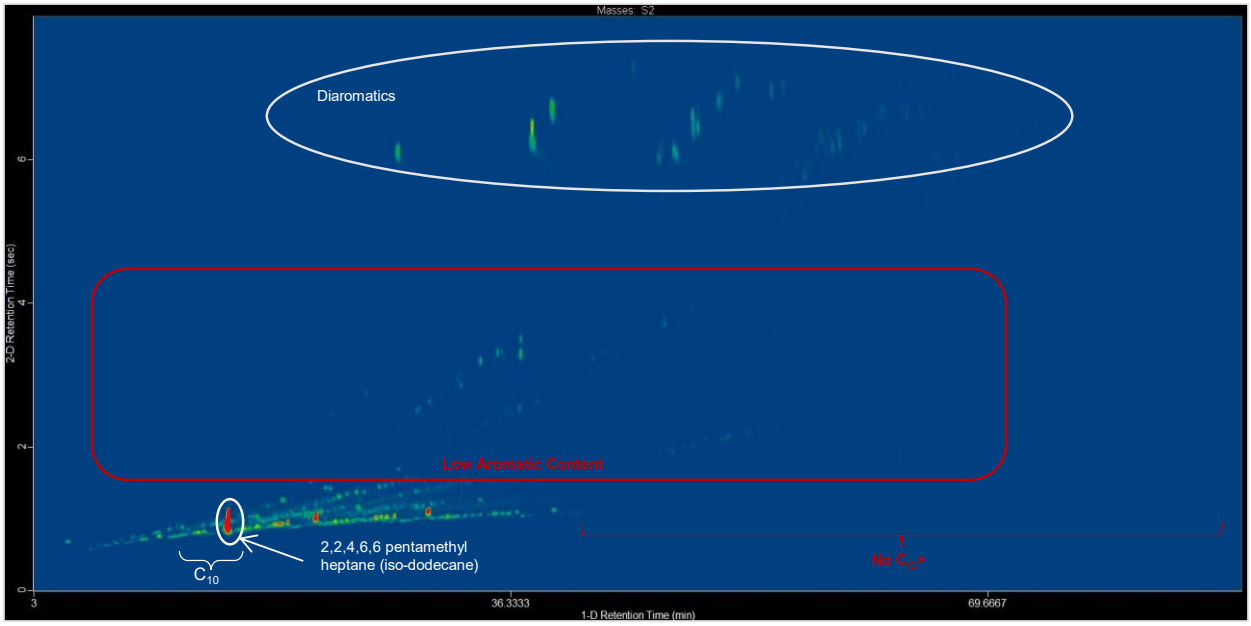

Figure 56 : Two dimensional chromatogram for CN30 from the GCxGC analysis.

Figure 57 illustrates the chromatogram for the next CN fuel with a cetane number of 35. The quantity of PMH drops for this fuel however it still accounts for a large weight fraction of the complete fuel at ~42%. The aromatic content of this fuel is lower than that for standard fuels like F-24 however it is significantly higher than that for CN30. The increase in aromatic content comes at the cost of a reduction in diaromatic content to incredibly low levels and in line with all other

fuels tested. The fuel has exceptionally low quantities of hydrocarbon larger than thirteen carbon atoms (C_{13}).

The analysis of CN40 (Figure 58) shows further reduction in PMH to ~33% by weight fraction while showing an increase in the aromatics. The quantity of cyclo-alkanes, primarily dicyclo-paraffins like decalin starts to rise from CN40 onwards. The trend of reduction in PMH continues through the CN fuels, until it reaches ~13% for CN50 and CN55, shown in Figure 60 and Figure 61 respectively. The composition of CN50 and CN55 is remarkably similar, which is in line with the fact that CN55 is prepared by adding cetane enhancing compounds in CN50 [95]. However, it is worth noting that in terms of cetane number, CN45 (Figure 59) and CN50 (Figure 60) should resemble the reference fuel, F24 (Figure 62), which has a similar cetane number but this is not the case.

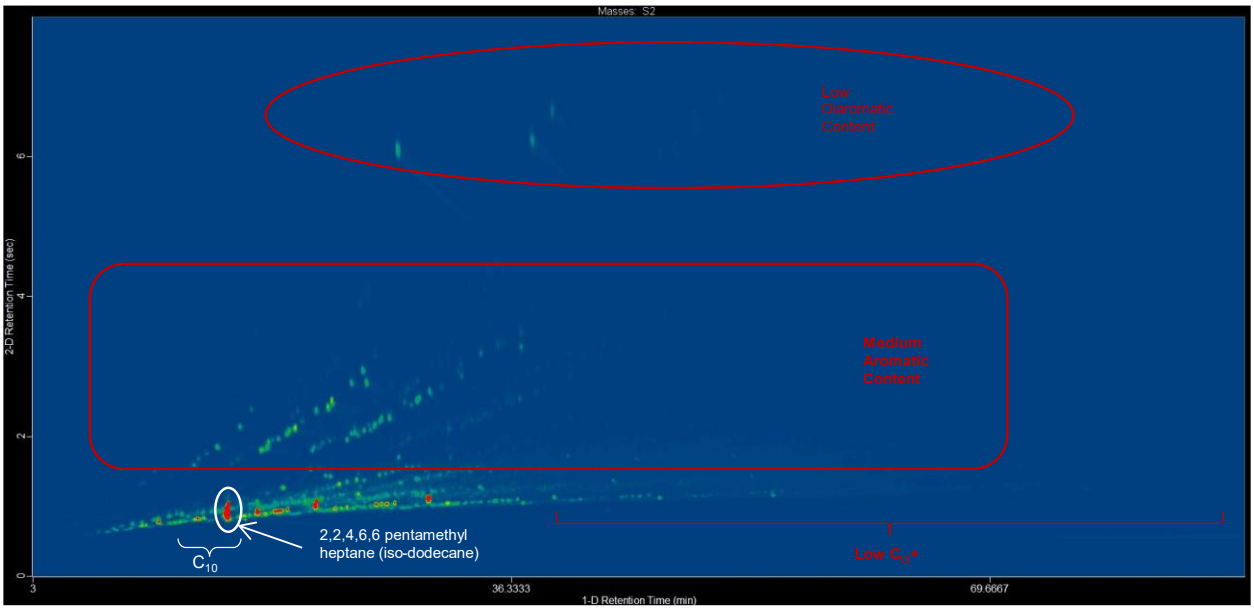

Figure 57 : Two dimensional chromatogram for CN35 from the GCxGC analysis.

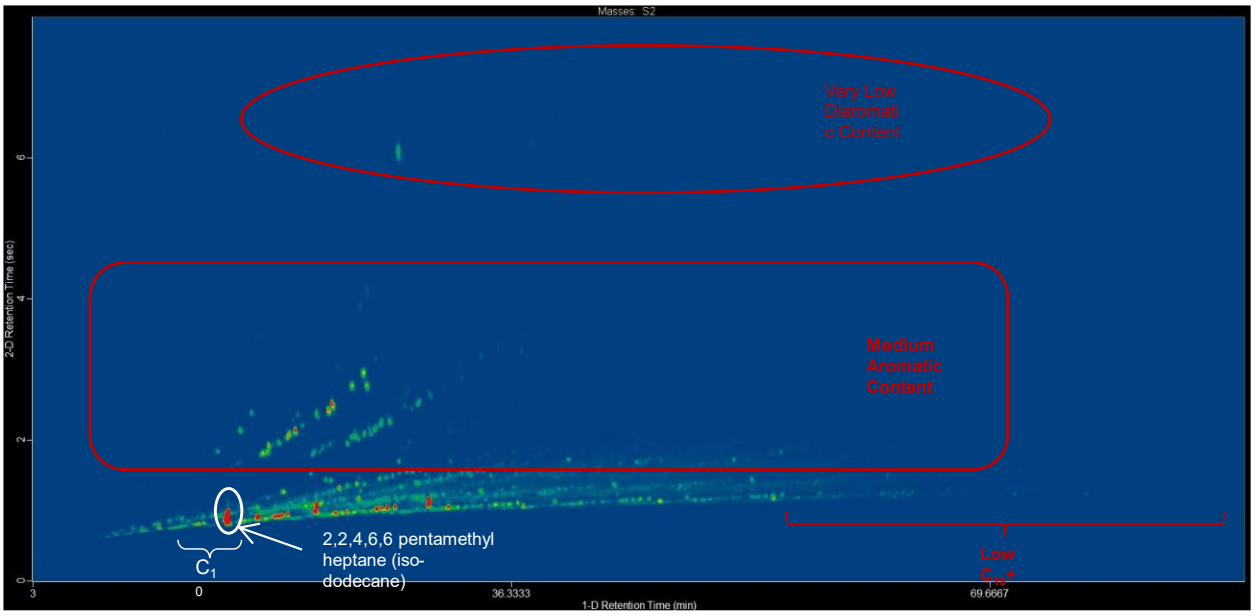

Figure 58 : Two dimensional chromatogram for CN40 from the GCxGC analysis.

The significant differences between the CN fuels and the distillate fuels show that while the CN fuels are specialty prepared fuels to target a particular cetane number, they are not representative of a distillate fuel and are close to being a single low cetane number component.

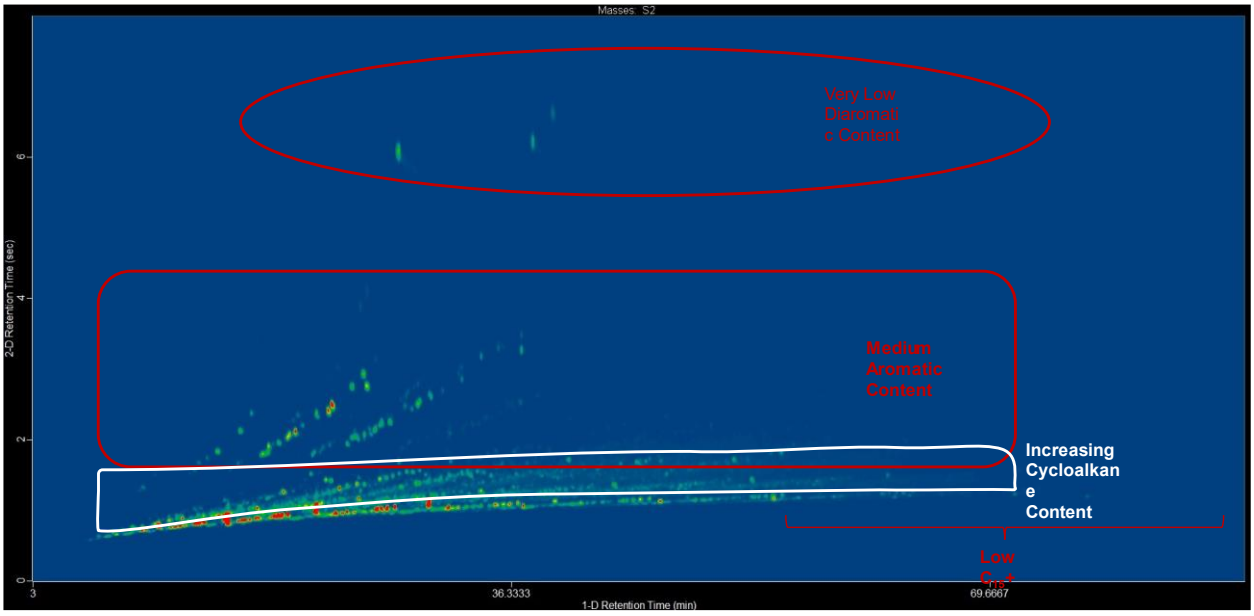

Figure 59 : Two dimensional chromatogram for CN45 from the GCxGC analysis.

The analysis of the distillate fuel Jet A1 is illustrated in Figure 63. Jet A1 has one of the highest quantities of n-Alkanes at about 18% by weight fraction, only second to F-24 (Figure 62) which has about 22% of n-Alkanes. The difference in normal alkane composition of the fuel is balanced by the iso alkane composition with F-24 having about 8% lower iso-alkane content than Jet A1. According to the properties provided by the fuel manufacturers, The expected cetane numbers for Jet A1 is 39.2 [55] and that for F-24 is 48.3. The large difference in the cetane numbers may be a result of this varying composition but the Jet A2 fuel and F-24 fuel are expected to have nearly the same cetane number of ~48 despite the differences in the fuel composition. Jet A2 (Figure 64) has about ~15% n-alkanes by mass whereas F-24 has ~25% by mass of n-alkanes. However, the difference in iso-alkanes between these fuels is extremely low, at about ~2%. The large difference in n-alkanes is balanced, by more cyclo-alkanes in Jet A2. In practice F-24 is a fuel equivalent to Jet A2, however containing trace amounts of additives that are required for meeting military specifications.

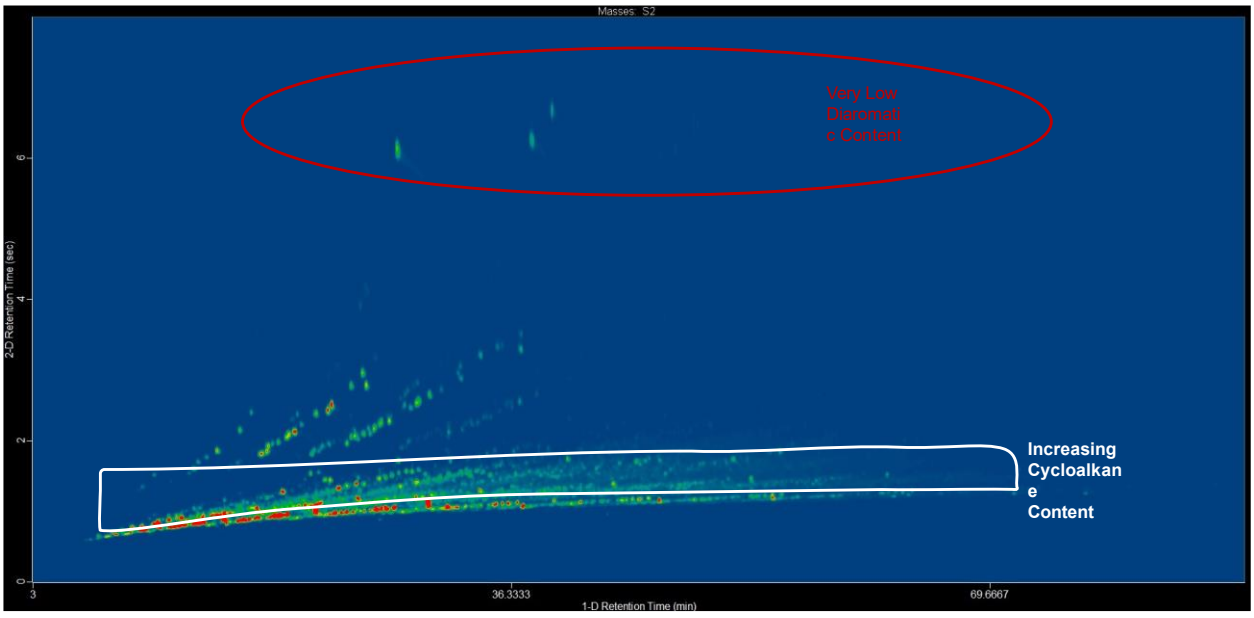

Figure 60 : Two dimensional chromatogram for CN50 from the GCxGC analysis.

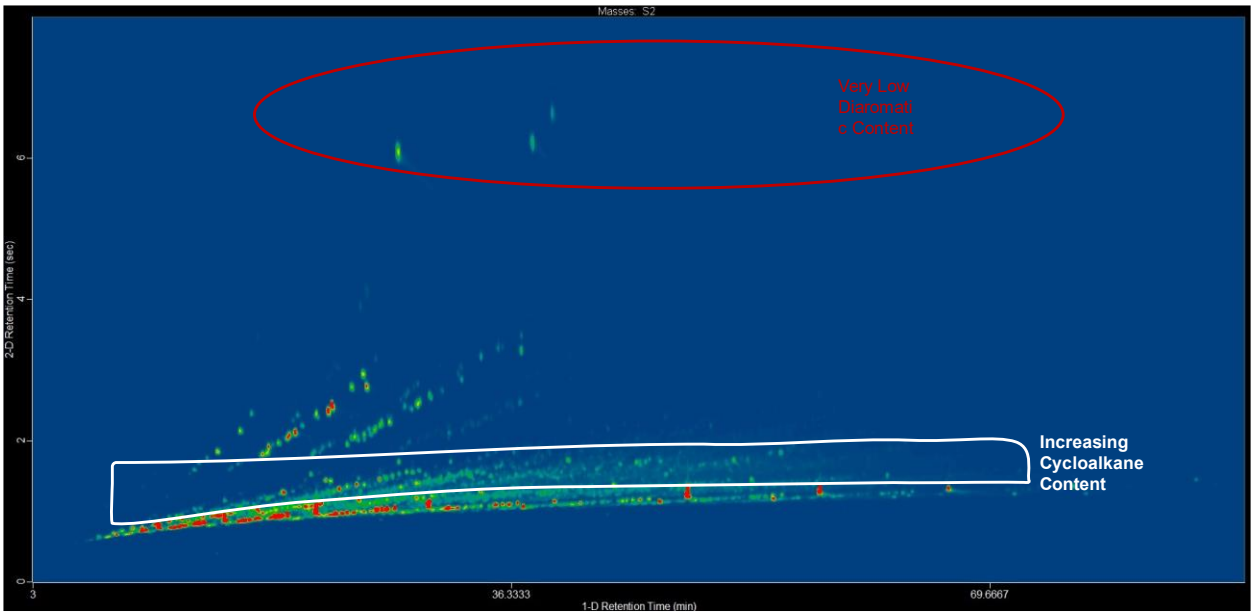

Figure 61 : Two dimensional chromatogram for CN55 from the GCxGC analysis.

The key difference among all distillate fuels tested is in Jet A3, which is also called JP-5 [36,55,97], Aviation Carrier Turbine Fuel (AVCAT). This fuel is a military fuel primarily used by the U.S. Navy for aircrafts operating from offshore installations like aircraft carriers. The physical and chemical property requirements of this fuel are different with consideration of point of use safety as well as having a different combustion behavior to assist with short runway take offs. The cetane number for Jet A3 [55] is ~48.5 which is the same as that for Jet A1 and F-24 but the composition differences are significant as evident in Figure 65. Jet A3 consists of a large number of aromatic compounds as well as cyclo-alkanes, particularly tri-cyclo-alkanes. The quantity of iso-alkanes in Jet A3 is almost half that of Jet A1 despite the same cetane number whereas it is about ~10% lower than that for Jet A2 and F-24. In addition to these difference, the cyclo-aromatics form about 8% of this fuel in comparison to ~1% for Jet A1, ~3% for Jet A2 and F-24. This makes it clear that while species composition does affect the cetane number of the fuel there is a more complex relationship between the composition and the cetane number.

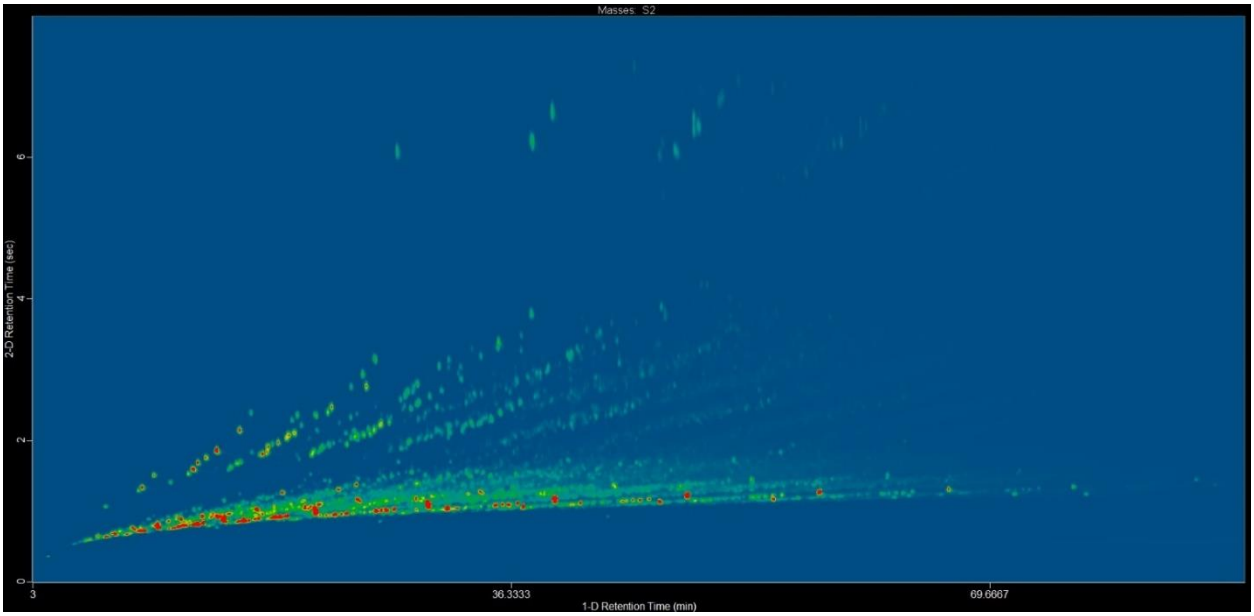

Figure 62 : Two dimensional chromatogram for F-24 from the GCxGC analysis.

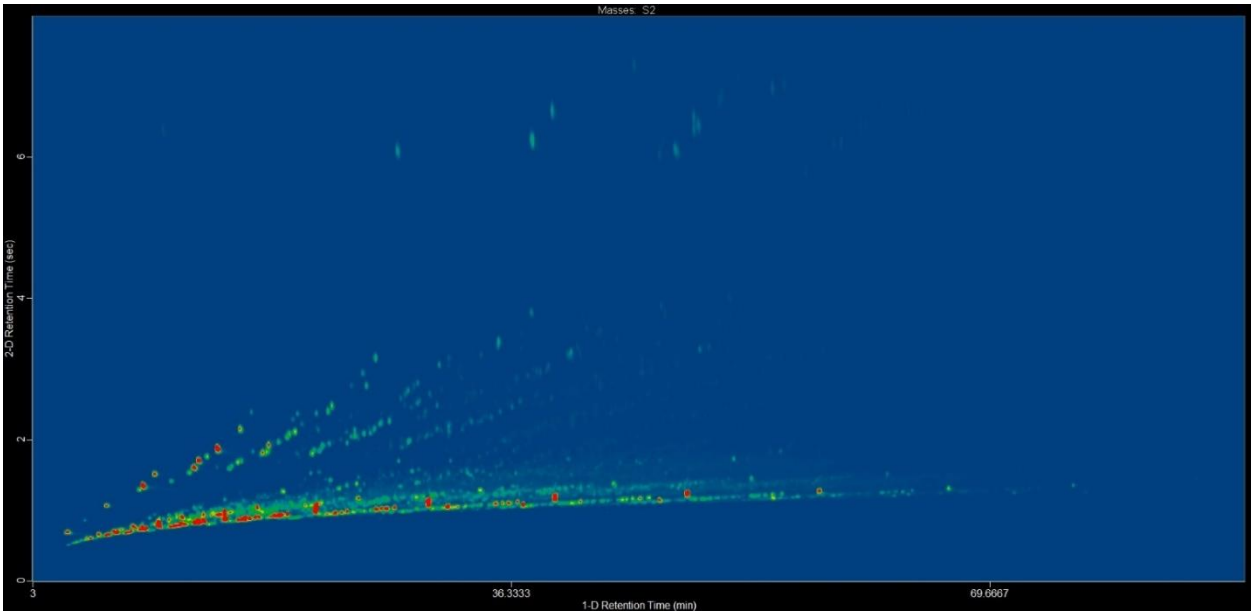

Figure 63 : Two dimensional chromatogram for Jet A1 (JP-8 POSF10264) from the GCxGC analysis.

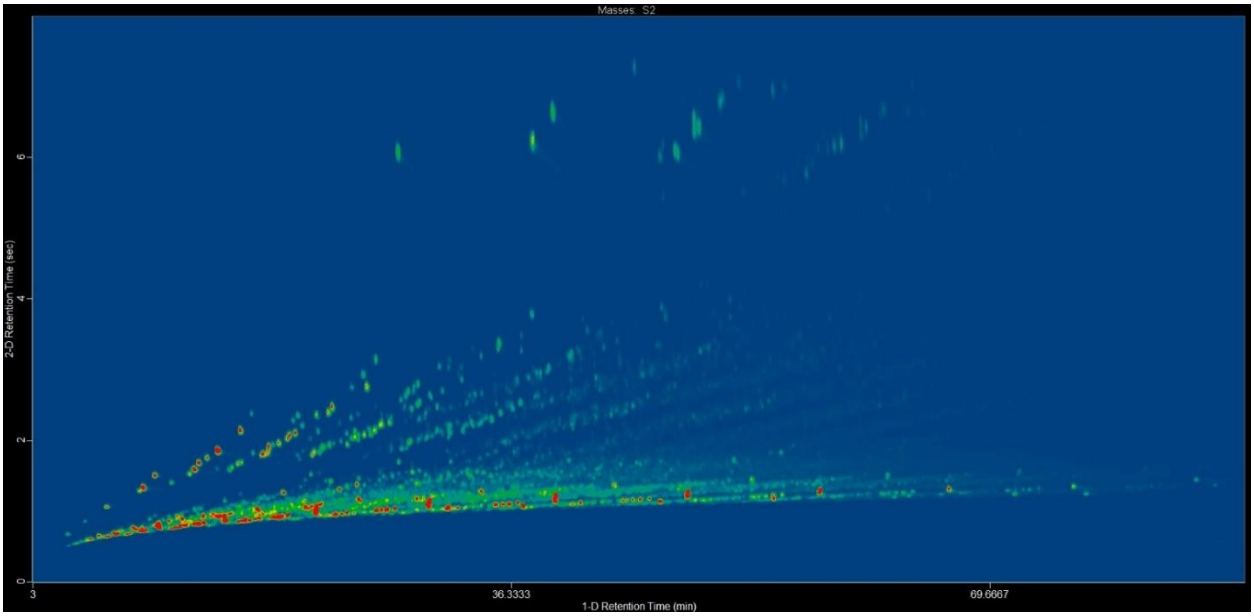

Figure 64 : Two dimensional chromatogram for Jet A2 (Jet A - POSF10325) from the GCxGC analysis.

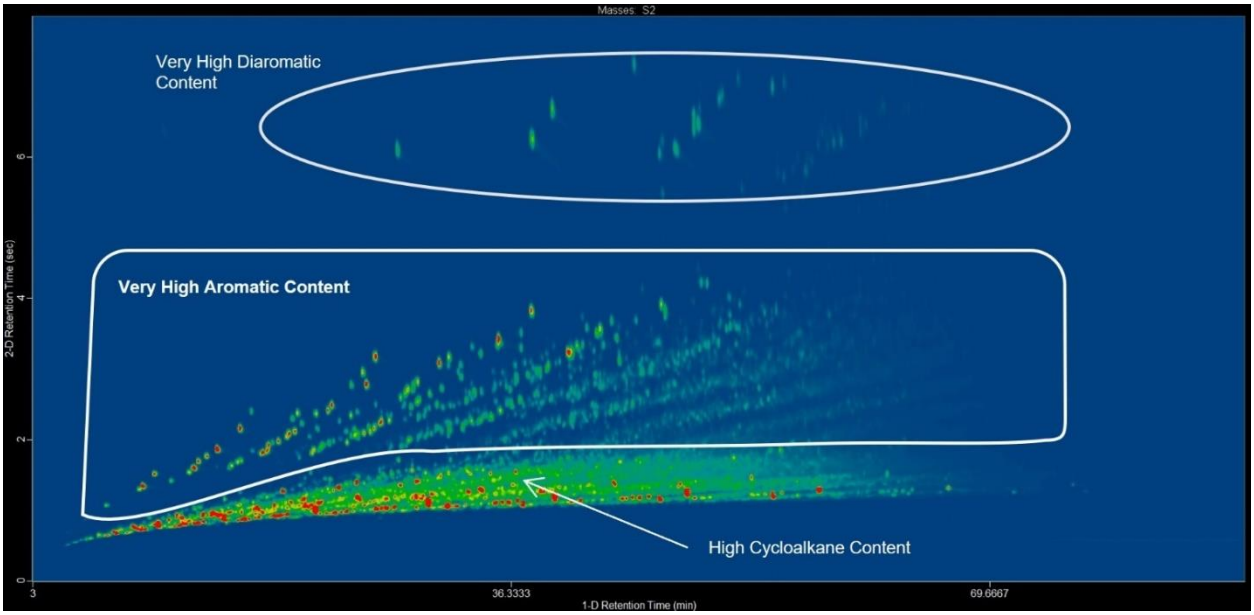

Figure 65 : Two dimensional chromatogram for Jet A3 (JP-5 POSF10289) from the GCxGC analysis.

3.5 *S2FG:* Species-to-Functional-Group

The GCxGC analysis provides the species composition of the fuels and the mixtures, but additional processing is necessary to convert this composition into the functional group based compositions which should display a more direct correlation to the ignition properties and the derived cetane number. Species-to-Functional-Groups (S2FG) is a software package developed for this exact purpose. S2FG takes the list of the compounds present in a mixture in the form of their SMILES molecular descriptors and the weight fractions of each compound as input and provides the list of chemical functional groups present and their weight fractions, along with the contribution of each compound to the functional groups.

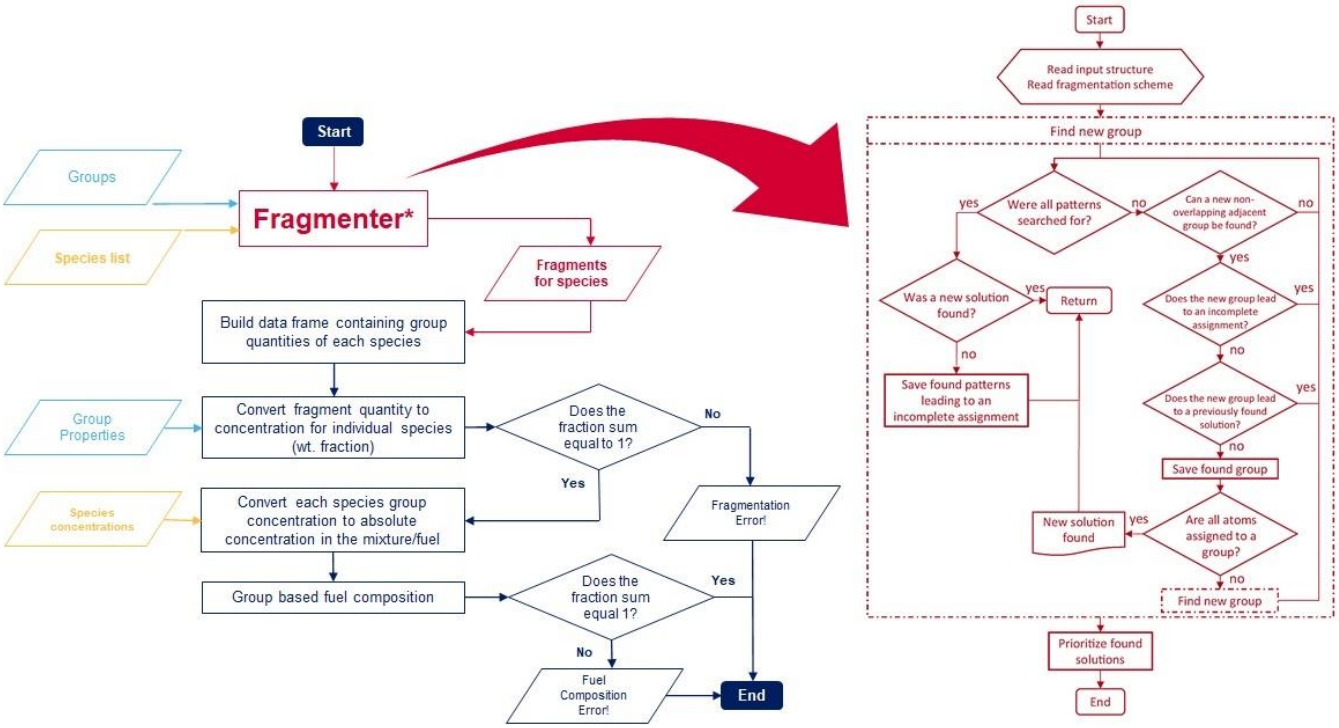

Figure 66 : The algorithm of S2FG along with the 'Fragmenter' algorithm by Muller [54].

S2FG uses a previously developed heuristic algorithm [54] to split the molecules into their constituent functional groups and provides the number of each functional group in the molecule. S2FG uses this information with the molecular weight of the group to compute the weight fraction

of each functional group within the molecule using equation 3.2. This process is repeated for every chemical functional group in the molecule, so that the individual chemical functional group composition of every compound can be obtained.

$$\hat{Y}_i^{FG} = \frac{N_i^{FG} \times W_i^{FG}}{MW_{compound}} \quad 3.2$$

where $\hat{Y}_i^{FG}$represents the weight fraction of the functional group in the molecule, N_i^{FG} quantity (number) of functional group that are present in the compound, W_i^{FG} is the weight of the functional group and $MW_{compound}$ is the total molecular weight of the compound.

This chemical functional group composition for each compound is then adjusted based on the weight fraction of the compound in the mixture to obtain the contribution of each functional group to the mixture by the compound using equation 3.3,

$$Y_i^{FG} = \hat{Y}_i^{FG} \times Y^{compound} \quad 3.3$$

where, Y_i^{FG} is the contribution of the compound to the overall functional group composition of the mixture and $Y^{compound}$ is the weight fraction of the compound in the mixture.

The individual contributions from all the compounds in the mixture can be summed up to obtain the total weight fraction of that functional group in the mixture. When this summation is repeated over all the functional groups present, the complete functional group composition of the mixture is obtained,

$$Y^{FG} = \sum Y_i^{FG}$$

3.4

The complete procedure is automated within S2FG. The chemical functional groups into which the molecule is split can be changed by changing the functional group input to the software. The software takes the chemical functional group properties from an input file which consists of the name of the chemical functional group, SMARTS representation of the chemical functional group and the weight of the functional group. S2FG splits the molecule using the heuristic algorithm [54] into the functional groups provided as input and uses its properties to complete the conversion of species based composition into the chemical functional group based composition. Figure 66 illustrates the structure of S2FG along with the heuristic algorithm from Muller [54] called 'Fragmenter'.

3.5.1 Chemical Functional Groups

There are several categories of the chemical functional groups that have been associated with specific properties and several methods have been developed to predict those various properties of the molecule using these chemical functional groups. The category of chemical functional groups chosen for this study has been the UNIFAC groups. CH3 (methyl), CH2 (methylene), ACH (aromatic carbon) are some examples of the UNIFAC groups. The UNIFAC groups can be used for predicting several properties of the fuels using well established and proven methods which can be generalized irrespective of the type and the source of the fuel. The UNIFAC method [53] was developed to predict activity coefficients of complex mixtures which is a correction factor used for calculating the real mixture effects from ideal mixture effects. The UNIFAC method has since been expanded to allow estimation of other physical and chemical properties of these mixtures [45]. The UNIFAC groups span purely hydrocarbon based groups (aliphatic and aromatic),

oxygenated hydrocarbon groups (alcohols, ketones, ethers, and esters), amides, cyanide and many more. In this study only hydrocarbon groups, shown in Table 1 have been observed since all the fuels and mixtures analyzed are purely hydrocarbon fuels. However, this approach can be extended to the other UNIFAC groups, particularly oxygenated hydrocarbons which are important for analysis of the gasoline and biofuels which include alcohols.

Table VIII : Major functional groups related to jet fuels from the complete the UNIFAC groups.

UNIFAC	**SMARTS**	**MW (g/mol)**
CH3	[CH3;X4]	15.035
CH2	[CH2;X4]	14.027
CH	[CH1;X4]	13.019
C	[CH0;X4]	12.011
CH2=CH	[CH2]=[CH]	27.046
CH=CH	[CH]=[CH]	26.038
CH2=C	[CH2]=[C]	26.038
CH=C	[CH]=[CH0]	25.03
ACH	[cH]	13
AC	[cH0]	12
ACCH3	[c][CH3;X4]	27
ACCH2	[c][CH2;X4]	26
ACCH	[c][CH;X4]	25
C=C	[CH0]=[CH0]	24.022

3.5.2 Testing

The more complex a molecule structure becomes, several splitting patterns without abandoning any part of the molecule is possible. The selection of the correct splitting pattern is important to ensure all key chemical functional groups within the molecule are correctly accounted for. Figure 67, using iso-propyl benzene (cumene), shows two different splitting patterns where all the parts

of the molecule are split into the UNIFAC groups. However only one of the patterns out of the two is the correct split to ensure all chemical functional groups responsible for the properties of the molecule are accounted for. Figure 67(b) shows the correct splitting pattern, where the bond between aromatic carbon (AC) and a paraffinic carbon group (CH) is correctly accounted for by fragmenting it as ACCH, unlike Figure 67(a) where they are separately accounted for. By using splitting like Figure 67(a), the chemical functional group composition does not provide any information about what group is substituted on the aromatic ring.

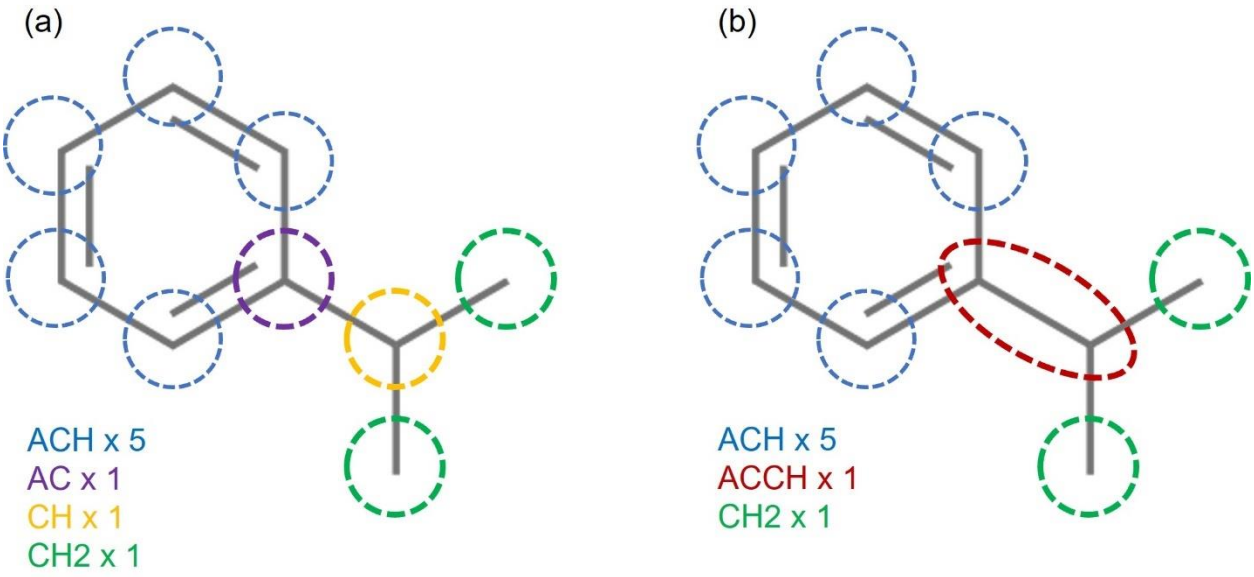

Figure 67 :The UNIFAC groups into which the iso-propyl benzene molecule can be split into. (a) The incorrect splitting of the molecule, which does not account for the UNIFAC group connected to the aromatic ring, (b) Correct splitting of the molecule which accounts for key features in the molecule.

The heuristic algorithm [54] used for splitting the molecule has different operating modes, one of which is the simple method where the first available splitting pattern is returned, and the other is the complex method where all possible splitting patterns are obtained. The splits are rated based on a hierarchy within the algorithm and the correct split of the molecule is provided. The use of this algorithm even for simple mixtures and fuels is recommended to avoid errors in obtaining the optimum molecule splitting. The S2FG code was tested on mixtures prepared in the

lab for this project. The mixtures were planned and intensively used for another complementary study [98]. The composition of the mixture was known and precisely controlled during preparation. Forty nine mixtures (UIC mixtures) were prepared in the lab having up to four components each from a pool of twenty one different pure compounds that are expected to be representative of the compounds present in jet fuels. The chemical functional group compositions of all of these mixtures and pure compounds were computed by S2FG from the species composition information of all the mixtures. The chemical functional group composition of the mixtures is provided in Appendix I. Figure 68 illustrates the output from S2FG for one of the mixtures, designated as P400001. The UNIFAC group split and their weight fractions for the individual components as well as the overall UNIFAC group composition is shown in Figure 68. The mixture P40001 includes one n-alkane (n-decane), one mono-cyclo-alkane (methylcyclohexane), one dicyclo-alkane (decahydronaphthalene) and one aromatic (benzene) compound. The complete mixture by weight contains 71% of CH2 group which is contributed by three out of the four components of this mixture. CH2 group is found in large quantities in n-alkanes as well as cyclo-alkanes. With only one aromatic component in the mixture, all the aromatic UNIFAC groups in the mixture are contributed by benzene alone.

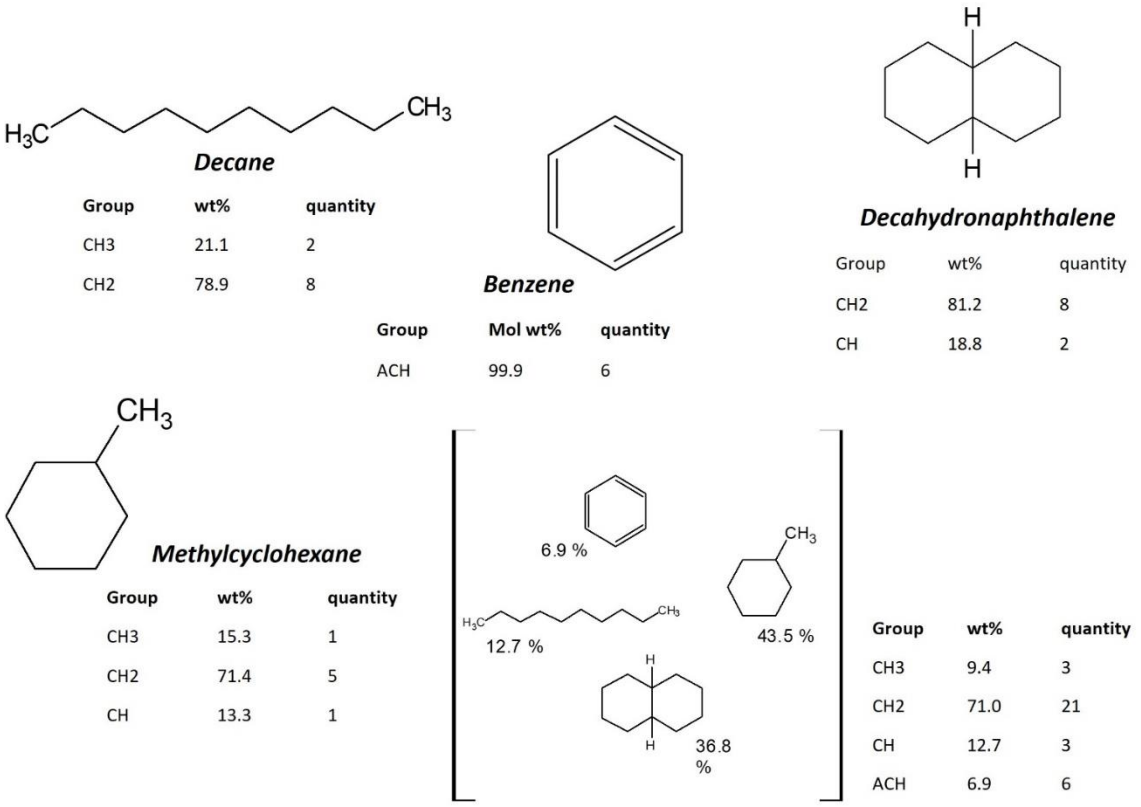

Figure 68 : Chemical functional group composition of P400001 mixture, with illustration of the various steps within S2FG.

The chemical functional group composition for all the mixtures obtained from S2FG was found to be as expected and the capability of S2FG to handle multi component mixtures appropriately was confirmed.

3.6 Chemical Functional Group Composition of Fuels

The S2FG was used to convert the hydrocarbon classification based composition of jet fuels analyzed using the GCxGC TOF-MS/FID into its chemical functional group based composition. The S2FG requires input of the molecule structure in the SMILES format to carry out the splitting and eventually converting to chemical functional group composition, but since the GCxGC TOF-MS/FID analysis of jet fuels was done using the hydrocarbon classification method, the composition was obtained in the form of hydrocarbon classifications, each of which could include multiple compounds in varying quantities. Thus, no single species is available from the analysis

to be fed to S2FG. To overcome this lack of species information, as previously mentioned, a representative species representing the fuel needs to be selected. All the fuels tested had significant variations as explained in section 3.4 and hence the appropriate representative species for each fuels may not be the same. Thus, the exact chemical functional group composition of the fuels cannot be estimated. To overcome this uncertainty, two computations using S2FG with the representative species of the two extreme conditions based on branching were conducted for each fuel. This analysis provides the two extreme chemical functional group compositions possible in the fuel for the same hydrocarbon classification composition.

Figure 69 shows the span over which ten key UNIFAC groups can be expected for the distillate fuels without the change in hydrocarbon classification compositions. In Figure 69 the distillate fuels, especially Jet A1, Jet A2 and F-24 have remarkably similar ranges for all the UNIFAC groups, with slightly larger span of CH3 and C group for Jet A1. It can be concluded again from these results that Jet A2 and F-24 seem to be nearly identical fuels. Jet A1 however seems to have a larger amount of CH3 and C groups when compared to Jet A2 and F-24. The Jet A3 has a more evident difference from the remaining fuels in the form of a reduced CH3 group composition along with a smaller maximum CH3 concentration which is about 8% less than the remaining distillate fuels but with a greater minimum CH2 group value which is about 6% higher than the remaining fuel. The remaining UNIFAC group ranges among the fuels show a similar span as well as minimum and maximum values.

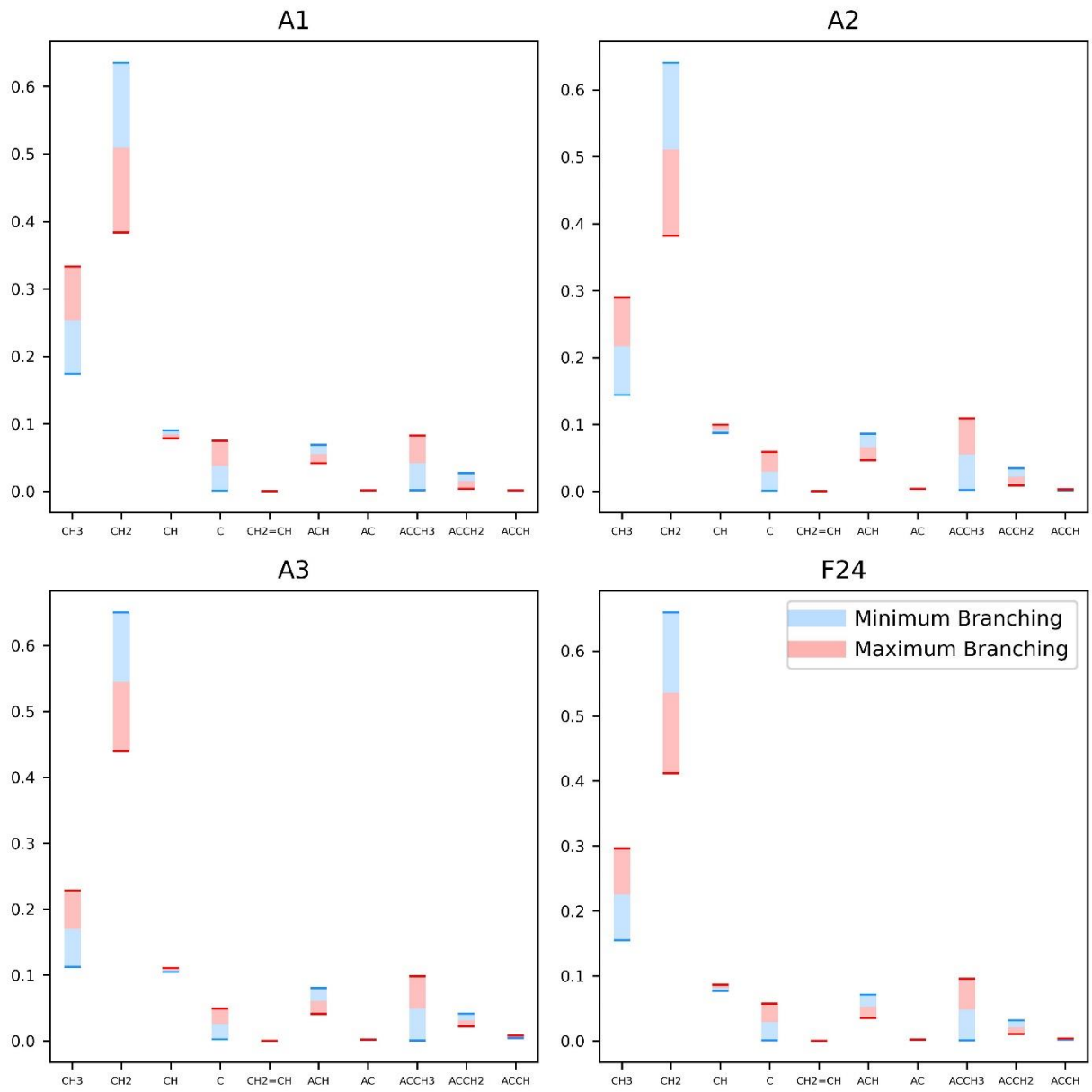

Figure 69 : UNIFAC group composition bounds for distillate jet fuels in weight fraction, the functional group composition for the fuel shifts into blue region as the branching reduces and shifts into red as the branching increases.

The CH2 group has the largest span over which the composition can change in a fuel based on the change in the constituents of each classifications. In addition to this large span, it shows an inverse behavior when compared to other paraffinic UNIFAC groups where the concentration of this group falls as the branching increases. This observation is in line with the fact that when branching increases in a molecule, the CH2 are replaced by the CH and the C groups depending

on the nature of branching. In addition to the increase in C and CH as a replacement, an increase in CH3 is also expected since terminal locations of carbon atoms in an alkane have a CH3 configuration and with increasing branches multiple terminal carbon atoms exist. Thus, CH2 is the paraffinic group which is inversely affected by branching compared to the remaining three paraffinic groups.

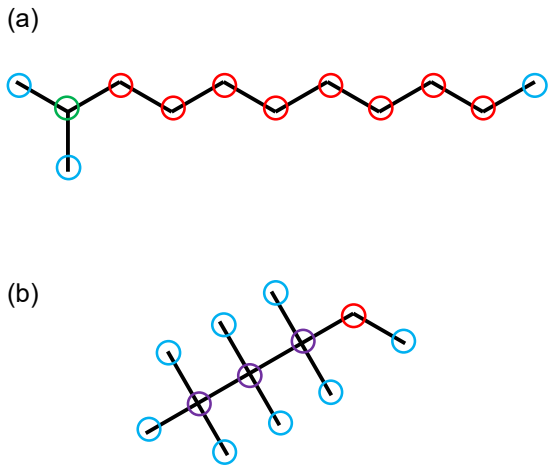

Figure 70 : Molecular structures of two isomers of iso-dodecane - (a) 2-methylundecane; (b) 2,2,3,3,4,4-hexamethylhexane. The different carbon atoms of the molecule have been marked based on the UNIFAC group they represent within the molecule – CH3 (blue), CH2(red), CH (green), C(purple).

Figure 70 shows the molecular structure for two different isomers of iso-dodecane ($C_{12}H_{26}$), 2-methylundecane and 2,2,3,3,4,4-hexamethylhexane, which fall in the same hydrocarbon classification of C12-isoAlkane and have the same atomic composition as well as the molecular weight. However, the physical and chemical properties vary between the two molecules as a result of the different arrangement of the atoms. For example, the boiling point of 2-methylundecane is 209°C and that of 2,2,3,3,4,4-hexamethylhexame is 194°C. This difference in arrangement shows up in the form of a different chemical functional group composition between

the two molecules as well and thus reiterates the fact that the functional groups impart physical and chemical properties to the molecule irrespective of the constituent atomic composition.

Additionally, this 2-methylundecane is a C_{12} hydrocarbon with one branch and has three CH3 groups, eight CH2 groups and one CH group whereas 2,2,3,3,4,4-hexamethylhexane has six branches resulting in eight CH3 groups, one CH2 group and three C groups. In this particular situation, the number of CH2 groups in the molecule is reduced by seven when number of branches increases by five whereas the number of CH3 increases by four when branching increases by five. This explains how the inverse relation between the two paraffinic groups exists as a result of branching. A similar relationship can be seen within the aromatic carbon based UNIFAC groups as well. However, it is the ACCH3 group that has an inverse relation with the rest of the aromatic groups – ACCH2, ACCH, ACH and AC.

This difference in chemical functional group composition based on branching, especially for iso-dodecane, is critical for CN fuels. As previously described in section 3.4, the CN fuels consist of large quantities of iso-dodecane. Thus, error in the selection of the correct isomer as a representative compound would result in a much larger error than inherent to this method. However, in the case of CN fuels, the largest contributor to C12-isoAlkane is one specific isomer – 2,2,4,6,6-pentamethylheptane which has been previously discussed in section 3.3.3. PMH appears with n-decane on the GCxGC analysis and was identified using the TOF-MS signal and quantified appropriately as discussed.

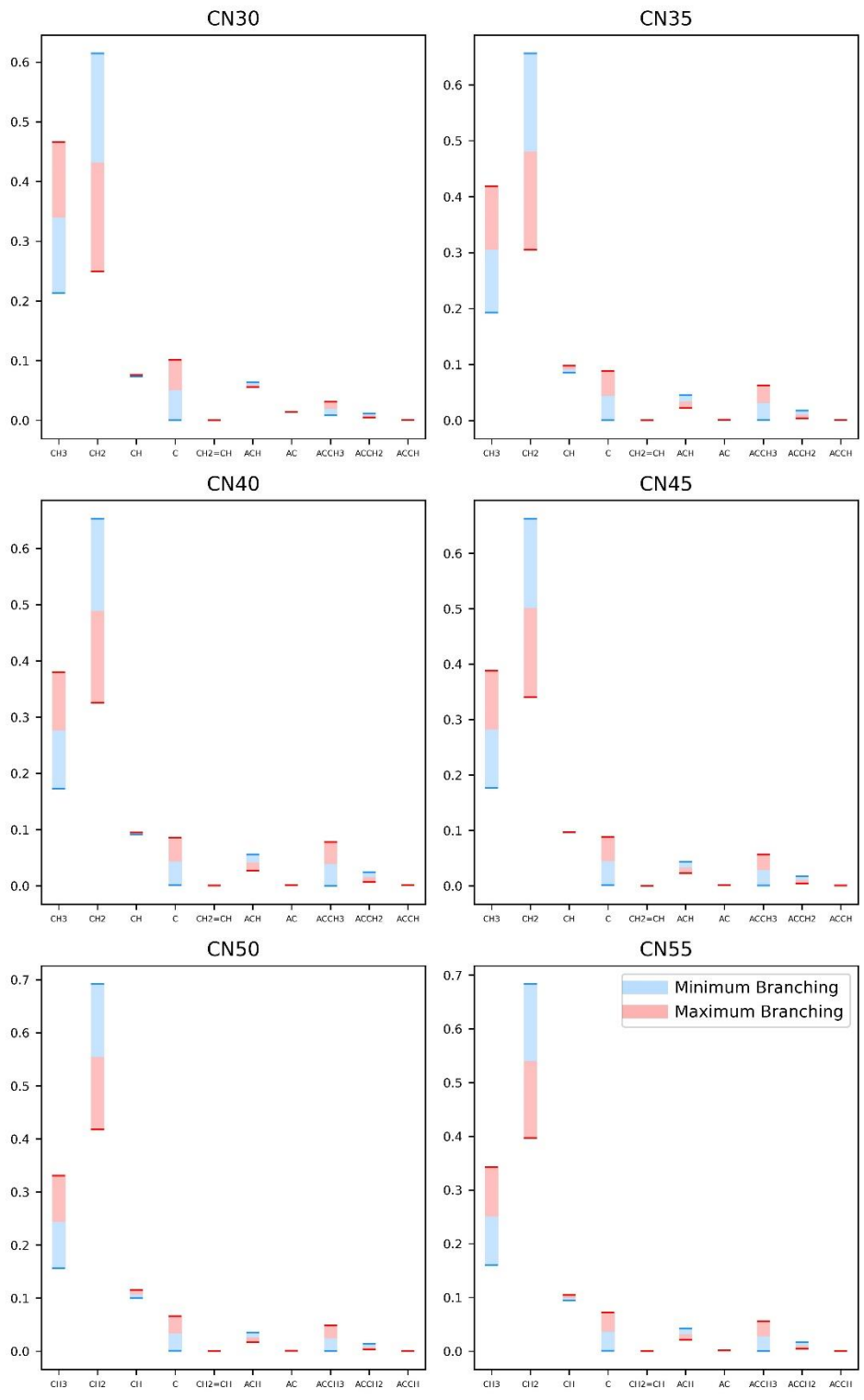

Figure 71 : The UNIFAC group composition bounds for CN fuels in weight fraction, the functional group composition for the fuel shifts into blue region as the branching reduces and shifts into red as the branching increases.

Figure 71 shows the UNIFAC group regions for all the CN fuels tested in this analysis and the difference between the fuels is much more significant for the CN fuels. However, all the lower cetane number fuels (30,35 and 40) are biased by the presence of extensive amount of PMH. The reduction in quantities of PMH in CN fuels as the cetane number increases results in a reduction of the span of CH3 group in the fuels. CN30 has a weight fraction span of ~0.28 for CH3 whereas CN55 has an approximately half the weight fraction span of ~0.14. However, the maximum quantity of CH3 changes from ~0.48 in CN30 to ~0.34 for CN50 and CN55, while the minimum value only has a change of about 0.02. The CN40 and CN45 fuels have a remarkably similar spread of the expected UNIFAC group composition, like CN50 and CN55. The CN35 values are also significantly different from those of CN30 with the CH3 group having a much shorter span as well as shorter range. In addition, for CN35 and above, the CH2 group composition is 0.65 or higher (goes higher with increase in cetane number) with CN50 and CN55 having ~0.70. CN30 however maxes out at ~0.6 weight fraction for CH2. Despite the significant differences in aromatic composition of the fuels as discussed in section 3.4, the span and range of all aromatic groups is similar among all the groups, with ACCH3 being lowest for CN30 and highest for CN40. No olefinic compounds were observed in the fuels analyzed.

3.6.1 Chemical Functional Groups and Fuel Surrogates

Jet fuels are complex mixtures with significant compositional variation, despite being specified for the same applications, as evident in this work as well as several research studies [28,33,34,55,93,97,99]. The knowledge of underlying chemical kinetic behavior as well as physical and chemical properties of these fuels plays an especially vital role in development of systems that operate on these fuels. To simplify the study of these complex fuels, surrogate approaches [5,26,33,91,100,101] are used for research studies to develop predictive models that

are capable of replicating the fuel behavior without actually knowing the exact composition of the fuels. The surrogate approach assumes that the surrogate composition covers all the key chemical characteristics of the fuel under consideration. The surrogates are used for performing experimental and modeling analysis to develop new models or optimize previous models for that particular fuel. Recent studies have further simplified the approach by suggesting that the fuels undergo a standard breakdown pathway forming select key species in different concentrations along the way. This latter approach has been implemented in a hybridized chemistry model, HyChem [15,16,27]. However, this approach does not provide the same level of predictive accuracy [28,102] that a surrogate based model [26,100,103] provides. Thus, selection of the surrogate composition [104] is key to developing high quality predictive models for jet fuels.

Table IX : Jet fuel surrogates which are used for comparison with the UNIFAC group composition of the distillate fuels evaluated in this study.

Name	***Component 1 (weight %)***	***Component 2 (weight %)***	***Component 3 (weight %)***	***Component 4 (weight %)***
UM1 [105]	n-dodecane (45.6%)	iso-cetane (23.4%)	methylcyclohexane (16%)	toluene (15%)
UM2 [105]	n-dodecane (33.2%)	iso-cetane (21.7%)	decahydronaphthalene (29.7%)	toluene (15.4%)
Malewicki et al. [26]	n-dodecane (49.6%)	iso-octane (23.6%)	n-propyl benzene (20.4%)	1,3,5-trimethyl benzene (6.4%)
Liu et al. [101]	n-dodecane (73%)	n-propyl benzene (12.3%)	1,3,5-trimethyl cyclohexane (14.7%)	-

Four proven jet fuel surrogate compositions developed over the years, shown in Table IX, were chosen and S2FG was used to obtain their UNIFAC group compositions. The UNIFAC group compositions of these surrogates was compared to the UNIFAC group composition range for the distillate fuels analyzed in this study. Figure 72 shows the comparison between F-24 and the four jet fuel surrogates. The CH3 composition of the surrogates is well within the range with the UM2 and Malewicki et al. [26], having similar values on the maximum branch side while the UM2 [105] and Liu et al. [101] surrogate having similar values on the minimum branch side. The difference

in the CH2 group is however more significant with the Liu et al. surrogate being at the limit of minimum branched conditions while the UM1 sits right at the average value. The Malewicki et al. surrogate has the lowest quantity of the CH2 putting it in the most branched condition with respect to the CH2 group. The CH group for all the surrogates is out of the limits with the UM1[105] having the highest amount of the group, remarkably close to the limit of minimum branched conditions for the CH group.

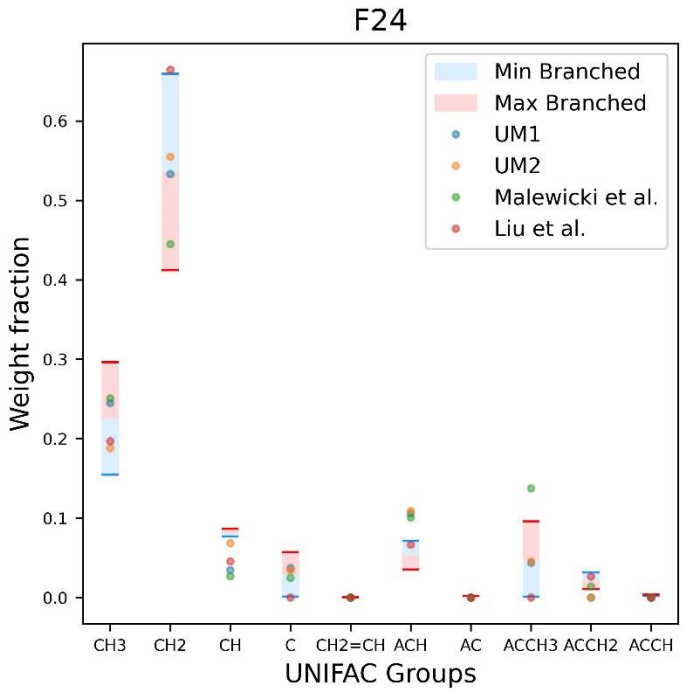

Figure 72 : UNIFAC group composition ranges for F-24 fuel analyzed in this study and the chemical functional group composition of the four surrogates – UM1 (blue), UM2(yellow), Malewicki et al. (green) and Liu et al. (red).

The surrogates are expected to represent Jet A (Jet A2 in this study). Figure 73 shows how the surrogate UNIFAC group composition to the range of Jet A2 compares. The comparison with Jet A2 is remarkably similar to that with F-24. The major difference is in the CH2 group, where the UM1 has moved further away from the average value into the minimum branched side. The CH2 group composition of the Liu et al. surrogate is outside the span of the CH2 group on the minimum

branched side. Other than that, the Liu et al. surrogate nearly matches the average value for the ACH group as opposed to being on the edge of minimum branched region for F-24. The four surrogates fall very well within the UNIFAC group ranges of fuels analyzed in this study and may be good surrogates for research studies including these fuels.

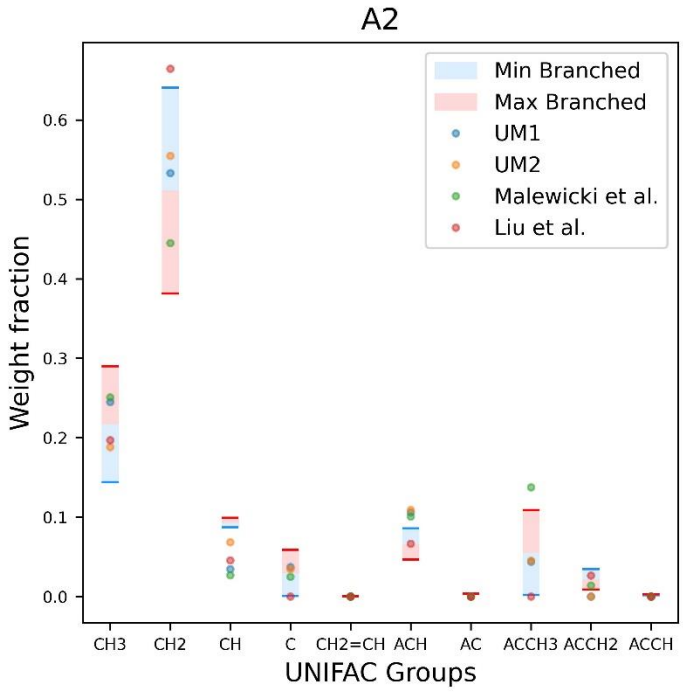

Figure 73 : UNIFAC group composition ranges for the Jet A2 fuel analyzed in this study and the chemical functional group composition of the four surrogates – UM1 (blue), UM2(yellow), Malewicki et al. (green) and Liu et al. (red).

In addition to the surrogates, the mixtures (UIC mixtures) prepared in the lab for the complementary study were also compared to the different fuels analyzed in this study. The mixtures span the complete range of the F-24 fuel, as evident in Figure 74, however substantial amounts of the UNIFAC groups like the CH2=CH2 group are present in these mixtures which are absent in all the fuels analyzed in this study. If the fuel samples analyzed in this study represent the population of jet fuels, it can be expected that no olefinic chemical functional groups should be present in the jet fuels. The information of UNIFAC group compositions in these fuels can thus

be used to optimize mixture preparation to better represent the jet fuel population. In addition to the CH2=CH2 groups, the composition of the aromatic UNIFAC groups is also high in these mixtures.

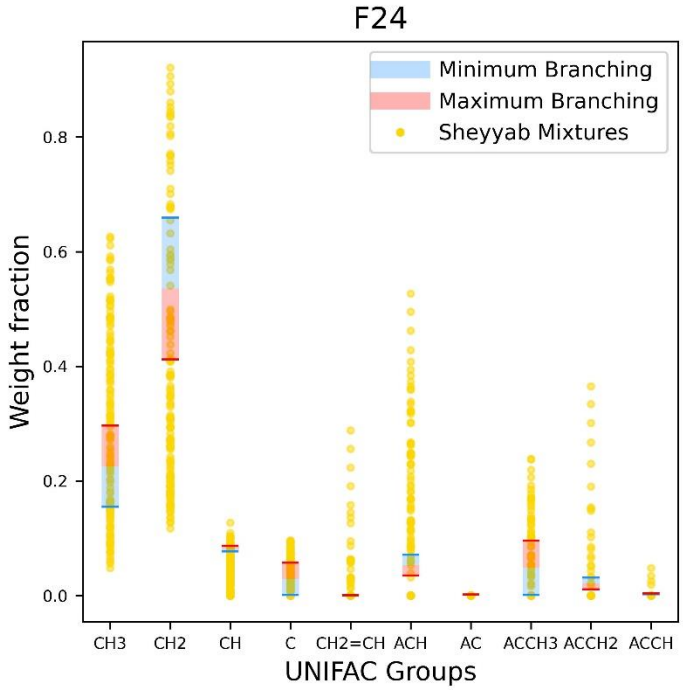

Figure 74 : UNIFAC group composition ranges for F-24 with the UNIFAC group composition of UIC mixtures.

3.7 Future Work

3.7.1 Nuclear Magnetic Resonance Spectroscopy (NMR)

The NMR spectroscopy can determine the atomic structure of a molecule and can provide the chemical functional group composition of a molecule. The NMR spectroscopy uses a high powered magnetic field to excite the nuclei of the molecule being analyzed and the localized magnetic field around the nuclei are detected using radio receivers. The resonant frequency is unique and characteristic of a molecule and the shift in the field can be used to identify the molecule. The shifts in an NMR spectra correspond to the various chemical functional groups and

the neighboring chemical functional groups which allow direct identification of the chemical functional groups present in a molecule. Quantitative analysis can also be conducted using NMR spectroscopy to obtain the quantity of chemical functional group of the molecules. This technique is most effective for single molecules.

The use of NMR spectroscopy to develop predictive models has made some significant strides in the recent years. The NMR spectroscopic analysis of jet fuels and surrogate mixtures has been used in recent studies [48,49,92] to develop models capable of predicting the ignition properties such as the derived cetane number (DCN) and several physical and chemical properties using Quantitative Structure Property Relations (QSPR). The predictive models presented by these studies provide satisfactory results however the use of NMR spectroscopy for several fuels is not the most cost effective approach.

The instrumentation required for NMR spectroscopy has an exceptionally large installation and operating cost. NMR systems usually consume massive quantities of liquid nitrogen and liquid helium to maintain the temperature of the high frequency magnets as well as use expensive deuterated solvents for sample preparation. The operating costs of the facilities required for NMR spectroscopy are also extremely large since the system is highly susceptible to environmental conditions. Additionally, to obtain sufficient signal to noise ratio for identification and quantification of all the chemical functional groups present in the molecule long run times are expected, further increasing the operating costs. Thus, NMR spectroscopy should be used only for studying new fuels with unexpected composition as well as to verify measurements from other analytical techniques.

3.7.2 Gas Chromatography – Infrared Spectrometry (GC-IR/FTIR)

Gas chromatography and IR spectroscopy are independently used in studies related to fuels and combustion however they are seldom used in conjunction with each other. The high level of separation of components of a mixture obtained from gas chromatography can be combined with IR based detection, replacing the MS when the focus is to identify isomers in a mixture. The use of IR leads to lower detection sensitivity than what can be achieved using an MS but provides superior identification of isomers. The IR system can be tuned to different spectral ranges to simplify analysis while targeting spectral features of interest. This is particularly useful when the focus of the analysis is chemical functional group composition. The spectral range corresponding to different chemical functional groups can be analyzed to directly obtain chemical function group composition of the analyte (peak). Simultaneous analysis using the FID, which is done in this current study, can be used for accurate quantification of the various chemical functional groups detected using IR.

The GC-IR technique is used within the pharmaceutical industry to identify and develop new drugs as well as to rebuild the structures based on IR analysis. This has resulted in several off the shelf available systems that can connect gas chromatographs to FTIR instruments for the GC-IR analysis. Nicolet© provides a GC interface to connect their iS50 FTIR system to a gas chromatograph. This system uses a transfer line through which the outlet end of the column is connected to a light pipe which is a glass gas cell through which the analyte from the column passes and the FTIR analysis of the sample within the glass cell is conducted. The FTIR scanning parameters are dependent on the FTIR instrument.

Similarly, Analytical Solutions and Providers (ASAP) has a vapor phase FTIR system, IRD3, which can be directly coupled to the GC (like an MSD) to provide vapor phase IR analysis

of the analytes leaving the column. This system also has the option of extending the analytical capabilities to GC-IR-MS by allowing the analytes from the FTIR to be transferred to an MSD. This arrangement allows complementary analysis of analytes. The addition of the FID in this system would further improve the quantitative performance of this system.

One drawback of GC-IR systems as it currently stands is that it is limited to one dimensional GC analysis and does not take advantage of the superior separation from the GCxGC. This can be in part be due to technological limitations as well as relatively longer scan times needed for IR detection. The possibility of using a GCxGC with IR is something that is worth investigating as that will allow direct measurement of chemical functional group composition in complex fuels without the need for expensive techniques like the NMR spectroscopy.

4 CONCLUDING REMARKS

The need for finding alternative fuels which are sustainable as well as economical has risen over the past decade. In addition to the environmental concerns, depleting fossil fuel reserves justify the need for alternate fuels. Natural gas which has been a domestic fuel source for centuries has shown immense potential over the last 25 years for becoming a clean and sustainable fuel source for the future [42]. However, most of this anticipation is based on the basic properties of natural gas like simple molecular structure and low cost but the detailed studies of natural gas a potential replacement fuel for all the applications beyond domestic use are scarce. Natural gas is already widely used in the transportation sector, in internal combustion engines. However, there is much room for improvement [106–109] of these systems if natural gas is to successfully replace all the applications including heavy duty engines [110]. These previous studies have focused on the application and optimization of natural gas to internal combustion engines but there has been growing interest in using natural gas for applications beyond the transportation sector and into military and high performance applications like propulsion and rocket engines [111]. While the focus on research studies applicable to these systems is increasing, there is a large void in scientific understanding of natural gas which needs to be filled for successful adoption of natural gas in these applications.

The study of natural gas in this current work contributed towards providing high pressure and high temperature data for the oxidation of natural gas, which is scarce in literature. The study investigated the effect of mixture conditions (stoichiometry) on the chemical kinetic breakdown of natural gas using speciation data from single pulse shock tube experiments as well as the effect of varying natural gas composition on its chemical kinetic breakdown. The studies were carried out at different pressures (~60 atm and ~240 atm) to provide large data set which can be used for

validation and optimization of current chemical kinetic models. This study also looked into some of the well-established chemical kinetic models and their capability to model the natural gas breakdown at these conditions and compared them to experimental observations. The models tested showed a difference in predictions among themselves and had a very limited match with the experimental data. The ARAMCO 3.0 [4] and the USC Mech 2 [76] showed the best agreement overall while still missing the experimental observations at several conditions.

The overall conclusion from this study is the need to re-optimize the chemical kinetic mechanisms for natural gas oxidation by remeasuring or readjusting reaction rate parameters for the key reactions and validating with target properties beyond ignition delay times and flame speeds. Recent studies [82,84,112] by other groups focused on rectifying the reaction rate parameters show a significant improvement in the predictions from these chemical reactions and further justify this conclusion. More focus on research towards validation of reaction rate parameters along with confirmation from theoretical studies [87,113] are necessary to make these chemical kinetic mechanism suitable for use with natural gas applications.

With natural gas being in the preliminary stages of research towards becoming the fuel of choice, there is a need for optimization of currently used hydrocarbon fuels, particularly for military applications. The systems currently in use are heavily dependent on distillate hydrocarbon fuels. Depleting distillate hydrocarbon resources along with the logistical difficulty of supplying fuels that meet operation specifications across the world has made use of these fuels uneconomical. There is an interest in moving towards fuel independence so that indigenous and synthetic fuels can be easily used for all applications. The fuels currently in use are significantly different in molecular structure when compared to the synthetic and sustainable fuels, requiring additional chemical kinetic studies to investigate the feasibility of using these fuels. The chemical functional

group approach provides a pathway to simplify this study by facilitating the application of already available research data towards the goal of fuel independence. In the short run, fuel independence is key for military operations. However eventually fuel independence could penetrate the consumer market to unburden the fossil fuel reserves while benefiting the sustainability.

The chemical functional group based studies [46,48,49,92] of fuel combustion allow understanding the behavior of the fuel as a function of general descriptors which have been scientifically shown to have unique properties. The knowledge about how these general descriptors (chemical functional groups) affect the fuel combustion can be easily applied to any fuel under consideration. Conventional studies [15,16,26–28,33,103,114] of fuels have concentrated on the fuel composition and have evaluated the combustion behavior of the fuel as a whole as a function of its constituent components, which limits the application of these studies to a limited group of fuels. In addition to the general understanding, the knowledge of chemical functional groups within the fuel can be used towards development of several types of sensors which can be used onboard or offboard to optimize engine performance and emissions in real time based on the fuel being used. This will not only ensure reliable operation but also maintain emissions under control especially when applied to consumer applications.

A methodology for fuel analysis along with a method to obtain chemical functional group composition of the fuel from its composition was developed and applied to eleven different fuels. The outcome of the study provided a range within which the chemical functional group (UNIFAC) can be present within a fuel based on its composition. The chemical functional group composition of various fuel surrogates previously used for the chemical kinetic model development for a specific jet fuel were compared to the corresponding distillate jet fuels analyzed. The surrogates were found to be well within the range of the chemical functional group compositions obtained in

this study, however there was variation within them. The information about the chemical functional group composition of fuels can be extremely useful for development of surrogates in the future which would better represent the real fuel under consideration. This approach has been successfully applied using fuel surrogates [49], however the application of this approach can be limited since it is based on the fuel composition. If chemical functional group composition of the fuel is instead used to reverse engineer new synthetic fuel molecules, a universal method which could match the performance of the distillate jet fuels better can be developed.

The chemical functional group composition of fuels can also assist in estimating physical and chemical properties of the current and new fuels which are necessary for engineering applications while developing auxiliary systems necessary to facilitate use of the fuel like pumps and injectors. The use of UNIFAC groups [53] as the chemical functional groups in this study was motivated by the universal proven application of UNIFAC groups to estimate molecular properties [45]. There are additional promising studies [98,115] underway which are developing correlations between the UNIFAC groups and combustion target properties like ignition delay times and derived cetane number to extend the application of UNIFAC groups to large scale applications.

5 APPENDICIES

Appendix A

License Details

This Agreement between University of Illinois at Chicago -- Jai Mehta ("You") and John Wiley and Sons ("John Wiley and Sons") consists of your license details and the terms and conditions provided by John Wiley and Sons and Copyright Clearance Center.

Print Copy

License Number	5291650731512
License date	Apr 17, 2022
Licensed Content Publisher	John Wiley and Sons
Licensed Content Publication	International Journal of Chemical Kinetics
Licensed Content Title	Experimental speciation study of natural gas oxidation using a single pulse shock tube
Licensed Content Author	Kenneth Brezinsky, Jai M. Mehta
Licensed Content Date	Mar 11, 2021
Licensed Content Volume	53
Licensed Content Issue	7
Licensed Content Pages	23
Type of Use	Dissertation/Thesis
Requestor type	Author of this Wiley article
Format	Print and electronic
Portion	Full article
Will you be translating?	No
Title	A study of conventional fuels for unconventional applications
Institution name	University of Illinois at Chicago
Expected presentation date	Jun 2022
Requestor Location	University of Illinois at Chicago 842 W Taylor St , 2039 ERF CHICAGO, IL 60607 United States Attn: University of Illinois at Chicago
Publisher Tax ID	EU826007151
Total	**0.00 USD**

Appendix B

Test Mixture (Mole Fraction / ppm) – NG-RF-01						
Fuel				**Oxidizer**	***Bath Gas***	***φ***
CH4	C2H6	C3H8	Others	O2	Ar	
808.7	29.8	8.3	0.0	2161.0	996992.2	0.82
Carbon Content		893				

Shock No.	***Pressure (atm)***	***Time (sec)[1]***	***Temperature (K)***		***Mole Fraction (ppm)***								***Carbon Total***
			Ideal	**Calibrated[2]**	**CO**	**CO_2**	**CH_4**	**C_2H_6**	**C_2H_4**	**C_2H_2**	**C_3H_8**	**O_2**	
2	66	0.00265	1350.5	1342.5	41.1	23.5	778.9	31.0	10.2	0.0	3.5	2048.7	936.3
3	61	0.00260	1425.6	1413.4	44.4	25.9	740.0	32.0	20.1	0.0	0.9	1987.4	917.2
4	59	0.00276	1317.7	1310.9	32.7	14.2	760.3	29.4	5.4	0.0	5.0	2106.5	892.0
5	65	0.00258	1398.1	1387.6	24.0	23.3	742.5	31.4	16.5	1.0	1.5	2049.6	892.2
6	62	0.00237	1504.5	1485.7	94.0	30.6	651.0	30.4	37.5	4.8	0.0	1990.3	920.9
7	58	0.00241	1589.7	1561.7	241.0	501.0	131.6	6.9	11.4	5.8	0.2	817.5	922.5
8	60	0.00242	1566.9	1541.5	313.4	186.4	284.4	15.2	30.6	12.2	0.3	1385.8	901.3
9	62	0.00252	1476.7	1460.5	65.5	16.0	684.8	30.9	28.7	3.3	0.2	1950.9	892.7
10	69	0.00277	1353.0	1344.9	22.6	15.2	779.2	31.0	10.1	0.0	4.2	2098.6	911.7
11	59	0.00238	1625.3	1592.8	195.9	665.2	60.6	3.2	4.9	3.4	0.3	667.8	945.6
12	55	0.00240	1595.0	1566.3	173.1	666.6	64.9	3.5	5.2	3.3	0.0	729.4	928.6
13	59	0.00225	1672.4	1633.4	69.3	863.5	15.0	0.8	0.0	1.2	0.0	409.2	951.8
14	59	0.00234	1287.8	1281.8	23.1	11.8	777.7	29.6	5.2	0.0	6.4	2051.7	901.2
15	55	0.00245	1160.1	1153.3	12.8	12.2	796.7	29.4	2.0	0.0	7.9	2153.7	908.2
16	55	0.00241	1191.4	1185.4	24.0	8.8	779.0	28.8	0.0	0.0	7.6	1990.7	892.2
17	57	0.00234	1235.5	1229.6	27.3	8.2	771.4	28.7	1.4	0.0	7.3	2004.2	888.9
18	54	0.00246	1283.4	1276.8	21.8	10.0	777.7	29.6	3.7	0.0	6.1	2031.9	894.4
19	60	0.00229	1670.3	1631.5	61.7	884.0	11.9	0.5	0.0	0.9	0.0	458.6	960.4
20	49	0.00238	1262.2	1256.6	29.3	10.7	772.9	29.5	3.6	0.0	6.4	1965.9	898.3
21	54	0.00264	1392.6	1382.5	34.3	16.4	728.4	31.6	21.3	1.5	0.6	2028.6	889.9
22	58	0.00237	1397.4	1386.9	24.6	12.5	757.3	32.5	16.6	0.0	1.1	2097.8	895.6
23	60	0.00243	1447.1	1433.3	51.0	14.4	709.4	31.4	24.5	2.1	0.4	1994.0	892.2
24	61	0.00234	1606.3	1576.2	205.5	595.0	79.5	4.2	6.9	4.1	0.3	645.4	911.2
25	67	0.00230	1578.5	1551.8	368.9	238.0	218.6	11.5	24.9	11.4	0.2	1196.8	921.7
26	65	0.00244	1473.9	1457.8	74.5	16.4	665.1	31.0	34.4	4.6	0.3	1891.6	896.7
28	60	0.00237	1533.3	1511.6	278.1	99.2	368.9	20.0	41.3	15.5	0.0	1572.9	899.9
29	53	0.00222	1675.4	1635.9	42.7	874.4	17.6	0.9	0.0	0.0	0.0	577.0	936.6
30	68	0.00216	1711.5	1666.6	37.7	887.7	13.6	0.6	0.0	0.0	0.0	378.6	940.2
31	67	0.00220	1754.9	1702.7	35.8	906.1	7.6	0.3	0.0	0.0	0.0	433.1	950.2
32	66	0.00218	1772.7	1717.2	32.3	914.7	7.9	0.4	0.0	0.0	0.0	467.2	955.5
33	64	0.00218	1690.6	1647.9	68.8	828.8	19.0	0.9	3.4	1.5	0.0	573.3	928.1
34	67	0.00222	1699.8	1655.3	43.1	873.3	10.6	0.5	0.0	0.0	0.0	423.7	928.1
35	58	0.00228	1606.8	1574.9	104.3	737.2	53.8	2.7	7.2	2.7	0.0	687.1	920.5

Test Mixture (Mole Fraction / ppm) – NG-RF-02

Fuel				**Oxidizer**	***Bath Gas***	***φ***
CH4	C2H6	C3H8	Others	O2	Ar	
857.8	31.7	8.8	0.0	3839.3	995262.3	0.49
Carbon Content		947.82				

Shock No.	***Pressure (atm)***	***Time (sec)*[1]**	***Temperature (K)***		***Mole Fraction (ppm)***								***Carbon Total***
			Ideal	**Calibrated[2]**	**CO**	**CO_2**	**CH_4**	**C_2H_6**	**C_2H_4**	**C_2H_2**	**C_3H_8**	**O_2**	
1	69	0.00235	1414.0	1402.6	54.3	12.9	770.5	35.6	25.2	1.5	0.9	3579.8	964.9
2	64	0.00233	1354.5	1346.3	42.5	14.2	806.9	34.5	15.5	1.5	2.8	3635.0	975.0
3	65	0.00246	1412.7	1401.3	55.8	14.2	759.8	36.1	26.9	1.5	0.8	3637.5	961.1
4	63	0.00257	1428.6	1416.1	77.8	18.7	720.1	35.3	32.5	2.1	0.6	3549.1	958.1
7	60	0.00245	1455.2	1440.7	237.7	55.3	493.5	27.7	43.9	6.2	0.3	3252.1	943.0
8	62	0.00224	1610.4	1579.8	67.5	915.8	19.9	1.0	0.0	0.0	0.0	2005.2	1005.2
9	62	0.00231	1554.8	1530.8	179.5	721.6	65.1	3.6	9.9	1.5	0.0	2094.7	996.1
10	61	0.00243	1530.9	1509.4	311.8	581.1	96.5	4.9	7.7	1.9	0.2	2410.6	1019.0
11	61	0.00255	1488.3	1471.0	359.9	190.8	303.9	17.1	30.8	5.6	0.3	2889.7	962.7
12	60	0.00239	1553.3	1529.5	197.5	732.7	61.7	3.5	5.2	1.5	0.0	2096.4	1012.2
13	59	0.00228	1582.6	1555.4	88.8	863.7	34.4	1.9	4.6	0.9	0.0	2139.1	1001.8
14	56	0.00214	1267.2	1261.5	17.4	5.1	844.9	31.9	3.3	0.0	7.1	3874.4	959.0
15	56	0.00227	1211.8	1206.1	24.3	2.5	841.8	31.1	1.6	0.0	8.3	3864.2	958.7
16	55	0.00230	1178.1	1171.8	16.1	2.6	858.3	31.7	0.0	0.0	8.6	3839.3	966.4
17	47	0.00233	1209.0	1203.0	19.1	2.5	848.9	31.4	0.0	0.0	8.2	3827.1	957.9
18	53	0.00241	1279.1	1272.5	32.0	3.8	824.6	31.4	4.1	0.0	6.6	3794.5	951.1
19	54	0.00254	1333.7	1326.4	38.9	11.5	805.3	33.1	11.0	0.0	3.7	3569.7	955.1
20	53	0.00226	1293.5	1287.3	35.3	2.4	816.3	31.8	5.7	0.0	5.9	3686.5	946.7
21	52	0.00261	1359.4	1351.0	33.2	10.1	804.1	35.5	17.9	0.0	1.7	3614.0	959.4
23	52	0.00222	1442.3	1428.9	163.7	40.6	591.4	31.4	37.2	4.4	0.4	3504.6	943.0
24	53	0.00220	1394.1	1383.8	52.6	8.1	758.9	35.9	24.8	1.6	0.8	3591.4	946.6
25	51	0.00231	1435.1	1422.2	134.9	23.9	622.9	33.7	40.4	4.8	0.4	3422.2	940.7
26	68	0.00243	1525.3	1504.5	343.9	444.7	129.2	6.8	11.7	3.5	0.2	2400.8	962.3
27	71	0.00233	1483.1	1466.3	295.5	93.7	421.5	23.2	40.3	6.4	0.3	3327.1	951.4
28	69	0.00213	1631.8	1598.4	34.9	945.7	15.5	0.7	0.0	0.0	0.0	1983.4	997.5
29	63	0.00221	1637.4	1603.3	29.7	951.8	13.8	0.7	0.0	0.0	0.0	2214.1	996.8
30	65	0.00211	1776.6	1721.1	25.7	1012.9	6.4	0.3	0.0	0.0	0.0	2088.7	1045.6
31	67	0.00218	1754.2	1702.1	19.4	998.0	9.9	0.5	0.0	0.0	0.0	1992.0	1028.1
32	67	0.00216	1657.6	1620.0	30.2	957.3	16.6	0.8	0.0	0.0	0.0	2008.9	1005.8
33	68	0.00217	1691.4	1648.5	23.4	971.5	7.5	0.3	0.0	0.0	0.0	2088.1	1003.1
34	65	0.00218	1663.9	1624.7	27.5	953.5	15.1	0.8	0.0	0.0	0.0	2085.3	997.7
35	64	0.00234	1549.5	1524.4	205.8	670.3	75.9	4.0	10.3	1.5	0.0	1214.6	983.5

Test Mixture (Mole Fraction / ppm) – NG-RF-03

Fuel				**Oxidizer**	***Bath Gas***	***φ***
CH4	C2H6	C3H8	Others	O2	Ar	
875.6463	32.9391	8.986296	0	1284	997798.43	1.49
Carbon Content		968.4834				

Shock No.	***Pressure (atm)***	***Time (sec)[1]***	***Temperature (K)***		***Mole Fraction (ppm)***								***Carbon Total***
			Ideal	**Calibrated[2]**	**CO**	**CO_2**	**CH_4**	**C_2H_6**	**C_2H_4**	**C_2H_2**	**C_3H_8**	**O_2**	
1	57.5	0.0	1240.7	1235.2	9.2	14.2	874.2	32.9	2.1	0.0	8.1	1505.6	992.1
2	50.6	0.0	1098.6	1088.7	7.9	6.5	870.9	32.2	0.0	0.0	8.8	2732.4	976.2
3	61.4	0.0	1216.8	1211.2	17.6	17.4	850.2	31.8	2.0	0.0	8.1	1227.0	977.0
4	49.0	0.0	1088.8	1078.3	32.1	12.5	843.3	31.4	0.0	0.0	8.7	3342.2	976.7
5	69.9	0.0	1276.0	1270.2	0.4	19.8	867.0	33.0	4.2	0.0	6.8	1274.9	982.0
6	68.8	0.0	1389.5	1379.5	20.9	17.9	844.5	33.7	10.6	0.8	4.2	1338.0	986.2
7	46.4	0.0	1229.7	1224.1	7.7	13.5	880.0	33.4	1.9	0.0	8.6	1562.2	997.7
8	46.6	0.0	1176.2	1169.8	0.6	12.0	873.2	32.5	1.2	0.0	8.7	1284.8	979.2
9	61.6	0.0	1368.1	1359.3	18.5	19.9	848.2	33.2	8.2	0.8	5.3	1215.2	987.0
10	56.1	0.0	1330.8	1323.6	4.7	11.8	858.2	32.9	4.4	0.0	6.5	1388.1	968.9
11	49.4	0.0	1297.7	1291.5	8.1	13.5	866.9	33.4	3.7	0.0	7.2	1999.3	984.2
13	55.1	0.0	1417.0	1405.3	15.3	18.0	836.0	34.6	13.5	0.6	2.4	1405.0	973.9
14	56.6	0.0	1456.7	1442.1	36.4	28.5	818.4	32.9	22.5	2.9	1.4	2088.5	1004.3
16	53.8	0.0	1501.5	1483.0	35.6	22.9	802.0	29.6	30.1	4.1	0.7	2006.7	990.3
17	45.1	0.0	1270.3	1264.3	8.7	13.2	866.8	33.4	4.1	0.0	7.1	2053.1	985.1
18	48.6	0.0	1475.5	1458.7	35.3	22.0	804.3	31.6	24.9	4.1	0.9	1504.5	985.7
19	52.9	0.0	1590.4	1562.2	107.7	31.6	674.2	22.7	44.3	19.3	0.8	1143.8	988.4
20	56.2	0.0	1627.9	1595.0	160.6	41.4	605.8	19.5	47.4	31.2	1.0	1234.6	1007.0
25	59.8	0.0	1684.0	1643.3	307.2	79.7	488.7	16.1	50.7	49.7	1.7	249.5	1113.7
29	56.8	0.0	1867.5	1795.4	690.6	123.1	86.9	1.0	4.2	94.0	0.8	504.2	1101.5
30	55.5	0.0	1763.0	1709.8	374.5	79.4	373.5	10.8	37.0	49.9	0.8	875.9	1025.1
31	61.1	0.0	1844.0	1776.0	609.2	107.8	136.8	1.6	7.8	81.1	0.9	701.3	1037.3
33	50.7	0.0	1510.1	1489.7	47.9	26.3	770.7	27.6	33.0	6.0	0.7	1523.0	980.1
34	57.0	0.0	1773.6	1717.2	399.1	81.5	339.7	8.7	34.0	69.5	1.0	1118.3	1047.7

Test Mixture (Mole Fraction / ppm) - NG-RF-04

Fuel				**Oxidizer**	***Bath Gas***	***φ***
CH4	C2H6	C3H8	Others	O2	Ar	
873.1	32.3	9.0	0.0	630.0	998455.6	3.0
Carbon Content		964.6				

Shock No.	***Pressure (atm)***	***Time (sec)[1]***	***Temperature (K)***		***Mole Fraction (ppm)***							***Carbon Total***
			Ideal	**Calibrated[2]**	**CO**	**CO_2**	**CH_4**	**C_2H_6**	**C_2H_4**	**C_2H_2**	**C_3H_8**	**O_2**	
1	54	0.00322	1136.9	1129.2	0.0	1.3	861.3	32.0	1.0	0.0	8.7	622.3	954.7
2	53	0.00293	1179.9	1173.6	0.0	1.9	894.8	33.2	1.1	0.0	9.0	610.3	992.1
3	52	0.00245	1165.4	1158.7	0.0	2.5	890.9	33.4	2.2	0.0	9.0	630.2	991.7
4	60	0.00282	1277.3	1271.5	8.1	6.4	857.8	32.7	3.5	0.0	6.9	619.2	965.5
5	56	0.00292	1259.9	1254.3	5.9	3.0	855.5	32.3	2.8	0.0	7.2	598.0	956.3
6	58	0.00284	1300.6	1294.4	8.1	5.7	854.0	33.1	5.7	0.0	5.7	617.9	962.5
7	57	0.00281	1325.0	1318.0	7.8	7.4	850.2	33.9	9.1	0.0	3.7	584.1	962.5
8	57	0.00275	1370.1	1361.2	9.3	9.2	855.1	34.4	13.6	0.0	1.5	569.0	974.1
9	58	0.00262	1455.9	1441.4	19.1	9.6	835.6	29.4	22.9	2.3	0.5	468.6	975.0
10	55	0.00286	1391.6	1381.5	23.5	7.7	830.6	32.6	16.6	0.0	0.9	499.5	963.0
11	57	0.00250	1519.6	1499.4	31.1	11.2	792.1	22.6	32.4	7.7	0.6	493.5	961.5
12	56	0.00270	1444.6	1431.0	17.2	7.2	828.1	29.5	21.8	2.2	0.5	517.6	960.9
13	52	0.00266	1510.4	1491.0	26.4	11.0	816.2	25.4	30.1	6.1	0.5	473.4	978.1
14	52	0.00268	1578.3	1551.6	64.0	17.4	753.3	21.4	38.7	15.2	0.5	459.9	986.8
15	51	0.00248	1637.2	1603.1	97.9	20.6	643.2	14.2	41.7	42.2	0.6	409.8	959.6
16	62	0.00237	1647.9	1612.3	119.6	23.3	609.6	12.6	40.4	45.8	0.8	684.4	952.2
18	63	0.00245	1667.2	1628.2	243.3	31.8	406.4	5.6	25.8	82.7	0.3	281.9	910.7
19	64	0.00210	1831.9	1766.6	353.5	34.6	140.8	0.9	6.4	180.9	0.4	86.3	906.6
20	59	0.00234	1679.5	1639.5	264.1	31.2	348.1	4.2	21.6	121.4	0.5	239.3	939.2
21	61	0.00219	1751.7	1700.4	335.5	36.7	205.6	1.7	11.2	144.7	0.4	198.9	894.1
22	63	0.00217	1751.9	1700.5	316.7	34.0	237.7	2.1	12.7	138.8	0.5	193.0	897.2
23	65	0.00226	1720.8	1674.4	293.1	31.6	288.3	3.0	16.2	125.3	0.4	177.1	903.0
24	65	0.00229	1792.4	1734.2	366.9	37.9	125.1	0.9	6.3	158.4	0.3	70.2	862.0

Test Mixture (Mole Fraction / ppm) - NG-RF-05

Fuel				**Oxidizer**	***Bath Gas***	***φ***
CH4	C2H6	C3H8	Others	O2	Ar	
1012.364	37.13307	10.18247	0	0	998940.32	∞
Carbon Content		1117.18				

Shock No.	***Pressure (atm)***	***Time (sec)[1]***	***Temperature (K)***		***Mole Fraction (ppm)***								***Carbon Total***
			Ideal	**Calibrated[2]**	**CO**	**CO_2**	**CH_4**	**C_2H_6**	**C_2H_4**	**C_2H_2**	**C_3H_8**	**O_2**	
1	52	0.00337	1195.8	1189.9	0.0	0.0	1012.4	37.3	0.9	0.0	10.0	0.0	1118.8
2	55	0.00297	1135.2	1127.4	0.0	0.0	1012.5	37.2	0.8	0.0	10.1	0.0	1118.9
3	49	0.00301	1128.2	1120.0	0.0	0.0	1012.8	37.5	0.8	0.0	10.3	0.0	1120.2
5	53	0.00303	1239.7	1234.2	0.0	0.0	971.4	37.5	5.7	0.0	8.3	0.0	1082.5
7	53	0.00297	1329.0	1321.9	0.0	0.0	1003.8	40.2	0.0	0.0	3.6	0.0	1095.0
8	51	0.00302	1266.5	1260.8	0.0	0.0	977.1	36.8	4.8	0.0	7.7	0.0	1083.2
9	58	0.00281	1364.4	1355.8	0.0	0.0	986.2	37.7	15.5	0.0	1.7	0.0	1097.7
10	55	0.00276	1380.7	1371.3	0.0	0.0	1005.0	38.5	14.9	0.0	1.7	0.0	1116.9
11	52	0.00285	1391.1	1381.0	0.0	0.0	972.8	37.5	16.8	0.0	1.5	0.0	1086.1
12	57	0.00234	1613.8	1582.7	0.0	0.0	894.1	15.0	41.7	21.8	0.6	0.0	1053.0
13	57	0.00243	1561.4	1536.6	0.0	0.0	955.3	20.6	38.2	14.4	0.5	0.0	1103.5
14	63	0.00239	1624.9	1592.4	0.0	0.0	884.0	12.8	40.8	32.6	0.6	0.0	1058.1
15	55	0.00273	1412.4	1401.0	0.0	0.0	989.9	32.0	23.2	2.3	0.5	0.0	1106.3
16	52	0.00287	1420.8	1408.8	0.0	0.0	973.8	32.4	22.6	2.0	0.5	0.0	1089.6
17	52	0.00269	1507.2	1487.8	0.0	0.0	958.5	23.8	30.8	6.0	0.4	0.0	1080.7
18	57	0.00229	1672.8	1633.0	0.0	0.0	774.4	8.5	40.8	76.6	0.4	0.0	1027.3
19	59	0.00245	1577.2	1550.6	0.0	0.0	956.3	18.3	37.8	15.7	0.4	0.0	1100.9
20	63	0.00214	1664.9	1626.9	0.0	0.0	811.1	9.5	42.3	63.5	0.3	0.0	1042.7
21	51	0.00266	1435.3	1422.4	0.0	0.0	989.4	32.0	23.3	2.4	0.5	0.0	1106.2
22	53	0.00246	1502.8	1484.2	0.0	0.0	962.0	23.9	31.0	6.2	0.3	0.0	1085.1
23	48	0.00281	1353.5	1345.4	0.0	0.0	988.3	37.6	16.3	0.0	1.0	0.0	1099.3
24	50	0.00237	1612.0	1581.2	0.0	0.0	880.5	13.7	42.2	31.2	0.3	0.0	1055.8
25	63	0.00254	1539.1	1516.8	0.0	0.0	990.8	23.1	32.0	7.5	0.4	0.0	1117.1
26	67	0.00224	1663.5	1625.7	0.0	0.0	831.1	9.6	40.8	60.9	0.4	0.0	1054.7
27	68	0.00213	1756.4	1704.3	0.0	0.0	364.3	2.6	18.2	188.3	0.5	0.0	784.0
28	66	0.00210	1819.3	1756.2	0.0	0.0	336.9	1.3	13.7	269.4	0.4	0.0	906.9
29	65	0.00213	1696.2	1653.6	0.0	0.0	688.7	5.6	35.1	113.8	0.3	0.0	998.7
30	62	0.00225	1733.7	1685.3	0.0	0.0	581.6	3.8	28.1	159.1	0.0	0.0	963.5
31	58	0.00233	1655.3	1618.3	0.0	0.0	790.9	9.0	41.1	57.7	0.4	0.0	1007.5
32	64	0.00221	1794.2	1734.9	0.0	0.0	445.8	2.3	20.4	213.7	0.6	0.0	920.3
34	57	0.00237	1611.6	1579.5	0.0	0.0	880.4	12.8	42.5	33.5	0.2	0.0	1058.7

Test Mixture (Mole Fraction / ppm) – NG-RF-06

Fuel				**Oxidizer**	***Bath Gas***	***φ***
CH4	C2H6	C3H8	Others	O2	Ar	
950.4	34.7	9.6	0	2083	996922.2	0.99
Carbon Content		1048.80				

Shock No.	***Pressure (atm)***	***Time (sec)¹***	***Temperature (K)***		***Mole Fraction (ppm)***								***Carbon Total***
			Ideal	**Calibrated²**	**CO**	**CO_2**	**CH_4**	**C_2H_6**	**C_2H_4**	**C_2H_2**	**C_3H_8**	**O_2**	
1	52	0.00250	1114.5	1105.6	28.7	5.1	941.3	34.7	0.0	0.0	9.6	1897.5	1073.3
2	50	0.00254	1169.5	1163.0	15.9	3.0	942.1	34.4	0.7	0.0	9.4	2019.0	1059.6
3	53	0.00213	1164.9	1158.2	13.1	3.1	950.0	34.6	0.9	0.0	9.3	2211.5	1065.2
4	49	0.00276	1132.2	1124.2	21.6	3.2	936.9	34.2	0.9	0.0	9.3	2113.3	1059.9
5	50	0.00266	1203.3	1197.5	45.2	4.1	915.2	33.9	1.8	0.0	8.8	2488.1	1062.1
6	47	0.00272	1189.3	1183.3	15.4	5.4	949.0	34.8	2.0	0.0	9.2	2170.3	1071.1
7	47	0.00268	1199.6	1193.8	17.7	3.8	945.8	34.7	1.6	0.0	9.2	2078.7	1067.4
8	56	0.00244	1270.7	1265.0	23.8	9.6	918.6	35.7	7.4	0.0	5.7	2197.1	1055.1
9	57	0.00249	1274.5	1268.8	13.1	8.0	925.7	35.3	6.1	0.0	6.4	2052.4	1048.7
10	50	0.00292	1210.9	1205.2	14.8	7.0	939.8	34.7	2.4	0.0	8.5	2044.9	1061.1
11	55	0.00247	1363.8	1355.2	25.9	11.1	891.5	37.2	17.4	0.0	1.9	2045.1	1043.4
13	55	0.00232	1395.9	1385.6	50.8	10.9	896.2	38.6	21.8	1.5	2.0	1966.2	1087.5
14	55	0.00224	1429.5	1417.0	35.0	11.8	865.8	37.3	26.6	2.0	0.9	1794.0	1046.9
17	59	0.00256	1490.1	1472.3	182.0	33.9	651.4	32.7	53.5	12.3	0.5	1413.2	1065.7
18	55	0.00276	1476.6	1459.6	74.9	13.6	790.3	35.6	40.9	6.4	0.5	1711.8	1045.9
19	62	0.00266	1530.4	1509.0	246.3	56.2	532.9	26.6	50.5	13.0	0.6	1189.6	1017.1
20	57	0.00285	1414.2	1402.7	45.4	9.1	869.7	37.1	27.1	2.0	0.7	2183.3	1058.3
21	62	0.00257	1541.1	1518.6	403.1	169.0	333.2	16.5	37.8	15.8	0.5	939.0	1047.2
22	64	0.00243	1639.9	1605.4	242.4	876.2	38.4	1.8	6.5	4.9	0.5	245.8	1185.1
23	63	0.00243	1620.3	1588.4	259.0	792.1	54.3	2.6	4.8	4.9	0.5	579.5	1131.4
24	60	0.00255	1544.8	1521.9	428.3	227.4	307.7	15.3	35.2	16.6	0.8	1085.7	1100.0
25	62	0.00243	1605.6	1575.6	265.9	783.4	65.7	3.0	10.0	5.6	0.6	424.5	1153.8
26	55	0.00252	1581.3	1554.3	364.4	417.8	218.0	10.7	26.4	9.7	0.6	519.6	1095.6
28	57	0.00228	1689.0	1647.6	297.6	861.4	28.6	1.4	5.3	4.5	0.4	138.3	1211.3
30	62	0.00226	1668.1	1629.6	177.2	903.8	21.8	1.1	5.1	2.7	0.4	238.0	1121.7
31	62	0.00216	1776.9	1721.3	180.6	945.3	12.1	0.6	0.0	5.1	0.3	121.7	1150.3
32	60	0.00222	1742.6	1692.8	175.4	937.1	13.7	0.6	0.0	3.6	0.2	157.1	1135.2
33	58	0.00287	1322.9	1316.0	10.5	9.8	938.4	38.5	16.2	0.0	3.5	1993.6	1078.6

Test Mixture (Mole Fraction / ppm) – NG-ID-00

Fuel				**Oxidizer**	***Bath Gas***	***φ***
CH4	C2H6	C3H8	Others	O2	Ar	
981.7	43.9	4.7	14.6	2345	996610	0.89
Carbon Content		1083.73				

Shock No.	***Pressure (atm)***	***Time (sec)[1]***	***Temperature (K)***		***Mole Fraction (ppm)***								***Carbon Total***
			Ideal	**Calibrated[2]**	**CO**	**CO_2**	**CH_4**	**C_2H_6**	**C_2H_4**	**C_2H_2**	**C_3H_8**	**O_2**	
1	48	0.00299	1108.7	1099.5	29.3	13.8	976.9	43.8	1.2	0.0	4.6	2345.2	1123.8
2	51	0.00330	1164.9	1158.2	21.6	14.2	973.7	43.9	4.6	0.0	4.4	2361.3	1119.5
3	51	0.00311	1202.3	1196.5	22.4	13.9	970.2	43.8	4.8	0.0	4.3	2304.9	1116.4
4	47	0.00329	1176.9	1170.5	22.2	14.0	968.6	43.7	4.2	0.0	4.3	2405.8	1113.6
5	46	0.00332	1171.5	1165.0	23.5	13.7	965.9	43.3	3.1	0.0	4.3	2483.7	1108.7
6	45	0.00341	1187.7	1181.6	14.6	15.7	994.8	45.1	6.0	0.0	4.1	2398.8	1139.5
7	39	0.00332	1156.8	1149.8	22.2	15.1	974.2	43.8	3.9	0.0	4.3	2334.4	1119.7
8	51	0.00273	1282.3	1276.4	20.9	17.5	958.7	45.3	16.2	0.0	1.6	2176.5	1124.9
9	55	0.00279	1352.6	1344.5	25.3	16.4	956.1	45.1	16.4	0.0	1.4	2553.5	1124.8
10	51	0.00307	1290.9	1284.8	29.0	16.0	952.1	43.6	6.6	0.0	3.5	2436.4	1108.0
11	54	0.00310	1261.3	1255.7	18.9	17.8	980.1	44.5	7.8	0.0	3.7	2574.7	1132.5
13	47	0.00298	1378.1	1368.8	91.5	24.5	879.9	49.8	66.7	13.7	0.4	2433.8	1257.5
14	49	0.00278	1404.1	1393.2	120.6	29.0	795.8	41.0	60.8	14.8	0.3	2277.2	1179.2
15	51	0.00265	1438.6	1425.4	201.7	40.1	664.7	32.8	57.2	18.7	0.4	1793.3	1124.9
16	48	0.00263	1505.6	1486.7	426.1	143.8	385.2	19.1	40.7	20.9	0.4	1267.3	1117.8
20	50	0.00274	1530.5	1509.1	492.9	251.1	287.6	14.1	38.2	16.6	0.5	855.3	1170.8
21	60	0.00256	1588.4	1560.5	645.9	431.3	79.8	3.4	16.1	15.6	0.6	400.3	1229.0
22	60	0.00269	1565.4	1540.2	507.5	692.7	131.3	6.6	26.0	13.3	0.7	636.0	1425.7
23	57	0.00236	1645.9	1610.6	657.2	559.1	68.6	2.9	15.2	14.4	0.8	237.3	1352.2
24	59	0.00225	1680.1	1639.9	491.0	782.8	22.2	0.8	0.0	8.1	0.5	146.5	1315.2
25	58	0.00224	1704.5	1660.7	475.3	819.3	13.2	0.5	0.0	8.8	0.4	10.5	1327.7
27	54	0.00237	1760.5	1707.7	464.2	777.1	13.3	0.4	0.0	10.1	0.4	0.0	1276.8
28	53	0.00263	1829.5	1764.6	447.9	785.3	10.0	0.3	0.0	10.1	0.3	0.0	1265.0
29	44	0.00295	1313.4	1306.8	35.4	26.2	937.4	44.5	18.3	1.1	0.9	2648.2	1129.3
30	43	0.00286	1390.9	1380.9	50.1	28.3	899.2	41.9	26.4	2.3	0.5	2674.2	1120.3
31	47	0.00274	1442.2	1428.7	207.2	51.0	710.3	36.5	59.8	19.4	0.5	1699.2	1201.2
32	44	0.00283	1490.9	1473.4	437.1	123.1	510.7	27.7	60.0	26.9	0.5	1401.7	1301.5
33	53	0.00241	1589.3	1561.3	513.8	415.5	143.2	6.6	24.0	13.0	0.4	536.9	1160.8

Test Mixture (Mole Fraction / ppm) – NG-KY-01

Fuel				**Oxidizer**	**Bath Gas**	**φ**
CH4	C2H6	C3H8	Others	O2	Ar	
936	79	3	9	2065	996909	1.04
Carbon Content	1101.32					

Shock No.	***Pressure (atm)***	***Time (sec)[1]***	***Temperature (K)***		***Mole Fraction (ppm)***								***Carbon Total***
			Ideal	**Calibrated[2]**	**CO**	**CO_2**	**CH_4**	**C_2H_6**	**C_2H_4**	**C_2H_2**	**C_3H_8**	**O_2**	
1	48	0.00229	1011.3	994.0	2.9	8.8	921.9	77.7	0.0	0.0	2.6	2480.4	1096.8
2	49	0.00240	1096.5	1086.5	3.4	9.3	934.2	78.3	0.0	0.0	2.7	2423.8	1111.5
3	46	0.00248	1147.6	1140.3	4.2	9.1	939.4	78.5	0.0	0.0	2.7	1946.4	1118.0
4	54	0.00195	1246.2	1240.6	5.4	13.0	936.6	76.7	7.0	3.2	2.4	2064.7	1135.8
5	48	0.00284	1218.0	1212.4	10.6	13.2	910.5	74.9	5.7	2.3	2.5	2006.3	1107.5
6	51	0.00242	1269.4	1263.7	16.9	16.3	892.9	71.4	15.4	4.4	1.8	2508.5	1113.8
7	48	0.00264	1280.6	1274.8	8.4	15.9	920.6	71.8	22.5	5.3	1.4	2138.4	1148.4
8	43	0.00276	1285.6	1279.7	8.2	18.5	917.5	71.0	25.3	5.0	1.3	2910.9	1150.6
9	40	0.00278	1326.4	1319.4	13.0	19.7	898.2	68.3	29.3	5.5	1.1	2878.3	1140.4
11	54	0.00278	1361.8	1353.3	32.3	19.9	863.4	58.4	53.9	9.0	0.7	2056.4	1160.4
12	50	0.00254	1419.2	1407.4	70.3	23.8	797.7	47.9	81.3	13.4	0.5	2078.3	1178.6
13	47	0.00256	1463.8	1448.6	144.1	33.6	673.8	37.9	100.1	23.1	0.5	1613.8	1175.2
14	51	0.00235	1664.5	1626.6	632.1	498.0	60.2	2.8	13.0	21.3	0.7	546.8	1266.6
16	44	0.00268	1399.2	1388.6	59.2	21.2	802.8	49.4	75.3	9.6	0.4	1856.6	1153.1
17	45	0.00247	1543.4	1520.3	437.8	172.0	326.4	18.2	68.4	23.6	0.4	1372.7	1157.6
21	60	0.00245	1437.7	1424.6	91.1	18.9	741.9	42.0	90.1	11.1	0.2	1685.8	1139.1
22	56	0.00243	1479.6	1463.1	260.3	53.5	539.2	30.2	100.3	23.2	0.4	1664.8	1161.4
23	56	0.00242	1609.8	1579.2	521.7	388.0	130.3	7.1	26.8	12.7	0.3	576.1	1134.0
24	57	0.00236	1617.1	1585.6	520.1	401.5	119.7	6.5	24.6	9.9	0.4	875.0	1124.4
25	58	0.00238	1549.9	1526.4	478.7	199.3	275.9	15.3	61.3	18.6	0.2	1640.3	1145.1
26	54	0.00225	1723.3	1676.6	405.9	687.8	19.6	1.0	2.7	7.3	0.3	314.2	1136.2
27	50	0.00236	1724.4	1677.5	396.7	701.1	21.6	1.3	2.3	6.6	0.2	461.9	1140.4
28	48	0.00245	1769.8	1715.4	405.4	704.7	9.2	0.4	0.0	9.4	0.2	379.9	1139.5
29	51	0.00232	1839.6	1772.8	429.1	725.6	9.4	0.5	0.0	11.7	0.0	315.0	1188.4

Test Mixture (Mole Fraction / ppm) – NG-TN-01

Fuel				**Oxidizer**	***Bath Gas***	***φ***
CH4	C2H6	C3H8	Others	O2	Ar	
962.2	70.2	2.0	10.6	2199.8	996755.3	0.98
Carbon Content		1108.64				

Shock No.	***Pressure (atm)***	***Time (sec)[1]***	***Temperature (K)***		***Mole Fraction (ppm)***								***Carbon Total***
			Ideal	**Calibrated[2]**	**CO**	**CO_2**	**CH_4**	**C_2H_6**	**C_2H_4**	**C_2H_2**	**C_3H_8**	**O_2**	
1	46	0.00336	982.3	961.7	0.0	2.8	962.2	70.2	0.0	0.0	2.0	3313.0	1111.5
2	50	0.00222	1181.2	1174.9	3.6	8.8	945.9	68.6	0.0	0.0	1.8	2398.1	1100.9
3	48	0.00207	1056.9	1044.0	5.0	8.5	944.9	68.7	0.0	0.0	2.0	2176.9	1101.7
4	50	0.00199	1110.6	1101.4	5.3	8.9	952.1	69.3	0.0	0.0	2.0	2546.0	1110.8
5	59	0.00227	1491.2	1473.7	119.3	34.9	747.7	40.6	86.8	26.9	1.1	1919.5	1213.7
6	49	0.00192	1202.3	1196.5	3.7	11.3	971.2	69.9	3.7	1.2	1.9	2551.4	1141.6
7	53	0.00238	1336.9	1329.5	16.4	16.6	913.7	62.5	19.6	4.6	1.1	2342.1	1123.2
8	57	0.00200	1308.9	1302.4	12.9	12.2	923.8	65.2	11.0	2.0	1.4	2584.1	1109.4
9	49	0.00194	1299.4	1293.2	13.0	11.6	929.1	66.5	6.6	1.7	1.7	2383.0	1108.4
11	53	0.00230	1414.9	1403.4	31.9	19.9	874.9	53.4	47.6	8.4	0.5	1873.2	1147.0
12	45	0.00256	1403.8	1393.0	26.4	17.8	879.4	54.2	44.0	6.7	0.5	1973.6	1134.9
14	46	0.00258	1527.5	1506.4	305.0	82.6	524.3	29.1	94.3	29.0	0.7	1950.5	1218.9
15	45	0.00252	1566.9	1541.5	415.7	136.4	397.5	22.2	79.5	32.2	1.0	1399.1	1220.4
16	46	0.00244	1624.9	1592.4	471.3	462.7	161.3	9.2	29.7	20.2	0.8	867.7	1215.7
17	49	0.00249	1646.2	1610.5	436.0	547.5	120.0	7.0	21.4	15.9	0.6	934.8	1193.7
18	42	0.00285	1183.3	1176.4	6.7	10.7	953.3	69.0	0.0	0.0	1.8	2340.2	1114.3
19	41	0.00283	1171.8	1165.3	6.4	13.0	954.6	69.0	2.5	1.3	2.0	1598.3	1125.7
20	45	0.00250	1293.0	1286.9	21.4	15.6	946.4	67.3	8.8	3.9	1.7	1740.2	1148.7
21	46	0.00229	1251.0	1245.5	8.3	12.5	943.7	67.5	4.1	1.8	1.9	1860.4	1117.0
22	41	0.00267	1349.7	1341.8	9.6	19.3	938.7	64.2	21.5	6.0	1.1	2433.5	1154.1
23	50	0.00252	1453.3	1439.0	92.7	32.2	776.8	42.9	83.0	24.5	0.9	1908.3	1205.1
24	46	0.00245	1592.1	1563.8	511.0	322.7	235.3	12.8	47.8	31.8	1.3	1023.5	1257.4
25	54	0.00248	1581.5	1554.4	469.1	217.9	282.6	15.4	58.4	11.6	0.9	0.0	1142.8
26	52	0.00236	1690.2	1648.5	423.3	801.1	24.8	1.2	1.4	33.1	0.7	808.7	1322.9
30	50	0.00225	1714.1	1668.8	426.2	830.3	18.9	0.8	2.9	16.4	0.4	298.4	1317.0
31	49	0.00267	1772.6	1717.8	344.5	845.5	14.5	0.6	2.3	16.1	0.4	222.8	1243.8
32	54	0.00244	1027.3	1011.7	5.3	10.1	960.7	69.9	0.0	0.0	1.9	2199.8	1121.5

Test Mixture (Mole Fraction / ppm) – NG-OH-01

Fuel				**Oxidizer**	***Bath Gas***	***φ***
CH4	C2H6	C3H8	Others	O2	Ar	
997.6	62.9	3.1	0.2	1981.1	996955.0	1.12
Carbon Content		1132.94				

Shock No.	***Pressure (atm)***	***Time (sec)[1]***	***Temperature (K)***		***Mole Fraction (ppm)***								***Carbon Total***
			Ideal	**Calibrated[2]**	**CO**	**CO_2**	**CH_4**	**C_2H_6**	**C_2H_4**	**C_2H_2**	**C_3H_8**	**O_2**	
1	53	0.00207	953.5	929.1	3.5	7.7	977.8	62.0	0.0	0.0	3.0	1593.3	1122.3
2	46	0.00242	1094.8	1084.7	2.4	8.4	984.1	62.0	0.0	0.0	3.0	2615.4	1128.0
3	45	0.00236	1088.3	1077.8	6.0	7.3	979.0	61.7	0.0	0.0	3.2	1981.1	1125.1
4	53	0.00210	1205.5	1199.7	9.9	10.1	981.2	61.4	3.8	1.2	2.8	2283.3	1142.5
5	47	0.00232	1125.3	1116.9	6.3	7.8	980.6	61.6	0.0	0.0	3.1	1971.6	1127.2
6	48	0.00264	1191.5	1185.5	1.4	9.5	1002.9	63.0	2.3	0.7	3.1	2498.8	1155.0
7	51	0.00212	1245.2	1239.7	9.4	11.5	969.8	60.5	6.1	1.6	2.6	2077.9	1134.8
8	49	0.00253	1284.3	1278.4	6.4	11.4	974.2	59.6	14.0	2.4	1.7	2022.4	1149.1
11	53	0.00245	1431.9	1419.2	86.2	19.7	817.2	41.5	83.4	13.1	0.0	1639.1	1199.2
12	53	0.00251	1357.8	1349.5	11.7	10.9	950.6	55.3	29.2	2.5	0.6	2006.4	1149.0
13	53	0.00251	1417.2	1405.6	30.2	14.1	907.5	49.2	55.0	4.8	0.3	1827.5	1171.0
14	46	0.00249	1428.4	1415.9	79.9	19.1	836.6	43.2	80.7	12.2	0.3	2059.4	1208.5
15	50	0.00239	1448.8	1434.8	107.0	22.5	774.1	39.8	87.5	14.7	0.0	1785.0	1187.6
16	46	0.00240	1543.3	1520.5	483.7	385.0	191.2	9.9	36.8	15.3	0.3	948.3	1184.9
17	48	0.00230	1606.8	1576.3	347.2	730.9	77.6	4.4	8.7	8.8	0.4	537.3	1200.5
18	44	0.00231	1579.8	1552.2	410.6	654.4	79.4	4.4	8.5	8.0	0.3	516.7	1187.3
19	48	0.00247	1442.6	1429.1	78.3	18.9	812.9	41.5	76.1	9.7	0.2	1559.7	1165.6
20	45	0.00247	1447.6	1433.7	81.6	20.6	824.8	42.1	77.6	11.3	0.3	1717.4	1189.9
21	57	0.00233	1513.3	1493.6	409.7	147.2	394.6	21.1	74.2	22.7	0.5	1470.6	1189.0
23	61	0.00230	1526.6	1505.6	487.8	220.1	275.5	14.7	51.9	18.3	0.4	2345.1	1154.3
24	58	0.00241	1444.7	1431.0	71.8	18.1	831.0	42.5	73.9	8.1	0.2	1861.5	1170.5
25	60	0.00230	1525.0	1504.2	492.9	192.8	292.5	15.3	58.7	19.5	0.4	1223.1	1166.3
26	55	0.00238	1569.5	1543.8	463.3	572.6	90.6	4.8	12.4	7.9	0.3	654.3	1177.5
27	54	0.00210	1862.1	1791.1	404.1	776.5	10.1	8.6	0.0	16.5	0.3	213.4	1241.9
28	47	0.00263	1563.9	1538.8	425.7	523.9	157.7	8.7	20.6	9.4	0.3	955.2	1185.8
29	48	0.00240	1675.3	1635.8	370.1	751.4	39.8	2.2	2.4	6.4	0.2	772.9	1184.1
30	47	0.00248	1644.6	1609.4	372.1	731.9	36.9	1.9	3.9	4.8	0.2	540.0	1162.9
31	47	0.00248	1761.0	1708.1	384.5	765.3	16.5	0.8	0.0	11.0	0.2	657.7	1190.7
32	46	0.00265	1494.4	1476.5	338.2	109.8	474.3	25.7	81.8	20.9	0.3	1627.8	1179.8
33	44	0.00271	1460.2	1445.4	136.9	27.1	734.6	38.4	91.5	14.4	0.2	1981.3	1187.8

Test Mixture (Mole Fraction / ppm) – NG-NC-01

Fuel				**Oxidizer**	***Bath Gas***	***φ***
CH4	C2H6	C3H8	Others	O2	Ar	
1048.6	33.3	1.9	10.4	2175.2	996730.7	1.02
Carbon Content		1120.78				

Shock No.	***Pressure (atm)***	***Time (sec)[1]***	***Temperature (K)***		***Mole Fraction (ppm)***								***Carbon Total***
			Ideal	**Calibrated[2]**	**CO**	**CO_2**	**CH_4**	**C_2H_6**	**C_2H_4**	**C_2H_2**	**C_3H_8**	**O_2**	
1	51	0.00212	1000.1	981.6	3.1	10.6	1034.1	32.9	0.0	0.0	1.8	1621.8	1118.9
2	51	0.00243	1094.3	1084.2	4.1	12.1	1042.8	33.2	0.0	0.0	1.8	2291.5	1130.8
3	49	0.00243	1099.3	1089.5	-1.1	14.1	1044.0	33.2	0.0	0.0	1.8	3333.3	1128.7
4	48	0.00263	1108.0	1098.7	5.2	14.6	1046.0	33.4	0.0	0.0	1.8	2441.9	1138.0
5	47	0.00253	1124.7	1116.3	7.8	14.1	1037.6	33.1	0.0	0.8	1.8	2206.1	1132.7
6	42	0.00277	1096.5	1086.5	5.1	13.4	1031.1	32.9	0.0	0.0	1.9	2175.2	1120.9
7	44	0.00285	1151.1	1143.9	4.1	16.9	1059.6	33.8	0.0	1.9	1.9	2170.1	1157.7
8	41	0.00298	1148.7	1141.4	8.0	16.7	1039.7	33.3	0.0	1.5	1.8	2846.3	1139.4
9	42	0.00268	1222.3	1216.7	5.2	14.8	1038.7	33.3	2.6	1.6	1.7	2010.7	1138.7
10	44	0.00280	1309.0	1302.5	14.1	14.8	1009.9	33.5	9.5	1.9	0.6	2013.2	1130.5
13	51	0.00262	1306.0	1299.6	12.4	12.8	1038.4	34.1	7.4	1.0	0.8	2307.7	1150.9
14	54	0.00260	1244.5	1238.9	5.4	12.6	1031.7	33.3	3.1	0.0	1.6	2268.1	1127.3
15	51	0.00269	1279.1	1273.3	10.3	12.8	1039.2	34.0	4.9	1.1	1.2	2193.4	1145.8
16	50	0.00253	1383.5	1373.9	22.6	14.4	983.9	33.5	20.4	2.0	0.3	2093.1	1133.5
17	50	0.00258	1355.7	1347.2	16.2	13.8	1012.3	33.8	12.8	1.3	0.3	2224.4	1139.0
18	45	0.00273	1400.9	1389.5	46.9	16.0	932.4	34.0	39.9	3.8	0.3	2089.4	1151.5
19	45	0.00275	1438.0	1424.9	170.8	43.3	724.2	31.7	71.2	13.1	0.2	2012.3	1171.1
20	47	0.00256	1546.3	1523.3	346.1	610.3	136.5	6.0	16.2	6.1	0.3	664.3	1150.5
21	44	0.00282	1443.3	1429.8	193.8	56.7	663.0	29.3	68.4	12.7	0.3	1798.7	1135.1
22	45	0.00283	1461.9	1446.9	277.5	100.9	557.8	25.4	66.6	14.8	0.3	1873.0	1150.6
23	45	0.00274	1511.6	1492.1	350.7	391.7	278.9	12.6	35.2	9.9	0.2	1039.3	1137.4
24	43	0.00277	1506.7	1487.7	352.6	331.4	328.5	14.4	38.8	9.7	0.3	1203.0	1138.9
25	57	0.00255	1399.8	1389.3	50.5	16.6	937.3	34.8	42.5	3.9	0.2	2216.8	1167.5
26	51	0.00264	1462.6	1447.6	267.2	96.0	557.1	25.3	68.4	15.5	0.3	1577.6	1139.5
27	55	0.00250	1555.8	1531.7	291.2	745.9	71.9	3.1	6.7	3.7	0.3	465.6	1136.6
28	52	0.00256	1558.3	1533.9	263.6	808.8	46.1	2.0	3.6	3.5	0.2	366.5	1137.2
29	54	0.00240	1712.0	1667.0	251.8	869.9	15.8	0.8	0.0	3.8	0.2	346.0	1147.3
30	52	0.00239	1635.6	1601.7	257.3	849.4	21.6	0.9	2.2	2.5	0.3	410.0	1140.3
31	56	0.00230	1693.6	1651.4	262.8	869.3	23.9	1.1	0.0	3.4	0.3	300.7	1165.8
34	57	0.00228	1628.9	1595.9	291.3	766.5	45.8	2.1	6.4	3.3	0.3	422.1	1128.0
35	48	0.00240	1538.9	1516.7	350.9	571.3	146.5	7.1	23.4	7.9	0.0	776.4	1145.6

Test Mixture (Mole Fraction / ppm) – NG-SC-01

Fuel				**Oxidizer**	***Bath Gas***	***φ***
CH4	C2H6	C3H8	Others	O2	Ar	
985.2	27.9	1.6	6.5	1964.0	997014.8	1.05
Carbon Content		1045.82				

Shock No.	***Pressure (atm)***	***Time (sec)[1]***	***Temperature (K)***		***Mole Fraction (ppm)***								***Carbon Total***
			Ideal	**Calibrated[2]**	**CO**	**CO_2**	**CH_4**	**C_2H_6**	**C_2H_4**	**C_2H_2**	**C_3H_8**	**O_2**	
1	53	0.00229	969.7	947.5	3.0	17.4	975.8	27.7	0.0	0.0	1.7	1964.0	1056.6
2	48	0.00273	1070.6	1058.8	8.0	17.7	959.6	27.2	0.0	0.0	1.6	2081.9	1044.4
3	47	0.00280	1094.2	1084.1	7.0	17.9	974.3	27.6	0.0	0.0	1.6	2099.2	1059.3
4	48	0.00254	1137.9	1130.2	10.7	19.1	958.6	27.3	0.0	0.0	1.6	2392.1	1048.0
5	47	0.00269	1179.4	1173.1	6.2	19.4	984.2	28.0	0.0	0.9	1.7	2237.7	1072.7
6	42	0.00299	1170.1	1163.6	6.7	20.3	990.9	28.4	0.0	1.1	1.6	2375.9	1081.9
7	45	0.00284	1204.0	1198.2	5.1	19.4	967.2	27.6	0.0	1.1	1.5	1940.6	1053.7
8	43	0.00291	1222.4	1216.8	6.8	19.7	965.7	27.9	2.5	1.3	1.4	1939.4	1059.9
9	46	0.00286	1309.4	1302.9	12.2	24.0	960.1	29.7	11.5	3.5	0.5	2047.8	1087.1
10	44	0.00291	1291.2	1285.2	13.3	21.1	945.1	28.3	6.0	2.0	0.8	2050.7	1054.6
11	46	0.00285	1277.6	1271.7	10.6	20.2	951.0	28.1	5.4	2.2	1.0	2249.0	1056.5
12	43	0.00280	1315.8	1309.1	9.7	24.3	945.4	29.3	12.5	4.9	0.6	2129.8	1074.4
13	39	0.00279	1356.2	1348.0	26.9	29.5	933.4	30.8	21.4	5.8	0.4	3247.1	1107.0
14	52	0.00267	1386.3	1376.5	30.0	26.3	921.0	29.7	22.3	7.3	0.4	2356.1	1097.2
15	50	0.00273	1405.7	1394.8	37.0	26.2	892.6	29.8	27.3	8.3	0.5	2000.6	1087.8
16	48	0.00263	1443.3	1429.7	58.9	28.1	842.1	30.3	40.0	10.0	0.4	2075.8	1090.9
17	42	0.00275	1472.1	1455.9	108.1	38.3	771.0	31.1	61.3	17.1	0.4	2018.5	1137.7
18	43	0.00260	1564.7	1538.8	423.3	449.6	176.8	8.4	30.2	17.5	0.7	980.1	1164.1
19	46	0.00247	1572.6	1546.6	415.1	612.3	81.6	3.7	13.3	13.5	0.6	863.4	1171.9
20	49	0.00247	1556.4	1532.2	401.0	242.4	308.0	14.5	51.5	23.1	0.7	1182.9	1131.9
21	51	0.00245	1519.2	1498.9	287.8	120.3	491.9	22.8	67.8	23.9	0.6	1693.3	1131.0
22	45	0.00266	1423.2	1411.1	48.8	27.8	860.0	29.9	33.9	9.1	0.4	1959.6	1083.7
23	51	0.00247	1511.6	1492.1	255.5	99.3	521.4	23.7	66.7	21.6	0.5	1636.5	1101.6
24	50	0.00265	1483.5	1466.6	186.9	70.8	615.3	27.3	68.3	19.9	0.5	1812.4	1105.4
25	49	0.00234	1638.7	1604.4	326.3	787.5	29.0	1.4	1.4	17.6	0.4	381.7	1184.9
27	56	0.00225	1697.2	1654.5	315.1	802.5	18.0	0.8	0.0	19.1	0.4	383.0	1176.9
28	58	0.00225	1711.9	1666.9	314.6	799.1	18.9	0.8	2.4	14.6	0.4	456.2	1169.2
29	50	0.00224	1589.9	1561.8	316.5	740.5	38.3	1.8	4.4	9.6	0.4	602.2	1128.4
30	55	0.00222	1564.7	1539.6	425.9	393.7	185.3	8.6	34.2	18.4	0.6	1000.9	1129.4
31	57	0.00220	1568.1	1542.6	410.7	525.2	122.6	5.6	20.8	15.3	0.7	711.9	1144.1
32	55	0.00219	1558.5	1534.1	412.5	335.2	238.2	11.0	39.0	18.3	0.5	863.1	1123.9
33	55	0.00206	1787.5	1730.1	354.3	813.4	10.6	0.4	0.0	29.4	0.5	348.1	1239.3
34	54	0.00227	1497.4	1479.2	213.8	79.6	590.8	26.6	69.0	21.3	0.5	2106.6	1119.6

Test Mixture (Mole Fraction / ppm) – NG-RF-08

Fuel			**Oxidizer**	***Bath Gas***	***φ***
CH4	C2H6	C3H8	O2	Ar	
956.0	35.1	9.8	2050.0	996949.2	1.02
Carbon Content		1055			

Shock No.	***Pressure - P5 (atm)***	***Time (sec)[1]***	***Temperature (K)***		***Mole Fraction (ppm)***								
			Ideal	**Calibrated[2]**	**CO**	**CO_2**	**CH_4**	**C_2H_6**	**C_2H_4**	**C_2H_2**	**C_3H_8**	**O_2**	**H_2**
2	239	0.00250	1234.5	1189.1	-23.2	18.8	918.2	34.8	8.8	1.9	8.5	2681.2	0.0
4	242	0.00246	1288.3	1242.6	-34.7	22.9	940.4	36.3	15.6	5.3	7.6	2214.6	0.0
5	233	0.00242	1333.9	1287.0	-78.8	23.2	972.8	38.6	26.2	6.3	5.4	2325.3	6.0
7	239	0.00263	1374.4	1325.9	32.1	38.9	863.8	36.5	48.6	9.6	2.2	1875.0	12.5
8	235	0.00262	1405.4	1355.2	68.6	43.9	806.9	35.0	62.1	12.4	1.3	1791.5	23.6
9	226	0.00271	1402.0	1352.0	74.4	46.7	796.1	34.8	65.1	13.6	1.3	1786.4	25.5
10	227	0.00263	1452.9	1399.5	161.6	60.0	670.0	30.8	87.6	20.9	1.2	1562.1	53.8
12	234	0.00243	1620.8	1550.3	535.6	628.5	93.9	3.4	18.2	37.7	1.4	6617.0	109.2
13	240	0.00256	1470.7	1415.9	93.7	34.9	733.1	32.2	59.7	11.0	1.1	3465.6	24.6
14	238	0.00260	1458.8	1404.9	162.9	40.0	666.2	30.6	68.7	8.9	1.0	5324.3	26.7
15	234	0.00243	1507.1	1449.1	111.4	37.4	722.6	32.6	74.9	12.7	0.8	1959.5	40.0
16	230	0.00244	1527.8	1467.5	230.0	58.2	590.0	26.8	83.1	21.3	1.1	1287.9	66.9
17	236	0.00253	1544.6	1482.2	380.5	94.9	425.4	19.8	82.4	23.8	1.2	1675.8	88.3
18	231	0.00245	1580.6	1514.9	522.9	170.4	263.2	11.8	58.8	26.1	1.3	911.6	94.7
19	230	0.00246	1589.0	1522.4	607.0	235.0	165.0	6.9	40.1	24.3	1.2	639.2	89.4
20	248	0.00234	1364.8	1316.7	-15.2	33.8	899.0	36.1	26.3	5.2	5.6	8326.1	0.0
21	218	0.00248	1643.0	1569.6	600.2	498.0	55.2	2.0	14.9	25.6	1.1	1110.5	66.0
22	225	0.00242	1697.2	1616.2	297.7	779.0	18.0	0.6	0.0	10.1	0.6	1353.6	54.3
23	221	0.00246	1615.3	1545.4	465.0	532.0	54.7	2.2	12.0	10.8	0.5	513.3	51.2
24	224	0.00243	1629.4	1557.8	458.6	653.0	34.8	1.4	8.6	14.7	0.7	641.7	50.4
25	221	0.00243	1633.1	1561.0	509.9	565.0	40.1	1.4	10.5	17.1	0.9	502.8	54.4
26	223	0.00245	1639.9	1566.9	512.2	572.0	40.5	1.6	9.9	17.4	0.9	365.5	53.3
27	215	0.00241	1719.0	1634.7	288.2	819.0	12.6	0.4	0.0	0.8	0.4	367.6	48.5
28	205	0.00234	1753.6	1663.9	289.3	813.0	9.9	0.5	0.0	21.0	0.5	178.4	54.5
29	179	0.00270	1475.3	1420.2	68.5	39.3	747.0	33.4	62.8	7.1	0.3	1940.3	36.6

Test Mixture (Mole Fraction / ppm) – NG-RF-09

Fuel			**Oxidizer**	***Bath Gas***	***φ***
CH4	C2H6	C3H8	O2	Ar	
932.0	33.9	8.9	3600.0	995425.3	0.56
Carbon Content		1026			

Shock No.	***Pressure - P5 (atm)***	***Time (sec)[1]***	***Temperature (K)***		***Mole Fraction (ppm)***							
			Ideal	**Calibrated[2]**	**CO**	**CO_2**	**CH_4**	**C_2H_6**	**C_2H_4**	**C_2H_2**	**C_3H_8**	**O_2**	**H_2**
1	248	0.00234	1145.3	1097.7	-17.5	0.0	923.4	33.5	0.0	0.0	8.6	3701.9	0.0
2	242	0.00240	1201.2	1155.3	-12.7	32.7	915.9	33.2	0.0	0.0	8.2	3672.1	0.0
3	241	0.00244	1224.3	1178.7	-9.7	34.2	914.3	33.1	1.9	0.0	7.9	3174.5	0.0
4	234	0.00241	1299.9	1254.0	-18.6	35.0	892.2	32.7	10.6	2.9	6.2	3909.7	0.0
7	239	0.00242	1327.1	1280.4	-3.4	33.2	874.6	32.3	15.1	3.0	4.9	2494.9	0.0
8	235	0.00259	1339.3	1292.2	14.6	31.8	856.1	32.2	17.3	2.4	4.2	2978.4	0.0
9	224	0.00247	1380.7	1331.9	54.2	46.4	774.8	31.6	40.2	6.6	2.0	2863.1	0.0
10	250	0.00253	1372.7	1324.2	21.5	46.3	843.2	33.0	30.6	6.0	2.8	3795.7	0.0
11	247	0.00228	1432.3	1380.4	176.2	76.4	642.0	27.4	58.8	9.4	1.0	2377.6	0.1
13	226	0.00241	1679.0	1600.6	107.3	1133.0	8.7	0.2	0.0	0.0	0.3	3189.8	0.0
14	236	0.00210	1429.8	1378.0	106.9	43.7	741.0	31.6	54.2	8.7	2.0	3427.1	0.1
15	236	0.00180	1456.9	1403.2	169.0	57.3	658.0	27.8	56.6	7.3	1.5	2767.5	0.1
17	244	0.00251	1449.1	1395.3	368.7	106.0	429.0	19.2	64.0	9.1	0.8	2531.9	0.1
18	246	0.00263	1447.8	1394.8	519.2	149.0	308.0	13.5	62.6	11.9	0.5	2209.5	0.1
19	241	0.00250	1505.5	1447.7	527.7	538.0	66.7	2.6	13.3	7.2	0.6	1898.4	0.0
20	243	0.00255	1487.0	1430.8	544.1	435.0	73.7	2.9	15.5	5.5	0.2	1544.9	0.1
21	240	0.00246	1553.3	1490.7	255.9	791.0	18.3	0.8	3.4	2.3	0.0	1296.6	0.0
22	237	0.00240	1600.0	1532.1	90.9	1020.0	7.9	0.3	0.0	4.0	0.3	1546.7	0.0
23	228	0.00241	1597.3	1529.7	115.1	1010.0	6.9	0.4	1.4	5.0	0.3	1277.2	0.0
24	235	0.00255	1522.2	1462.7	369.3	686.8	32.2	1.5	6.0	4.0	0.2	1392.9	0.0
25	243	0.00253	1437.2	1384.9	400.2	131.0	383.1	16.9	59.0	7.3	0.5	2028.4	0.1
26	241	0.00255	1460.7	1406.7	433.7	102.2	372.9	16.7	69.7	7.5	0.4	2120.8	0.1
27	237	0.00241	1630.3	1558.6	78.8	1058.3	6.4	0.3	0.0	2.9	0.2	1197.8	0.0
28	233	0.00242	1588.3	1521.8	174.4	968.0	10.7	0.5	0.0	4.3	0.3	1362.3	0.0
29	239	0.00248	1544.6	1482.9	325.1	757.9	27.6	1.3	4.8	5.0	0.3	1404.2	0.0
30	229	0.00237	1654.6	1579.7	82.7	1125.4	4.3	0.5	0.0	5.5	0.3	1174.0	0.0
31	224	0.00229	1730.5	1644.5	70.1	1175.0	3.2	0.0	0.0	5.3	0.2	1446.4	0.0
32	218	0.00225	1876.9	1765.3	96.1	1319.5	2.4	0.0	0.0	10.7	0.3	1174.5	0.0

Test Mixture (Mole Fraction / ppm) – NG-RF-10

Fuel			**Oxidizer**	***Bath Gas***	***φ***
CH4	C2H6	C3H8	O2	Ar	
997.0	37.1	10.3	1160.0	997795.6	1.87
Carbon Content		1102			

Shock No.	***Pressure - P5 (atm)***	***Time (sec)[1]***	***Temperature (K)***		***Mole Fraction (ppm)***								
			Ideal	**Calibrated[2]**	**CO**	**CO_2**	**CH_4**	**C_2H_6**	**C_2H_4**	**C_2H_2**	**C_3H_8**	**O_2**	**H_2**
1	243	0.00243	1240.9	1195.4	-6.4	13.3	979.5	37.2	10.6	1.5	9.0	1125.0	1.9
2	244	0.00245	1209.1	1163.3	-10.4	7.9	987.0	37.0	5.4	1.3	9.6	1009.3	0.0
3	239	0.00241	1277.1	1231.5	-7.0	11.3	959.9	36.8	12.9	2.9	8.2	1466.2	3.1
4	242	0.00245	1290.0	1244.2	-9.7	11.2	965.4	37.2	16.7	2.6	7.6	1036.6	3.8
5	233	0.00264	1276.6	1231.0	-2.8	14.9	982.4	37.9	14.9	1.8	8.1	1264.3	0.0
6	242	0.00236	1329.6	1282.9	2.0	20.3	956.3	37.8	26.5	10.8	6.6	1251.1	6.8
7	235	0.00267	1341.8	1294.6	-23.2	15.4	953.4	37.7	25.6	4.6	5.8	1302.0	5.8
8	233	0.00234	1333.1	1286.3	0.5	17.3	965.9	38.6	27.8	3.0	6.4	1296.5	5.5
11	225	0.00267	1419.9	1368.8	22.4	18.6	909.2	37.2	50.5	8.6	1.2	1222.8	21.2
12	229	0.00264	1434.1	1382.1	19.2	14.2	908.9	36.5	55.6	7.0	0.7	1111.4	23.3
13	235	0.00250	1311.2	1265.0	-5.3	13.8	975.4	38.0	21.0	0.0	6.9	1212.6	0.0
14	228	0.00257	1363.9	1315.9	-2.2	15.0	946.4	37.9	34.1	3.6	3.5	1114.8	9.1
19	246	0.00250	1497.0	1440.0	70.8	15.9	830.0	30.9	82.2	11.7	0.4	1077.8	55.3
20	239	0.00251	1522.7	1463.2	116.4	23.2	760.0	27.7	87.7	22.5	0.6	861.9	87.9
23	238	0.00249	1536.7	1475.9	110.9	20.0	751.0	27.4	85.7	18.8	0.4	1066.9	81.0
25	215	0.00256	1604.1	1535.7	194.0	37.1	666.0	23.5	89.7	34.0	1.1	761.6	121.0
26	213	0.00260	1573.2	1508.4	131.7	27.8	738.0	26.7	92.0	24.7	0.2	904.7	97.9
28	221	0.00247	1645.8	1572.0	411.4	74.3	408.0	12.4	72.6	52.4	0.5	759.8	222.3
30	220	0.00240	1705.9	1623.6	581.2	108.0	275.0	5.3	38.9	72.2	0.8	534.4	271.1
32	232	0.00232	1688.9	1609.1	542.6	102.8	349.1	9.9	60.7	54.7	0.4	422.1	247.0
33	233	0.00230	1714.5	1630.9	514.7	94.0	345.3	9.1	53.7	62.2	0.4	456.5	243.6
34	223	0.00226	1720.7	1636.2	610.9	118.9	285.8	5.4	38.3	68.0	0.5	527.7	269.3
35	222	0.00224	1740.0	1652.5	654.6	123.9	252.7	3.9	28.0	75.5	0.4	246.5	290.6
36	220	0.00217	1851.6	1744.8	726.3	138.6	139.4	0.8	9.6	107.2	0.3	401.4	357.3
37	221	0.00221	1802.2	1704.2	702.9	133.5	184.5	1.6	15.4	87.4	0.4	426.8	320.2
38	226	0.00229	1675.6	1597.7	503.2	93.6	375.4	10.3	64.8	61.9	0.7	810.9	237.3
40	223	0.00231	1656.6	1581.4	398.8	72.8	491.0	15.7	82.3	57.8	0.6	710.9	203.2
41	219	0.00231	1728.4	1642.6	615.7	116.3	287.3	5.9	39.6	73.6	0.5	381.8	276.4

Test Mixture (Mole Fraction / ppm) – NG-ID-03

Fuel			**Oxidizer**	***Bath Gas***	***φ***
CH4	C2H6	C3H8	O2	Ar	
977.0	43.9	4.8	2150.0	996824.3	0.98
Carbon Content		1079			

Shock No.	***Pressure - P5 (atm)***	***Time (sec)[1]***	***Temperature (K)***		***Mole Fraction (ppm)***								
			Ideal	**Calibrated[2]**	**CO**	**CO_2**	**CH_4**	**C_2H_6**	**C_2H_4**	**C_2H_2**	**C_3H_8**	**O_2**	**H_2**
1	252	0.00247	1174.7	1128.1	-24.2	0.0	956.2	43.4	0.0	0.0	4.6	1842.8	0.0
2	244	0.00256	1224.1	1178.5	-27.5	16.6	960.2	43.4	1.8	0.6	4.5	1799.0	0.0
3	250	0.00240	1266.7	1221.3	-18.9	20.5	935.2	42.7	11.1	2.6	4.0	2175.2	1.9
4	237	0.00254	1266.7	1221.2	-21.4	18.1	957.7	43.3	10.9	1.2	4.0	1757.7	1.9
5	240	0.00253	1305.5	1259.4	-11.5	26.9	940.9	43.0	22.6	1.4	3.0	1924.9	1.9
6	238	0.00255	1350.4	1302.9	-6.2	25.7	912.8	41.6	33.4	3.1	2.1	2016.0	4.3
7	232	0.00262	1381.7	1332.8	16.9	27.6	875.7	40.6	45.1	4.9	1.1	1923.8	12.8
8	235	0.00259	1451.9	1398.6	124.5	36.4	724.0	34.0	85.7	10.4	0.5	1547.0	44.8
9	222	0.00257	1496.8	1439.7	379.9	87.3	432.6	20.6	84.4	18.6	0.6	1405.2	89.8
10	248	0.00254	1514.9	1456.2	464.6	114.1	337.6	15.6	71.4	17.5	0.5	1078.4	90.6
11	249	0.00243	1538.7	1477.7	516.4	376.7	180.8	2.9	25.0	13.6	0.6	609.1	55.1
12	233	0.00246	1612.0	1542.6	212.7	823.4	36.2	1.6	7.9	7.8	0.4	339.5	32.1
13	237	0.00249	1589.3	1522.7	242.0	760.4	47.8	2.1	7.2	6.5	0.4	372.3	27.2
14	232	0.00237	1681.3	1602.6	187.3	905.0	16.2	0.5	3.1	8.4	0.4	272.9	39.2
15	231	0.00233	1732.2	1645.8	141.7	924.6	10.5	0.4	1.4	7.4	0.3	506.2	27.7
17	239	0.00242	1244.3	1198.9	-23.2	17.8	954.0	43.1	2.4	0.0	4.5	1925.0	0.0
18	235	0.00240	1269.1	1223.6	-18.3	17.0	950.0	43.2	7.9	0.0	4.3	2024.2	0.0
22	248	0.00251	1290.3	1244.6	-17.1	20.6	946.0	43.0	18.5	3.1	3.4	2121.8	3.2
23	232	0.00264	1414.7	1363.9	59.3	27.1	819.0	38.0	69.3	7.8	0.6	1717.1	26.0
24	235	0.00257	1477.3	1421.9	229.6	47.0	572.0	27.3	93.0	12.1	0.3	1559.1	72.4
25	224	0.00258	1531.6	1471.2	579.2	269.0	155.0	7.0	33.7	11.8	0.4	730.2	69.5
26	228	0.00245	1625.4	1554.3	219.6	874.0	19.6	0.8	5.2	6.1	0.4	388.9	49.9
27	232	0.00246	1610.0	1540.8	289.9	759.0	31.9	1.3	6.9	5.5	0.4	331.3	41.2
28	242	0.00242	1583.9	1517.9	386.6	621.9	52.3	2.3	10.8	5.5	0.3	399.3	40.3
29	243	0.00241	1584.7	1518.6	371.4	640.2	53.1	2.5	11.3	5.2	0.3	459.1	40.4
30	248	0.00244	1580.3	1514.7	384.5	657.1	46.9	2.0	9.5	5.4	0.4	625.2	39.8
31	234	0.00242	1683.2	1604.2	197.8	894.0	15.2	0.5	2.7	6.0	0.3	368.2	44.7

Test Mixture (Mole Fraction / ppm) – NG-ID-04

Fuel			**Oxidizer**	***Bath Gas***	***φ***
CH4	C2H6	C3H8	O2	Ar	
953.0	43.1	4.7	1010.0	997989.2	2.03
Carbon Content		1053			

Shock No.	***Pressure - P5 (atm)***	***Time (sec)[1]***	***Temperature (K)***		***Mole Fraction (ppm)***								
			Ideal	**Calibrated[2]**	**CO**	**CO_2**	**CH_4**	**C_2H_6**	**C_2H_4**	**C_2H_2**	**C_3H_8**	**O_2**	**H_2**
1	254	0.00253	1196.5	1150.5	-22.1	0.0	963.5	43.6	2.7	0.0	4.6	1009.8	0.0
2	250	0.00247	1227.0	1181.5	-29.3	0.0	956.1	43.5	5.2	0.0	4.3	1001.6	1.2
3	244	0.00246	1263.8	1218.3	-23.5	0.3	950.2	43.5	9.7	1.0	4.1	1155.4	1.7
4	254	0.00241	1323.1	1276.5	-17.8	2.1	946.8	43.6	20.9	1.5	2.9	1068.9	3.1
5	245	0.00252	1326.8	1280.1	-16.0	2.2	928.6	43.0	20.8	2.0	2.8	1557.5	4.8
6	239	0.00259	1349.2	1301.7	-14.1	6.9	941.3	44.2	28.9	2.5	2.4	1450.1	7.9
7	237	0.00257	1410.6	1360.1	-2.2	2.4	911.6	40.8	44.6	4.3	0.7	902.0	12.2
8	232	0.00256	1455.5	1401.9	14.0	6.3	879.1	37.7	56.9	5.5	0.3	1231.7	25.6
14	228	0.00238	1725.9	1640.5	613.9	131.6	186.6	4.5	27.4	44.8	0.5	440.9	142.4
15	224	0.00242	1654.2	1579.3	376.8	56.3	408.0	13.1	72.6	50.0	0.5	638.3	151.0
16	217	0.00239	1727.1	1641.6	539.9	91.0	256.0	5.4	36.2	58.1	0.3	478.2	191.6
17	231	0.00257	1263.6	1217.4	-28.5	1.1	947.0	42.9	6.9	0.0	4.3	1060.1	0.0
18	255	0.00233	1309.9	1263.7	-15.7	2.5	938.0	43.3	16.5	1.1	3.6	1141.7	0.0
19	239	0.00265	1382.9	1334.0	-13.3	2.5	914.0	41.9	28.9	3.6	1.5	1034.8	7.9
20	235	0.00267	1420.0	1368.9	-1.6	2.7	893.0	39.6	40.9	4.0	0.6	1179.8	11.6
21	238	0.00251	1509.9	1451.7	49.5	6.1	789.0	29.5	72.2	11.8	0.3	1099.8	41.6
25	216	0.00248	1654.4	1579.5	336.7	54.4	449.0	14.6	78.1	47.4	0.5	903.0	180.1
26	222	0.00250	1637.9	1565.1	291.7	40.9	484.4	16.5	83.3	41.1	0.5	917.1	166.3
27	220	0.00246	1665.5	1589.0	405.5	64.6	383.2	11.5	65.7	49.7	0.5	926.1	200.9
28	226	0.00246	1627.6	1556.2	242.1	33.2	537.6	18.7	87.1	36.7	0.3	860.5	115.2
29	234	0.00246	1608.7	1539.7	206.8	28.0	586.5	21.1	91.0	30.3	0.4	1214.1	110.0
30	234	0.00251	1559.5	1496.2	92.0	11.1	729.2	27.0	83.7	16.8	0.2	1090.0	61.3
31	234	0.00247	1607.7	1538.8	140.1	18.2	659.8	24.2	90.4	22.6	0.4	1053.4	98.2
32	231	0.00252	1594.8	1527.5	123.5	15.8	699.5	25.7	89.1	20.1	0.3	1172.7	77.6
33	221	0.00244	1706.2	1623.8	523.2	88.1	281.3	6.5	43.5	60.2	0.3	719.7	217.6
34	218	0.00240	1722.6	1637.7	525.9	88.7	265.2	5.6	37.4	59.5	0.4	541.4	238.9

Test Mixture (Mole Fraction / ppm)

Fuel			**Oxidizer**	***Bath Gas***	***φ***
CH4	C2H6	C3H8	O2	Ar	
958.0	43.3	4.6	3670.0	995324.1	0.56
Carbon Content		1059			

Shock No.	***Pressure - P5 (atm)***	***Time (sec)[1]***	***Temperature (K)***		***Mole Fraction (ppm)***								
			Ideal	**Calibrated[2]**	**CO**	**CO_2**	**CH_4**	**C_2H_6**	**C_2H_4**	**C_2H_2**	**C_3H_8**	**O_2**	**H_2**
1	263	0.00241	1181.1	1134.7	-24.3	0.0	957.4	43.3	2.5	0.0	4.6	3670.8	0.0
2	258	0.00237	1241.7	1196.3	-21.4	18.3	945.9	42.6	8.1	1.6	4.2	3635.6	0.0
4	244	0.00256	1290.5	1244.7	-17.7	19.4	935.7	42.0	14.7	1.3	3.4	3619.6	0.0
5	248	0.00254	1339.1	1292.0	-2.5	20.7	898.3	39.9	26.9	1.8	2.0	3740.7	4.2
6	249	0.00261	1396.5	1346.9	96.2	29.6	751.9	34.5	68.5	3.1	0.6	3408.0	23.4
7	248	0.00253	1450.0	1396.8	519.5	148.0	319.0	14.6	61.6	6.4	0.2	2891.7	45.3
8	236	0.00253	1468.3	1413.7	555.6	225.2	203.6	9.2	37.0	5.5	0.3	2684.0	44.0
9	226	0.00252	1588.5	1521.9	198.8	836.1	24.8	1.1	3.4	2.8	0.2	2123.5	4.9
10	227	0.00257	1547.4	1485.4	458.7	570.7	43.4	1.9	7.6	2.3	0.2	2221.7	14.4
11	237	0.00265	1502.9	1445.3	609.6	277.5	140.9	6.2	28.5	5.6	0.2	2577.1	39.7
12	224	0.00248	1616.5	1546.6	106.6	965.6	16.6	0.8	2.7	2.4	0.2	2226.2	12.2
13	224	0.00241	1670.9	1593.7	52.4	1040.8	8.0	0.3	0.0	1.2	0.3	2024.1	0.0
14	222	0.00243	1633.1	1561.0	82.6	1000.0	9.5	0.4	1.5	1.2	0.2	2111.4	0.0
15	215	0.00247	1668.8	1591.8	40.6	1060.0	6.5	0.4	0.0	1.3	0.2	2119.3	0.0
16	261	0.00244	1194.5	1148.1	-50.3	19.1	960.0	43.4	4.3	0.0	4.5	3623.8	0.0
17	244	0.00254	1362.3	1313.6	-3.9	23.6	871.0	39.4	42.6	2.3	1.6	3683.4	8.6
18	232	0.00270	1380.4	1331.6	10.6	26.6	859.0	38.9	49.8	1.8	1.0	3629.5	13.9
19	245	0.00251	1407.3	1357.0	125.7	36.5	702.0	32.7	78.0	3.7	0.4	3384.7	36.5
20	244	0.00255	1413.7	1363.0	182.3	45.1	631.0	29.5	84.2	4.6	0.3	3341.6	47.3
21	246	0.00258	1442.0	1389.4	414.2	102.0	388.0	17.5	70.8	6.3	0.3	3158.5	68.2
22	244	0.00259	1414.4	1363.6	125.3	34.4	676.0	31.2	73.2	3.2	0.4	3388.4	40.9
23	235	0.00254	1455.0	1401.5	513.9	152.0	274.0	12.2	53.4	5.7	0.3	2631.7	63.0
24	239	0.00260	1437.7	1385.4	348.4	79.1	452.6	20.9	77.2	5.2	0.4	3052.6	56.5
25	233	0.00261	1510.3	1452.0	622.8	291.1	135.3	5.9	27.4	4.7	0.3	2648.2	59.3
26	227	0.00259	1533.8	1473.2	561.1	291.9	133.0	5.8	23.7	3.0	0.2	2676.4	35.3
27	236	0.00252	1563.0	1499.3	402.5	637.6	37.5	1.6	6.8	2.0	0.2	2281.4	16.4
28	230	0.00253	1544.5	1482.9	510.5	474.0	62.4	2.7	11.3	2.5	0.2	2572.1	23.7
30	226	0.00241	1680.4	1601.8	38.6	1068.4	6.1	0.5	0.0	0.0	0.1	2141.2	0.0
31	224	0.00236	1748.6	1659.7	19.3	1091.0	3.7	0.3	0.0	0.0	0.2	2052.1	0.0
32	223	0.00241	1712.1	1628.9	25.1	1132.7	4.0	0.4	0.0	1.5	0.2	1918.8	0.0
33	217	0.00237	1761.2	1670.2	24.8	1135.8	3.6	1.3	0.0	1.3	0.2	2016.2	0.0

Appendix C

Gas Chromatograph Calibration for Natural Gas Experiments

The gas chromatographs were calibrated using calibration gas samples obtained from SCOTTY® with known concentrations of various components. This sample was run neat to get the first calibration point and then it was subsequently diluted to get multiple points at varying concentrations. The sample was injected and diluted in the same sampling system used for all experiments to ensure consistency and to avoid any new sources of random errors. The relationship obtained between the normalized area under the peak of the chromatogram for a species and the known concentration of species is used as the calibration factor for that species. The intercept of the trend was set to zero. The measured area is normalized by the pressure in the sampling lines (injection pressure) to account for variation in the injection pressure from run to run during calibration as well as actual experiments.

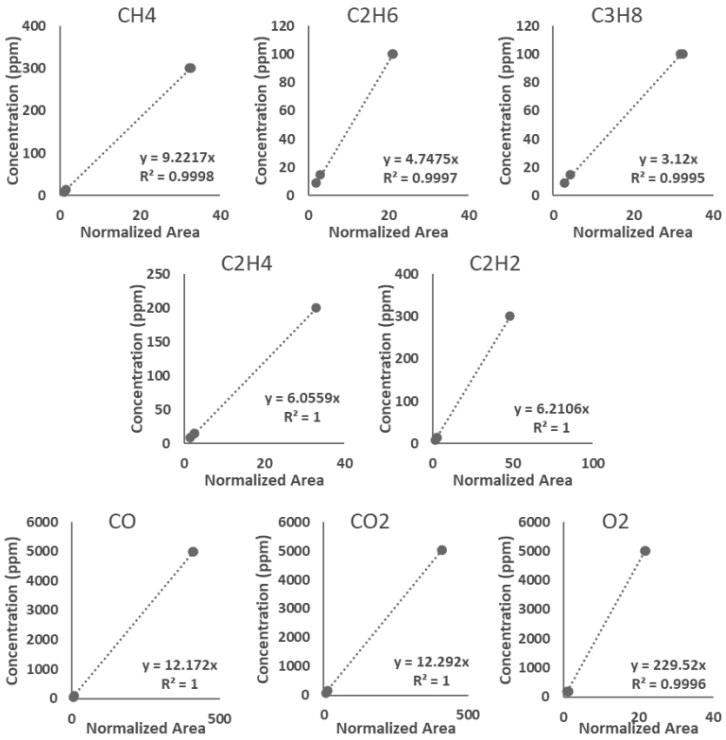

The uncertainty in the measurements can result from the uncertainty of the calibration mixtures, errors in integrating the peak area in the chromatograms, errors in injection pressure and losses in the sampling lines. However, since the sample handling system used for calibration is the same as that used for the experiments, any random effects and systematic errors are already factored into the calibration which results in uncertainty of the composition of calibration mixtures as the only major source of uncertainty which is 2% for most of the calibration mixtures used, except for that used for O_2 and H_2 measurements having 5% uncertainty. Any loss of samples due to adsorption in the lines is mitigated by using Sulfinert® coated stainless steel tubing which is heated to a temperature of 150°C.

Appendix D

Gas Chromatographs Methods Used for Natural Gas Experiments

```
======================================================================
                          Agilent 7890B
======================================================================

GC
GC Summary
Run Time                                  39.5 min
Post Run Time                             0 min

Oven
Equilibration Time                        0.5 min
Max Temperature                           185 °C
Maximum Temperature Override              Disabled
Slow Fan                                  Disabled
Temperature
Setpoint                                  On
(Initial)                                 35 °C
Hold Time                                 15 min
Post Run                                  180 °C
Program
#1 Rate                                   10 °C/min
#1 Value                                  180 °C
#1 Hold Time                              10 min



Thermal Aux 1 (Nickel Catalyst)
Temperature
Setpoint                                  On
(Initial)                                 375 °C
Post Run                                  0 °C


Column
Column Outlet Pressure                    0 psi
Column #1
Column Information                        Agilent 19091P-UO4
HP-PLOT U
Temperature Range                         -60 °C—190 °C (190 °C)
Dimensions                                30 m x 320 µm x 10 µm
Column lock                               Unlocked
In                                        Aux EPC 1 He
Out                                       Back Detector FID
(Initial)                                 35 °C
Pressure                                  6.1983 psi
Flow                                      1 mL/min
Average Velocity                          19.924 cm/sec
Holdup Time                               2.5096 min
Flow
Setpoint                                  On
(Initial)                                 1 mL/min
Hold Time                                 14.5 min
Post Run                                  1.25 mL/min
Program
#1 Rate                                   1 mL/min per min
#1 Value                                  2 mL/min
#1 Hold Time                              0 min



Column #2
Column Information                        Supelco 25467
Carboxen-1010
Temperature Range                         -60 °C—250 °C (250 °C)
```

```
 method: C:\Chem32\1\Methods\Methane_NaturalGas_A.M
Modified on: 6/14/2021 at 1:42:36 PM
    Dimensions                                  30 m x 530 µm x 30 µm
    Column lock                                 Unlocked
    In                                          Aux EPC 2 ArMe
    Out                                         Front Detector TCD
    (Initial)                                   35 °C
    Pressure                                    2.6071 psi
    Flow                                        2 mL/min
    Average Velocity                            18.199 cm/sec
    Holdup Time                                 2.7474 min
    Flow
    Setpoint                                    On
    (Initial)                                   2 mL/min
    Post Run                                    2 mL/min



    Front Detector TCD
    Makeup                                      He
    Heater                                      On    210 °C
    Reference Flow                              On    24 mL/min
    Makeup Flow                                 On    5 mL/min
    Filament                                    On
    Negative Polarity                           On

    Back Detector FID
    Makeup                                      He
    Heater                                      On    320 °C
    H2 Flow                                     On    40 mL/min
    Air Flow                                    On    450 mL/min
    Makeup Flow                                 On    30 mL/min
    Carrier Gas Flow Correction                 Does not affect Makeup or Fuel Flow
    Flame                                       On

    Valve 1
    Type                                        Gas Sampling Valve
    GSV Loop Volume                             0.25 mL
    Load Time                                   0.01 min
    Inject Time                                 2 min

    Valve 2
    Type                                        Gas Sampling Valve
    GSV Loop Volume                             1 mL
    Load Time                                   0.01 min
    Inject Time                                 2 min

    Aux EPC 1,2,3
    Aux EPC 1 He
    Aux EPC 1 He                                Supplies Column 1

    Aux EPC 2 ArMe
    Aux EPC 2 ArMe                              Supplies Column 2

    Aux EPC 3 N2
                                                ***Excluded from Affecting GC's Readiness State***
    Pressure
    Setpoint                                    Off
    (Initial)                                   10 psi
    Post Run                                    0 psi



    Valve Box
    Heater                                      On    150 °C

    Signals
```

```
 method: C:\Chem32\1\Methods\Methane_NaturalGas_A.M
Modified on: 6/14/2021 at 1:42:36 PM
    Signal #1:  Front Signal
    Description                              Front Signal
    Details                                  Front Signal (TCD)
    Save                                     On
    Data Rate                                200 Hz

    Signal #2:  Back Signal
    Description                              Back Signal
    Details                                  Back Signal (FID)
    Save                                     On
    Data Rate                                20 Hz

    Signal #3:
    Description                              None

    Signal #4:
    Description                              None


    Run Time Events
    Run Time Events
    #1 Time                                  0.001 min
    #1 Event                                 Valve
    #1 Position                              Valve 1
    #1 Setpoint                              On
    #2 Time                                  0.001 min
    #2 Event                                 Valve
    #2 Position                              Valve 2
    #2 Setpoint                              On
```

method: C:\Chem32\1\Methods\PLOT_U_LNG_Surrogate.M
Modified on: 4/15/2019 at 6:40:31 PM

Agilent 7890B

GC	
GC Summary	
Run Time	40 min
Post Run Time	10 min
Oven	
Equilibration Time	0.5 min
Max Temperature	185 °C
Maximum Temperature Override	Disabled
Slow Fan	Disabled
Temperature	
Setpoint	On
(Initial)	35 °C
Hold Time	10 min
Post Run	180 °C
Program	
#1 Rate	5 °C/min
#1 Value	100 °C
#1 Hold Time	10 min
#2 Rate	20 °C/min
#2 Value	180 °C
#2 Hold Time	3 min
Thermal Aux 1 (Nickel Catalyst)	
Temperature	
Setpoint	On
(Initial)	375 °C
Post Run	0 °C
Column	
Column Outlet Pressure	0 psi
Column #1	
Column Information	Agilent 19091P-UO4
HP-PLOT U	
Temperature Range	-60 °C—190 °C (190 °C)
Dimensions	30 m x 320 µm x 10 µm
Column lock	Unlocked
In	Aux EPC 1 He
Out	Back Detector FID
(Initial)	35 °C
Pressure	8.6893 psi
Flow	1.5 mL/min
Average Velocity	27.732 cm/sec
Holdup Time	1.803 min
Flow	
Setpoint	On
(Initial)	1.5 mL/min
Post Run	0.46015 mL/min
Column #2	
Column Information	J&W 19095P-MS0E
HP-MOLSIV Megabore	
Temperature Range	-60 °C—300 °C (325 °C)
Dimensions	30 m x 530 µm x 50 µm
Column lock	Unlocked
In	Aux EPC 2 ArMe

```
 method: C:\Chem32\1\Methods\PLOT_U_LNG_Surrogate.M
Modified on: 4/15/2019 at 6:40:31 PM
    Out                                     Front Detector TCD
    (Initial)                               35 °C
    Pressure                                3.3417 psi
    Flow                                    2 mL/min
    Average Velocity                        21.228 cm/sec
    Holdup Time                             2.3554 min
    Flow
    Setpoint                                On
    (Initial)                               2 mL/min
    Hold Time                               30 min
    Post Run                                5 mL/min
    Program
    #1 Rate                                 2.5 mL/min per min
    #1 Value                                5 mL/min
    #1 Hold Time                            10 min



    Front Detector TCD
    Makeup                                  He
    Heater                                  On    250 °C
    Reference Flow                          On    20 mL/min
    Makeup Flow                             On    7 mL/min
    Filament                                On
    Negative Polarity                       On

    Back Detector FID
    Makeup                                  He
    Heater                                  On    320 °C
    H2 Flow                                 On    40 mL/min
    Air Flow                                On    450 mL/min
    Makeup Flow                             On    30 mL/min
    Carrier Gas Flow Correction             Does not affect Makeup or Fuel Flow
    Flame                                   On

    Valve 1
    Type                                    Gas Sampling Valve
    GSV Loop Volume                         0.25 mL
    Load Time                               0.01 min
    Inject Time                             2 min

    Valve 2
    Type                                    Gas Sampling Valve
    GSV Loop Volume                         1 mL
    Load Time                               0.01 min
    Inject Time                             2 min

    Aux EPC 1,2,3
    Aux EPC 1 He
    Aux EPC 1 He                            Supplies Column 1

    Aux EPC 2 ArMe
    Aux EPC 2 ArMe                          Supplies Column 2

    Aux EPC 3 N2
                                            ***Excluded from Affecting GC's Readiness State***
    Pressure
    Setpoint                                Off
    (Initial)                               10 psi
    Post Run                                0 psi



    Valve Box
```

method: C:\Chem32\1\Methods\PLOT_U_LNG_Surrogate.M
Modified on: 4/15/2019 at 6:40:31 PM

Heater	On 150 °C
Signals	
Signal #1: Front Signal	
Description	Front Signal
Details	Front Signal (TCD)
Save	On
Data Rate	200 Hz
Signal #2: Back Signal	
Description	Back Signal
Details	Back Signal (FID)
Save	On
Data Rate	20 Hz
Signal #3:	
Description	None
Signal #4:	
Description	None
Run Time Events	
Run Time Events	
#1 Time	0.001 min
#1 Event	Valve
#1 Position	Valve 1
#1 Setpoint	On
#2 Time	0.001 min
#2 Event	Valve
#2 Position	Valve 2
#2 Setpoint	On

method: C:\Chem32\2\Methods\GasPro_LNG_Surrogates.M
Modified on: 10/14/2020 at 3:23:10 PM

Agilent 7890B

GC
GC Summary

Run Time	44.5 min
Post Run Time	0 min

Oven

Equilibration Time	0.5 min
Max Temperature	290 °C
Maximum Temperature Override	Disabled
Slow Fan	Disabled
Temperature	
Setpoint	On
(Initial)	45 °C
Hold Time	14 min
Post Run	270 °C
Program	
#1 Rate	10 °C/min
#1 Value	250 °C
#1 Hold Time	10 min

Column

Column Outlet Pressure	0 psi
Column #1	
Column Information	Agilent 113-4362
GS-GasPro	
Temperature Range	-80 °C–260 °C (300 °C)
Dimensions	60 m x 320 µm x 0 µm
Column lock	Unlocked
In	Aux EPC 2 He
Out	Front Detector FID
(Initial)	45 °C
Pressure	15.885 psi
Flow	2 mL/min
Average Velocity	27.579 cm/sec
Holdup Time	3.626 min
Flow	
Setpoint	On
(Initial)	2 mL/min
Post Run	0.52288 mL/min

Column #2

Column Information	Agilent 19091J-413
HP-5	
Temperature Range	-60 °C–325 °C (350 °C)
Dimensions	30 m x 320 µm x 0.25 µm
Column lock	Unlocked
In	Aux EPC 1 He
Out	Back Detector FID
(Initial)	45 °C
Pressure	7.3804 psi
Flow	1.5 mL/min
Average Velocity	26.243 cm/sec
Holdup Time	1.9052 min
Flow	
Setpoint	On
(Initial)	1.5 mL/min
Post Run	0.4496 mL/min

method: C:\Chem32\2\Methods\GasPro_LNG_Surrogates.M
Modified on: 10/14/2020 at 3:23:10 PM

Front Detector FID	
Makeup	He
Heater	On 320 °C
H2 Flow	On 30 mL/min
Air Flow	On 300 mL/min
Makeup Flow	On 30 mL/min
Carrier Gas Flow Correction	Does not affect Makeup or Fuel Flow
Flame	On
Back Detector FID	
	Excluded from Affecting GC's Readiness State
Makeup	He
Heater	Off
H2 Flow	Off
Air Flow	Off
Makeup Flow	Off
Carrier Gas Flow Correction	Does not affect Makeup or Fuel Flow
Flame	Off
Valve 2	
Type	Gas Sampling Valve
GSV Loop Volume	0.25 mL
Load Time	0.01 min
Inject Time	2 min
Aux EPC 1,2,3	
Aux EPC 1 He	
	Excluded from Affecting GC's Readiness State
Aux EPC 1 He	Supplies Column 2
Aux EPC 2 He	
Aux EPC 2 He	Supplies Column 1
Aux EPC 3 N2	
	Excluded from Affecting GC's Readiness State
Pressure	
Setpoint	Off
(Initial)	10 psi
Post Run	0 psi
Valve Box	
Heater	On 150 °C
Signals	
Signal #1: Front Signal	
Description	Front Signal
Details	Front Signal (FID)
Save	On
Data Rate	20 Hz
Signal #2: Back Signal	
Description	Back Signal
Details	Back Signal (FID)
Save	Off
Data Rate	20 Hz
Signal #3:	
Description	None
Signal #4:	
Description	None

method: C:\Chem32\2\Methods\GasPro_LNG_Surrogates.M
Modified on: 10/14/2020 at 3:23:10 PM

Run Time Events	
Run Time Events	
#1 Time	0.001 min
#1 Event	Valve
#1 Position	Valve 2
#1 Setpoint	On
#2 Time	2 min
#2 Event	Valve
#2 Position	Valve 2
#2 Setpoint	Off

method: C:\CHEM32\2\METHODS\Methane_NaturalGas_B.M
Modified on: 7/27/2021 at 4:50:12 PM

Agilent 7890B

GC	
GC Summary	
Run Time	35.5 min
Post Run Time	0 min
Oven	
Equilibration Time	0 min
Max Temperature	290 °C
Maximum Temperature Override	Disabled
Slow Fan	Disabled
Temperature	
Setpoint	On
(Initial)	45 °C
Hold Time	10 min
Post Run	270 °C
Program	
#1 Rate	10 °C/min
#1 Value	250 °C
#1 Hold Time	5 min
Column	
Column Outlet Pressure	0 psi
Column #1	
Column Information	Agilent 113-4362
GS-GasPro	
Temperature Range	-80 °C–260 °C (300 °C)
Dimensions	60 m x 320 µm x 0 µm
Column lock	Unlocked
In	Aux EPC 2 He
Out	Front Detector FID
(Initial)	45 °C
Pressure	12.788 psi
Flow	1.5 mL/min
Average Velocity	22.427 cm/sec
Holdup Time	4.459 min
Flow	
Setpoint	On
(Initial)	1.5 mL/min
Post Run	0.52288 mL/min
Column #2	
Column Information	Agilent 19091J-413
HP-5	
Temperature Range	-60 °C–325 °C (350 °C)
Dimensions	30 m x 320 µm x 0.25 µm
Column lock	Unlocked
In	Aux EPC 1 He
Out	Back Detector FID
(Initial)	45 °C
Pressure	5.2264 psi
Flow	1 mL/min
Average Velocity	18.692 cm/sec
Holdup Time	2.675 min
Flow	
Setpoint	On
(Initial)	1 mL/min
Post Run	0.4496 mL/min

method: C:\CHEM32\2\METHODS\Methane_NaturalGas_B.M
Modified on: 7/27/2021 at 4:50:12 PM

Front Detector FID	
Makeup	He
Heater	On 320 °C
H2 Flow	On 40 mL/min
Air Flow	On 450 mL/min
Makeup Flow	On 30 mL/min
Carrier Gas Flow Correction	Does not affect Makeup or Fuel Flow
Flame	On
Back Detector FID	
	Excluded from Affecting GC's Readiness State
Makeup	He
Heater	On 100 °C
H2 Flow	Off
Air Flow	Off
Makeup Flow	Off
Carrier Gas Flow Correction	Does not affect Makeup or Fuel Flow
Flame	Off
Valve 2	
Type	Gas Sampling Valve
GSV Loop Volume	0.25 mL
Load Time	0.01 min
Inject Time	2 min
Aux EPC 1,2,3	
Aux EPC 1 He	
	Excluded from Affecting GC's Readiness State
Aux EPC 1 He	Supplies Column 2
Aux EPC 2 He	
Aux EPC 2 He	Supplies Column 1
Aux EPC 3 N2	
	Excluded from Affecting GC's Readiness State
Pressure	
Setpoint	Off
(Initial)	10 psi
Post Run	0 psi
Valve Box	
Heater	On 150 °C
Signals	
Signal #1: Front Signal	
Description	Front Signal
Details	Front Signal (FID)
Save	On
Data Rate	20 Hz
Signal #2: Back Signal	
Description	Back Signal
Details	Back Signal (FID)
Save	Off
Data Rate	20 Hz
Signal #3:	
Description	None
Signal #4:	
Description	None

method: C:\CHEM32\2\METHODS\Methane_NaturalGas_B.M
Modified on: 7/27/2021 at 4:50:12 PM

Run Time Events	
Run Time Events	
#1 Time	0.001 min
#1 Event	Valve
#1 Position	Valve 2
#1 Setpoint	On
#2 Time	2 min
#2 Event	Valve
#2 Position	Valve 2
#2 Setpoint	Off

method: C:\Chem32\1\Methods\PLOT_Q_Carboxen1010.M
Modified on: 5/21/2019 at 5:00:48 PM

==========

Agilent 7890B

==========

GC	
GC Summary	
Run Time	45 min
Post Run Time	0 min
Oven	
Equilibration Time	0.5 min
Max Temperature	250 °C
Maximum Temperature Override	Disabled
Slow Fan	Disabled
Temperature	
Setpoint	On
(Initial)	35 °C
Hold Time	10 min
Post Run	180 °C
Program	
#1 Rate	5 °C/min
#1 Value	100 °C
#1 Hold Time	10 min
#2 Rate	20 °C/min
#2 Value	250 °C
#2 Hold Time	4.5 min
Thermal Aux 1 (Nickel Catalyst)	
Temperature	
Setpoint	On
(Initial)	375 °C
Post Run	0 °C
Column	
Column Outlet Pressure	0 psi
Column #1	
Column Information	Agilent 19091P-QO4
HP-PLOT Q	
Temperature Range	-60 °C—270 °C (290 °C)
Dimensions	30 m x 320 µm x 20 µm
Column lock	Unlocked
In	Aux EPC 1 He
Out	Back Detector FID
(Initial)	35 °C
Pressure	10.839 psi
Flow	1.5 mL/min
Average Velocity	29.933 cm/sec
Holdup Time	1.6704 min
Flow	
Setpoint	Off
(Initial)	1.5 mL/min
Post Run	0.46015 mL/min
Column #2	
Column Information	Supelco 25467
Carboxen-1010	
Temperature Range	-60 °C—250 °C (250 °C)
Dimensions	30 m x 530 µm x 0 µm
Column lock	Unlocked
In	Aux EPC 2 ArMe

```
 method: C:\Chem32\1\Methods\PLOT_Q_Carboxen1010.M
Modified on: 5/21/2019 at 5:00:48 PM
    Out                                     Front Detector TCD
    (Initial)                               35 °C
    Pressure                                1.2623 psi
    Flow                                    1.5 mL/min
    Average Velocity                        11.223 cm/sec
    Holdup Time                             4.455 min
    Flow
    Setpoint                                Off
    (Initial)                               1.5 mL/min
    Post Run                                5 mL/min



    Front Detector TCD
    Makeup                                  He
    Heater                                  On    250 °C
    Reference Flow                          On    20 mL/min
    Makeup Flow                             On    7 mL/min
    Filament                                On
    Negative Polarity                       On

    Back Detector FID
    Makeup                                  He
    Heater                                  On    320 °C
    H2 Flow                                 On    40 mL/min
    Air Flow                                On    450 mL/min
    Makeup Flow                             On    30 mL/min
    Carrier Gas Flow Correction             Does not affect Makeup or Fuel Flow
    Flame                                   On

    Valve 1
    Type                                    Gas Sampling Valve
    GSV Loop Volume                         0.25 mL
    Load Time                               0.01 min
    Inject Time                             2 min

    Valve 2
    Type                                    Gas Sampling Valve
    GSV Loop Volume                         1 mL
    Load Time                               0.01 min
    Inject Time                             2 min

    Aux EPC 1,2,3
    Aux EPC 1 He
    Aux EPC 1 He                            Supplies Column 1

    Aux EPC 2 ArMe
    Aux EPC 2 ArMe                          Supplies Column 2

    Aux EPC 3 N2
                                            ***Excluded from Affecting GC's Readiness State***
    Pressure
    Setpoint                                Off
    (Initial)                               10 psi
    Post Run                                0 psi



    Valve Box
    Heater                                  On    150 °C

    Signals
    Signal #1:  Front Signal
    Description                             Front Signal
    Details                                 Front Signal (TCD)
```

```
 method: C:\Chem32\1\Methods\PLOT_Q_Carboxen1010.M
Modified on: 5/21/2019 at 5:00:48 PM
    Save                                    On
    Data Rate                               200 Hz

    Signal #2:  Back Signal
    Description                             Back Signal
    Details                                 Back Signal (FID)
    Save                                    On
    Data Rate                               20 Hz

    Signal #3:
    Description                             None

    Signal #4:
    Description                             None


    Run Time Events
    Run Time Events
    #1 Time                                 0.001 min
    #1 Event                                Valve
    #1 Position                             Valve 1
    #1 Setpoint                             On
    #2 Time                                 0.001 min
    #2 Event                                Valve
    #2 Position                             Valve 2
    #2 Setpoint                             On
```

Appendix E

High Pressure Shock Tube Extension – Part Drawings

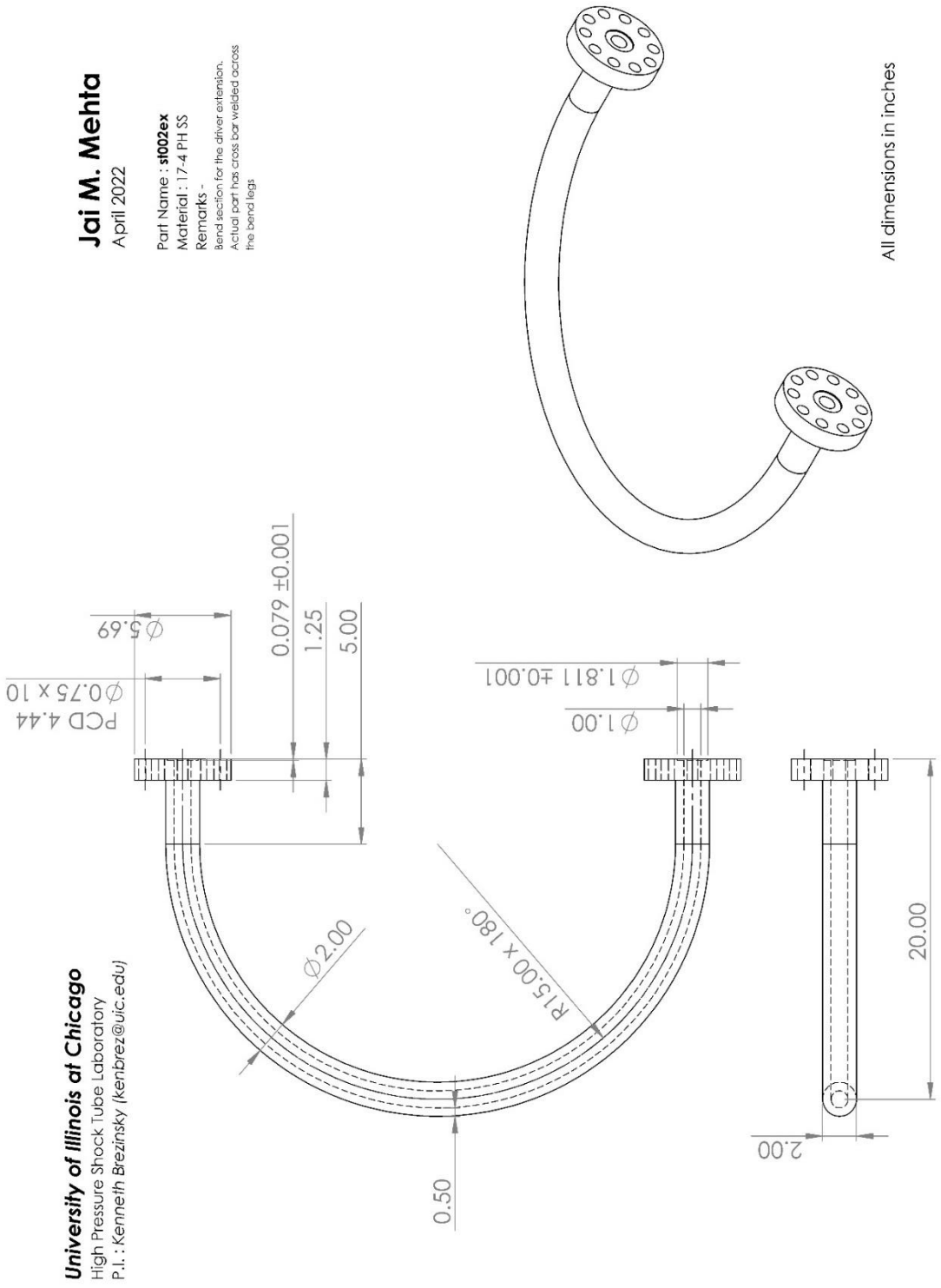

University of Illinois at Chicago
High Pressure Shock Tube Laboratory
P.I. : *Kenneth Brezinsky (kenbrez@uic.edu)*

Jai M. Mehta
April 2022

Part Name : **st003ex**
Material : 17-4 PH SS
Remarks -
Two differnet versions of this design exist with varying lenghts. Every other dimension remains the same

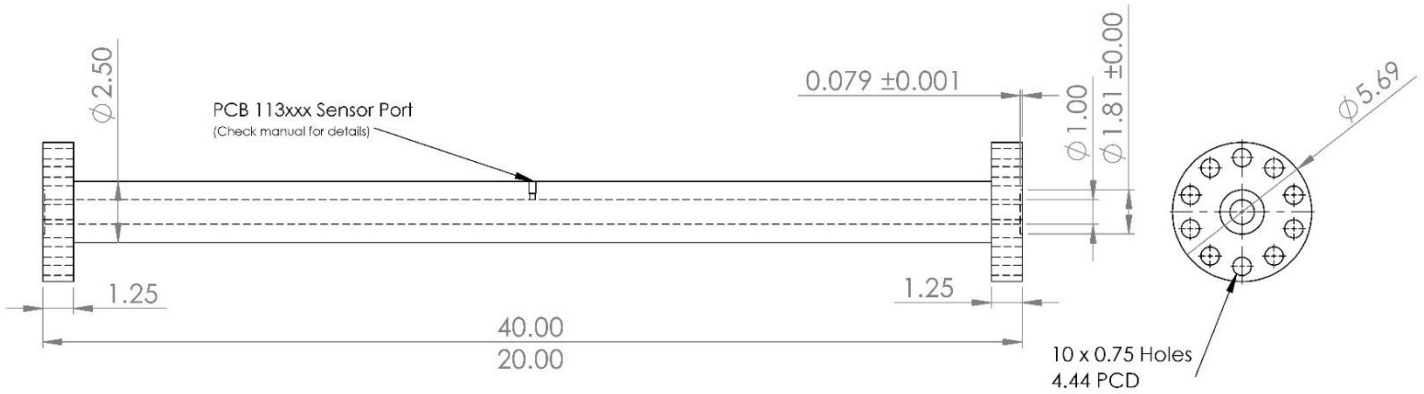

All dimensions in inches

University of Illinois at Chicago
High Pressure Shock Tube Laboratory
P.I. : *Kenneth Brezinsky (kenbrez@uic.edu)*

Jai M. Mehta
April 2022

Part Name : **st004ex**
Material : 17-4 PH SS
Remarks -
Driver Section Endwall with mounting for insert

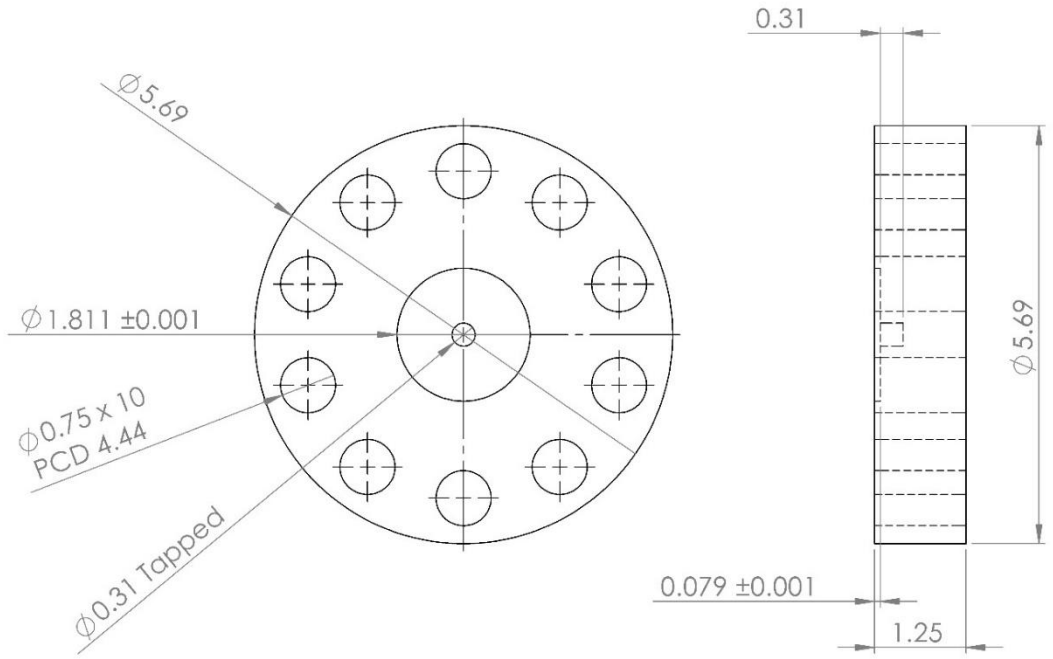

All dimensions in inches

University of Illinois at Chicago
High Pressure Shock Tube Laboratory
P.I. : *Kenneth Brezinsky (kenbrez@uic.edu)*

Jai M. Mehta
April 2022

Part Name : **st005exA**
Materail : 17-4 PH SS
Remarks -
Coupler to connect original shock tube to the extension.

Threads match the driver threads as of April 2022.
Template Gauge avialable in the lab
Non standard bastards threads - resulting from re-cutting threads of the driver in 2020

Use Following Thread Dimensions
Major : 3.950
Minor : 3.793

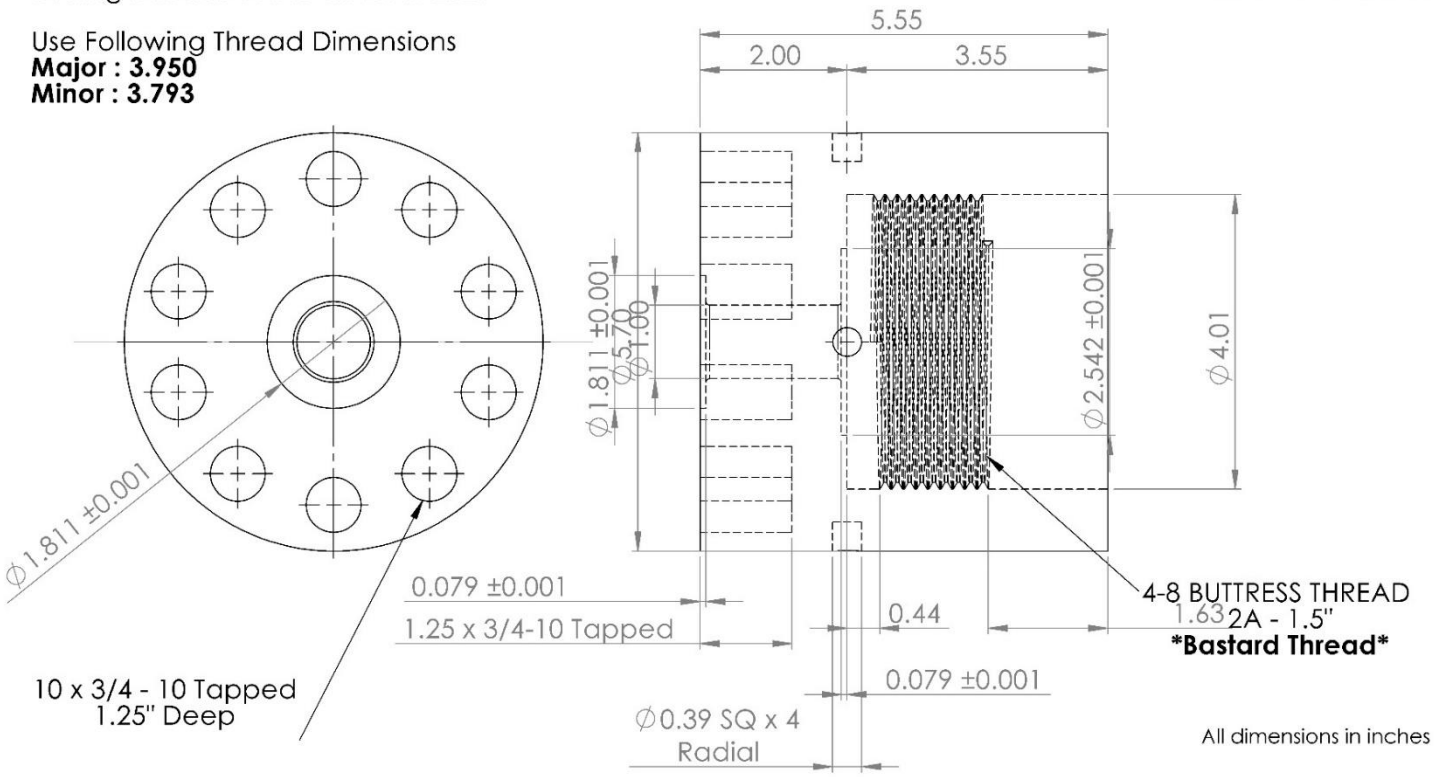

All dimensions in inches

University of Illinois at Chicago
High Pressure Shock Tube Laboratory
P.I. : *Kenneth Brezinsky (kenbrez@uic.edu)*

Jai M. Mehta
April 2022

Part Name : **st005exC**
Materail : 17-4 PH SS
Remarks -
Coupler to connect original shock tube to the extension.

Threads match the driver threads as of April 2022.
Template Gauge avialable in the lab
Non standard bastards threads - resulting from re-cutting threads of the driver in 2020

Use Following Thread Dimensions
Major : 3.950
Minor : 3.793

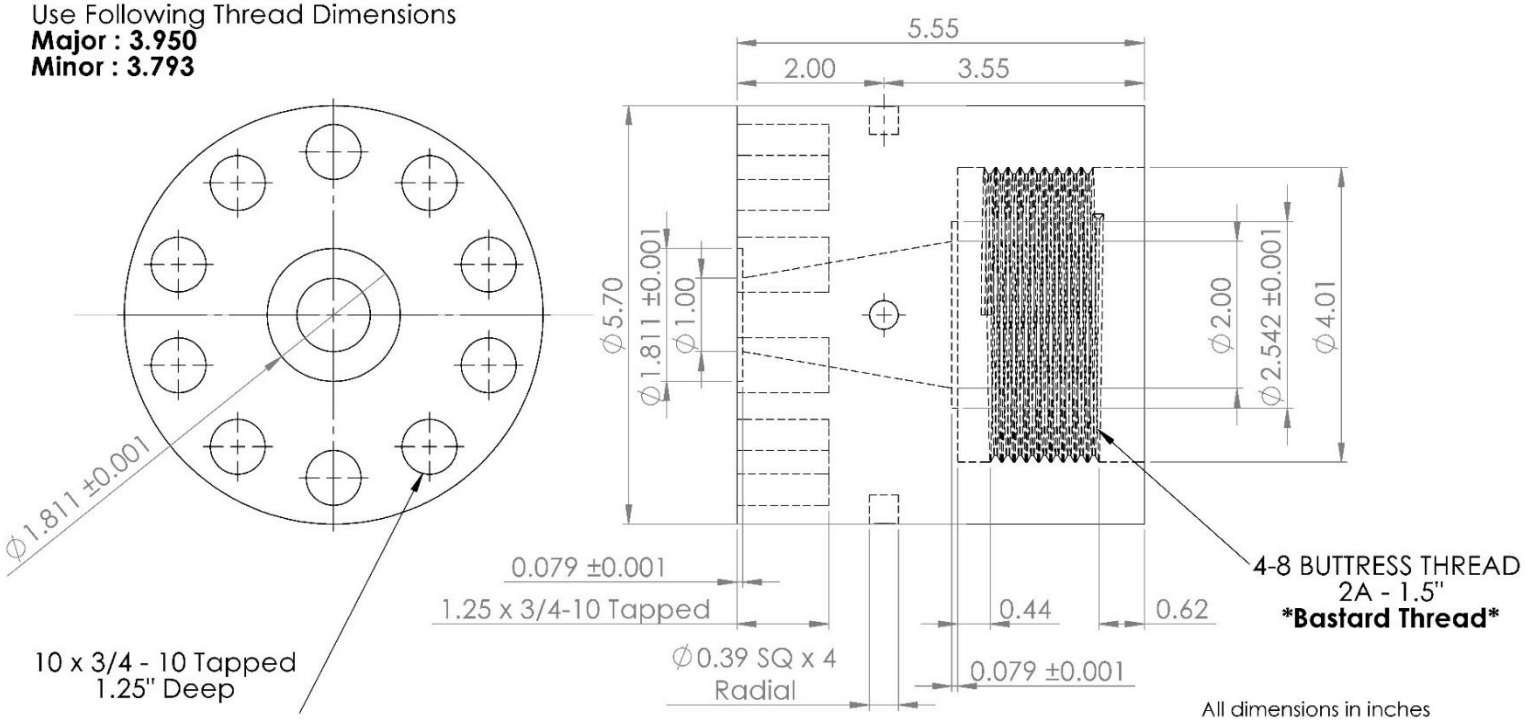

All dimensions in inches

Appendix F

Circuit Diagrams for Auxiliary Systems of High Pressure Shock Tube

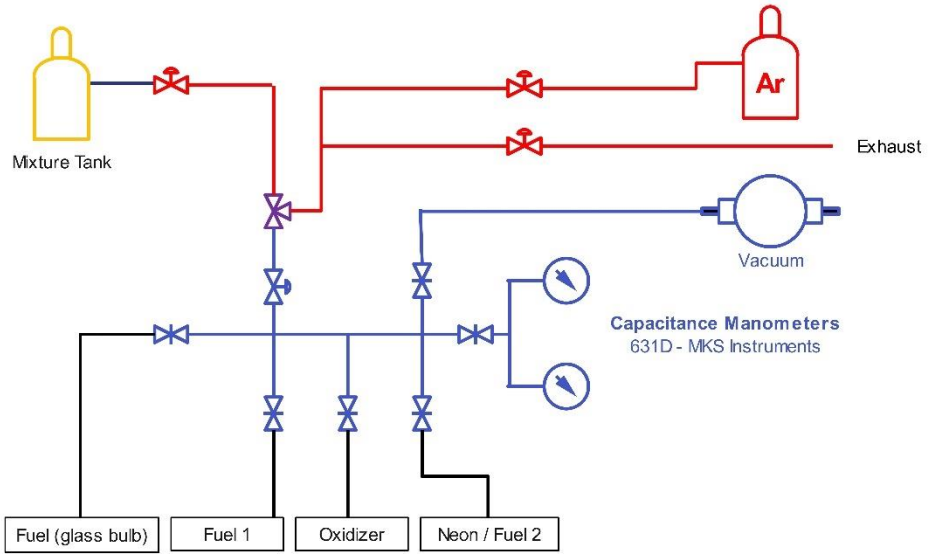

Figure 75 : Flow Diagram - Fuel Mixing Rig

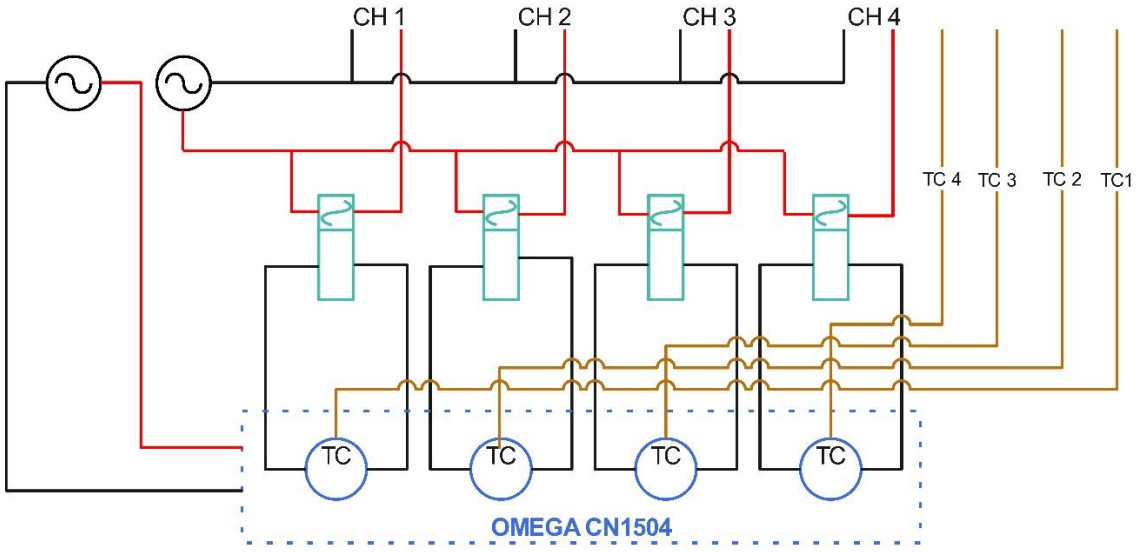

Figure 76 : Circuit Diagram - Temperature Controllers

Appendix G

GCxGC and MS Method used in Chemical Functional Group Analysis

- Petro-WAX : TOF+FID : 23 Friday, April 29, 2022 7:46 AM

Hardware control:

◉ Agilent© 7890	Agilent© 7890 Gas Chromatograph
○ Agilent© 6890	Agilent© 6890 Gas Chromatograph
○ Shimadzu© GC-2010	Shimadzu© GC-2010
○ Generic	Generic Gas Chromatograph
○ Direct Inlet	Direct Inlet to Calibration Compound

Option:

☐ MACH/LTM Oven

☑ LECO© GCxGC

Capillary Configuration:

No problems detected with column configuration.

Flow Path 1:

#	Type	Location	Length(m)	Int. Diameter(µ	Max Temp	Film Thickness	Phase	Bleed Masses
1*	Inlet	Front						
2	Capillary	GC Oven	50.000	200.00	325.0	0.50	DB - Pet	
3	Capillary	Modulator	0.100	100.00	260.0	0.10	DB-WAX	
4	Capillary	Secondary	1.700	100.00	260.0	0.10	DB-WAX	
5	Capillary	Detector o	0.200	100.00	260.0	0.10	DB-WAX	
6	Detector	TOF						

Add | Delete | Promote | Demote | Copy | Paste

☑ Enable Flow Path 2

Flow Path 2:

#	Type	Location	Length(m)	Int. Diameter(µ	Max Temp	Film Thickness	Phase	Bleed Masses
1*	Inlet	Back						
2	Capillary	GC Oven	50.000	200.00	325.0	0.50	DB - Pet	
3	Capillary	Modulator	0.100	100.00	260.0	0.10	DB-WAX	
4	Capillary	Secondary	1.700	100.00	260.0	0.10	DB-WAX	
5	Capillary	Detector o	0.200	100.00	260.0	0.10	DB-WAX	
6	Detector	Back						

6	Detector	Back							M

Add | Delete | Promote | Demote | Copy | Paste

Mass Selection for Auto Mass Defect Tracking

(Set Auto Mass Defect Mode in MS method. Select masses between 130 to 384 inclusive.)

◉ Excluded Masses in Auto Mass Defect Mode

(For general unknown analyses. Select column bleed, matrix, interfering, and non-target masses.)

○ Included Masses in Auto Mass Defect Mode

(Generally for target analyses. Select significant masses of target analytes, minimum of 2 masses required.)

Carrier Gas:

Helium

Front Inlet Type:

None

Back Inlet Type:

None

Active Inlet Location:

◉ Front ○ Back

The active inlet must be present in the capillary configuration.

No problems detected with pressure / flow.

☑ Corrected constant flow via pressure ramps

Use this mode when in GCxGC mode or using short (< 5 m) single column or two columns.

Column 1 / Front Inlet flow(s):

#	Rate (mL/min²)	Target Flow (mL/min)	Duration (min)
1*	Initial	1.25	Entire Run

Column 2 / Back Inlet flow(s):

#	Rate (mL/min²)	Target Flow (mL/min)	Duration (min)
1*	Initial	1.25	Entire Run

No problems detected with oven temperatures.

Oven Equilibration Time (sec):

60

Note: All oven temperature ramps (except the secondary oven) will have the same duration. This is accomplished by extending the final hold time.

Enter oven temperature ramp below:

#	Rate (°C/min)	Target Temp (°C)	Duration (min)
1*	Initial	100	0.20
2	1.25	200	6.70

Add

Remove

Coolant to Column Oven ○ On ◉ Off Coolant timeout 10

☑ Enable Secondary Oven

☑ Use Advanced Secondary Temperature Programming

#	Rate (°C/min)	Target Temp (°C)	Duration (min)
1*	Initial	105	1.00
2	1.25	205	6.70

Add

Remove

+5 °C relative to the GC oven is recommended.

☑ Modulator Enabled

Modulator Temperature Offset (°C, relative to the secondary oven temperature):

40

+15 °C is recommended

☐ Use Advanced Modulator Temperature Programming

- Petro-WAX : TOF+FID : 23 Friday, April 29, 2022 7:46 AM

Purge Pulse Time (sec):

0

Modulation For 1D GC set second dimension time to 0

T #	Start	End	Modulation Period (s)	Hot Pulse Time	Cool Time Between Stages
1*	Start of Run	End of Run	8.00	1.75	2.25

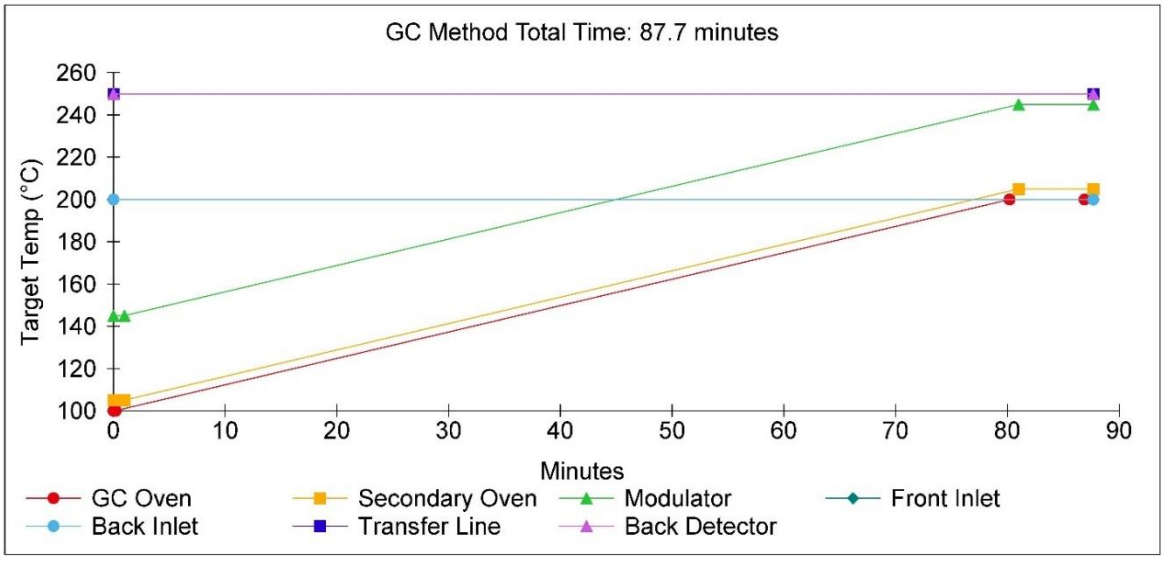

Transfer Line Temperature Equilibration Time (sec):

0

Transfer Line Temperature (°C):

250

☑ Specify Additional Detectors & Auxiliary Pneumatics

☐ Store Signal 1 Data

☑ Store Signal 2 Data

Signal Assignment:

Back Detector

Data Collection Rate (50Hz is maximum rate for ECD detectors):

200

Acquisition Delay (sec):

0

☐ Specify Acquisition Time

☐ Enable Front Detector

☑ Enable Back Detector

Detector Type:

FID

Temperature (°C):

250

Makeup Gas Type:

Helium

Makeup Gas Flow Mode:

○ Constant Makeup Flow ◉ Makeup + Column Flow is Constant

Makeup Flow + Column Flow:

30

Hydrogen Flow:

40

Air Flow:

400

AUX Pneumatic Zone #3: ○ On ◉ Off

AUX Pneumatic Zone #4: ○ On ◉ Off

AUX Pneumatic Zone #5: ○ On ◉ Off

Enter Valve/Relay settings below:

#	Time (min)	Valve 1	Valve 2	Valve 3	Valve 4	Valve 5	Valve 6	Valve 7	Valve 8

Add

Remove

Use GC method total time for MS method total time:

(●) Yes ( ) No

Acquisition delay

3 ( ) Sec. (●) Min.

The length of time from injection until the data system will start storing data from the mass spectrometer.

Enter time(s) when the filament should be turned off (min of 3 sec) in the grid below

#	Start	End	Filament
1*	Start of Run	3 minutes	Off
2	3 minutes	End of Run	On

Add

Remove

Required Disk Space

NA

Enter the mass spectrometer settings:

Start Mass (u)

35

End Mass (u)

300

Acquisition Rate (spectra / second)

50

Detector Voltage:

☑ Specify Relative Detector Voltage

Optimized Voltage Offset: 200

Electron Energy (Volts)

-70

Mass defect mode

(●) Auto (Select masses for automatic tracking in column information section of GC method.)

( ) Manual

Mass Defect (mu / 100 u)

0

Set the temperature for the Ion Source.

Ion Source (°C)

250

☑ Wait for ion source temperatures to reach set point before starting acquisition

Source Temperature Equilibration Time (Seconds)

30

Enter the masses to display during acquisition

TIC S2

Examples
t TIC
69,131 Masses 69 and 131
69+131 Sum of masses 69 and 131

Appendix H

Hydrocarbon Classification Composition of Fuels

Classification	***Weight Percentage***										
	A1	**A2**	**A3**	**CN30**	**CN35**	**CN40**	**CN45**	**CN50**	**CN55**	**F-24**	**ATJ**
Napthalene+C00	0.09267	0.23591	0.09830	0.92605	0.47625	0.44942	0.51491	0.37080	0.48716	0.10931	0.00181
Napthalene+C01	0.27484	0.68872	0.35541	4.37493	0.32575	0.02585	0.26335	0.24563	0.23828	0.36039	0.00456
Napthalene+C02	0.26933	0.79937	0.47472	2.06044	0.02502	0.00000	0.00371	0.01581	0.00558	0.42452	0.00367
Napthalene+C03	0.07781	0.34369	0.18950	1.10781	0.00000	0.00000	0.00000	0.00000	0.00000	0.20742	0.00000
Napthalene+C04	0.00188	0.07003	0.02286	0.39149	0.00281	0.00000	0.00000	0.00000	0.00000	0.03773	0.00000
Indane+C00	0.00000	0.00000	0.00000	0.00000	0.00280	0.00656	0.00281	0.00188	0.00375	0.00000	0.00000
Indane+C01	0.01609	0.02852	0.05930	0.00471	0.16092	0.49094	0.21282	0.12277	0.19552	0.05116	0.00000
Tetralin+C00	0.18265	0.42488	0.76615	0.04149	0.52323	1.10461	0.71191	0.40891	0.67155	0.47657	0.00466
Indane+C02	0.20555	0.47694	1.29362	0.11852	0.19588	0.10158	0.12878	0.15194	0.12062	0.67071	0.00375
Tetralin+C01	0.14845	0.27431	0.91083	0.84670	0.21197	0.06740	0.19790	0.16808	0.18330	0.36108	0.00375
Indane+C03	0.11090	0.20932	0.53625	0.02667	0.02186	0.00477	0.01332	0.01622	0.01240	0.21630	0.00094
Tetralin+C02	0.27819	0.67597	2.50058	0.24289	0.02662	0.00858	0.02188	0.02099	0.01908	0.87191	0.00471
Tetralin+C03	0.09597	0.26700	0.51408	0.03442	0.00000	0.00000	0.00000	0.00000	0.00000	0.30745	0.00000
Benzene+C00	0.01305	0.01404	0.00283	0.00000	0.00000	0.00000	0.00000	0.00000	0.00000	0.00187	0.00000
Benzene+C01	0.30529	0.17887	0.04762	0.00469	0.00094	0.00094	0.00188	0.00094	0.00282	0.05660	0.00093
Benzene+C02	2.30085	1.23753	0.54824	0.00379	0.04251	0.01042	0.04159	0.03602	0.00474	0.60393	0.00936
Benzene+C03	4.54002	3.36161	1.63774	0.00953	0.56087	0.32331	0.44899	0.45122	0.45702	2.52671	0.03203
Benzene+C04	2.27518	3.32352	2.08588	0.03829	3.85889	6.28014	4.14730	2.94435	4.06774	2.78759	0.02651
Benzene+C03 +Alkene	0.02275	0.02571	0.04024	0.00095	0.04148	0.10687	0.04905	0.03216	0.04636	0.04650	0.00000
Benzene+C04 +Alkene	0.04482	0.09099	0.15035	0.00000	0.03983	0.06088	0.03985	0.03140	0.03712	0.11838	0.00094
Benzene+C05	1.10366	2.24026	1.96084	0.19417	2.52206	2.56392	1.93143	1.94078	1.87178	2.17894	0.01901
Benzene+C06	0.50337	1.33492	1.69063	0.25945	0.31861	0.11202	0.16278	0.25115	0.15844	1.50990	0.00763
Indane+C04	0.07198	0.19953	0.72165	0.01147	0.00000	0.00096	0.00096	0.00000	0.00096	0.25173	0.00000
Benzene+C07	0.19998	0.65231	1.24708	0.10543	0.01545	0.01356	0.01159	0.02131	0.02325	0.81737	0.00000
Indane+C05	0.02889	0.11702	0.33380	0.01247	0.00000	0.00192	0.00287	0.00288	0.00288	0.11375	0.00000
Tetralin+C04	0.04429	0.15764	0.44960	0.02207	0.00000	0.00000	0.00000	0.00000	0.00000	0.19569	0.00000
C16-nAlkane	0.15602	0.44772	0.12390	0.00101	0.00000	0.00000	0.00202	0.00000	0.55814	0.34587	0.01996
C15-nAlkane	2.18354	3.00052	3.06650	0.00909	0.02016	0.18102	0.00000	0.00000	1.57020	2.55241	0.02797
C14-nAlkane	0.00000	0.00000	0.00000	0.00000	0.00000	0.00000	0.00000	0.00000	0.00000	0.00000	0.00000
C13-nAlkane	2.81818	0.82795	0.00000	0.24377	0.17565	0.22990	0.41619	0.26947	0.43467	2.95454	0.13404
C12-nAlkane	3.98725	3.98535	3.60679	2.88032	3.89312	4.43591	3.69752	4.59728	3.75329	4.08947	0.10012
C11-nAlkane	1.69773	1.41706	3.48318	5.33103	2.01289	1.40446	1.60429	0.26899	3.66088	5.50024	0.60637
C10-nAlkane	0.22611	0.69563	1.88281	0.98437	1.64885	0.81389	0.06182	0.88626	0.11792	4.51926	0.18566
C09-nAlkane	4.13764	2.42421	1.41974	0.56817	1.48812	0.57703	2.07176	8.11007	2.82327	2.40208	0.02211
C08-nAlkane	1.44530	0.84798	0.36984	0.07231	0.11689	0.06118	0.24206	0.39880	0.33460	0.71119	0.07150
C07-nAlkane	0.36787	0.27788	0.04971	0.02348	0.00713	0.00307	0.01122	0.01125	0.00920	0.14670	0.01514
C06-Alkanes -Minus	0.00000	0.00000	0.00727	0.00307	0.00102	0.00000	0.00102	0.00000	0.00103	0.00206	0.00000

C17-nAlkane	0.02126	0.11797	0.00614	0.00000	0.00101	0.00404	0.00000	0.00303	0.10207	0.07299	0.00000
C18-Alkane-Plus	0.00405	0.04066	0.00000	0.00000	0.00000	0.00101	0.00000	0.00000	0.01515	0.01824	0.00000
Decalin+C00	0.01089	0.08350	0.12303	0.08677	0.06397	0.07503	0.13688	0.09579	0.15409	0.11989	0.00000
Decalin+C01	0.46576	0.98338	1.68866	1.22334	1.63775	2.26786	1.83506	2.01630	1.97609	1.02882	0.01074
Decalin+C02	7.18854	1.69092	3.54548	0.75715	1.10290	1.83094	1.69987	2.25908	1.61192	2.08076	0.02835
Benzene+C08	0.09440	0.35188	0.64720	0.05139	0.01064	0.04660	0.05035	0.04079	0.04662	0.35464	0.00000
Benzene+C09	0.02536	0.18023	0.32330	0.26527	0.00194	0.02140	0.02911	0.01946	0.03017	0.18453	0.00000
Adamantane	0.25064	0.39670	0.39032	0.36729	0.46742	0.45143	0.49976	0.59460	0.08663	0.35539	0.00384
Admantane+C01	0.03031	0.05598	0.05040	0.05164	0.08946	0.09950	0.08076	0.10831	0.08198	0.02545	0.00096
Admantane+C02	0.02646	0.08859	0.08816	0.04199	0.07017	0.08702	0.05461	0.06259	0.08705	0.03827	0.00000
Admantane+C03	1.00841	1.00790	3.91402	0.08805	0.35052	1.24598	1.37077	1.33449	1.44350	1.51286	0.00871
C16-Cyclo	0.02510	0.03025	0.01421	0.00000	0.00000	0.00000	0.05695	0.06312	0.00000	0.00000	0.00791
C15-Cyclo	0.00000	0.00000	0.00000	0.00000	0.00000	0.00000	0.00000	0.00000	0.00000	0.00000	0.00000
C14-Cyclo	0.00000	0.00000	0.00000	0.00000	0.00000	0.00000	0.00000	0.00000	0.00000	0.00000	0.00000
C13-Cyclo	0.00000	0.00000	0.09641	0.00700	0.00000	0.02805	0.02798	0.00000	0.02806	0.11359	0.03067
C18-isoAlkane -Plus	0.02429	0.15452	0.00409	0.00000	0.00403	0.03534	0.02216	0.04444	0.02828	0.11754	0.20343
C07-isoAlkane	0.33406	0.19452	0.04143	0.00306	0.00102	0.00102	0.00306	0.00511	0.00409	0.10874	0.00000
C08-isoAlkane	0.96592	0.43220	0.15496	0.07536	0.07521	0.03467	0.16476	0.19277	0.22953	0.48197	0.41795
C09-isoAlkane	3.69898	1.80227	0.65368	0.34151	0.82065	0.28088	1.32264	2.96531	1.78071	1.77603	0.17288
C10-isoAlkane	9.15246	4.45717	2.00119	1.66632	2.97866	1.43573	5.61059	1.80912	7.00287	4.87105	0.54994
C11-isoAlkane	9.06235	5.74385	2.77174	7.53539	6.80740	8.62361	8.90607	9.53841	9.65068	6.24366	15.76950
C12-isoAlkane	5.81627	8.24829	3.65711	56.32462	42.85667	33.37879	27.67531	13.71682	13.72319	5.50857	65.79950
C13-isoAlkane	4.56025	4.74238	3.85181	2.59650	3.07189	3.81509	4.61643	4.22334	4.71951	4.84801	0.62017
C14-isoAlkane	2.96205	3.54458	3.67041	0.15969	0.63448	2.18081	2.12069	3.00535	2.09367	3.16957	10.91040
C15-isoAlkane	2.16834	2.54744	2.92102	0.00707	0.57457	2.18641	2.24837	2.47326	2.25110	2.62142	1.74792
C16-isoAlkane	0.30292	0.77233	0.52119	0.00000	0.06850	0.43864	0.47884	0.20320	0.36906	0.80837	0.13875
C17-isoAlkane	0.04658	0.22171	0.04401	0.00000	0.01510	0.05859	0.06650	0.07073	0.07276	0.14395	0.52279
Cyclohexane+C08	0.26709	0.92580	1.44817	0.00000	0.12680	0.59501	0.33370	0.23546	2.35299	0.37998	0.23843
Cyclohexane+C09	0.10844	0.15027	0.30648	0.00000	0.03495	0.14424	0.12489	0.16733	0.21345	0.19401	0.00495
Cyclohexane+C07	0.28717	0.96816	1.46441	0.01000	0.11183	0.44075	0.31472	0.39076	0.74658	1.18518	0.00000
Cyclohexane+C06	0.22391	0.92378	0.86768	0.30213	0.42834	0.49283	0.46958	0.24047	0.35175	1.31687	0.02770
Cyclohexane+C05	0.69483	1.46232	1.67651	0.88138	1.20114	1.39736	1.31484	1.46887	1.26569	1.56516	0.14642
Cyclohexane+C04	1.42079	1.34836	0.96612	0.26311	3.70726	0.25443	0.38866	1.55203	1.17549	0.94493	0.00000
Cyclohexane+C03	1.03422	0.84210	0.43739	0.57025	0.41935	0.51387	0.77132	4.46773	0.51610	0.85546	0.01088
Cyclohexane+C02	0.98100	0.76646	0.71140	0.08404	0.08886	0.08815	0.30873	0.31161	0.41388	0.64436	0.00297
Cyclohexane+C01	0.57535	0.37113	0.10148	0.00000	0.00000	0.00000	0.00000	0.07615	0.00000	0.19200	0.00000
C08-Dicyclo	0.05128	0.05546	0.04584	0.00196	0.00490	0.00295	0.01079	0.01574	0.01378	0.03554	0.00000
C09-Dicyclo	1.67081	1.76348	1.44003	0.03544	0.51877	0.06013	0.84749	3.24676	1.58470	1.53522	0.01168
C10-Dicyclo	8.31318	1.41149	1.16529	0.70108	0.79319	0.71085	1.33238	1.16038	2.29449	1.75371	0.02243
C11-Dicyclo	1.33385	2.36190	2.55302	0.59439	1.95210	1.63318	2.34486	1.65536	1.10970	2.84041	0.03125
C12-Dicyclo	0.00000	6.99885	3.37703	1.99074	7.02189	8.19370	7.54084	10.38169	6.84771	3.27558	0.07820
C13-Dicyclo	1.39317	3.23939	5.49380	0.27307	0.89756	2.72024	2.49982	3.02516	2.54402	2.94262	0.05479
C14-Dicyclo	0.84472	1.22273	2.57131	0.00099	0.17590	1.17680	1.23311	1.17910	4.94730	1.51626	0.04896
C11-Tricyclo	0.01956	0.04223	0.06128	0.01754	0.03403	0.02829	0.02724	0.02049	0.03025	0.02937	0.00000

C12-Tricyclo	0.48708	1.12609	2.41887	0.66400	1.33512	1.71587	2.00400	1.93636	2.07167	1.17053	0.01255
C14-Tricyclo	0.16987	0.43294	1.47371	0.00000	0.12498	0.53777	0.70444	0.51930	0.69284	0.40992	0.00290
C13-Tricyclo	0.06688	0.13829	0.69381	0.00686	0.06161	0.17955	0.17908	0.15702	0.24146	0.12898	0.00194
C15-Dicyclo	0.06992	0.29181	0.26378	0.00000	0.03624	0.23973	0.19305	0.11597	0.16317	0.24354	0.00194
C15-Tricyclo	0.02761	0.19411	0.41060	0.02358	0.03236	0.16231	0.21488	0.14956	0.16632	0.17769	0.00000
Unclassified	1.48552	3.72072	6.22416	0.97497	0.45131	0.64243	0.74649	0.90392	0.79432	1.53107	1.05047

Appendix I

UNIFAC Group Composition of Sheyyab Mixtures

Sheyyab Mixture	***Weight Fraction***									
	CH3	***CH2***	***CH***	***C***	***CH2=CH***	***ACH***	***AC***	***ACCH3***	***ACCH2***	***ACCH***
P200028	0.165	0.385	0	0	0	0.317	0	0.132	0	0
P200029	0.202	0.677	0	0	0	0.087	0	0	0	0.034
P200030	0.48	0.41	0.057	0.053	0	0	0	0	0	0
P200031	0.516	0.352	0.069	0.063	0	0	0	0	0	0
P200032	0.552	0.295	0.08	0.074	0	0	0	0	0	0
P200033	0.587	0.237	0.091	0.084	0	0	0	0	0	0
P200034	0.623	0.18	0.103	0.095	0	0	0	0	0	0
P200035	0.611	0.16	0.103	0.095	0.031	0	0	0	0	0
P200036	0.564	0.197	0.092	0.085	0.063	0	0	0	0	0
P200037	0.517	0.234	0.08	0.074	0.095	0	0	0	0	0
P200038	0.47	0.271	0.069	0.064	0.126	0	0	0	0	0
P200039	0.422	0.309	0.058	0.053	0.158	0	0	0	0	0
P200040	0.374	0.347	0.046	0.043	0.191	0	0	0	0	0
P200041	0.325	0.385	0.035	0.032	0.223	0	0	0	0	0
P200042	0.277	0.423	0.023	0.022	0.256	0	0	0	0	0
P200043	0.228	0.461	0.012	0.011	0.288	0	0	0	0	0
P200044	0.585	0.22	0.101	0.093	0	0	0	0	0	0
P200045	0.514	0.315	0.089	0.082	0	0	0	0	0	0
P200046	0.444	0.408	0.077	0.071	0	0	0	0	0	0
P200047	0.376	0.499	0.065	0.06	0	0	0	0	0	0
P200048	0.31	0.587	0.054	0.049	0	0	0	0	0	0
P200049	0.245	0.674	0.042	0.039	0	0	0	0	0	0
P200050	0.181	0.758	0.031	0.029	0	0	0	0	0	0
P200051	0.12	0.841	0.021	0.019	0	0	0	0	0	0
P200052	0.059	0.921	0.01	0.009	0	0	0	0	0	0
P200053	0.163	0.38	0	0	0	0.323	0	0.134	0	0
P200054	0.147	0.344	0	0	0	0.359	0	0.149	0	0
P200055	0.133	0.309	0	0	0	0.394	0	0.164	0	0
P200056	0.118	0.275	0	0	0	0.428	0	0.178	0	0

Sheyyab Mixture	*Weight Fraction*									
	CH3	*CH2*	*CH*	*C*	*CH2=CH*	*ACH*	*AC*	*ACCH3*	*ACCH2*	*ACCH*
P200057	0.104	0.242	0	0	0	0.462	0	0.192	0	0
P200058	0.09	0.209	0	0	0	0.495	0	0.206	0	0
P200059	0.076	0.177	0	0	0	0.527	0	0.219	0	0
P200060	0.569	0.135	0.099	0.091	0	0.053	0	0	0.053	0
P200061	0.487	0.146	0.084	0.078	0	0.102	0	0	0.102	0
P200062	0.411	0.156	0.071	0.066	0	0.148	0	0	0.148	0
P200063	0.34	0.166	0.059	0.054	0	0.19	0	0	0.19	0
P200064	0.274	0.175	0.047	0.044	0	0.23	0	0	0.23	0
P200065	0.212	0.183	0.037	0.034	0	0.267	0	0	0.267	0
P200066	0.154	0.191	0.027	0.025	0	0.301	0	0	0.301	0
P200067	0.099	0.199	0.017	0.016	0	0.334	0	0	0.334	0
P200068	0.048	0.206	0.008	0.008	0	0.365	0	0	0.365	0
P200069	0.626	0.174	0.104	0.096	0	0	0	0	0	0
P200070	0.551	0.295	0.08	0.074	0	0	0	0	0	0
P200071	0.14	0.86	0	0	0	0	0	0	0	0
P200072	0.148	0.852	0	0	0	0	0	0	0	0
P200073	0.155	0.845	0	0	0	0	0	0	0	0
P200074	0.163	0.837	0	0	0	0	0	0	0	0
P200075	0.12	0.88	0	0	0	0	0	0	0	0
P200076	0.107	0.893	0	0	0	0	0	0	0	0
P200077	0.094	0.906	0	0	0	0	0	0	0	0
P200078	0.137	0.835	0	0	0.028	0	0	0	0	0
P200079	0.141	0.802	0	0	0.057	0	0	0	0	0
P200080	0.145	0.767	0	0	0.087	0	0	0	0	0
P200081	0.125	0.819	0	0	0	0.039	0	0.016	0	0
P200082	0.118	0.771	0	0	0	0.078	0	0.032	0	0
P200083	0.104	0.677	0	0	0	0.154	0	0.064	0	0
P200084	0.09	0.586	0	0	0	0.229	0	0.095	0	0
P200085	0.083	0.541	0	0	0	0.266	0	0.11	0	0
P200086	0.076	0.496	0	0	0	0.302	0	0.125	0	0
P200087	0.069	0.452	0	0	0	0.338	0	0.14	0	0
P200088	0.063	0.409	0	0	0	0.373	0	0.155	0	0
P200089	0.056	0.366	0	0	0	0.408	0	0.169	0	0
P300027	0.218	0.484	0.026	0.024	0	0.081	0	0.168	0	0
P300069	0.453	0.309	0.06	0.056	0	0.086	0	0.036	0	0
P300070	0.393	0.268	0.052	0.048	0	0.169	0	0.07	0	0
P300071	0.335	0.229	0.045	0.041	0	0.247	0	0.103	0	0
P300072	0.281	0.192	0.037	0.034	0	0.321	0	0.134	0	0
P300073	0.484	0.258	0.07	0.065	0	0.086	0	0.036	0	0
P300074	0.42	0.224	0.061	0.056	0	0.168	0	0.07	0	0
P300075	0.359	0.192	0.052	0.048	0	0.247	0	0.102	0	0
P300076	0.3	0.16	0.044	0.04	0	0.321	0	0.133	0	0

Sheyyab Mixture	*Weight Fraction*									
	CH3	*CH2*	*CH*	*C*	*CH2=CH*	*ACH*	*AC*	*ACCH3*	*ACCH2*	*ACCH*
P300077	0.515	0.208	0.08	0.074	0	0.086	0	0.036	0	0
P300078	0.447	0.181	0.07	0.064	0	0.168	0	0.07	0	0
P300079	0.382	0.154	0.059	0.055	0	0.246	0	0.102	0	0
P300080	0.32	0.129	0.05	0.046	0	0.321	0	0.133	0	0
P300081	0.547	0.158	0.09	0.083	0	0.086	0	0.036	0	0
P300082	0.474	0.137	0.078	0.072	0	0.168	0	0.07	0	0
P300083	0.405	0.117	0.067	0.062	0	0.246	0	0.102	0	0
P300087	0.496	0.169	0.08	0.073	0	0.128	0	0.053	0	0
P300088	0.37	0.173	0.056	0.051	0	0.247	0	0.103	0	0
P300089	0.592	0.19	0.097	0.089	0.032	0	0	0	0	0
P300090	0.553	0.214	0.088	0.081	0.063	0	0	0	0	0
P300091	0.507	0.15	0.083	0.077	0	0.059	0	0.123	0	0
P300092	0.396	0.127	0.064	0.059	0	0.114	0	0.238	0	0
P300093	0.555	0.269	0.092	0.084	0	0	0	0	0	0
P300094	0.486	0.361	0.08	0.073	0	0	0	0	0	0
P300095	0.425	0.283	0.057	0.053	0	0.128	0	0.053	0	0
P300096	0.295	0.293	0.032	0.029	0	0.248	0	0.103	0	0
P300097	0.522	0.303	0.074	0.069	0.031	0	0	0	0	0
P300098	0.482	0.329	0.065	0.06	0.063	0	0	0	0	0
P300099	0.442	0.255	0.063	0.058	0	0.06	0	0.124	0	0
P300100	0.33	0.233	0.043	0.04	0	0.115	0	0.238	0	0
P300101	0.485	0.383	0.069	0.064	0	0	0	0	0	0
P300102	0.409	0.486	0.055	0.051	0	0	0	0	0	0
P400001	0.094	0.71	0.127	0	0	0.069	0	0	0	0
P400002	0.076	0.683	0.109	0	0	0.132	0	0	0	0
P400003	0.15	0.741	0.05	0	0	0.059	0	0	0	0
P400004	0.163	0.471	0	0	0	0.116	0	0	0.051	0.025
P400005	0.111	0.477	0	0	0	0.202	0	0	0.154	0.019
P400006	0.165	0.578	0	0	0	0.159	0	0	0.033	0.048
P400007	0.216	0.202	0.022	0.02	0	0.384	0	0.046	0.11	0
P400008	0.315	0.293	0.044	0.04	0	0.218	0	0.068	0.022	0
P400009	0.236	0.604	0.018	0.016	0	0.089	0	0.019	0.018	0
P400010	0.168	0.767	0	0	0	0.032	0	0	0.032	0
P400011	0.16	0.701	0	0	0	0.069	0	0	0.069	0
P400012	0.13	0.568	0	0	0	0.151	0	0	0.151	0
P400013	0.197	0.632	0	0	0	0.085	0	0	0.085	0
P400014	0.419	0.41	0.031	0.085	0.013	0	0	0	0	0
P400015	0.226	0.678	0.006	0.018	0.027	0	0	0	0	0
P400016	0.202	0.593	0.003	0.008	0.145	0	0	0	0	0
P400017	0.163	0.806	0.004	0.012	0.014	0	0	0	0	0
P400018	0.179	0.751	0.006	0.018	0.046	0	0	0	0	0
P400019	0.232	0.188	0	0	0	0.36	0	0.068	0	0

Sheyyab Mixture	*Weight Fraction*									
	CH3	*CH2*	*CH*	*C*	*CH2=CH*	*ACH*	*AC*	*ACCH3*	*ACCH2*	*ACCH*
P400020	0.256	0.391	0	0	0	0.111	0	0.114	0	0
P400021	0.249	0.273	0	0	0	0.264	0	0.066	0	0
P400022	0.149	0.438	0.01	0.009	0	0.208	0	0.185	0	0
P400023	0.188	0.655	0.009	0.008	0	0.069	0	0.071	0	0
P400024	0.087	0.414	0	0	0.136	0.229	0	0.068	0.065	0
P400025	0.151	0.595	0	0	0.021	0.131	0	0.021	0.081	0
P400026	0.272	0.462	0.028	0.026	0	0.127	0	0.042	0.043	0
P400027	0.459	0.191	0.072	0.066	0.03	0.128	0	0.053	0	0
P400028	0.423	0.21	0.064	0.059	0.061	0.129	0	0.053	0	0
P400029	0.334	0.177	0.049	0.045	0.022	0.262	0	0.109	0	0
P400030	0.303	0.207	0.041	0.038	0.059	0.248	0	0.103	0	0
P400031	0.504	0.155	0.082	0.076	0	0.096	0	0.086	0	0
P400032	0.386	0.146	0.061	0.056	0	0.181	0	0.17	0	0
P400033	0.427	0.263	0.068	0.062	0	0.127	0	0.053	0	0
P400034	0.308	0.258	0.045	0.042	0	0.245	0	0.102	0	0
P400035	0.358	0.358	0.055	0.051	0	0.126	0	0.052	0	0
P400036	0.242	0.349	0.033	0.031	0	0.243	0	0.101	0	0
P400037	0.386	0.308	0.049	0.045	0.03	0.129	0	0.053	0	0
P400038	0.347	0.333	0.04	0.037	0.061	0.129	0	0.054	0	0
P400039	0.26	0.312	0.024	0.023	0.029	0.248	0	0.103	0	0
P400040	0.222	0.336	0.016	0.015	0.059	0.249	0	0.103	0	0
P400041	0.432	0.271	0.059	0.055	0	0.096	0	0.086	0	0
P400042	0.314	0.26	0.038	0.035	0	0.193	0	0.159	0	0
P400043	0.352	0.384	0.044	0.04	0	0.127	0	0.053	0	0
P400044	0.228	0.385	0.02	0.018	0	0.246	0	0.102	0	0
P400045	0.28	0.483	0.03	0.028	0	0.126	0	0.052	0	0
P400046	0.159	0.481	0.007	0.007	0	0.244	0	0.101	0	0
P400047	0.314	0.26	0.038	0.035	0	0.181	0	0.171	0	0

Pure Component	***Weight Fraction***										
	CH3	**CH2**	**CH**	**C**	**CH2=CH**	**CH=C**	**ACH**	**ACCH3**	**ACCH2**	**ACCH**	**CH#C**
n-tetradecane	0.152	0.848	0	0	0	0	0	0	0	0	0
cyclohexane	0	1	0	0	0	0	0	0	0	0	0
n-heptane	0.3	0.7	0	0	0	0	0	0	0	0	0
decahydronaphthalene	0	0.812	0.188	0	0	0	0	0	0	0	0
2,5-dimethyl-2,4-hexadiene	0.546	0	0	0	0	0.454	0	0	0	0	0
2,2,4 trimethylpentane	0.658	0.123	0.114	0.105	0	0	0	0	0	0	0
1-octene	0.134	0.625	0	0	0.241	0	0	0	0	0	0
1,3,5 trimethylbenzene	0	0	0	0	0	0	0.324	0.674	0	0	0

toluene	0	0	0	0	0	0	0.705	0.293	0	0	0
benzene	0	0	0	0	0	0	0.999	0	0	0	0
methylcyclohexane	0.153	0.714	0.133	0	0	0	0	0	0	0	0
n-hexadecane	0.133	0.867	0	0	0	0	0	0	0	0	0
2,2,4,4,6,8,8 heptamethylnonane	0.598	0.186	0.057	0.159	0	0	0	0	0	0	0
tetrahydronaphthalene	0	0.212	0	0	0	0	0.393	0	0.393	0	0
indane	0	0.119	0	0	0	0	0.44	0	0.44	0	0
iso-propyl benzene	0.25	0	0	0	0	0	0.541	0	0	0.208	0
1-hexyne	0.183	0.512	0	0	0	0	0	0	0	0	0.304
n-dodecane	0.177	0.823	0	0	0	0	0	0	0	0	0
n-undecane	0.192	0.808	0	0	0	0	0	0	0	0	0
n-propyl benzene	0.125	0.117	0	0	0	0	0.541	0	0.216	0	0
n-decane	0.211	0.789	0	0	0	0	0	0	0	0	0

Appendix J

UNIFAC Group Composition of Fuels – Minimum and Maximum Branching Conditions

Fuel		*A1*	*A2*	*A3*	*CN30*	*CN35*	*CN40*	*CN45*	*CN50*	*CN55*	*F24*
CH3	**MIN**	0.174253	0.14403	0.112158	0.213537	0.192524	0.17314	0.17679	0.156679	0.159902	0.154582
	MAX	0.333133	0.289804	0.228318	0.466135	0.418284	0.379751	0.387871	0.330889	0.34234	0.296402
CH2	**MIN**	0.635263	0.640602	0.650222	0.614502	0.656058	0.65276	0.662196	0.691514	0.68312	0.659366
	MAX	0.383572	0.381486	0.439524	0.24938	0.304981	0.325772	0.340456	0.41759	0.397187	0.412066
CH	**MIN**	0.090353	0.087001	0.104762	0.073522	0.085153	0.090894	0.096306	0.09968	0.094518	0.076898
	MAX	0.078562	0.099116	0.110554	0.076452	0.09783	0.094911	0.097082	0.1148	0.104312	0.086634
C	**MIN**	0.000723	0.000788	0.002741	0.000131	0.000359	0.000982	0.001028	0.001031	0.001101	0.001067
	MAX	0.074836	0.058693	0.049065	0.10099	0.087863	0.085692	0.087903	0.066071	0.0723	0.057228
CH2=CH	**MIN**	0.000144	0.000245	0.0004	2.16E-06	0.000176	0.000369	0.000194	0.000138	0.000182	0.000349
	MAX	0.000144	0.000245	0.0004	2.16E-06	0.000176	0.000369	0.000194	0.000138	0.000182	0.000349
ACH	**MIN**	0.068792	0.085829	0.080597	0.063685	0.045264	0.055855	0.043495	0.035091	0.04197	0.071289
	MAX	0.041292	0.046349	0.041147	0.055785	0.022463	0.027151	0.022625	0.017345	0.021556	0.035039
AC	**MIN**	0.001163	0.003408	0.00181	0.014355	0.001484	0.000885	0.001414	0.001133	0.001323	0.001807
	MAX	0.001213	0.003545	0.002307	0.014362	0.001484	0.000886	0.001415	0.001133	0.001324	0.00198
ACCH3	**MIN**	0.001416	0.001832	0.000814	0.008321	0.000621	5.18E-05	0.000506	0.000469	0.000461	0.00085
	MAX	0.082431	0.108806	0.098212	0.031089	0.062262	0.077816	0.056992	0.048251	0.055658	0.09581
ACCH2	**MIN**	0.027051	0.034444	0.041669	0.011522	0.017592	0.023831	0.017332	0.013669	0.016733	0.031543
	MAX	0.00348	0.008839	0.022059	0.004943	0.003829	0.006349	0.004663	0.003141	0.004399	0.01062
ACCH	**MIN**	0.000696	0.001637	0.004639	0.000286	0.000673	0.001113	0.000649	0.000521	0.0006	0.002093
	MAX	0.001129	0.002845	0.008142	0.000706	0.000681	0.001118	0.000661	0.000528	0.00061	0.003637

6 CITED LITERATURE

[1] Buras ZJ, Safta C, Zádor J, Sheps L. Simulated production of OH, HO2, CH2O, and CO2 during dilute fuel oxidation can predict 1st-stage ignition delays. Combustion and Flame 2020;216:472–84. https://doi.org/10.1016/j.combustflame.2019.12.013.

[2] Kogekar G, Karakaya C, Liskovich GJ, Oehlschlaeger MA, DeCaluwe SC, Kee RJ. Impact of non-ideal behavior on ignition delay and chemical kinetics in high-pressure shock tube reactors. Combustion and Flame 2018;189:1–11. https://doi.org/10.1016/j.combustflame.2017.10.014.

[3] Campbell MF, Wang S, Goldenstein CS, Spearrin RM, Tulgestke AM, Zaczek LT, et al. Constrained reaction volume shock tube study of n-heptane oxidation: Ignition delay times and time-histories of multiple species and temperature. Proceedings of the Combustion Institute 2015;35:231–9. https://doi.org/10.1016/j.proci.2014.05.001.

[4] Zhou CW, Li Y, Burke U, Banyon C, Somers KP, Ding S, et al. An experimental and chemical kinetic modeling study of 1,3-butadiene combustion: Ignition delay time and laminar flame speed measurements. Combustion and Flame 2018;197:423–38. https://doi.org/10.1016/j.combustflame.2018.08.006.

[5] Michelbach C, Tomlin A. An experimental and kinetic modeling study of the ignition delay and heat release characteristics of a five component gasoline surrogate and its blends with iso-butanol within a rapid compression machine. International Journal of Chemical Kinetics 2021;53:787–808. https://doi.org/10.1002/kin.21483.

[6] Shao J, Zhu Y, Wang S, Davidson DF, Hanson RK. A shock tube study of jet fuel pyrolysis and ignition at elevated pressures and temperatures. Fuel 2018;226:338–44. https://doi.org/10.1016/j.fuel.2018.04.028.

[7] Shao J, Ferris AM, Choudhary R, Cassady SJ, Davidson DF, Hanson RK. Shock-induced ignition and pyrolysis of high-pressure methane and natural gas mixtures. Combustion and Flame 2020;221:364–70. https://doi.org/10.1016/j.combustflame.2020.08.010.

[8] Turbiez A, el Bakali A, Pauwels JF, Rida A, Meunier P. Experimental study of a low pressure stoichiometric premixed methane, methane/ethane, methane/ethane/propane and synthetic natural gas flames. Fuel 2004;83:933–41. https://doi.org/10.1016/j.fuel.2003.10.017.

[9] el Bakali A, Dagaut P, Pillier L, Desgroux P, Pauwels J-F, Rida A, et al. Experimental and modeling study of the oxidation of natural gas in a premixed flame, shock tube, and jet-stirred reactor. Combustion and Flame 2004;137:109–28. https://doi.org/10.1016/j.combustflame.2004.01.004.

[10] Xiao H, Duan Q, Sun J. Premixed flame propagation in hydrogen explosions. Renewable and Sustainable Energy Reviews 2018;81:1988–2001. https://doi.org/10.1016/j.rser.2017.06.008.

[11] Marinov NM, Pitz WJ, Westbrook CK, Vincitore AM, Castaldi MJ, Senkan SM, et al. Aromatic and polycyclic aromatic hydrocarbon formation in a laminar premixed n-butane flame. Combustion and Flame 1998;114:192–213. https://doi.org/10.1016/S0010-2180(97)00275-7.

[12] Wang Y, Movaghar A, Wang Z, Liu Z, Sun W, Egolfopoulos FN, et al. Laminar flame speeds of methane/air mixtures at engine conditions: Performance of different kinetic models and power-law correlations. Combustion and Flame 2020;218:101–8. https://doi.org/10.1016/j.combustflame.2020.05.004.

[13] Liu J, Dumitrescu CE. Flame development analysis in a diesel optical engine converted to spark ignition natural gas operation. Applied Energy 2018;230:1205–17. https://doi.org/10.1016/j.apenergy.2018.09.059.

[14] Velásquez M, Mondragón F, Santamaría A. Chemical characterization of soot precursors and soot particles produced in hexane and diesel surrogates using an inverse diffusion flame burner. Fuel 2013;104:681–90. https://doi.org/10.1016/j.fuel.2012.04.033.

[15] Xu R, Wang K, Banerjee S, Shao J, Parise T, Zhu Y, et al. A physics-based approach to modeling real-fuel combustion chemistry – II. Reaction kinetic models of jet and rocket fuels. Combustion and Flame 2018;193:520–37. https://doi.org/10.1016/j.combustflame.2018.03.021.

[16] Tao Y, Xu R, Wang K, Shao J, Johnson SE, Movaghar A, et al. A Physics-based approach to modeling real-fuel combustion chemistry – III. Reaction kinetic model of JP10. Combustion and Flame 2018;Submitted:466–76. https://doi.org/10.1016/j.combustflame.2018.08.022.

[17] Lundberg SM, Lee SI. A unified approach to interpreting model predictions. Advances in Neural Information Processing Systems 2017;2017-Decem:4766–75.

[18] Smith GP, Tao Y, Wang H. Foundational Fuel Chemistry Model Version 1.0 (FFCM-1) 2016. http://nanoenergy.stanford.edu/ffcm1.

[19] Lopez JG, Rasmussen CL, Alzueta MU, Gao Y, Marshall P, Glarborg P. Experimental and kinetic modeling study of C2H4 oxidation at high pressure. Proceedings of the Combustion Institute 2009;32 I:367–75. https://doi.org/10.1016/j.proci.2008.06.188.

[20] Petersen EL, Kalitan DM, Simmons S, Bourque G, Curran HJ, Simmie JM. Methane/propane oxidation at high pressures: Experimental and detailed chemical kinetic modeling. Proceedings of the Combustion Institute 2007;31:447–54. https://doi.org/10.1016/j.proci.2006.08.034.

[21] Malewicki T, Comandini A, Brezinsky K. Experimental and modeling study on the pyrolysis and oxidation of iso-octane. Proceedings of the Combustion Institute 2013;34:353–60. https://doi.org/10.1016/j.proci.2012.06.137.

[22] Sarathy SM, Westbrook CK, Mehl M, Pitz WJ, Togbe C, Dagaut P, et al. Comprehensive chemical kinetic modeling of the oxidation of 2-methylalkanes from C7 to C20. Combustion and Flame 2011;158:2338–57. https://doi.org/10.1016/j.combustflame.2011.05.007.

[23] Sun W, Hamadi A, Abid S, Chaumeix N, Comandini A. Detailed experimental and kinetic modeling study of toluene/C2 pyrolysis in a single-pulse shock tube. Combustion and Flame 2021;226:129–42. https://doi.org/10.1016/j.combustflame.2020.11.044.

[24] Malewicki T, Brezinsky K. Experimental and modeling study on the pyrolysis and oxidation of n-decane and n-dodecane. Proceedings of the Combustion Institute 2013;34:361–8. https://doi.org/10.1016/j.proci.2012.06.156.

[25] El-Sabor Mohamed AA, Panigrahy S, Sahu AB, Bourque G, Curran HJ. An experimental and kinetic modeling study of the auto-ignition of natural gas blends containing C1–C7

alkanes. Proceedings of the Combustion Institute 2021;38:365–73. https://doi.org/10.1016/j.proci.2020.06.015.

[26] Malewicki T, Gudiyella S, Brezinsky K. Experimental and modeling study on the oxidation of Jet A and the n-dodecane/iso-octane/n-propylbenzene/1,3,5-trimethylbenzene surrogate fuel. Combustion and Flame 2013;160:17–30. https://doi.org/10.1016/j.combustflame.2012.09.013.

[27] Wang H, Xu R, Wang K, Bowman CT, Hanson RK, Davidson DF, et al. A physics-based approach to modeling real-fuel combustion chemistry - I. Evidence from experiments, and thermodynamic, chemical kinetic and statistical considerations. Combustion and Flame 2018. https://doi.org/10.1016/j.combustflame.2018.03.019.

[28] Han X, Liszka M, Xu R, Brezinsky K, Wang H. A high pressure shock tube study of pyrolysis of real jet fuel Jet A. Proceedings of the Combustion Institute 2019;37:189–96. https://doi.org/10.1016/j.proci.2018.05.136.

[29] Mehta JM, Brezinsky K. Experimental speciation study of natural gas oxidation using a single pulse shock tube. International Journal of Chemical Kinetics 2021;53:845–67. https://doi.org/10.1002/kin.21487.

[30] Mehta JM, Wang W, Brezinsky K. Shock tube study of natural gas oxidation at propulsion relevant conditions. Proceedings of The Combustion Institute 2022;39.

[31] Anderson RB. Fischer-Tropsch synthesis. London: Academic Press; 1984. https://doi.org/https://doi.org/.

[32] Chauvy R, Verdonck D, Dubois L, Thomas D, de Weireld G. Techno-economic feasibility and sustainability of an integrated carbon capture and conversion process to synthetic natural gas. Journal of CO2 Utilization 2021;47. https://doi.org/10.1016/j.jcou.2021.101488.

[33] Guzman J, Brezinsky K. Experimental and modeling study of the oxidation of F-24 jet fuel, and its mixture with an iso-paraffinic synthetic jet fuel, ATJ. Combustion and Flame 2021;224:108–25. https://doi.org/10.1016/j.combustflame.2020.12.008.

[34] Ryu JI, Kim K, Min K, Scarcelli R, Som S, Kim KS, et al. Data-driven chemical kinetic reaction mechanism for F-24 jet fuel ignition. Fuel 2021;290:119508. https://doi.org/10.1016/j.fuel.2020.119508.

[35] Pandey V, Badruddin IA, Terfasa TT, Tesfamariam BB, Sayeed Ahmed GM, Ahamed Saleel C, et al. Experimental investigation of the impact of CeO2 nanoparticles in Jet-A and Jatropha-SPK blended fuel in an aircraft can-combustor at flight conditions. Fuel 2022;317:123393. https://doi.org/10.1016/j.fuel.2022.123393.

[36] Tran S, Brown A, Olfert JS. Comparison of Particle Number Emissions from In-Flight Aircraft Fueled with Jet A1, JP-5 and an Alcohol-to-Jet Fuel Blend. Energy & Fuels 2020;34:7218–22. https://doi.org/10.1021/acs.energyfuels.0c00260.

[37] Crane J, Shi X, Xu R, Wang H. Natural gas versus methane: Ignition kinetics and detonation limit behavior in small tubes. Combustion and Flame 2022;237:111719. https://doi.org/10.1016/j.combustflame.2021.111719.

[38] Cassady SJ, Choudhary R, Pinkowski NH, Shao J, Davidson DF, Hanson RK. The thermal decomposition of ethane. Fuel 2020;268:117409. https://doi.org/10.1016/j.fuel.2020.117409.

[39] Nadiri S, Agarwal S, He X, Kühne U, Fernandes R, Shu B. Development of the chemical kinetic mechanism and modeling study on the ignition delay of liquefied natural gas (LNG) at intermediate to high temperatures and high pressures. Fuel 2021;302:121137. https://doi.org/10.1016/j.fuel.2021.121137.

[40] Healy D, Kalitan DM, Aul CJ, Petersen EL, Bourque G, Curran HJ. Oxidation of C1−C5 Alkane Quinternary Natural Gas Mixtures at High Pressures. Energy & Fuels 2010;24:1521–8. https://doi.org/10.1021/ef9011005.

[41] Sahu AB, Mohamed AAE-S, Panigrahy S, Bourque G, Curran H. Ignition Studies of C1–C7 Natural Gas Blends at Gas-Turbine-Relevant Conditions. Journal of Engineering for Gas Turbines and Power 2021;143. https://doi.org/10.1115/1.4050063.

[42] Increased Conversion to Natural Gas Vehicles in Asia Global Alternative Fuels Agenda Overview Regional Snapshot of Natural Gas Use in Asian Transportation Sector Background. 2016.

[43] Tranter RS, Brezinsky K, Fulle D. Design of a high-pressure single pulse shock tube for chemical kinetic investigations. Review of Scientific Instruments 2001;72:3046–54. https://doi.org/10.1063/1.1379963.

[44] Mehta J. Optimization of Pressure and Temperature Characteristics of a High Pressure Shock Tube. MS Thesis. University of Illinois at Chicago, 2018.

[45] Rezakazemi M, Marjani A, Shirazian S. Development of a group contribution method based on UNIFAC groups for the estimation of vapor pressures of pure hydrocarbon compounds. Chemical Engineering and Technology 2013;36:483–91. https://doi.org/10.1002/ceat.201200422.

[46] Carpenter D, Nates S, Dryer FL, Won SH. Evaluating ignition propensity of high cycloparaffinic content alternative jet fuel by a chemical functional group approach. Combustion and Flame 2021;223:243–53. https://doi.org/10.1016/j.combustflame.2020.09.024.

[47] Dussan K, Won SH, Ure AD, Dryer FL, Dooley S. Chemical functional group descriptor for ignition propensity of large hydrocarbon liquid fuels. Proceedings of the Combustion Institute 2019;37:5083–93. https://doi.org/10.1016/j.proci.2018.05.079.

[48] Dussan K, Won SH, Ure AD, Dryer FL, Dooley S. Chemical functional group descriptor for ignition propensity of large hydrocarbon liquid fuels. Proceedings of the Combustion Institute 2019;37:5083–93. https://doi.org/10.1016/j.proci.2018.05.079.

[49] Won SH, Haas FM, Dooley S, Edwards T, Dryer FL. Reconstruction of chemical structure of real fuel by surrogate formulation based upon combustion property targets. Combustion and Flame 2017;183:39–49. https://doi.org/10.1016/j.combustflame.2017.04.032.

[50] Burger JL, Widegren JA, Lovestead TM, Bruno TJ. ^{1}H and ^{13}C NMR Analysis of Gas Turbine Fuels As Applied to the Advanced Distillation Curve Method. Energy & Fuels 2015;29:4874–85. https://doi.org/10.1021/acs.energyfuels.5b01035.

[51] Wang Y, Wei W, Zhang Y, Hanson RK. A new strategy of characterizing hydrocarbon fuels using FTIR spectra and generalized linear model with grouped-Lasso regularization. Fuel 2021;287:119419. https://doi.org/10.1016/j.fuel.2020.119419.

[52] Wang Y, Ding Y, Wei W, Cao Y, Davidson DF, Hanson RK. On estimating physical and chemical properties of hydrocarbon fuels using mid-infrared FTIR spectra and regularized linear models. Fuel 2019;255:115715. https://doi.org/10.1016/j.fuel.2019.115715.

[53] Fredenslund A, Jones RL, Prausnitz JM. Group-contribution estimation of activity coefficients in nonideal liquid mixtures. AIChE Journal 1975;21:1086–99. https://doi.org/10.1002/aic.690210607.

[54] Müller S. Flexible heuristic algorithm for automatic molecule fragmentation: Application to the UNIFAC group contribution model. Journal of Cheminformatics 2019;11:1–12. https://doi.org/10.1186/s13321-019-0382-3.

[55] Colket M, Heyne J, Rumizen M, Gupta M, Edwards T, Roquemore WM, et al. Overview of the National Jet Fuels Combustion Program. AIAA Journal 2017;55:1087–104. https://doi.org/10.2514/1.J055361.

[56] Gaydon AG, Hurle IR. The Shock Tube in High Temperature Chemical and Physics. New York: Reinhold Publishing Corporation; 1963.

[57] Anderson JD. Modern Compressible Flow with Historic Perspective. Third. McGraw Hill Education (India); 2012.

[58] Gaydon AG, Hurle IR. The Shock Wave in an Ideal Gas. The shock tube in high-temperature chemical physics, Reinhold Pub. Corp.; 1963, p. 9–27.

[59] Mackay D, Trass O. Contact surface tailoring in a chemical shock tube. AIAA Journal 2008;1:2161–3. https://doi.org/10.2514/3.2019.

[60] Hong Z, Davidson DF, Hanson RK. Contact surface tailoring condition for shock tubes with different driver and driven section diameters. Shock Waves 2009;19:331–6.

[61] Hong Z, Pang GA, Vasu SS, Davidson DF, Hanson RK. The use of driver inserts to reduce non-ideal pressure variations behind reflected shock waves. Shock Waves 2009;19:113–23.

[62] Hidaka Y, Nakamura T, Miyauchi A, Shiraishi T, Kawano H. Thermal decomposition of propyne and allene in shock waves. International Journal of Chemical Kinetics 1989;21:643–66. https://doi.org/10.1002/kin.550210805.

[63] Han X, Mehta JM, Brezinsky K. Temperature approximations in chemical kinetics studies using single pulse shock tubes. Combustion and Flame 2019;209:1–12. https://doi.org/10.1016/j.combustflame.2019.07.022.

[64] Tang W, Brezinsky K. Chemical kinetic simulations behind reflected shock waves. International Journal of Chemical Kinetics 2006;38:75–97.

[65] Tranter RS, Sivaramakrishnan R, Srinivasan N, Brezinsky K. Calibration of reaction temperatures in a very high pressure shock tube using chemical thermometers. International Journal of Chemical Kinetics 2001;33:722–31. https://doi.org/10.1002/kin.1069.

[66] Tsang W, Lifshitz A. Kinetic stability of 1,1,1-trifluoroethane. International Journal of Chemical Kinetics 1998;30:621–8.

[67] Matsugi A, Yasunaga K, Shiina H. Thermal decomposition of 1,1,1-trifluoroethane revisited. Journal of Physical Chemistry A 2014;118:11688–95. https://doi.org/10.1021/jp510227k.

[68] Matsugi A. Dissociation of 1,1,1-Trifluoroethane Is an Intrinsic RRKM Process: Classical Trajectories and Successful Master Equation Modeling. The Journal of Physical Chemistry A 2015;119:1846–58. https://doi.org/10.1021/acs.jpca.5b00796.

[69] Giri BR, Tranter RS. Dissociation of 1,1,1-trifluoroethane behind reflected shock waves: Shock tube/time-of-flight mass spectrometry experiments. Journal of Physical Chemistry A 2007;111:1585–92. https://doi.org/10.1021/jp066232n.

[70] Schofield K. The enigmatic mechanism of the flame ionization detector: Its overlooked implications for fossil fuel combustion modeling. Progress in Energy and Combustion Science 2008;34:330–50. https://doi.org/10.1016/j.pecs.2007.08.001.

[71] Comandini A, Malewicki T, Brezinsky K. Online and offline experimental techniques for polycyclic aromatic hydrocarbons recovery and measurement. Review of Scientific Instruments 2012;83. https://doi.org/10.1063/1.3692748.

[72] Liszka MK. High Pressure and Temperature Study of Cyclohexane, Methylcyclohexane, and 6-Bromo-1-hexene Pyrolysis. University of Illinois at Chicago, 2018.

[73] Ranzi E, Frassoldati A, Stagni A, Pelucchi M, Cuoci A, Faravelli T. Reduced kinetic schemes of complex reaction systems: Fossil and biomass-derived transportation fuels. International Journal of Chemical Kinetics 2014;46:512–42. https://doi.org/10.1002/kin.20867.

[74] Ranzi E, Cavallotti C, Cuoci A, Frassoldati A, Pelucchi M, Faravelli T. New reaction classes in the kinetic modeling of low temperature oxidation of n-alkanes. Combustion and Flame 2015;162:1679–91. https://doi.org/10.1016/j.combustflame.2014.11.030.

[75] Bagheri G, Ranzi E, Pelucchi M, Parente A, Frassoldati A, Faravelli T. Comprehensive kinetic study of combustion technologies for low environmental impact: MILD and OXY-fuel combustion of methane. Combustion and Flame 2020;212:142–55. https://doi.org/10.1016/j.combustflame.2019.10.014.

[76] Wang H, You X, Joshi A v., Davis SG, Laskin A, Egolfopoulos F, et al. High-Temperature Combustion Reaction Model of H2/CO/C1-C4 Compounds. USC Mech Version II 2007. http://ignis.usc.edu/USC_Mech_II.htm.

[77] Wang H, Dames E, Sirjean B, Sheen DA, Tangko R, Violi A, et al. A hightemperature chemical kinetic model of n-alkane (up to n-dodecane), cyclohexane, and methyl-, ethyl-, n-propyl and n-butyl-cyclohexane oxidation at high temperatures, JetSurF version 2.0; September 19, 2010. URL (Http://Melchior Usc Edu/JetSurF/JetSurF2 0) Cited on Page 2010;192.

[78] Goodwin D. Cantera: An object-oriented software toolkit for chemical kinetics, thermodynamics, and transport properties 2009. https://doi.org/10.5281/zenodo.1174508.

[79] Williams FA, Seshadri K, Cattolica R. San Diego Mechanism: Chemical-Kinetic Mechanisms for Combustion Applications 2011.

[80] Tranter RS, Sivaramakrishnan R, Brezinsky K, Allendorf MD. High pressure, high temperature shock tube studies of ethane pyrolysis and oxidation. Physical Chemistry Chemical Physics 2002;4:2001–10. https://doi.org/10.1039/b110702j.

[81] Oehlschlaeger MA, Davidson DF, Hanson RK. High-temperature ethane and propane decomposition. Proceedings of the Combustion Institute 2005;30:1119–27. https://doi.org/10.1016/j.proci.2004.07.032.

[82] Shao J, Wei W, Choudhary R, Davidson DF, Hanson RK. Shock Tube Measurement of the CH3+C2H6→CH4+C2H5 Rate Constant. The Journal of Physical Chemistry A 2019;123:9096–101. https://doi.org/10.1021/acs.jpca.9b07691.

[83] Petersen EL, Hanson RK. Nonideal effects behind reflected shock waves in a high-pressure shock tube. Shock Waves 2001;10:405–20. https://doi.org/10.1007/PL00004051.

[84] Shao J, Choudhary R, Peng Y, Davidson DF, Hanson RK. Shock Tube Measurement of the C 2 H 4 + H ⇔ C 2 H 3 + H 2 Rate Constant. Journal of Physical Chemistry A 2019;123:15–20. https://doi.org/10.1021/acs.jpca.8b09452.

[85] Sivaramakrishnan R, Michael J v., Ruscic B. High-temperature rate constants for H/D + C2H6 and C3H8. International Journal of Chemical Kinetics 2012;44:194–205. https://doi.org/10.1002/kin.20607.

[86] Peukert SL, Labbe NJ, Sivaramakrishnan R, Michael J v. Direct Measurements of Rate Constants for the Reactions of CH_3 Radicals with C_2H_6, C_2H_4, and C_2H_2 at High Temperatures. The Journal of Physical Chemistry A 2013;117:10228–38. https://doi.org/10.1021/jp4073153.

[87] Sivaramakrishnan R, Goldsmith CF, Peukert S, Michael J v. Direct measurements of channel specific rate constants in OH + C3H8 illuminates prompt dissociations of propyl radicals. Proceedings of the Combustion Institute 2019;37:231–8. https://doi.org/10.1016/j.proci.2018.05.130.

[88] Lynch PT, Annesley CJ, Tranter RS. Dissociation of ortho-benzyne radicals in the high temperature fall-off regime. Proceedings of the Combustion Institute 2015;35:145–52. https://doi.org/10.1016/j.proci.2014.05.049.

[89] Ferris AM, Davidson DF, Hanson RK. A combined laser absorption and gas chromatography sampling diagnostic for speciation in a shock tube. Combustion and Flame 2018;195:40–9. https://doi.org/10.1016/j.combustflame.2018.04.032.

[90] MIL-STD-3004D - Department of Defense Standard Practice Quality Assurance/Surveillance for Fuels, Lubricants and Related Products. 2016.

[91] Luning Prak DJ, Jones MH, Trulove P, McDaniel AM, Dickerson T, Cowart JS. Physical and Chemical Analysis of Alcohol-to-Jet (ATJ) Fuel and Development of Surrogate Fuel Mixtures. Energy & Fuels 2015;29:3760–9. https://doi.org/10.1021/acs.energyfuels.5b00668.

[92] Abdul Jameel AG, Naser N, Emwas AH, Dooley S, Sarathy SM. Predicting Fuel Ignition Quality Using 1H NMR Spectroscopy and Multiple Linear Regression. Energy and Fuels 2016;30:9819–35. https://doi.org/10.1021/acs.energyfuels.6b01690.

[93] Striebich RC, Shafer LM, Adams RK, West ZJ, DeWitt MJ, Zabarnick S. Hydrocarbon Group-Type Analysis of Petroleum-Derived and Synthetic Fuels Using Two-Dimensional Gas Chromatography. Energy & Fuels 2014;28:5696–706. https://doi.org/10.1021/ef500813x.

[94] Xu R, Wang H, Colket M, Edwards T. Thermodynamic Properties of Jet Fuels. 2015.

[95] Meininger RD, Kweon C-BM, Szedlmayer MT, Dang KQ, Jackson NB, Lindsey CA, et al. Knock criteria for aviation diesel engines. International Journal of Engine Research 2017;18:752–62. https://doi.org/10.1177/1468087416669882.

[96] Geleynse S, Brandt K, Garcia-Perez M, Wolcott M, Zhang X. The Alcohol-to-Jet Conversion Pathway for Drop-In Biofuels: Techno-Economic Evaluation. ChemSusChem 2018;11:3728–41. https://doi.org/10.1002/cssc.201801690.

[97] Luning Prak DJ, Foley MP, Dorn L, Trulove PC, Cowart JS, Durkin DP. Determining the Thermal Properties of Military Jet Fuel JP-5 and Surrogate Mixtures Using Differential Scanning Calorimetry/Thermogravimetric Analysis and Differential Scanning Calorimetry Methods. Energy & Fuels 2020;34:4046–54. https://doi.org/10.1021/acs.energyfuels.9b04028.

[98] Sheyyab M, Mehta JM, Lynch PT, Mayhew E, Brezinsky K. Prediction of derived cetane number from chemical functional group compositions of hydrocarbon mixtures with machine learning models. Submitted 2022.

[99] Edwards T. Reference jet fuels for combustion testing. AIAA SciTech Forum - 55th AIAA Aerospace Sciences Meeting 2017:1–58. https://doi.org/10.2514/6.2017-0146.

[100] Kim D, Martz J, Violi A. A surrogate for emulating the physical and chemical properties of conventional jet fuel. Combustion and Flame 2014;161:1489–98. https://doi.org/10.1016/j.combustflame.2013.12.015.

[101] Liu Y-X, Richter S, Naumann C, Braun-Unkhoff M, Tian Z-Y. Combustion study of a surrogate jet fuel. Combustion and Flame 2019;202:252–61. https://doi.org/10.1016/j.combustflame.2019.01.022.

[102] Han X. A Shock tube Study of the Pyrolysis of Real Jet Fuels Jet A and JP10. PhD Thesis. University of Illinois at Chicago, 2018.

[103] Malewicki T. Development of a high temperature chemical surrogate for jet a using a high pressure shock tube. PhD Thesis. University of Illinois at Chicago, 2012.

[104] Kim D, Violi A. On the importance of species selection for the formulation of fuel surrogates. Proceedings of the Combustion Institute 2021;38:5615–24. https://doi.org/10.1016/j.proci.2020.06.243.

[105] Kim D, Martz J, Violi A. A surrogate for emulating the physical and chemical properties of conventional jet fuel. Combustion and Flame 2014;161:1489–98. https://doi.org/10.1016/j.combustflame.2013.12.015.

[106] Lopatin OP. Natural gas combustion in diesel engine. IOP Conference Series: Earth and Environmental Science 2020;421:072019. https://doi.org/10.1088/1755-1315/421/7/072019.

[107] Chen H, He J, Zhong X. Engine combustion and emission fuelled with natural gas: A review. Journal of the Energy Institute 2019;92:1123–36. https://doi.org/10.1016/j.joei.2018.06.005.

[108] Cho HM, He B-Q. Combustion and Emission Characteristics of A Lean Burn Natural Gas Engine. International Journal of Automotive Technology 2008;9:415–22. https://doi.org/10.1007/s12239−008−0050−5.

[109] Sehgal AK, Saxena M, Pandey S, Malhotra RK. Improving Performance of Compressed Natural Gas Fueled Passenger Car Engine by Addition of Hydrogen. Journal of Scientific & Industrial Research 2018;77:61–5.

[110] Liu J, Ulishney CJ, Dumitrescu CE. Experimental investigation of a heavy-duty natural gas engine performance operated at stoichiometric and lean operations. Energy Conversion and Management 2021;243:114401. https://doi.org/10.1016/j.enconman.2021.114401.

[111] Exhaust Plume Calculations for SpaceX Raptor Booster Engine. 2019.

[112] Wang S, Dames EE, Davidson DF, Hanson RK. Reaction rate constant of CH2O + H = HCO + H2 revisited: A combined study of direct shock tube measurement and transition state theory calculation. Journal of Physical Chemistry A 2014;118:10201–9. https://doi.org/10.1021/jp5085795.

[113] Jasper AW, Sivaramakrishnan R, Klippenstein SJ. Nonthermal rate constants for CH 4∗ + X → CH 3 + HX, X = H, O, OH, and O 2. Journal of Chemical Physics 2019;150. https://doi.org/10.1063/1.5090394.

[114] Luning Prak DJ, Jones MH, Trulove P, McDaniel AM, Dickerson T, Cowart JS. Physical and chemical analysis of alcohol-to-jet (ATJ) fuel and development of surrogate fuel mixtures. Energy and Fuels 2015;29:3760–9. https://doi.org/10.1021/acs.energyfuels.5b00668.

[115] Dalmiya A, Sheyyab M, Brezinksy K, Mayhey E, Lynch PT. DCN prediction of jet fuels and their functional group surrogates using liquid phase IR absorption. Proceedings of the Combustion Institute 2022;39.

7 VITA

EDUCATION

Doctorate (PhD) - *Mechanical Engineering*, 2022 (4.0/4.0)
University of Illinois at Chicago, Chicago, USA

Master of Science (MS) - *Mechanical Engineering*, 2018 (4.0/4.0)
University of Illinois at Chicago, Chicago, USA

Bachelor of Engineering (B.E.) - *Mechanical Engineering*, 2016 (8.72/10.0)
University of Mumbai, Mumbai, India

Diploma in Mechanical Engineering, 2013 (8.89/10.0)
Shri Bhagubhai Mafatlal Polytechnic, Mumbai, India

EXPERIENCE

***University of Illinois at Chicago**, Chicago, USA* - **Research Assistant**, *High Pressure Shock Tube Laboratory,* 2017 – present

- *Study of natural gas and methane for propulsion applications – Shock Tube*
- *Compressible flow and boundary layer characterization for a shock tube*
- *Analysis of military jet fuels for prediction of ignition properties – GC x GC – TOF/FID*
- *Designing and manufacturing of high-pressure high temperature supersonic flow equipment*
- *Development of high flow rate mixing apparatus*
- *Computational analysis of high-speed flows.*
- *Chemical kinetic analysis of natural gas and military jet fuels*
- *Ignition Quality Testing (IQT)*

***B.E.S.T Undertaking**, Mumbai, India* – **Engineer,** *Transportation Engineering, 2013*

- Overhauling and modification of powertrain components – gearbox, differential, engines, transfer case etc.
- Conversion by retrofitting of diesel engines to natural gas powered engines.
- Improvement of hydraulic clutch actuation system to reduce maintenance cycle and reduce driver fatigue

***Air India Ltd.**, Mumbai, India* – **Engineer**, *Engine Overhauling Division, 2011*

- Overhauling of turbofan engines - GE-90, GE-CF60/80C2, PW 4000 series and CFM56 and APUs
- Turbofan engine and APU static testing

- Overhauling of aircraft hydraulic system and fuel supply system.
- Gas Turbine Engine Testing

PUBLICATIONS

- ***Mehta, J M****, Brezinsky, K.* Experimental speciation study of natural gas oxidation using a single pulse shock tube. Int J Chem Kinet. 2021; 53: 845– 867. https://doi.org/10.1002/kin.21487
- *Dalmiya, A.,* ***Mehta, J M.****, Tranter, R S., Lynch P T.* High pressure, high flow rate batch mixing apparatus for high throughput experiments. Rev. Sci. Instrum. 2021; 92. 114104 https://doi.org/10.1063/5.0071472
- *Han, X.,* ***Mehta, J M.****, Brezinsky, K.* Temperature approximations in chemical kinetics studies using single pulse shock tubes. Combust. Flame. 2019; 209; 1-12. https://doi.org/10.1016/j.combustflame.2019.07.022
- ***Mehta, J M***. Optimization of Pressure and Temperature Characteristics of a High Pressure Shock Tube. University of Illinois at Chicago. Thesis. 2018. https://hdl.handle.net/10027/22678
- ***Mehta, J M****, Wang, W, Brezinsky, K.* Shock tube study of natural gas oxidation at propulsion relevant conditions. Proc. Combust. Inst. 2022; 39. [In Press]

POSTERS AND PRESENTATIONS

- ***Mehta J M.****, Lynch P T., Brezinsky K.* Estimation of UNIFAC group composition of fuels using hydrocarbon group type analysis, 2022 Spring Technical Meeting of CSSCI, Detroit, MI, May 15-17,2022**.**
- ***Mehta, J M.****, Abdulrahman M., Lynch P T., Brezinsky K.* Ignition property prediction model, 3rd CUP Workshop, Madison, WI, November 17-18,2021.
- ***Mehta J M.****, Brezinsky K.* Optimization of shock tube performance in the reaction region at high temperatures and pressures, 11th U. S. National Combustion Meeting, Pasadena, CA, March 24-27,2019**.**
- *Sheyyab M.,* ***Mehta J M.****, Lynch P T., Brezinsky K.* Prediction of derived cetane number from UNIFAC group compositions of hydrocarbon mixtures with machine learning models, 2022 Spring Technical Meeting of CSSCI, Detroit, MI, May 15-17,2022**.**
- *Han X.,* ***Mehta J M.****, Brezinsky K.,* A Revisit of Constant Temperature Approximation in Chemical Kinetics Study Using Single Pulse Shock Tubes with Speciation, 11th U. S. National Combustion Meeting, Pasadena, CA, March 24-27,2019.
- *Dalmiya, A.,* ***Mehta, J M.****, Laich, A., Lynch P T.* High pressure, high flow rate batch mixing apparatus, 11th U. S. National Combustion Meeting, Pasadena, CA, March 24-27,2019.

PROJECTS

Design of Intake and Exhaust System for Formula SAE Car, 2016

- *Design of a new intake manifold based on ram induction theory to overcome the effect of restricted air flow*
- *Design of exhaust system to compliment the intake system and to minimize the exhaust noise to below 110 dBc*
- *CFD analysis of the system using ANSYS Fluent and Solidworks*
- *Prototyping and manufacturing of the intake system using additive manufacturing (SLS)*

Computer Numeric Controlled (CNC) milling machine, 2013

- *Design and fabrication of 3-axis stepper motor-controlled mill*
- *Electronic and control board to operate the mill using G and M codes*

LEADERSHIP EXPERIENCE

- Head of Engine Department at DJS Racing (Formula SAE Team – Dwarkadas J. Sanghvi College of Engineering)
- Driver at DJS Racing (Formula SAE Team – Dwarkadas J. Sanghvi College of Engineering) – Formula Student India 2016
- Cultural Secretary in Student Council – Shri Bhagubhai Mafatlal Polytechnic
- Treasurer - Indian Graduate Student Association of UIC